

กรณีแปรสัณฐานยุคใหม่ตามแนวรอยเลื่อนปัว จังหวัดน่าน
ภาคเหนือของประเทศไทย โดยอาศัยหลักฐานจาก
ข้อมูลโทรมัมผัสและการหาอายุตะกอน
ด้วยวิธีเปล่งแสงด้วยความร้อน

นายกิตติ ขาววิเศษ

วิทยานิพนธ์นี้เป็นส่วนหนึ่งของการศึกษาตามหลักสูตรปริญญาวิทยาศาสตรมหาบัณฑิต
สาขาวิชาธรณีวิทยา ภาควิชาธรณีวิทยา
คณะวิทยาศาสตร์ จุฬาลงกรณ์มหาวิทยาลัย
ปีการศึกษา 2550
ลิขสิทธิ์ของจุฬาลงกรณ์มหาวิทยาลัย

NEOTECTONICS ALONG THE PUA FAULT IN CHANGWAT NAN,
NORTHERN THAILAND: EVIDENCE FROM REMOTE SENSING
AND THERMOLUMINESCENCE DATING

Mr. Kitti Khaowiset

A Thesis Submitted in Partial Fulfillment of the Requirements
for the Degree of Master of Science Program in Geology

Department of Geology

Faculty of Science

Chulalongkorn University

Academic Year 2007

Copyright of Chulalongkorn University

Thesis Title NEOTECTONICS ALONG THE PUA FAULT IN
CHANGWAT NAN, NORTHERN THAILAND:
EVIDENCE FROM REMOTE SENSING AND
THERMOLUMINESCENCE DATING


By Mr. Kitti Khaowiset

Field of Study Geology

Thesis Advisor Associate Professor Punya Charusiri, Ph.D.

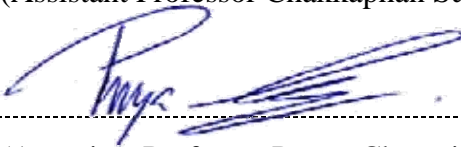
Thesis Co-Advisor Mr. Suwith Kosuwan, M.Sc.


Accepted by the Faculty of Science, Chulalongkorn University in
Partial Fulfillment of the Requirements for the Master's Degree

 Dean of the Faculty of Science
(Professor Supot Hannongbua, Ph.D.)

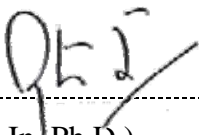
THESIS COMMITTEE

 Chairman
(Assistant Professor Chakkaphan Sutthirat, Ph.D.)

 Thesis Advisor
(Associate Professor Punya Charusiri, Ph.D.)

 Thesis Co-Advisor
(Suwith Kosuwan, M.Sc.)

 Member
(Assistant Professor Montri Choowong, Ph.D.)

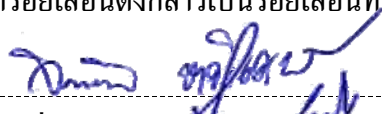
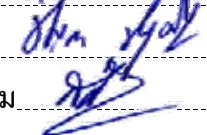

 Member
(Krit Won-In, Ph.D.)

กิตติ ขาววิเศษ : ธรณีแปรสัณฐานยุคใหม่ตามแนวรอยเลื่อนปัว จังหวัดน่าน ภาคเหนือของประเทศไทยโดยอาศัยหลักฐานจากข้อมูลโทรมัมผัสและการหาอายุตะกอนด้วยวิธีเปล่งแสงด้วยความร้อน. (NEOTECTONICS ALONG THE PUA FAULT IN CHANGWAT NAN, NORTHERN THAILAND: EVIDENCE FROM REMOTE SENSING AND THERMOLUMINESCENCE DATING) อ.ที่ปรึกษา: รศ. ดร. ปัญญา จารุศิริ, อ.ที่ปรึกษาร่วม: สุวิทย์ โคสุวรรณ, 218 หน้า.

การศึกษารณีแปรสัณฐานยุคใหม่บริเวณจังหวัดน่าน ครอบคลุมพื้นที่ส่วนใหญ่ของแอ่งปัวและแอ่งน่าน โดยการประยุกต์ใช้ข้อมูลโทรมัมผัสในการประเมินโอกาสเกิดแผ่นดินไหวของกลุ่มรอยเลื่อนปัว วัตถุประสงค์ของการศึกษาเพื่อบ่งชี้ถึงธรณีสัณฐานที่เกิดขึ้นสัมพันธ์กับรอยเลื่อน กำหนดตำแหน่งแนวรอยเลื่อนมีพลัง ทิศทางการวางตัวและลักษณะการเคลื่อนตัวของรอยเลื่อนมีพลัง ตลอดจนช่วงเวลาของการเคลื่อนตัวของกลุ่มรอยเลื่อนดังกล่าว

ผลการศึกษาวิจัยพบว่า กลุ่มรอยเลื่อนปัว วางตัวในแนวเหนือ-ใต้ เลื่อนตัวแบบเฉียง มีความยาวรวมทั้งสิ้นประมาณ 130 กิโลเมตร ต่อเนื่องมาจากชายแดนไทย-ลาว ลงมาถึงขอบด้านใต้ของแอ่งน่าน สามารถแบ่งออกเป็น 14 รอยเลื่อนย่อย มีความยาวตั้งแต่ 6 ถึง 39 กิโลเมตร รอยเลื่อนส่วนใหญ่วางตัวในทิศค่อนข้างเหนือ-ใต้ และวางตัวขนานตามขอบแอ่งยุคซีโนโซอิก โดยเฉพาะขอบด้านตะวันออกของแอ่งปัว รอยเลื่อนปรากฏให้เห็นชัดเจน ผลการแปลความหมายข้อมูลโทรมัมผัสรวมกับการสำรวจภาคสนาม พบลักษณะธรณีสัณฐานที่สัมพันธ์กับรอยเลื่อน ได้แก่ ฝาสามเหลี่ยม ธารเหลี่ยม ฝารอยเลื่อน หุบเขาเส้นตรง หุบเขาแก้วไวน์ และ สันเขาปิดกั้น ซึ่งธรณีสัณฐานดังกล่าวสามารถพบได้ตลอดแนวรอยเลื่อน

ผลการตรวจสอบภาคสนามและชุดร่องสำรวจ จำนวน 3 พื้นที่ ได้แก่ 1) บริเวณบ้านทุ่งอ้าว พบรอยเลื่อนย่อยทุ่งอ้าว มีความยาวของรอยเลื่อน 22 กม. และมีการเคลื่อนตัวในแนวตั้งประมาณ 1.2 เมตร จากระยะการเคลื่อนตัวของในแนวตั้งรอยเลื่อนบ่งชี้ว่าสามารถก่อให้เกิดแผ่นดินไหวในอดีตได้สูงสุด 6.67 ริกเตอร์ 2) พื้นที่บ้านตุ้ ครอบคลุมรอยเลื่อนย่อยบ้านตุ้ ยาวประมาณ 7 กม.และมีระยะการเคลื่อนตัวในแนวตั้งประมาณ 1.75 เมตร จากระยะการเคลื่อนตัวในแนวตั้งสามารถก่อให้เกิดแผ่นดินไหวสูงสุด 6.79 ริกเตอร์ และ 3) พื้นที่บ้านเวียงสอง อยู่ใกล้กับรอยเลื่อนย่อยเวียงสอง มีความยาว 6 กม. สามารถเกิดแผ่นดินไหวขนาดสูงสุดขนาดประมาณ 6.03 ริกเตอร์ ผลการศึกษาแสดงว่าในอดีตรอยเลื่อนมีการเคลื่อนตัวตามอิทธิพลส่วนใหญ่ของรอยเลื่อนแบบปกติร่วมกับการเลื่อนในแนวราบ ทั้งแบบเหลี่ยมขวาและเหลี่ยมซ้าย ผลการหาอายุของชั้นตะกอนในร่องสำรวจที่สัมพันธ์กับรอยเลื่อน บ่งชี้ว่ารอยเลื่อนมีอัตราการเคลื่อนตัวที่ 0.3 มิลลิเมตรต่อปี และเคยทำให้เกิดแผ่นดินไหวมาแล้วอย่างน้อย 4 ครั้ง ครั้งแรกเกิดก่อน 70,000 ปี ครั้งที่สองเกิดเมื่อประมาณ 5,000 ปี ครั้งที่สามเมื่อประมาณ 2,000 ปี และครั้งล่าสุดเมื่อ 180 ปี และมีคาบอุบัติซ้ำประมาณ 1,500 ถึง 2,000 ปี จัดว่ารอยเลื่อนดังกล่าวเป็นรอยเลื่อนที่มีพลัง

ภาควิชา.....	ธรณีวิทยา.....	ลายมือชื่อนิสิต.....	
สาขาวิชา.....	ธรณีวิทยา.....	ลายมือชื่ออาจารย์ที่ปรึกษา.....	
ปีการศึกษา.....	2550.....	ลายมือชื่ออาจารย์ที่ปรึกษาร่วม.....	

##4772220323: MAJOR GEOLOGY




KEYWORD: PUA FAULT / MORPHOTECTONIC / THERMOLUMINESCENCE
DATING / PALEOSEISMIC

KITTI KHAOWISET: NEOTECTONICS ALONG THE PUA FAULT IN CHANGWAT
NAN, NORTHERN THAILAND: EVIDENCE FROM REMOTE SENSING AND
THERMOLUMINESCENCE DATING. THESIS ADVISOR: ASSOC. PROF. PUNYA
CHARUSIRI, Ph.D., THESIS COADVISOR: SUWITH KOSUWAN, 218 pp.

Neotectonic investigation in Nan area, northern Thailand was selected for identifying the detailed characteristics of active faults. The remote-sensing data was applied for evaluating the occurrence of paleoseismicity in the study area. The main purposes of this study constitute events of earthquake faulting, paleoearthquake magnitudes, and slip-rates of these fault movements.

Results from the remote-sensing interpretation indicate that the Pua Fault Zone is the north-south trending, normal-oblique fault with a total length of about 130 km. The fault zone can be traced from Thai-Lao border throughout the Pua basin to south of Nan basin. A number of fourteen fault segments, ranging in length from 6 to 39 km, are recognized and most of all which run along the boundary of Cenozoic basins, particularly faults on the western flank of Pua basin. Based on the remote-sensing interpretation together with the ground-truth surveys reveal that several morphotectonic features, particularly triangular facets, offset streams, scarplets, linear valleys, fault scarp, wine-glass canyon, and shutter ridges, were clearly observed sporadically within the area under investigation.

Detailed field investigations with exploratory trenching were done in 3 areas. Ban Thung Ao area consists of the 22 km-long Thung Ao fault segment. This segment has vertical displacement of 1.2 m and used to produce the maximum paleoearthquake of 6.67 M. Ban Doo area is located in the southern part of Ban Doo fault segment which is 7 km-long. Based on the vertical movement of 1.75 m, this segment fault used to produce the maximum paleoearthquake of 6.79 M. The Ban Wiang Song area comprises the 6 km-long Wiang Song segment with paleoearthquake of about 6.03 M. Based on morphotectonic evidences most faults in Pua Fault Zone are normal-oblique fault which the slips are both right-lateral and left-lateral. The TL dating results of sedimentary layers related to faults indicate the average slip rate of these faults of about 0.3 mm/yr. The faults have ever been triggered four major earthquake events. The first event took place at the ages of about more than 70,000 years ago, the second event took place at about 5,000 years ago, and the third event occurred at about 2,000 years ago, and the last event at about 180 year. The recurrence interval of the Pua Fault is around 1,500 to 2,000 years. Consequently, various pieces of evidences indicate that the Pua Fault Zone is still active till present.

Department:..... Geology..... Student's signature: 
Field of study:..... Geology..... Advisor's signature: 
Academic year:..... 2007..... Co-advisor's signature: 

ACKNOWLEDGMENTS

The author wishes to express his profound and sincere appreciation to his advisor, Associate Professor Punya Charusiri, and the thesis co-advisor, Mr. Suwith Kosuwan, for their enthusiastic support, continuous guidance and invaluable advice throughout the period of this study.

Sincere thanks and appreciation are extended to the Research Institute of Materials and Resources, Akita University, Professor Isao Takashima and his research assistants, Dr. Krit Won-in and Mr. Myint Soe for their technical assistance and support all the facilities and their hospitality during his visit in Japan.

The author would like to thank the Global Land Cover Facility website for the grants and accessibility to the satellites images from the Landsat 7 ETM⁺, Earth Remote Sensing Data Analysis Center (ERSDAC) for Aster data and USGS for SRTM DEM and Pointasia website (www.pointasia.com) for high IKONOS images.

A special thank to the Secretary and staff of Office of Atoms for Peace (OAEP), especially Mr. Pisarn Tungpitayakul for his help in sample analysis with NAA method. The author also would like to express his sincerely gratitude to Mr. Arag Vitittheeranon for his help in working in gamma ray issues.

Thanks are also extended to Mr. Somsak Potisat, the Director General of Department of Mineral Resources (DMR), Mrs. Benja Sekteera and Mrs. Benjawan Charukalat the director of Bureau of Geological Survey, DMR and Dr. Assanee Meesook the director of Geological Division 4, for providing permission suggestions in his graduate study.

Special thanks extend to Mr. Preecha Saithong, Mr. Rachata Meetuwong, Mr. Pitsanupong Kanjanapayont, and Mr. Pongpan Janpinij for their helps in fieldwork and manage collecting all samples. The author would like to thank to Assistant Professor Dr. Motri Chuwong, Assistant Professor Dr. Thasinee Charoentitirat and staffs of the Department of Geology, Chulalongkorn University for all their help and support.

Finally, a very special thank to his family, his parents for continuous financial and emotional supports throughout the program. No amount of his gratitude to them would be sufficient. Last, but not least, his honored master, Dr. Assanee Meesook, thank you again for his help and being a proofreader. His responses make his work a better one.

CONTENTS

	PAGE
Abstract in Thai	iv
Abstract in English	v
Acknowledgments	vi
Contents	vii
List of Figures	x
List of Tables	xxiv
Chapter I Introduction	1
1.1 Background	1
1.2 Objective	4
1.3 Study Area	4
1.4 Methodology	4
1.5 Previous Active Fault Study in Thailand	9
1.6 A Brief Guide to the Thesis	22
Chapter II Literature Reviews	26
2.1 Regional Geologic setting	26
2.1.1 Geological setting	26
2.1.2 Structural setting	33
2.2 Tectonic Setting	35
2.2.1 Tectonic evolution during Cenozoic in the Sunda shelf and Northern Thailand	35
2.2.2 Development of Tertiary basins in northern Thailand	39
2.3 Seismicity in northern Thailand and Nan Area	41
2.4 Active faults in Thailand	43
2.4.1 Definition of active fault	43
2.4.2 Active faults in Thailand	48
2.4.3 Pua Fault	52
Chapter III Remote-sensing Interpretation	55
3.1 Results from satellite image interpretation	55
3.1.1 Satellite images acquisition	55
3.1.2 Result from Landsat 7 TM images and SRTM DEM interpretation	59
3.1.2.1 Lineaments	59
3.1.2.2 Cenozoic basins	60
3.1.3 Result from Aster image interpretation	66
3.1.3.1 Lineaments	66
3.1.3.2 Lithologic units	67

	PAGE
3.2 Fault segmentation	74
3.2.1 Concept of fault segmentation	74
3.2.2 Result of fault segmentation	78
3.3 Neotectonic Evidence and Faulting	80
3.3.1 Introduction to tectonic geomorphology	80
3.3.2 Result from Aerial photographs and Ikonos images interpretation ..	85
3.3.2.1 Area 1: Ban Thung Ao, Amphoe Thung Chang	85
3.3.2.2 Area 2: Ban Doo, Amphoe Chiang Klang	87
3.3.2.3 Area 3: Ban Teen Tok, Amphoe Pua	97
3.3.2.4 Area 4: Ban Thung Hao, Amphoe Pua	100
3.3.2.5 Area 5: Ban Sob Pua, Amphoe Pua	100
3.3.2.6 Area 6: Ban Muang Luang, Amphoe Muang Nan	105
Chapter IV Field Investigations.	109
4.1 Field evidence of tectonic geomorphology	109
4.1.1 Area 1: Ban Thung Ao, Amphoe Thung Chang	109
4.1.2 Area 2: Ban Doo, Amphoe Chiang Klang	113
4.1.3 Area 3: Ban Teen Tok, Amphoe Pua	119
4.1.4 Area 4: Ban Thung Hao, Amphoe Pua	123
4.1.5 Area 5: Ban Sob Pua, Amphoe Pua	125
4.1.6 Area 6: Ban Muang Luang, Amphoe Muang Nan	128
4.2 Paleoseismic Trenching	130
4.2.1 Site selection for paleoseismic trenching	130
4.2.2 Trench 1: Ban Thung Ao, Amphoe Thung Chang	133
4.2.2.1 Stratigraphic description	133
4.2.2.2 Evidence of faulting and folding	139
4.2.2.3 Structural geology	139
4.2.3 Trench 2: Ban Doo, Amphoe Chiang Klang	140
4.2.3.1 Stratigraphic description	141
4.2.3.2 Evidence of faulting and folding	145
4.2.3.3 Structural geology	145
4.2.4 Trench 3: Ban Wiang Song, Amphoe Thung Chang	146
4.2.4.1 Stratigraphic description	146
4.2.4.2 Evidence of faulting and folding	151
4.2.4.3 Structural geology	151
Chapter V Sedimentary Dating and Fault Evolution	153
5.1 Thermoluminescence dating	153
5.1.1 Basic concept	153
5.1.2 Paleodose and annual dose evaluation	156
5.1.3 Laboratory analysis	156
5.1.3.1 Crushing and sieving	158
5.1.3.2 Paleodose or equivalent dose evaluation	158
5.1.4 Regeneration technique	160
5.1.5 Residual test	160
5.1.6 Plateau test	163

	PAGE
5.1.7 Annual dose evaluation.....	163
5.1.8 Error determination.....	166
5.2 Thermoluminescence dating results.....	166
5.3 Fault evolution.....	168
5.3.1 Trench 1: Ban Thung Ao, Amphoe Thung Chang.....	168
5.3.1.1 Age of stratigraphic units.....	168
5.3.1.2 Evolution of sedimentation and faulting.....	171
5.3.2 Trench 2: Ban Doo, Amphoe Chiang Klang.....	171
5.3.2.1 Age of stratigraphic units.....	171
5.3.2.2 Evolution of sedimentation and faulting.....	171
5.3.3 Trench 3: Ban Wiang Song, Amphoe Thung Chang.....	171
5.3.3.1 Age of stratigraphic units.....	171
5.3.3.2 Evolution of sedimentation and faulting.....	175
Chapter VI Discussions	179
6.1 Characteristics of the Nan-Pua Fault.....	179
6.2 Paleomagnetism and slip rate.....	181
6.3 Neotectonic Evolution.....	187
6.4 Preliminary Seismic Hazard Evolution.....	190
Chapter VII Conclusions	197
References	199
Appendices	208
Biography	220

LIST OF FIGURES

	PAGE
Figure 1.1	Historical seismicity of Thailand and surrounding countries (Thai Meteorological Department, 2008). Note that lineaments and major structures are shown and the study region is shown in the red box. 2
Figure 1.2	Major active faults in Thailand showing preliminary TL dating results on earthquake events, locations of hot spring and epicenter distribution (after Charusiri et al., 2001). 3
Figure 1.3	Map of northern and north-western Thailand and eastern Myanmar showing the location of the study area (black square) in the Nan Province (Department of Highways, 2007). 5
Figure 1.4	Topological map of the study (white square) showing the mountain ranges (brown) Cenozoic basins and plains (yellow) and major streams and oriented in the north-south direction. Note that the regional structure extends northward to Myanmar and Lao. 6
Figure 1.5	Simplified flow chart illustrating investigation procedures for the research study. 7
Figure 1.6	Seismic source zones of Burma, Thailand and Indochina (modified after Nutalaya et al., 1985). Noted that seismic source zones were recognized only in the northern and western parts of Thailand. 11
Figure 1.7	Map showing active and suspected active faults in Thailand (modified after Hinthong, 1997). Note that the Pua Fault was not reported in the map. 12
Figure 1.8	Combined magnetic- radiometric - gravity data interpretation showing structural map of Central Plain with magnetic and radiometric lineaments underlain. Note that 1 = Phitsanulok Basin, 2 = Nong Bua Basin, 3 = Nakhon Sawan Basin, 4 = Lop Buri Basin, 5 = Supanburi Basin, 6 = Kamphaeng Saen Basin, 7 = Thon Buri Basin, 8 = Ayuthaya Basin (after Tulyatid and Charusiri, 1999). 14
Figure 1.9	a) Location of Ban Hat Chom Phu trench site, in the southern part of Mae Ai segment of Mae Chan Fault, Chiang Mai, Northern Thailand. b) Trench stratigraphy of the east wall side of the Ban Hat Chom Phu trench showing reverse fault movement and locations of samples for TL dating and their dates (Kosuwan et al., 1999). 15

Figure 1.10	Map of the Three Pagodas Fault showing the fault segments (after Won-In, 1999).	16
Figure 1.11	a) Geologic map along the trace of the Mae Kuang fault. P, undifferentiated Permian rocks; Cmt, Mae Tha Formation; SD, Silurian and Devonian Rocks; Pzph, Paleozoic phyllite; Pzv, Paleozoic metabasalt; Mzg, granitic rocks of the Fang-Mae Suai batholiths. B) Topographic map of a portion of the Mae Kuang Valley, showing the mapped trace of the Mae Kuang Fault. A, B, and C point to shutter ridges that have diverted northwest-flowing tributaries (after Rhodes et al., 2002).	18
Figure 1.12	Fault segments of the Phrae fault system northern Thailand, interpreted using Landsat 5 TM image data (after Udchachon et al., 2005).	19
Figure 1.13	Late Cenozoic faults and historical seismicity (1362 to 1996) of the Northern Basin and Range seismotectonic province (Fenton et al., 1997).	20
Figure 1.14	a) Location of Mae Yom I trench site, central part of Mae Yom Fault, Phare, Northern Thailand. b) Trench stratigraphy of the southwest wall of the Mae Yom 1 Phu trench showing both nor and reverse faulting and locations of samples for TL dating and their dates (Charusiri et al., 2006).	21
Figure 1.15	a) IKONOS satellite image showing locations of proposed dam sites (yellow lines) along the Salawin River. Datched red lines indicate the potential active fault, mostly trending in NW-SE direction. b) Trench-log stratigraphy showing fault orientation and TL ages of sedimentary layer, the Hutgyi dam area, the Salawin River. Lithostratigraphy compare with the age of sediment.	24
Figure 1.16	Map showing fault segments and their paleoearthquake magnitudes of the Moei-Mae Ping Fault Zone (Saithong, 2006).	25
Figure 2.1	Regional geological map of the eastern part of northern Thailand (Department of Mineral Resources, 1999). Note that black box is the study area.	27
Figure 2.2	Explanation of geological map (Department of Mineral Resources, 1999), showing in Figure 2.1.	28
Figure 2.3	Structural map of Northern Thailand showing relationship between conjugate strike-slip faults and the development of N-S trending pull-apart basins (after Polachan and Sattayarak, 1989).	34

Figure 2.4	Tectonic map of central-east Asia illustrating ‘extrusion’ model and its relationship with Cenozoic structures in the region. Numbers in white arrows indicate the relative order in which certain continental blocks were extruded toward the southeast (after Tapponnier et al., 1982).....	36
Figure 2.5	Three successive stages (I to III and IV to VI are in interpretation) of extrusional model experiment with plasticine (plain view). In unilaterally confined experiment, two major faults (F1 and F2) guide successive extrusion of two blocks. In stage VI, blocks 1 and 2 can be compared to Indochina and southern China, and open gap 1, 1+2, 2 to South China Sea, Andaman Sea, and northeastern China, respectively (after Tapponnier et al., 1982).....	37
Figure 2.6	Tectonic map of Southeast Asia showing major structural elements in relation to direction of present maximum horizontal stress (after Srisuwan, 2002).....	40
Figure 2.7	Seismotectonic provinces in Thailand (after Woodward-Clyde Federal Services, 1996).....	44
Figure 2.8	Late Cenozoic faults and historical seismicity (1362 to 1996) of the Northern Basin and Range seismotectonic province (Bott et al., 1997).....	45
Figure 2.9	Schematic focal mechanisms of Thailand and adjacent regions (Bott et al., 1997).....	46
Figure 2.10	Simplified map of the Pua Fault System showing fault segments and localities mentioned in the text (Fenton, 2003).....	53
Figure 2.11	Low angle fault scarp on surface of Late Quaternary alluvial fan, Thung Chang Segment, Pua Fault (Fenton et al., 2003).....	54
Figure 2.12	Wine-glass canyon developed where the Nam Khun crosses the Pua Fault (Fenton et al., 2003).....	54
Figure 2.13	Exposure of faulted alluvial gravels and lacustrine clays at the southern end of the Pau fault overall sense of displacement is down-to-the-west (Fenton et al., 2003).....	54
Figure 3.1	Electromagnetic radiation (or EMR) spread from sun impact to earth and reflex to atmosphere. Satellite can be detected these electromagnetic wave and convert to image. (www.ellie.cla.sc.edu).....	56
Figure 3.2	Electromagnetic wavelength with low frequency to high frequency, such as radio wave, microwave, visible wave, ultraviolet wave and grammar ray (http://www.nasa.gov).....	56

Figure 3.3	The reflection of electromagnetic wave of each object on earth (http://www.nasa.gov).	56
Figure 3.4	Enhanced Landsat 7 ETM+ by using the false-colored composite image data of bands 4 (red), 5 (green), and 7 (blue) showing physiographic features of the study area covered the eastern part of northern Thailand and western part of Lao PDR. Note that these exists some contrasting structural features between eastern and western blocks of the roughly N-trending Pua-Nan-Sirikkit Reservoir zone, suggesting the difference in tectonic regime between the two blocks.	61
Figure 3.5	Enhanced Landsat 7 ETM+ by using the false-colored composite image data of bands 6 (red), band ratio 3/2 (green), and band ratio 4/5 (blue) showing physiographic features of the study area covered the eastern part of northern Thailand and some part of Lao PDR. Note that identification of Cenozoic basins (shown herein as yellow-coloured) can be done easily after the enhancement process, and that a sharp lineament in the north-northeast trend connecting the Pua and the Nan basins. Interpreted result is shown in Figure 3.8.	62
Figure 3.6	Shade relief image from SRTM DEM data taken on February 11, 2000 showing contrasting hard-rock geology and structures between western and eastern blocks of the Pua-Nan-Sirikkit Reservoir zone. Note that not many Cenozoic Basin occur in east of the Pua-Nan-Sirikkit Reservoir zone. Also shown is a series of the ENE-trending faults in the eastern block that is quite distinct and non-cut the major structures and lithologies. See also Figure 3.7 for interpretation.	63
Figure 3.7	Map of the study region showing distribution of lineaments and Cenozoic basins interpreted using the enhanced Landsat 7 ETM+ image and SRTM DEM data in Figures 3.5 and 3.6. Note that Pua Basin contains more distinct sharp lineaments than those of Nan Basin.	64
Figure 3.8	Lineament maps after filtering process of enhancement showing a) the north-south-trending with 45 lineaments, b) the northeast-southwest-trending with 119 lineaments, c) the northwest-southeast-trending with 224 lineaments. d) Rose diagram based on 224 points with the majority of the lineaments in the northeast-southwest direction.	65

Figure 3.9	Enhanced Aster image by using the false-colored composite image data of band 3 (red), band 2 (green), and band 1 (blue) showing physiographic features of the study area covered. Note that eastern edge (blue/red boundary) of the Pua Basin is quite prominent. There exists the cross structure into the basin in the NE direction from Tha Wang Pha to Pua District. Similar situation also shown at north of Chiang Klang. The Nan Basin shows more subdue features.....	69
Figure 3.10	Enhanced Aster image by using the false-colored composite image data of bands 6 (red), band 3 (green), and band 1 (blue) showing physiographic features. Cenozoic basins are shown in pink and white and most hard-rock geology is depicted in green. Note that cross structures are clear. Linear features connecting the Pua and Nan basins are also distinct (Interpreted result is shown in Figure 3.12).....	70
Figure 3.11	Shade relief image from ASTER DEM data showing several morphotectonic landforms of the Nan-Pua study area. Note that the basins are shown as flat terrain or very low relief features whereas the mountainous areas are mainly with high-relief tonation. The interpreted result is shown in Figure 3.12.....	71
Figure 3.12	Interpretation map using the enhanced Aster images and Aster DEM data in Figures 3.9-3.11 shows major geology of the Cenozoic basin and the essential lineament features. Note that some lineaments cross cut the basins.....	72
Figure 3.13	Lineament maps after enhancement in the DEM format showing a) the north-trending with 99 lineaments, b) the northeast to east-northeast-trending with 314 lineament c) the northwest-trending with 214 lineaments. d) Rose diagram based on 627 points with the majority of the lineaments in the northeast-southwest direction.....	73
Figure 3.14	Map of the study area displaying locations of the Pua Faults (red line) and its major 14 inferred active fault segments with their length.....	79
Figure 3.15	Plan view of structures associated with an idealized strike-slip fault (after Christie-Blick and Biddle, 1985).....	81
Figure 3.16	Simple shear models associated with strike-slip fault (a) and producing contraction and extensional features (b), used in this study following the work done by Christie-Blick and Biddle (1985).....	81

Figure 3.17	Sags and pressure ridges associated with bends and steps along strike-slip faults (after Keller and Pinter, 1996).	83
Figure 3.18	Assemblage of landform associated with active tectonic strike-slip faulting (after Burbank and Anderson, 2001).	83
Figure 3.19	Idealized cross-section of extension tectonic environments (after Burbank and Anderson, 2001).	83
Figure 3.20	Basic slope elements that may be present on a fault scarp (after McCalpin, 1996).	84
Figure 3.21	Types of reverse fault scarps. (A) Simple reverse (or thrust) scarp. (B) Hanging-wall collapse scarp. (C) Simple pressure ridge. (D) Dextral pressure ridge. (E) Back-thrust pressure ridge. (F) Low-angle ridge. (G) En-echelon pressure ridge. 1, bed rock; 2, soft Quaternary sediments; 3, turf (after Phillip et al., 1992).	84
Figure 3.22	Map showing locations of the Pua Fault Zone (red line) and its major inferred active fault segments. Boxes with numbers indicate selected areas for remote-sensing and aerial photographic interpretations for detailed.	86
Figure 3.23	Aerial photograph (left), and interpreted morphotectonic landforms (right), along the Thung Ao fault segment in Area 1 (red box in an inserted map), Ban Thung Ao, Amphoe Thung Chang, Changwat Nan. Note that a green frame in morphotectonic map represent to location of Figures 3.24 – 3.26 paleoseismic studies.	88
Figure 3.24	The 3D model of IKONOS image (www.pointasia.com) at Ban Thung Ao area, Nan showing landform developed by fault (red lines) such as triangular facet (t), small fault scarp (s), offset stream (0) and linear valley (v).	89
Figure 3.25	The IKONOS image (www.pointasia.com) showing the orientation of the Thung Ao fault segment (dashed lines) in the north-northeast direction and offset spurs with the left lateral sense of movement.	90
Figure 3.26	The IKONOS image (www.pointasia.com) showing Ridge crest offset creating shutter ridge along the Thung Ao Fault east of Ban Thung Ao.	91
Figure 3.27	Aerial photograph (left) and interpreted morphotectonic landforms (right) along the Ban Doo fault segment in Area 2 (red box in an inserted), Ban Doo, Amphoe Chiang Klang, Changwat Nan.	93

Figure 3.28a	The IKONOS image (www.pointasia.com) showing of Ban Doo area showing location of the Ban Doo fault segment with a series of triangular facets and offset stream with the left-lateral sense of movement.....	94
Figure 3.28b	Development of pseudo-right lateral movement.....	95
Figure 3.29	The 3D model of ASTER image at Ban Doo area in Nan province showing geographic features, such as linear range front, steep drainage and large triangular facet with steep slopes dipping westward to the Pua Basin, indicating normal fault movement with rapid hanging wall subsidence and foot wall uplift.....	95
Figure 3.30	The 3D model of ASTER image at Ban Doo area showing a series of triangular faceted spurs along the Ban Doo segment (red dashed line). The over steepened base and the development of several erosional benches along the escarpment including at least 4 limes of fault movement in the Ban Doo area, Nan province.....	95
Figure 3.31	Development of faceted spurs produced by episodic vertical tectonic movement (after Hamblin, 1976).....	96
Figure 3.32	Aerial photograph (left) and interpreted morphotectonic landforms (right) along the Tin Tok fault segment in Area 3 (red box in an inserted map), Ban Tin Tok, Amphoe Pua, Changwat Nan. Note that a green frame in morphotectonic map represent to location of Figures 3.33.....	98
Figure 3.33	The 3D model of ASTER image showing a series of triangular facets and the v-shape valley with narrow canyon called “wineglass canyon” at the base of Phu Ka Mountain at Ban Tin Tok, east of Amphoe Pua normal fault movement.....	99
Figure 3.34	Formation of a wine-glass canyon seen in Figure 3.3 based on the interpretation reported earlier by Woodward-Clyde Federal Services (1996) at Ban Tin Tok.....	99
Figure 3.35	Aerial photograph (left) and interpreted morphotectonic landforms (right) along the Santisuk fault segment in Area 4 (red box in an inserted map), Ban Thung Hao, Amphoe Pua, Changwat Nan.....	101
Figure 3.36	The 3D model of ASTER image showing the development sub-basin in the upper part of the Santisuk basin bounded by normal faults probably in an extensional (rift) basin (see also Figure 3.37).....	102

	PAGE	
Figure 3.37	Extensional (rift) basin formation with the associated normal fault blocks caused by the strike-slip movement (after Koop and Stonely, 1982).	102
Figure 3.38	Aerial photograph (left) and interpreted morphotectonic landforms (right) along the Sob Pua fault segment in Area 5 (red box in an inserted map), Ban Sob Pua, Amphoe Pua, Changwat Nan. Note that the basin looks very much like an eye.	103
Figure 3.39	The 3D Model of ASTER image at Ban Sob Pua, west of Pua Basin showing eye-shape sub-basin as a result of the depression zone of the strike-slip movement.	104
Figure 3.40	Physical modeling of stresses produced at contractional and dilational step-overs along strike-slip faults suggesting plausible locations and orientations of secondary structures. Contours show where $\sigma_3 = 0$ outline region of tensile stress and zone of potential tensile fracturing for (A) a contraction step and (B) a dilational step. Representative tensile fractures (ladder-like symbols) are drawn perpendicular to local σ_3 . In (C) and (D), contours show shear-failure condition, F, for contraction step and dilational step, respectively. Potential shear-fractures are oriented at 30° to locate direction of maximum compression. Redrawn and modified from Segall and Pollard (1980).	104
Figure 3.41	Aerial photograph (left) and interpreted morphotectonic landforms (right) along the Nam Tuan fault segment in Area 6 (red box is an inserted map), Ban Muang Luang, Amphoe Muang, Changwat Nan.	107
Figure 3.42	The 3D model of ASTER image at Ban Muang Luang, north of Nan Basin showing Nam Tuan Segment (red dashed lines) and the neotectonic features, such as linear valley (a) and triangular facet with steep slopes (b), in comparison with landforms produced along recently active fault proposed by Sharp (1972).	108
Figure 4.1	Topographic map of Ban Thung Ao area, showing the location of the Thung Ao segment. Note that the yellow arrows represent the areas of photographs taken from field investigation.	110
Figure 4.2	a) Semi-consolidated alluvial deposits at Ban Ngop Nuea consisting of silty mud overlain by gravel beds which were cut by normal fault dipping to west (the author –Kitti Khaowiset- is to scale). b) A close-up view of plant fossils (dark coloured) in (grey) silty mud indicated Tertiary age (view looking to south at 699238 E / 2155615 N).	111

Figure 4.3	A panorama of the north-trending Doi Khun Huai Nam Ao mountain range, north of BanThung Ao, showing the west-dipping triangular facet covered mostly by corn field (A) in the lower part of the fault step (B) (view looking to west at 698473E/2151683N).....	111
Figure 4.4	A panoramic view of set of triangular facets (A) and facet spur (B) of the Thung Ao fault segment, and its north-trending, north of Ban Thung Ao, Amphoe Thung Chang, Changwat Nan (view looking to east at 699177E/2152622N).....	112
Figure 4.5	A physiographic feature showing the obvious geomorphotectonic evidences such as north-northeast-trending offset stream, small scarp, shutter ridge, compression ridge and offset ridge, suggesting the normal-oblique fault with a sinistral movement (view looking to NNE at 699051E/2152079N).....	113
Figure 4.6	Topographic map of Ban Doo area, showing the location of the Thung Ao segment. Note that the yellow arrows represent important tectonic geomorphic features along the fault segments.....	114
Figure 4.7	A linear front range with facet spurs (B) triangular facets (yellow) dipping to west of the Ban Doo fault segment, Doi Khun Satun situated on the east Pua basin, Ban Doo, Amphoe Chiang Klang. Note that the Nam Kon River is on the right.....	115
Figure 4.8	A scarplet (or small scarp) with a low-angle slope of Ban Doo segment (Pua Fault) cutting Late Quaternary alluvial deposit, Nan (located at 701177E/2134105N).....	116
Figure 4.9	Photograph showing the NNW-trending offset stream with the sinistral sense of movement (red arrowed) observed along the Ban Doo fault segment in Ban Doo area, Amphoe Chiang Klang, Changwat Nan (view looking at 701177E/2134105N to North).....	116
Figure 4.10	Meta-shale on the west flank of Doi Phu Sathan, east of Ban Phaya Kaeo, Amphoe Chiang Klang. Cleavage is dipping to the west.....	117
Figure 4.11	Series of triangular faceted spurs along the Den Phana segment, east of Ban Den Phana. Note that the over steepened base and the development of several erosional benches along the fault, suggesting 4 times of fault movement.....	118
Figure 4.12	Topographic map of Ban Tin Tok area, showing location of the Tin Tok segment. Note that the yellow arrows represent the areas of photograph taken from field investigation in this area.....	120

Figure 4.13	A panoramic view of Phu Kha showing the west dipping triangular facets along fault segment (view looking to east at 701366E/2122205N).	121
Figure 4.14	Triangular facets (A) and facet spurs (B) observed along the Tin Tok fault segment in Tin Tok area, Ban Tin Tok (view looking to NE at 704637E/2117997N).	121
Figure 4.15	A view of wine-glass canyon developed where the Nam Khun crosses the Tin Tok segment, Pua Fault. Note that compare canyon with figure 3.34 (view looking to east at 701366E/2122205N).	122
Figure 4.16	a) Foot of wine-glass canyon (figure 4.15) at Kaeng dam site, Ban Hua Nam, Nan. b) Close-up view at the foot of wine-glass canyon beside the dam showing meta sandstone cut by normal fault set. c) Small air bubbles observed at from water in the Kaeng reservoir (photo taken to southeast at 705966E/2117149N).	122
Figure 4.17	Topographic map of Ban Thung Hao area, showing the location of the Santisuk fault segment, Nan. Note that the yellow arrows represent the areas with distinct morphotectonic features.	123
Figure 4.18	A panoramic view show set of triangular faceted (A) and fault step (B) along the Santisuk fault segment Ban Thung Hao, north of Amphoe Santisuk (view looking at 703459E/2106129N to east).	124
Figure 4.19	A view looking to north at Ban Thung Hao showing a set of triangular facet and linear valley. Note that the Santisuk fault segment is shown by red dashed line (703459E/2106129N).	125
Figure 4.20	Topographic map of Ban Sob Pua area showing the location of the Sob Pua segment. Note that the yellow arrow represents the areas of photograph.	126
Figure 4.21	View looking northeast of the Pua river bank showing the point bar area in the west (left) and the erosional bank in the east (right) at Ban Sob Pua village (looking to east at 692366E/2122073N).	127
Figure 4.22	Prathat Din Whai – The Chedi at Wat Sala, Ban Nawong, Amphoe Pua was built in 1827 and named by the earthquake event on that year (locating at 692366E/ 2122073N).	127
Figure 4.23	Topographic map of Ban Muang Luang area, showing the location of the Nam Tuan segment. Note that the yellow arrow represents the areas with distinct triangular facets (Figure 4.29).	128
Figure 4.24	Triangular facets observed along the Nam Tuan fault segment in Ban Muang Luang valley (view looking to SE at 692193E / 2086241N).	129

Figure 4.25	IKONOS satellite image showing offset streams (os), shutter ridges (sr), offset ridges (or), triangular facets (tr), linear valleys (lv) and beheaded streams (bs) along the Thung Ao fault segment (Figure 3.15) of the Ban Thung Ao village, Amphoe Thung Chang, Nan. Note that the yellow box is the trench location.....	134
Figure 4.26	View of paleoseismic trench section (no.1) on the north wall, Ban Thung Ao village, Nan, showing Quaternary stratigraphy and fault orientation.....	135
Figure 4.27	Trench-log section of the north wall of the Ban Thung Ao Trench showing principal stratigraphy, major fault, and sample location for TL dating.....	136
Figure 4.28	View of paleoseismic trench section (no.1) on the south wall, Ban Thung Ao village, Nan, showing Quaternary stratigraphy and fault orientation.....	137
Figure 4.29	Trench-log section of the south wall of the Ban Thung Ao Trench showing principal stratigraphy, major fault, and sample location for TL dating.....	138
Figure 4.30	Close-up view (box in Figure 4.29) of the south wall, Ban Doo Trench, Nan, showing the west-dipping fault (F1) and location of TL dating sample. Fault (F1) cut into Layer D.....	140
Figure 4.31	IKONOS satellite image showing offset streams (os) and triangular facets (tr) along the Ban Doo fault segment (Figure 3.15) of the Ban Ban Doo village, Amphoe Chiang Klang, Nan. Note that the yellow box is the trench location.....	142
Figure 4.32	View of paleoseismic trench section (no.2) on the south wall, Ban Doo village, Nan, showing Quaternary stratigraphy and fault orientation.....	143
Figure 4.33	Trench-log section of the south wall of the Ban Doo Trench showing principal stratigraphy, major fault, and sample location for TL dating.	144
Figure 4.34	Close-up view of Figure 4.33 showing a fault contact (F1) between units C and B (left) and unit D and A (right). Note that several pebbles of units C and B showing steep dipping along the long axis.....	145
Figure 4.35	IKONOS image covering a small scarp (in Figure 3.15) of the Ban Thung Ao area, Amphoe Thung Chang, Changwat Nan. Note that yellow box is the trench location near road no. 1080. P1 and P = point-bar side, x = chute cut-off. The circle pink shows a boundary of the “Pa Haew” ancient community of Nan area. (Kaokaew, per. Com., 2008).....	147
Figure 4.36	a) Quarry at Ban Wiang Song, b) Trench excavation using tractor, c) decorate trench wall by using small spade, d) show sharp contact of each unit.....	148

Figure 4.37	View of paleoseismic trench section (no.3) on the west wall, Ban Wiang song village, Nan, showing Quaternary stratigraphy and fold. using small spade, d) show sharp contact of each unit.....	149
Figure 4.38	Trench-log section of the west wall of the Ban Wiang Song Trench showing principal stratigraphy, major structure, and sample location for TL dating.....	150
Figure 4.39	Close-up view of Figure 4.33 showing the alignment of pebbles in the forms of folding and steeply dipping features which were affected by fault nearby.....	152
Figure 5.1	A simplified model of lattice structure of an ionic crystal showing three simple types of defect which are negative-ion vacancy on the left, negative ion interstitial at the center, and substitution impurity center on the bottom right (After Aitken, 1985).....	153
Figure 5.2	Thermoluminescence-process diagram showing energy-level related to three processes; (i) irradiation process, caused by crystal exposed to nuclear radiation, ionized electrons are trapped at hole (T); (ii) Storage stage in which electrons have been trapped, need hole deep enough for electrons (E) during geological time period of sample; and (iii) Heating process, at optimum level of temperature, electrons are released and re-combined at luminescence center (L), and then light (TL) is released (After Aitken, 1985).....	155
Figure 5.3	Diagram of thermoluminescence instrument (After Aitken, 1985).....	157
Figure 5.4	A glow curve graph shows relationship between TL intensity versus temperature.....	157
Figure 5.5	Simplified flow chart illustrating laboratory analysis used in this research study. The red dash line is the annual dose procedure and the blue dash line is the equivalent dose procedure (Modified from Takashima and Honda, 1989).....	161
Figure 5.6	Graph showing relationship between TL ratio (artificial glow curves/natural glow curves) versus temperature (C). N is natural signal, H is heated sample at 320oC for 5 hours, and γ is known dosage that irradiated sample.....	162
Figure 5.7	Schematic charts of regeneration technique (Takashima et. al., 1989). Note that several portions are used for measurement of the TL intensity; N is natural sample; I_o is residual intensity from sample; H is 350oC heated sample; and γ is known dosage that irradiated sample.....	162

Figure 5.8	Plateau curve (solid line) is the ratio of the two glow-curves; N is represented the “natural” glow-curve and N+1,200 Gy is the “natural + artificial” glow-curve.....	164
Figure 5.9	Thermoluminescence remaining after bleaching by exposes to sunlight for various time (Aitken, 1985).....	164
Figure 5.10	Summary of neutron activation analysis (NAA) procedures with sample preparation and annual dose determination.....	165
Figure 5.11	Trench-log stratigraphy showing fault orientation (F1), lithostratigraphy, and TL ages of sedimentary layer, on north wall, Ban Thung Ao trench.....	169
Figure 5.12	Trench-log stratigraphy showing fault orientation, lithostratigraphy, and TL ages of sedimentary layer on south wall, Ban Thung Ao trench. ...	170
Figure 5.13	Evolution of faulting associated with sediment deposition in Ban Thung Ao trench from 5,000 year to present.....	172
Figure 5.14	Trench-log stratigraphy showing fault orientation, lithostratigraphy and TL ages of sedimentary layer, Ban Doo trench.....	173
Figure 5.15	Evolution of faulting associated with sediment deposition in Ban Doo trench from 6,200 year to present.....	174
Figure 5.16	Trench-log stratigraphy showing fault orientation and TL ages of sedimentary layer, Ban Doo trench.....	176
Figure 5.17	Evolution of faulting associated with sediment deposition in Ban Wiang Song trench from 110,000 year to present.....	177
Figure 6.1	Map of Nan and adjacent areas showing epicentral distribution from 1983 to 2008 (Data from Nutalaya et al., 1985; Thai Meteorological Department, 2004; and http://neic.usgs.gov/neis/epic/epic_global.html , 2008). Note that many epicenters are located in the basins, a few in the hard-rock terrain.....	180
Figure 6.2	Map showing active fault segments, their length and estimated maximum credible earthquakes or paloemagnitudes of the Pua Fault Zone.....	182
Figure 6.3	Graph showing relationship between surface rupture length and moment magnitude of the data from Pua Fault in comparison with those of the world data of Well and Coppersmith (1994).....	185
Figure 6.4	Trench log section at the south wall of Ban Thung Ao trench, Nan showing principal stratigraphy and TL ages of each sediment layer.....	185

Figure 6.5	Trench log section at the south wall of Ban Doo trench showing principal stratigraphy and TL ages of each sediment layer.....	186
Figure 6.6	Trench log section at the south wall of Ban Doo trench showing principal stratigraphy and TL ages of each sediment layer.....	186
Figure 6.7a	Map of Thailand showing major tectonic units, 1 = Shan-Thai plate 2 = Lampang-Chiang Rai plate, 3 = and Nakhon Thai plate, 4 = Indochina plate. Note that the Nan-Pua study area (black frame) is located nearby the Nan-Uttaradit suture zone (after Charusiri et al., 2002).....	188
Figure 6.7b	Plate tectonic model in Late Tertiary showing the major plate interaction, major structures, and Cenozoic tectonism (modified after Charusiri et al., 2002).....	188
Figure 6.8a	A model for the development of the Nan-Pua basins and associated structures by strike-slip tectonics (modified after Christie-Blick and Biddle, 1985 and Sylvester, 1988).....	189
Figure 6.8b	Present-day structure relationship between strike-slip faults, and the Cenozoic basins. SWF: Salween fault, NMF: Nam Ma Fault, MCF: Mae Chan fault, CKF: Chiang Khong fault, WHF: Wiang Haeng fault, PYF: Phayao fault, NGF: Ngao fault, LIF Li fault, MMF: Mae Moh fault, TNF: Thoen fault, UDFZ: Uttaradit fault zone, MPFZ: Mae Ping fault zone (after Uttamo et al., 2003).....	190
Figure 6.9a	Schematic diagram showing evolution of Nan-Pua basin during the Cenozoic time.....	193
Figure 6.9b	Schematic diagram showing evolution of Nan-Pua basin during the Cenozoic time.....	194
Figure 6.10	The 3D model of ASTER image showing sharp morphotectonic of Pua basin, particularly on the eastern flank of the basin which indicated an active tectonic of this area.....	195
Figure 6.11	Simplify map of Pua Fault zone showing faults are never generated earthquake (thick red lines). Note that the epicentral distribution from 1983 to 2008 (Data from Nutalaya et al., 1985; Thai Meteorological Department, 2002; and http://neic.usgs.gov/neis/epic/epic_global.html , 2008).....	196

LIST OF TABLES

	PAGE
Table 2.1 Active fault rank, criteria, and examples in Thailand (after Charusiri et al., 2001).	50
Table 2.2 Activity of faults in Thailand based upon age-dating data (after Charusiri et al., 2001).	51
Table 3.1 Types of fault segments and criteria used for active fault in this study mainly following McCalpin (1996).	76
Table 3.2 Comparison between the Pua Faults from this study and the important active faults as compiled by McCalpin (1996).	77
Table 4.1 Rating criteria and priority for selection of detailed investigation area for exploration trenching (Saithong, 2006).	131
Table 4.2 Rating of the selected areas suitable for the detailed field investigation.	132
Table 5.1 TL dating results of quartz concentrates sediments for sample collected from the study area in Nan, northern Thailand.	167
Table 5.2 Estimated timing of paleoearthquakes in the Pua-Nan area before present.	178

CHAPTER I

INTRODUCTION

1.1 Background

Earthquake is a natural phenomenon which is unable to control and unpredictable when it will be occurring. As known, earthquakes can cause large damages in many parts of the world including Thailand (Figure 1.1). Previously, annals and stone inscriptions indicate that land shaking or large earthquakes have been recorded many times in many parts of Thailand, particularly northern and western parts resulting in damaging for these regions. According to the annals, lands shaking of large earthquakes, including man-made structural damages, have been reported in Nan and Chiang Mai cities (Charisiri et al., 2000). Recently, earthquakes can be recorded throughout Thailand especially in the northern part by using seismographs. There are many records of earthquakes having the magnitude greater than M_L 5 (Richter scale) particularly in the Nan and adjacent areas. On 22 December 1925 and 12 February 1934, earthquakes with magnitude greater than M_L 6 have also been recorded northwest of Nan city in Lao P.D.R. and Amphoe Thung Chang, Changwat Nan, respectively. In addition, on 9 December 1995, a M_L 5.1 (Bott et al., 1997) earthquake occurred at Amphoe Rong Kwang southwest of Nan city. As mentioned above, both historical and instrumental records reveal that these regions have been suffered with the frequent earthquakes and have a tendency for future earthquakes. Accordingly, the imperative study of earthquakes is needed rapidly and incessantly in order to reduce impacts caused by hazardous earthquakes.

Fenton et al. (1997 and 2003) investigated Pua Fault located on the eastern flank of Pua basin, Changwat Nan. They observed neotectonic evidence, such as triangular facets, wine-glass canyons and offset streams along the fault line. This observation indicates that Pua Fault is still active and has a tendency to generate large earthquakes. However, the study lacks of detailed study in age dating, thus the precise age of the last displacement of this fault cannot be defined. Subsequently, Charusiri et al. (2001) studied and collected data of potentially active faults that can generate large earthquakes in northern Thailand. As a result, there are many active faults and potentially active faults in the study area including Pua Fault (Figure 1.2).

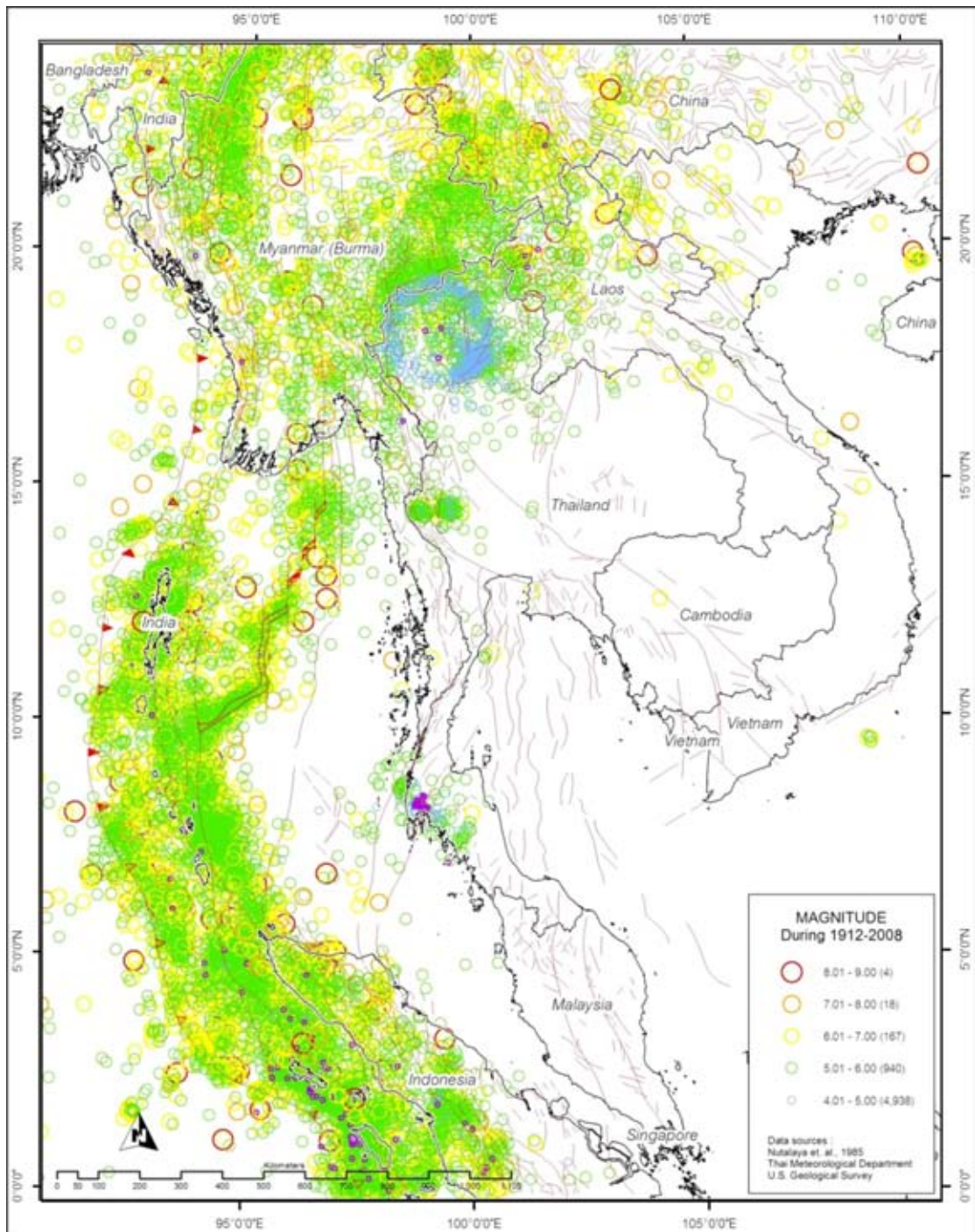


Figure 1.1 Historical seismicity of Thailand and surrounding countries (Thai Meteorological Department, 2008). Note that lineaments and major structures are shown and the study region is shown in the red box.

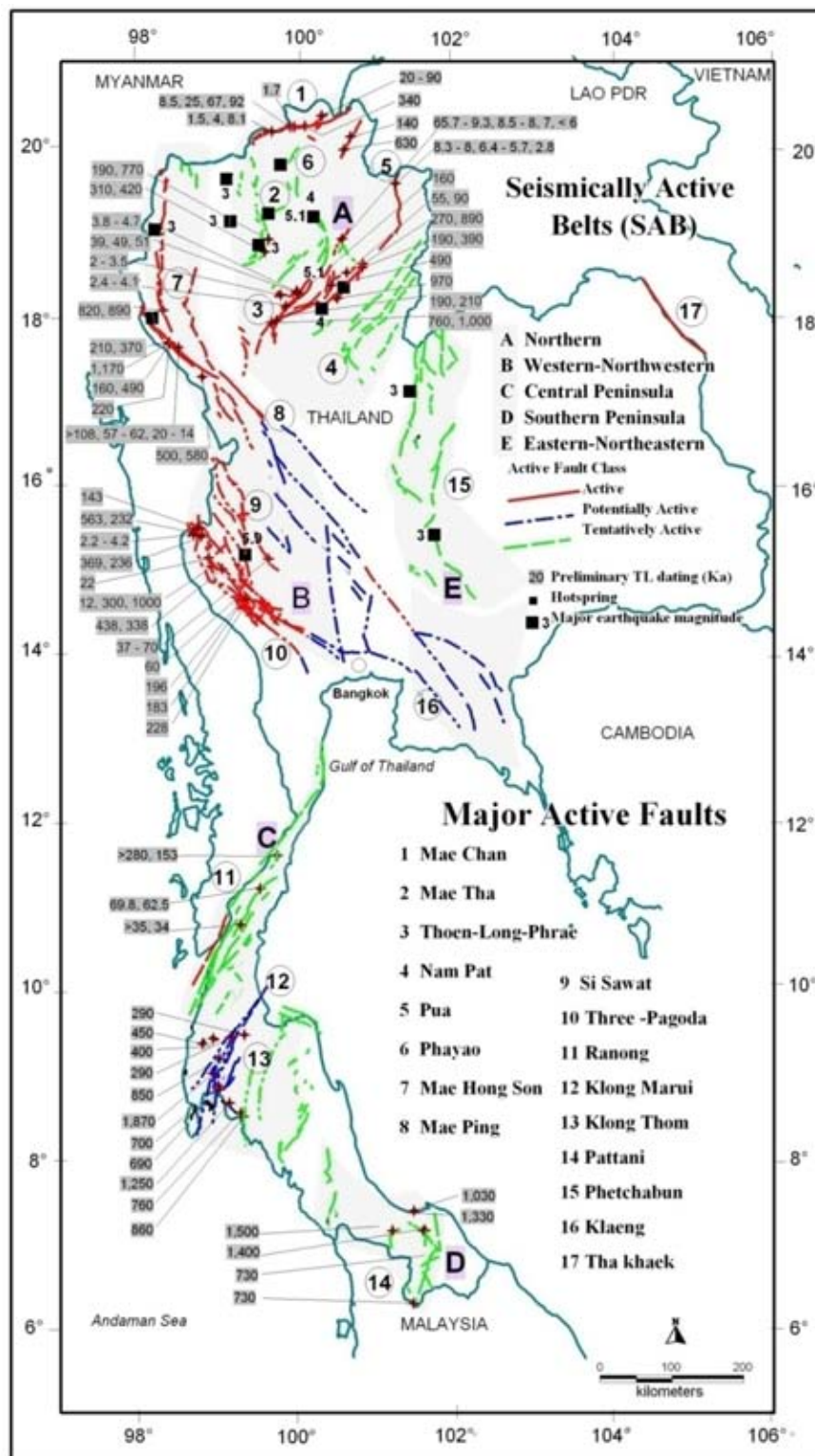


Figure 1.2 Major active faults in Thailand showing preliminary TL dating results on earthquake events, locations of hot spring and epicenter distribution (after Charusiri et al., 2001).

Therefore the study of Pua Fault and its vicinity in detail is confined to fault orientations and possibilities of large earthquakes in the near future. Chulalongkorn University granting expenditures for this thesis has a future plan to construct a new learning center (campus) at Changwat Nan where preliminary evaluation of earthquake risks are mentioned which the result of this study will be collected as database to help for the design of building or large construction.

1.2 Objective

The main purpose of this thesis is to study neotectonic evidences along Pua Fault in Changwat Nan, northern Thailand. The main knowledge and techniques used for neotectonic investigations in this study include remote-sensing interpretation and TL-dating. Results of thesis are to fulfill the following goals.

1. Morphotectonic study as a result of fault movement;
2. Delineation of active faults in the Pua fault zone;
3. Age determination of the Pua fault movement; and
4. Estimation of paleoearthquake magnitudes and slip-rates of these fault movements.

1.3 Study Area

The study area is separated into 2 aspects; i.e. regional- and small- scale studies. Firstly, in the regional-scale investigation remote-sensing interpretation covers the western part of northern Thailand and some parts of Lao P.D.R (Figure 1.3). The area under investigation lies within the latitudes 17° 15' N to 19° 45' N and longitudes 99° 30' E to 102° 00' E. Secondly, for the small-scale investigation, field investigation covers Nan and Pua basins, Changwat Nan (Figure 1.4). The total study area is about 10,500 km², and the study area is approximately 560 km north of Bangkok, the capital city of Thailand.

1.4 Methodology

The methodology of the study is divided into 6 steps, viz, planning and preparation of significant data, field reconnaissance, remote-sensing interpretation, field investigation, laboratory analysis and analyses of the results. A flow chart depicting the general procedure for this research study is shown in Figure 1.5.



Figure 1.3 Map of northern and north-western Thailand and eastern Myanmar showing the location of the study area (black square) in the Nan Province (Department of Highways, 2007).

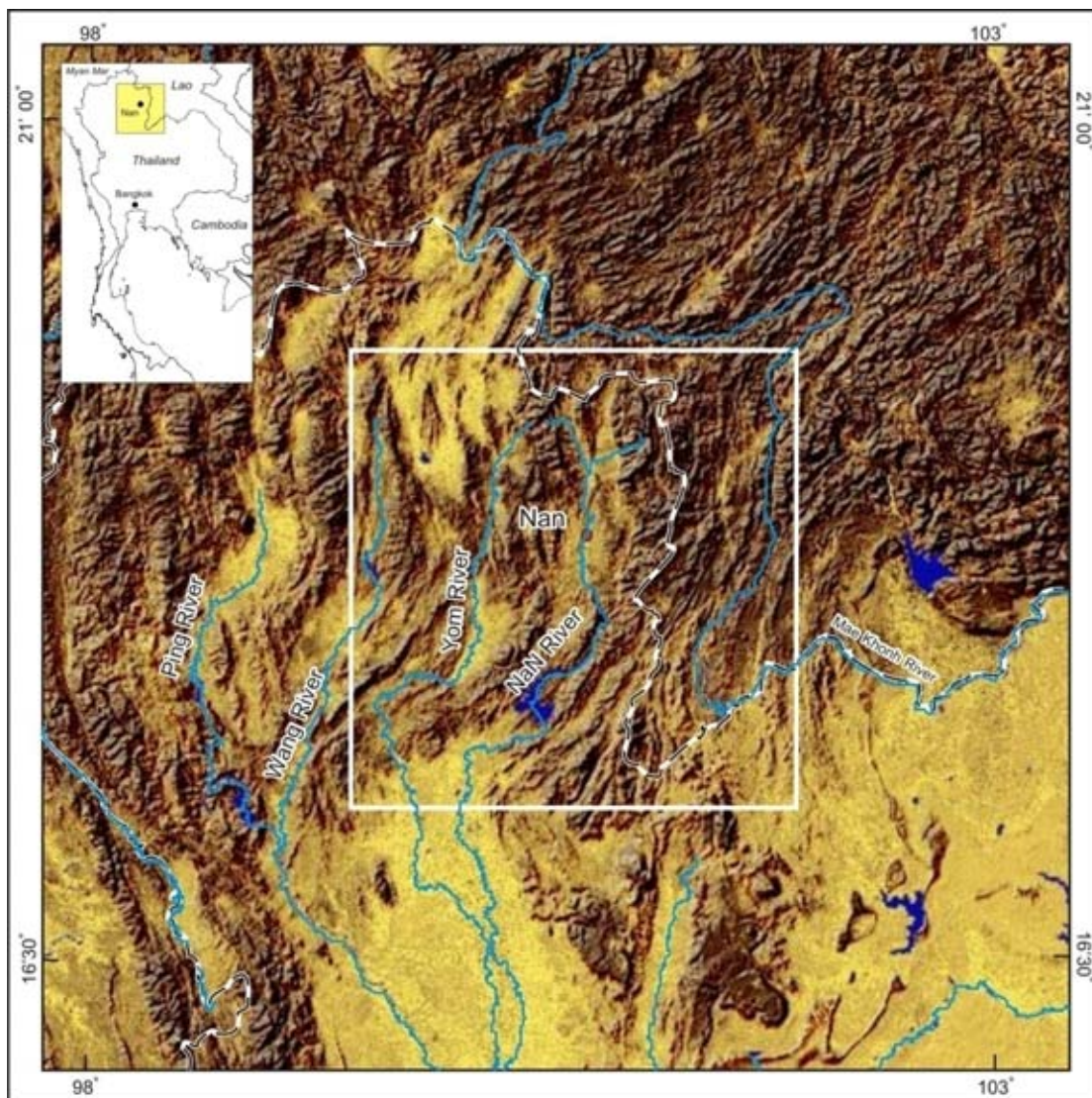


Figure 1.4 Topological map of the study (white square) showing the mountain ranges (brown) Cenozoic basins and plains (yellow) and major streams and oriented in the north-south direction. Note that the regional structure extends northward to Myanmar and Laos.

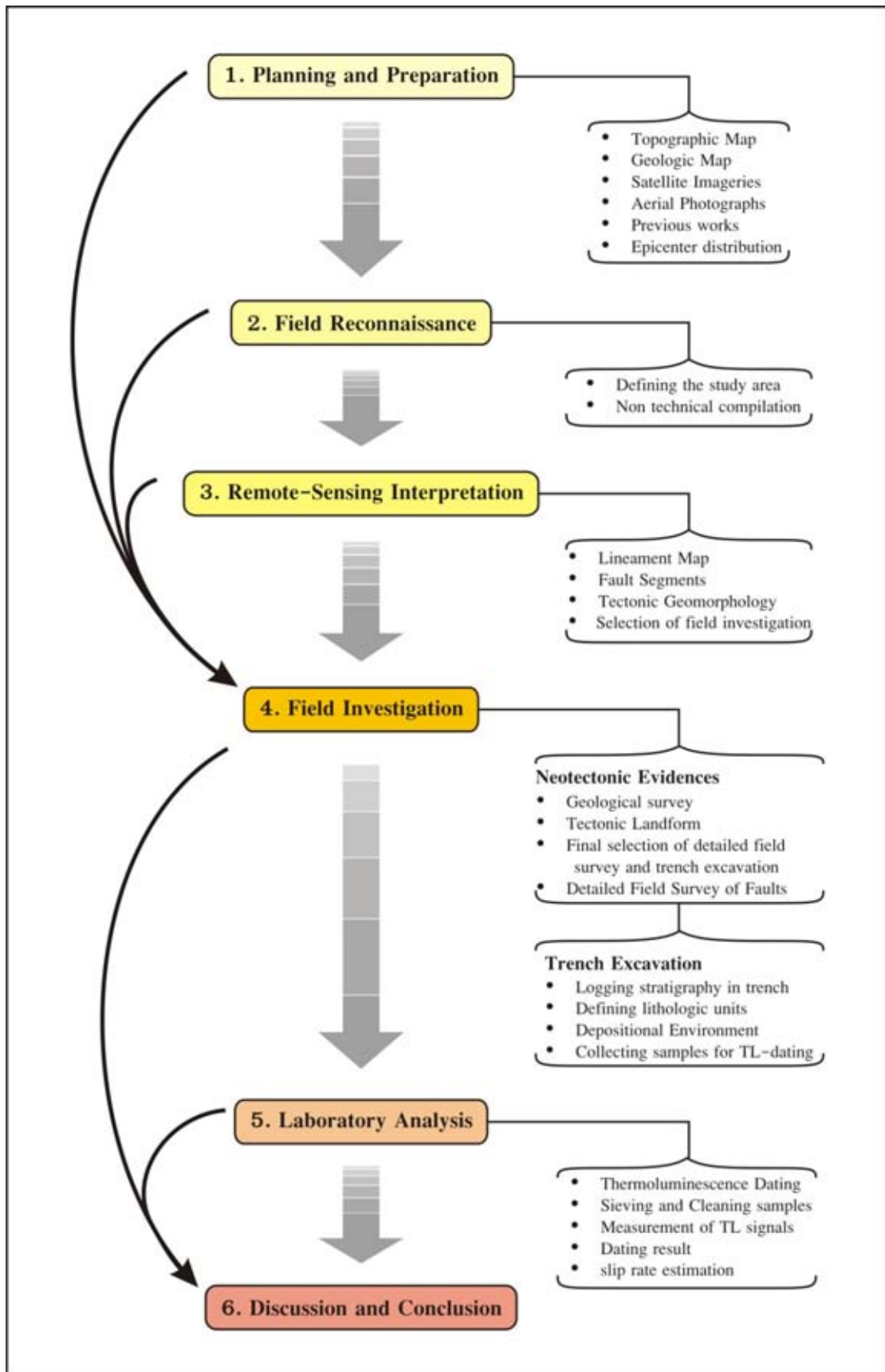


Figure 1.5 Simplified flow chart illustrating investigation procedures for the research study.

1.4.1 Planning and preparation

The first stage concerns with data collection in order to contribute preliminarily available data about the regional study area and to arrange and rearrange relevant data for subsequent steps. This includes literature surveys for previous work, finding base maps (topographic and geological maps), earthquake epicenters, and acquiring the satellite images and aerial photographs, collecting historical earthquake events, and the other related technical and nontechnical documents.

1.4.2 Field reconnaissance

Field reconnaissance is the second step of the main task in this thesis. It was launched to construct valuable guidelines for detailed investigations. This stage includes investigating route condition, approach to the areas and looking for residents for labor workers.

1.4.3 Remote-sensing interpretation

The third stage of this study deals with remote-sensing interpretation. Commencement of the stage is to study the small scale with satellite imagery to large scale with aerial photograph and IKONOS imagery. Basic data for the interpretation is enhanced Landsat 7 ETM⁺, SRTM DEM and ASTER satellite images for lineaments, their attitudes and orientations, and Cenozoic basins in the study area. Segmentation of fault is performed in this step for more detailed investigation, including defining individual characteristics of fault segments using photographs and IKONOS images. When the fault segments are already defined, progressing to detailed interpretation using the geomorphic evidence and structural geology that can help to indicate neotectonic and active areas for field investigation.

1.4.4 Field investigation

This stage starts with compilation of all collecting data and the interpretation of remote-sensing imagery for interesting and selected areas. These areas are on subsequent detailed geomorphic mapping related to the neotectonic evidence, as landform produced by fault movement and shifting of young sediment layers in trench. These evidences aid in evaluating location and nature of active faults and identifying sequences of fault movements in the interesting areas. Geological data are collected along fault segments for identifying characteristics of faults.

1.4.5 Laboratory analysis

Laboratory analysis is the fifth stage with the main purpose of collecting samples for dating by Thermoluminescence (TL) method. The dating method follows that of Takashima and Watanabe (1994), commencing at collecting geological material samples related to active faults, treatment of quartz-enriched samples for dating, and measuring both equivalent and annual dose of quartz concentrates.

1.4.6 Discussions and Conclusion

This stage includes integration of all results, including synthesizing, the previous works with the author's geomorphic evidence related to active faults along with the result of TL dating. Focus is made on estimating paleoearthquake magnitude from surface rupture length, identifying slip rates, and finally identification of active faults.

1.5 Previous study of active faults in Thailand

To date, no detailed investigations have been done relating to the precise age of the last movement of the Pua Fault. However, a few researches have been reported, more or less concerned with structural geology and tectonic geomorphology of the Nan and adjacent areas.

Nutalaya et al. (1985) studied the seismology of Thailand and structure framework of the Chao Phaya Basin and seismotectonic source zones are subsequently delineated. The seismic source zones in mainland Southeast Asia can be separated into twelve zones. They are located in Thailand within zones F and G on the west and the north, respectively (Figure 1.6). The Pua Fault is situated in the zone G (Northern Thailand) and characterized by complex fault zones with normal movements.

Siribhakdi (1986) studied seismogenic in Thailand and periphery and reported earthquakes in Thailand throughout her past 1,500 years history. Many of the earthquakes found have closed relation with four major faults including the Three Pagoda, the Si Sawat, the Moei-Uthai-Thani, and the Mae Hong Son-Mae Sariang Faults. He mentioned that the earthquakes in Thailand are associated with tectonism,

interpreted to be related to subduction and spreading ridge in the Andaman Sea. Pua Fault was not reported in his study.

Hinthong (1991) investigated the role of tectonic setting in earthquake events in Thailand. He reported that earthquakes in Thailand are closely related to two seismic source zones, Zone F of the Tenasserim Range and Zone G of the Northern Thailand (Natalaya et al., 1985). The faults within zone F are interpreted to be more active than those of zone G where the Pua Fault is located and inferred to be possibly potentially active faults.

Charusiri et al. (1996) applied the several remote sensing techniques to study geological structures related to earthquakes in Thailand and neighboring countries. The results are useful in determining the seismic source zones to indicate the earthquake-prone areas and purposed a new seismotectonic (or seismic-source) map.

Hinthong (1997) studied the project entitled “Study of Active Faults in Thailand”. According to various authors, three approaches to define active faults can be distinguished and applied, as general definition, engineering definition, and regulatory definition. Those three applications of definitions were discussed, based primarily on its original definition which was proposed in the context of a two-fold classification of dead and alive or active faults, and with respect to their potential for recurrence of displacement or offset. Based upon available data, and with the exclusion of the tentatively inactive and inactive classification, fault activity can be classified as three classes namely, active, potentially active, and tentatively active. Basically, there are three major criteria for recognition of active faults viz, geologic, historic, and seismologic criteria (Figure 1.7).

Bott et al. (1997) studied seismicity related to neotectonic and mentioned northern Thailand is similar to the Basin and Range province of Western United States of America in terms of earthquake processes and tectonics. Lastly, Fenton et al. (2003) reported the existence of Pua Fault for the first time. They indicated Cenozoic faults and historical seismicity within the northern Basin and Range seismotectonic province of Thailand as illustrated in Figure 2.8. Based on tectonic geomorphology, Pua Fault is defined to be an active fault.

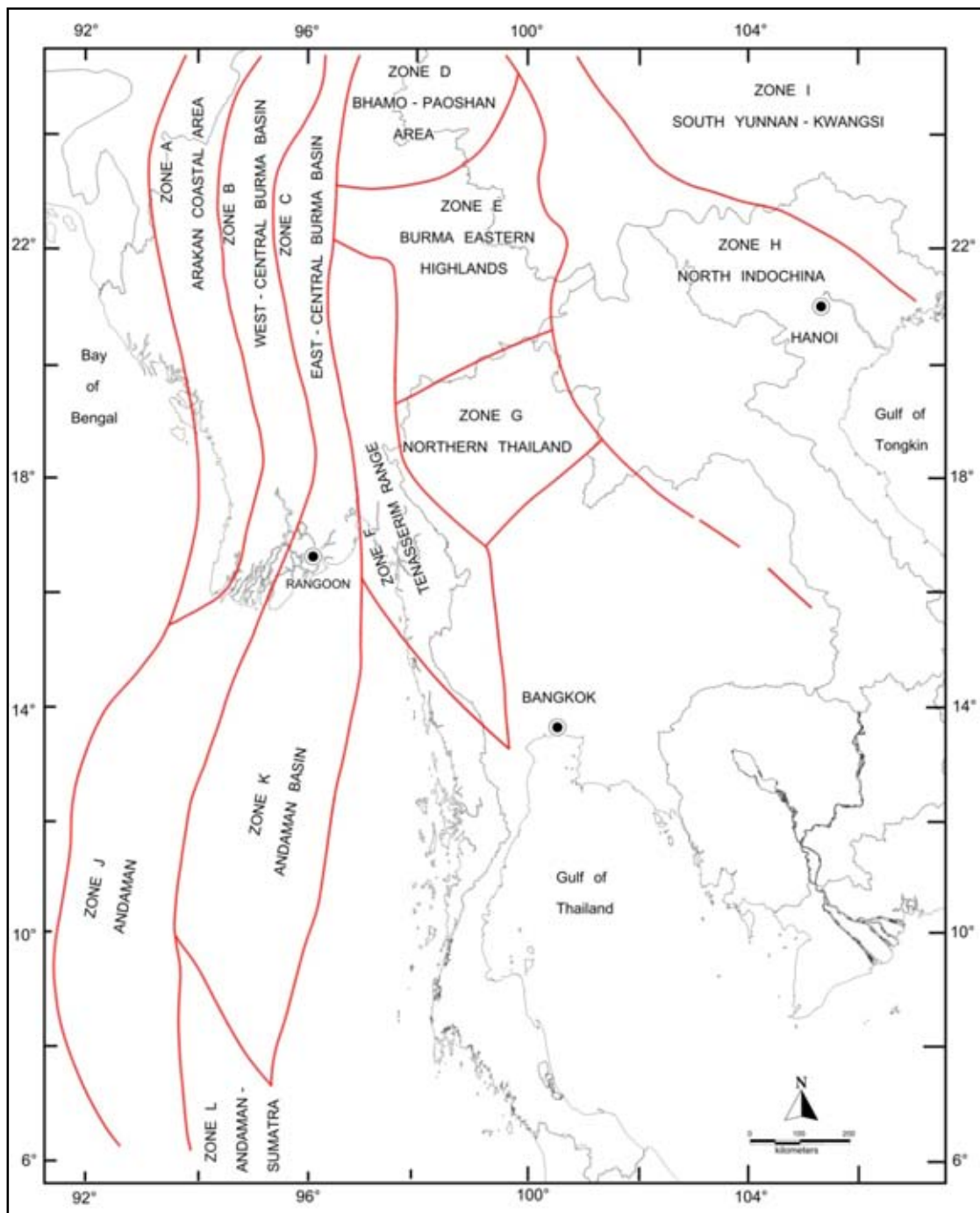


Figure 1.6 Seismic source zones of Burma, Thailand and Indochina (modified after Nutalaya et al., 1985). Noted that seismic source zones were recognized only in the northern and western parts of Thailand.

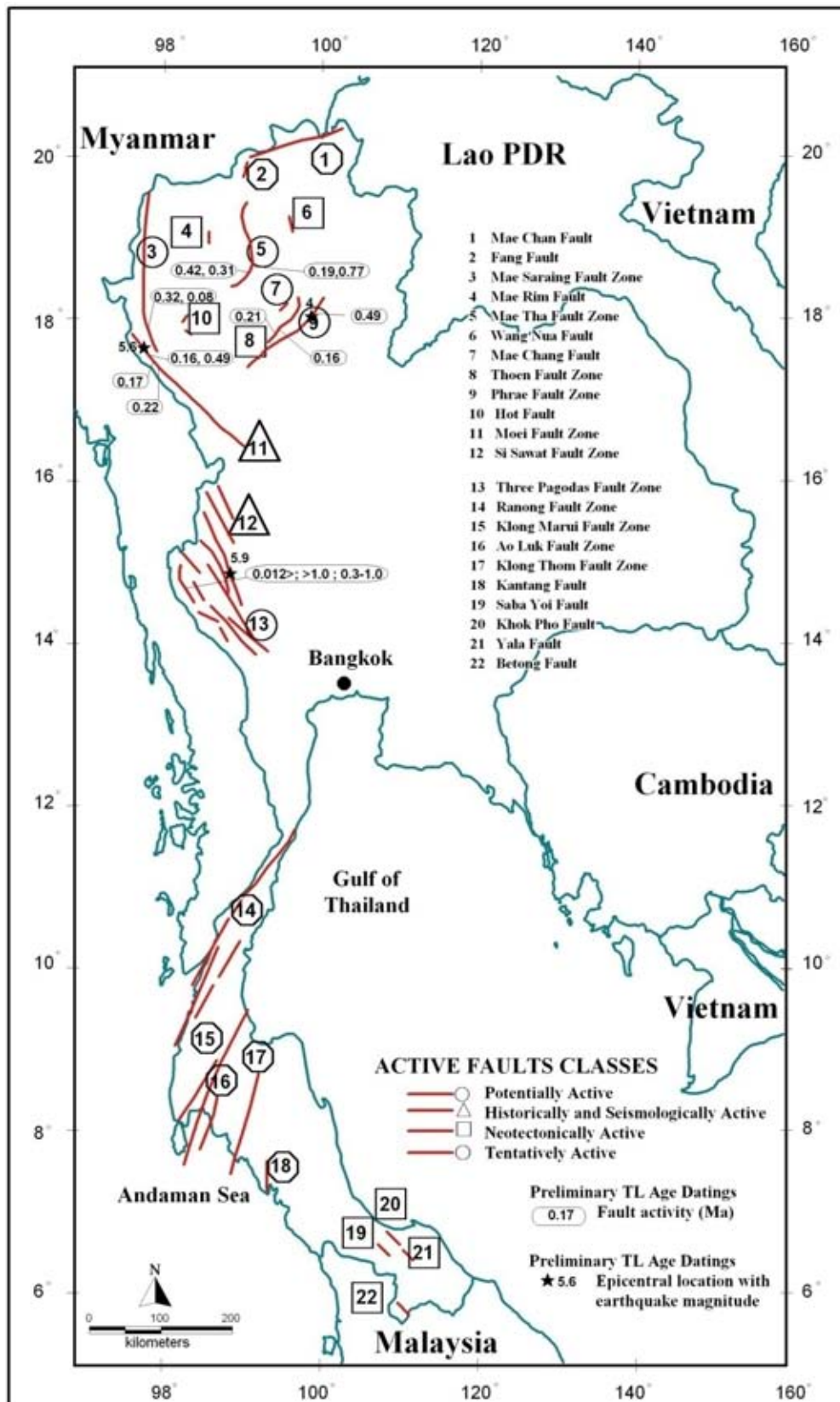


Figure 1.7 Map showing active and suspected active faults in Thailand (modified after Hinthong, 1997). Note that the Pua Fault was not reported in the map.

Tulyatid (1997) used airborne geophysical data to interpret extensional tectonism in the Central Thailand based on geological structures and Cenozoic basins. The magnetic data is useful to delineate a new fault pattern (for the Chao Phraya Fault Zone) and a new fault path for the Three Pagoda Fault Zone. The data also outline the Uttaradit Fault Zone (UTFZ) by showing a shift of high magnetic bodies, indicating sinistral movement along the fault zone (Figures 1.8).

Hongjaisee (1999) investigated the major faults and seismic hazard in northern Thailand. Based on tectonic morphology of faults, such as stream offsets, triangular facets, and canyon shapes, the high slip rates of the Mae Chan and Wang Nua faults are 0.1-3.7 and 0.8-3.5 mm/yr, respectively. The Thoen and Phrae faults have the low slip rates, in the range of about 0.01-0.1 mm/yr.

Kosuwan et al. (1999) applied remote-sensing, field investigation, dating data to evaluate paleoseismology of the Mae Chan Fault in the northern most part of Thailand. Based on dating result, fault movements gave rise to earthquake of about 92,000, 67,000, 48,000, 25,000 and 1,600 years in age. The 1,600 years ago event probably caused a characteristic earthquake with a magnitude greater than 7 Richter's scale (Figures 1.9).

Won-In (1999) used remote-sensing and ground-truth surveys to study neotectonic evidences along the Three Pagodas fault zones in Kanchanaburi, western Thailand. Based on geological and geomorphological analyses, the Three Pagodas fault can be separated into five segments with right lateral movements. Five events of earthquake faulting were reported based on geological evidence and dating results (Figure 1.10).

Charusiri et al. (2001) classified active faults in Thailand into five seismically active belts (SAB) by using geologic, geotectonic, geochronological, and seismological criteria. These belts can be classified into Northern, Western-Northwestern, Central Peninsula, Southern Peninsula and Eastern-Northeastern SABs. The study area is inferred in the Northern seismically active belt and hence Pua Fault is active based upon their study (see Figure 1.2).

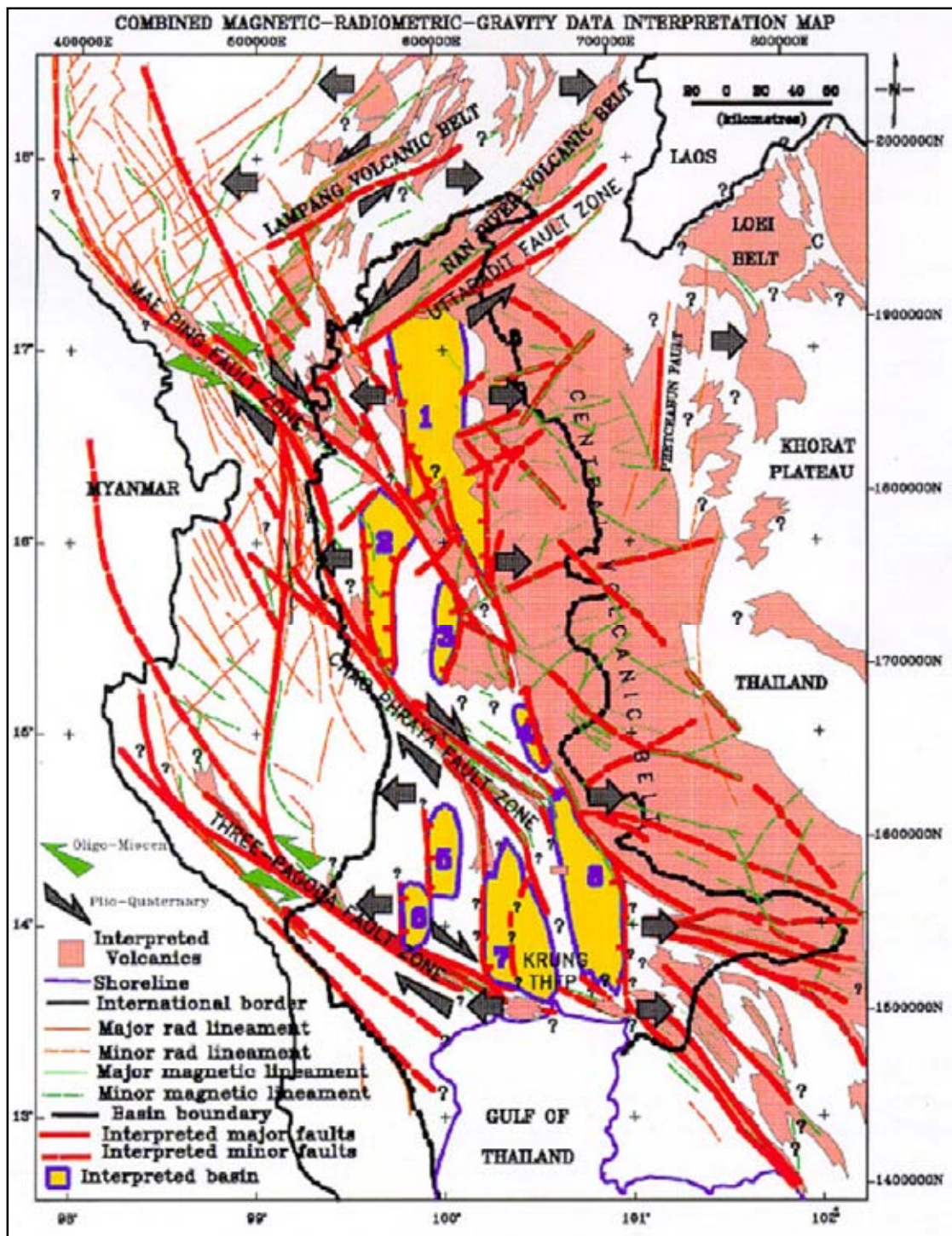


Figure 1.8 Combined magnetic- radiometric - gravity data interpretation showing structural map of Central Plain with magnetic and radiometric lineaments underlain. Note that 1 = Phitsanulok Basin, 2 = Nong Bua Basin, 3 = Nakhon Sawan Basin, 4 = Lop Buri Basin, 5 = Supanburi Basin, 6 = Kamphaeng Saen Basin, 7 = Thon Buri Basin, 8 = Ayuthaya Basin (after Tulyatid and Charusiri, 1999).

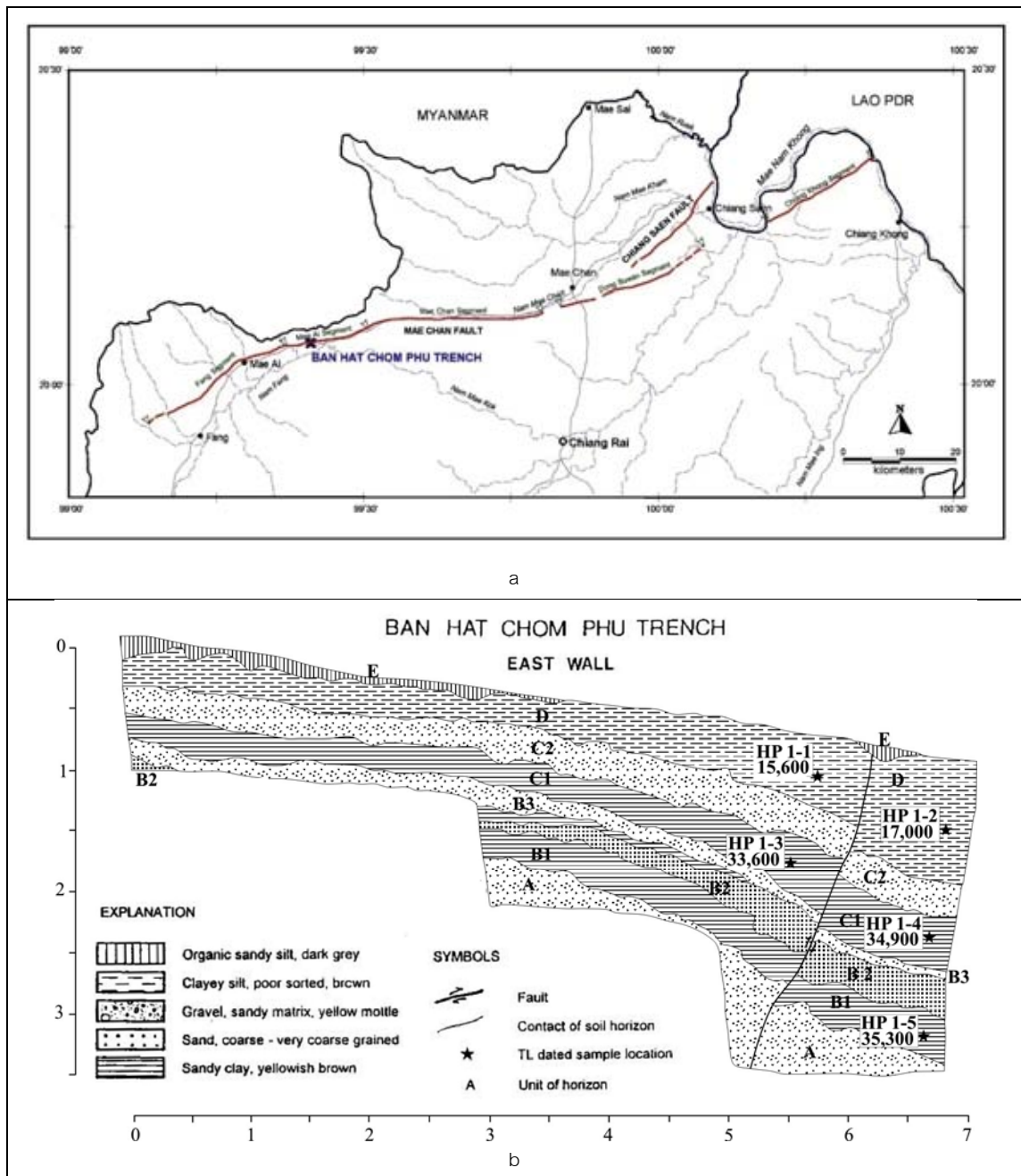


Figure 1.9 a) Location of Ban Hat Chom Phu trench site, in the southern part of Mae Ai segment of Mae Chan Fault, Chiang Mai, Northern Thailand. b) Trench stratigraphy of the east wall side of the Ban Hat Chom Phu trench showing reverse fault movement and locations of samples for TL dating and their dates (Kosuwat et al., 1999).

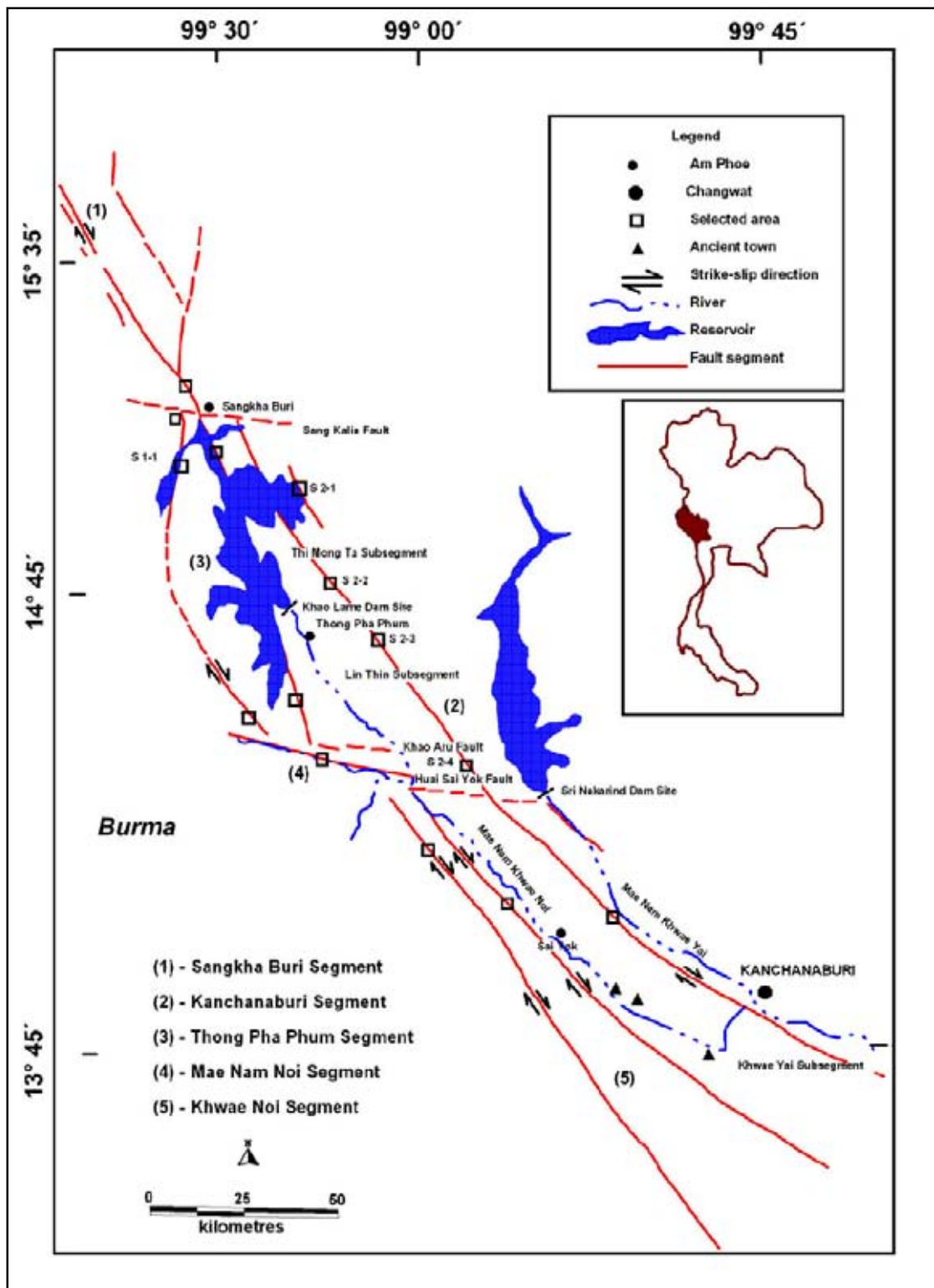


Figure 1.10 Map of the Three Pagodas Fault showing the fault segments (after Won-In, 1999).

Rhodes et al. (2002) studied kinematics of the Mae Kuang Fault and evidences from satellite images and aerial photographs. They suggested that the Mae Kuang fault accommodates the transfer of extension between Chiang Mai basin and Wiang Pa Pao basin which is sinistral offset between 400 and 700 m and the slip rate must be between 0.175 and 0.7 mm/yr (Figures 1.11).

Udchachon (2002) and Udchachon et al. (2005) investigated the neotectonics of the Phrae basin with integration of data from remote-sensing interpretation, field investigation, seismic profiles, and focal mechanism data. He estimated that the southeastern segment of the Phrae fault system is a potentially active fault with maximum slip-rate of 0.06 mm/yr. This evidence is consistent with the study on contemporary stress axis orientation in this area which reveals a roughly east-west trend and north-south trend of extensional and compressional axes, respectively (Figure 1.12).

Fenton et al. (2003) conducted the investigation of recent paleoseismic and identified a number of active faults in Northern and Western Thailand. Mae Chan fault and the Three Pagodas fault zones are determined as strike-slip faults, with slip-rates 0.1-0.3 mm/yr and damage earthquake of $M=7.5$. In the northern part of Thailand, six major faults show sense of movements as slip-rates between 0.5-2.0 mm/yr in normal-oblique fault, and damage earthquake about $M=7.0$ on the Richter scale. The Pua Fault is the one of six major faults in Northern Thailand with the slip-rate of 0.6 mm/yr and a maximum credible damage earthquake of $M=7.25$ (Figure 1.13).

Charusiri et al. (2006a) studied paleoearthquake along Mae Yom Fault Zone by the evidences of remote-sensing interpretation, field investigation, and GRP profiles. The appearances of sharp lineaments are well observed and they indicate the oblique-left-lateral sense of movement. The slip-rate of fault movement is 0.14-0.8 mm/yr and paleoearthquake magnitude using surface rupture length is 6.3-6.7 M_w (Figure 1.14).

Recently Charusiri et al. (2006b) investigated active faults at Hutgyi dam site project, Salawin River, Myanmar using remote sensing and geological survey, geochronological and related laboratory analyses. Four major faults are recognized including 1) Yinbaing Fault in the southernmost part, 2) Meseik Fault in

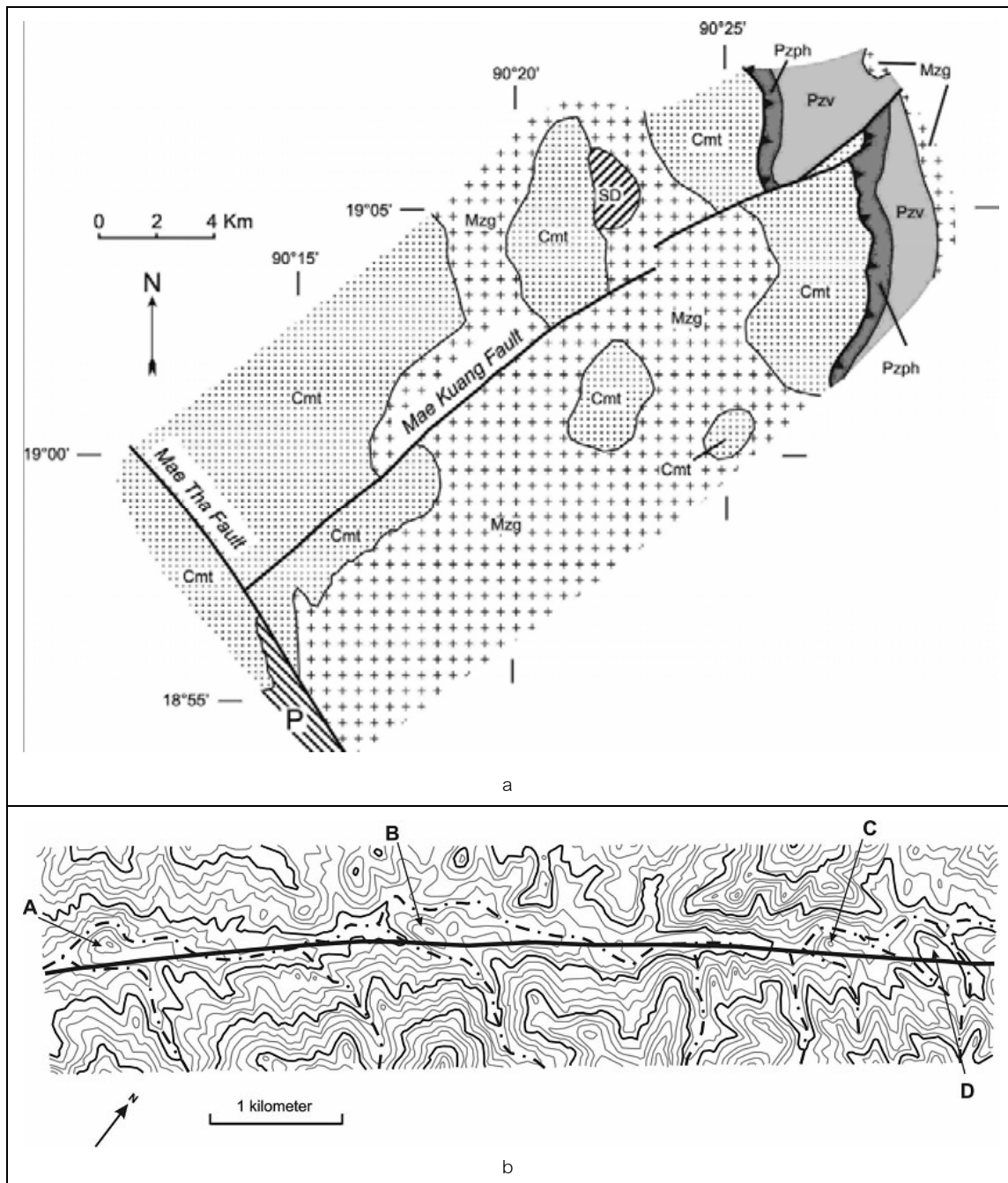


Figure 1.11 a) Geologic map along the trace of the Mae Kuang fault. P, undifferentiated Permian rocks; Cmt, Mae Tha Formation; SD, Silurian and Devonian Rocks; Pzph, Paleozoic phyllite; Pzv, Paleozoic metabasalt; Mzg, granitic rocks of the Fang-Mae Suai batholiths. B) Topographic map of a portion of the Mae Kuang Valley, showing the mapped trace of the Mae Kuang Fault. A, B, and C point to shutter ridges that have diverted northwest-flowing tributaries (after Rhodes et al., 2002).

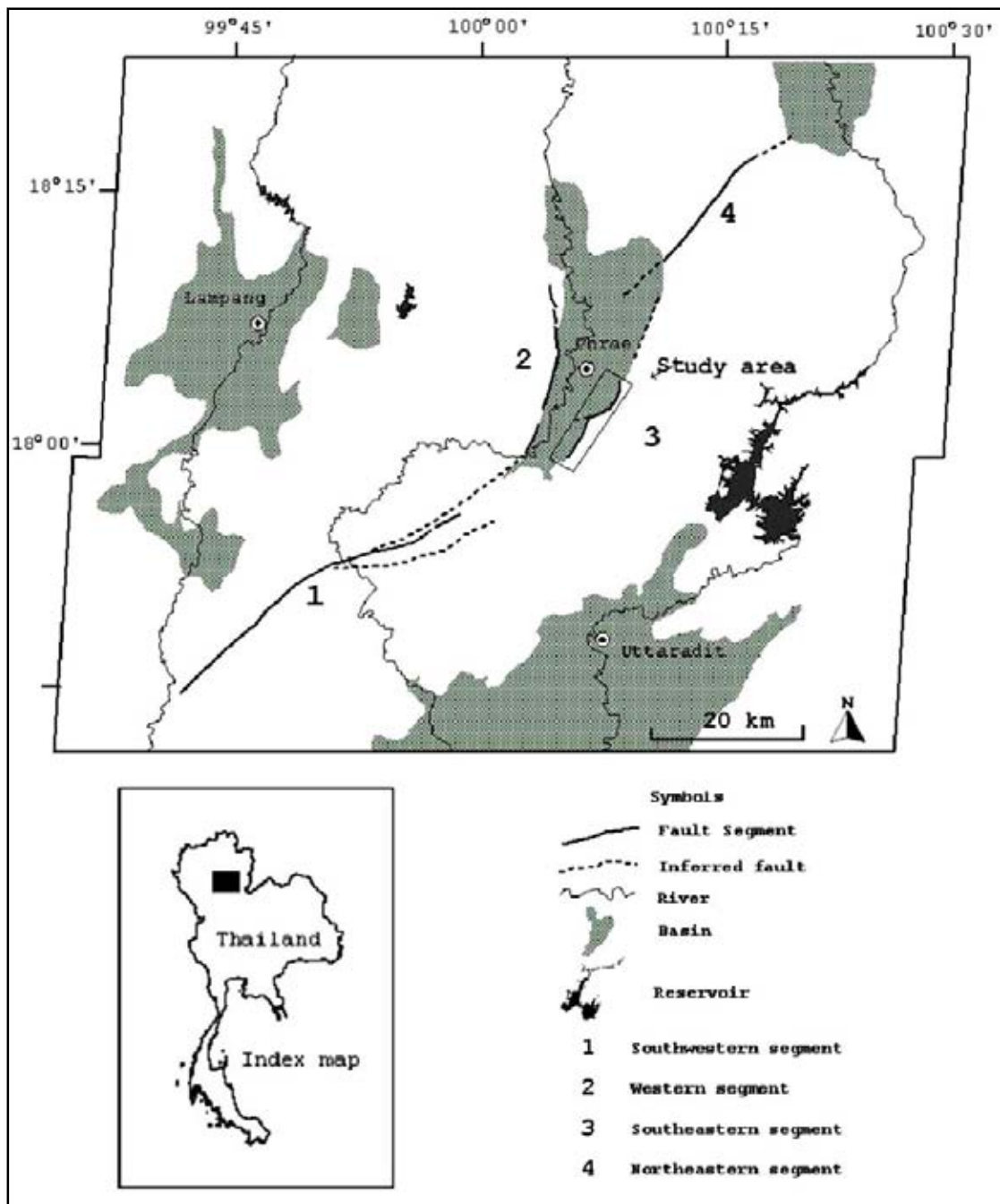


Figure 1.12 Fault segments of the Phrae fault system northern Thailand, interpreted using Landsat 5 TM image data (after Udchachon et al., 2005).

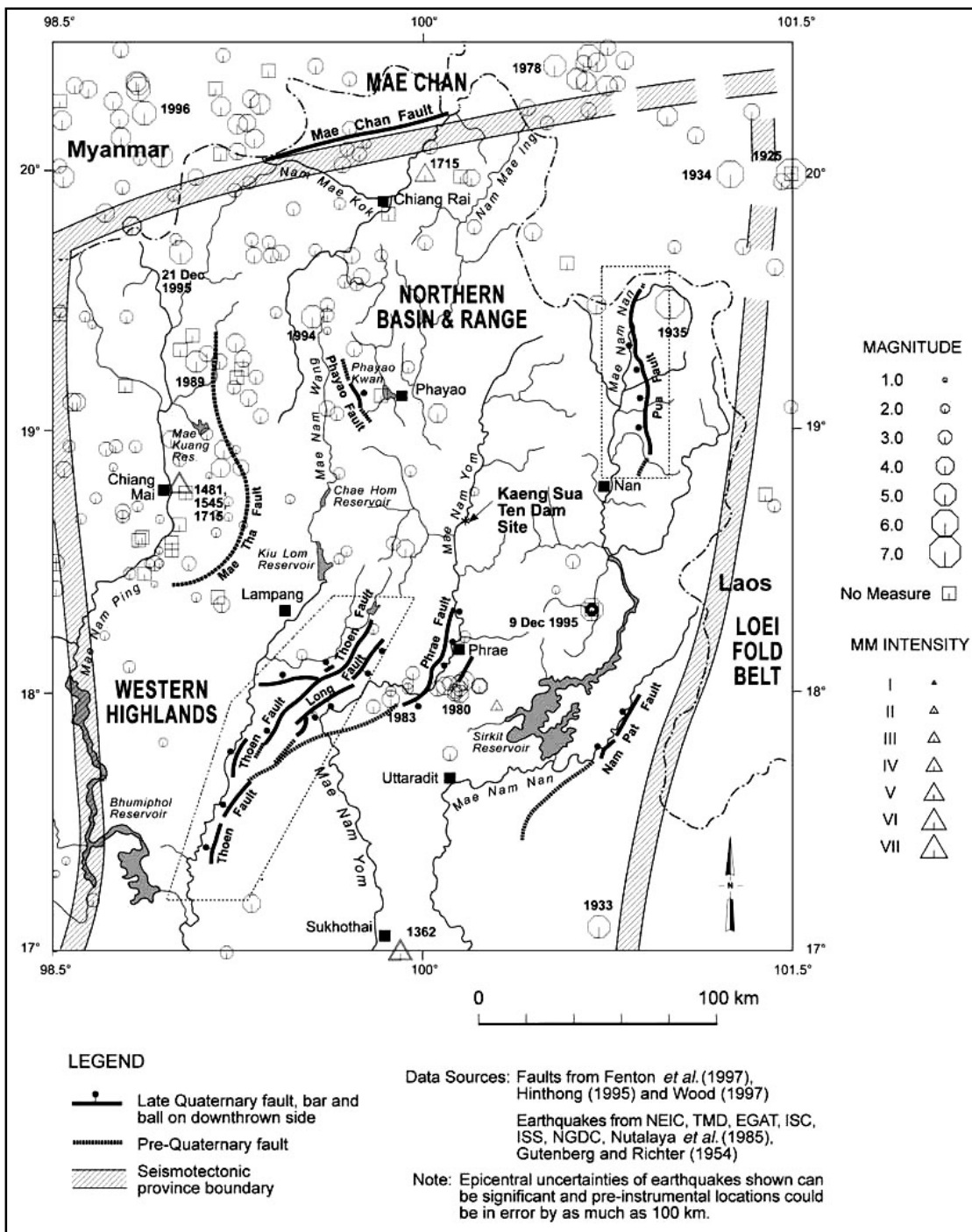


Figure 1.13 Late Cenozoic faults and historical seismicity (1362 to 1996) of the Northern Basin and Range seismotectonic province (Fenton *et al.*, 1997).

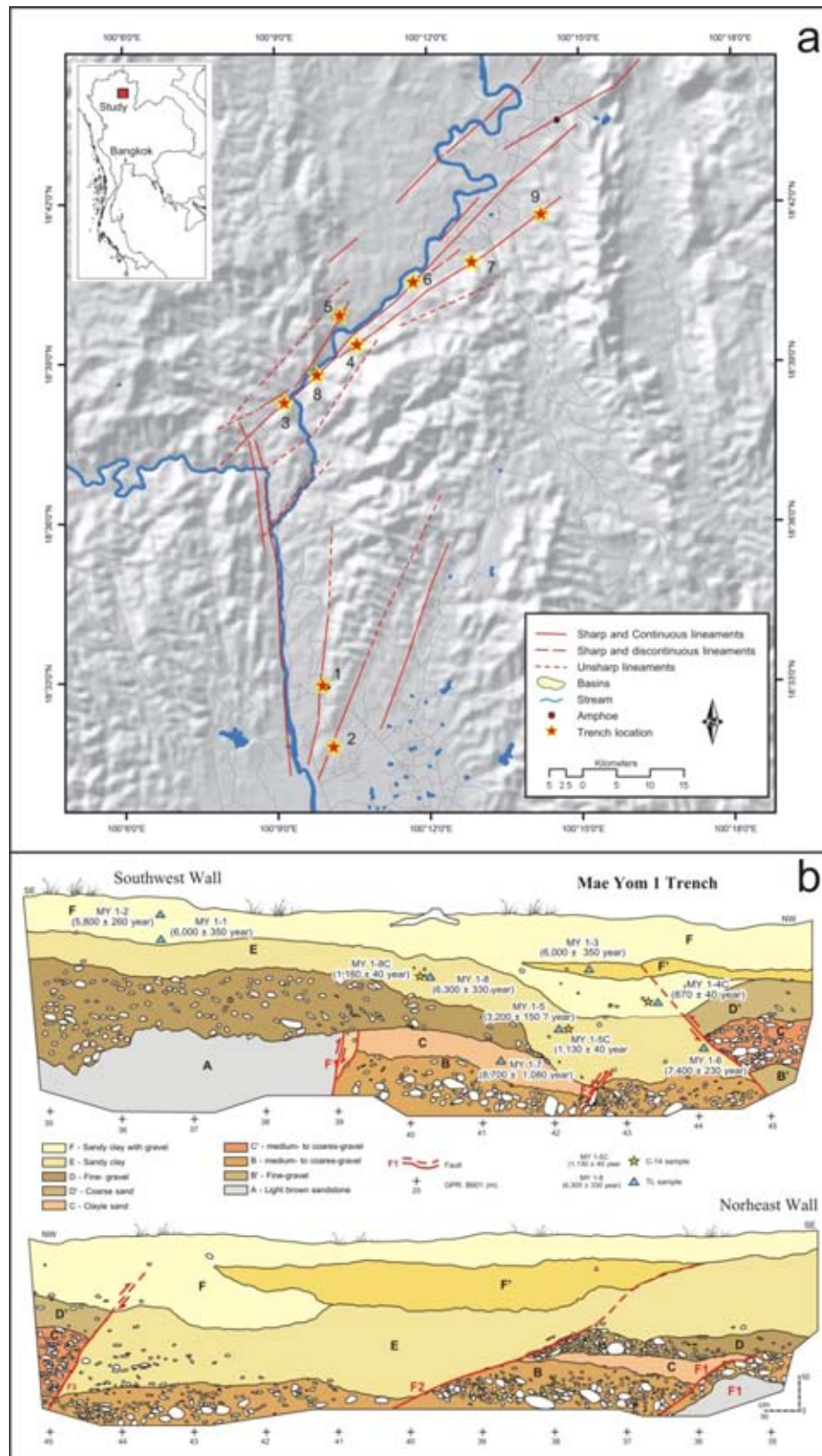


Figure 1.14 a) Location of Mae Yom I trench site, central part of Mae Yom Fault, Phare, Northern Thailand. b) Trench stratigraphy of the southwest wall of the Mae Yom 1 Phu trench showing both nor and reverse faulting and locations of samples for TL dating and their dates (Charusiri et al., 2006).

the south central part, 3) Koshwe-e-we fault in the north–central part, and 4) Kyoukeola Fault in the northern most part. These faults has the left–lateral movement with the slip-rate of 0.1-0.3 mm/yr and a maximum credible earthquake of $M=7.5$ (Figure 1.15).

Recently Saithong (2006) studied the Moei-Mae Ping Fault Zone (MPFZ) in Changwat Tak. Based on the remote-sensing interpretation, field investigation, and dating methods, the MPFZ is the northwest-southeast trending, oblique-slip fault with a total length of about 230 km. The slip rate of this fault segment is estimated as 0.17-0.73 mm/yr and maximum paleoearthquake of M_w 6.70 (Figure 1.16).

Very recently, Khaowiset et al. (2006) reported the movement along the southern extension of the NW-trending Mae Ping Fault may have occurred in pre Cenozoic (Triassic) and Cenozoic due to the change in tectonic regime.

1.6 A Brief Guide to the Thesis

This thesis provides a tectonic geomorphology and geochronology of Pua fault zone in succession of Chapters

Chapter I mentions about an introduction, objective, study area and methodology to the research project.

Chapter II includes regional geology of northern Thailand, tectonic setting and earthquake epicenter of mainland Southeast Asia and focuses on the study area. Active faults of northern Thailand are reviewed, including case study of active faults in Thailand.

Chapter III is part of remote-sensing interpretation. This chapter aims to understand tectonic geomorphology and evidence of faulting in the interested areas the northern Thailand region to.

Chapter IV provides the field investigation integrated with the remote-sensing interpretation. Leading to the interpretation geomorphology related to neotectonic and detailed study for displacement of sedimentary layers in trenches. Finally, collect samples for dating.

Chapter V concerns geochronology and particularly sedimentary age and evolution of fault movements.

Chapter VI is the discussion about characteristics of the Pua fault system, paleomagnetism and slip rate, and linkage of neotectonic evolution in the study area

Chapter VII concludes results of the study project.

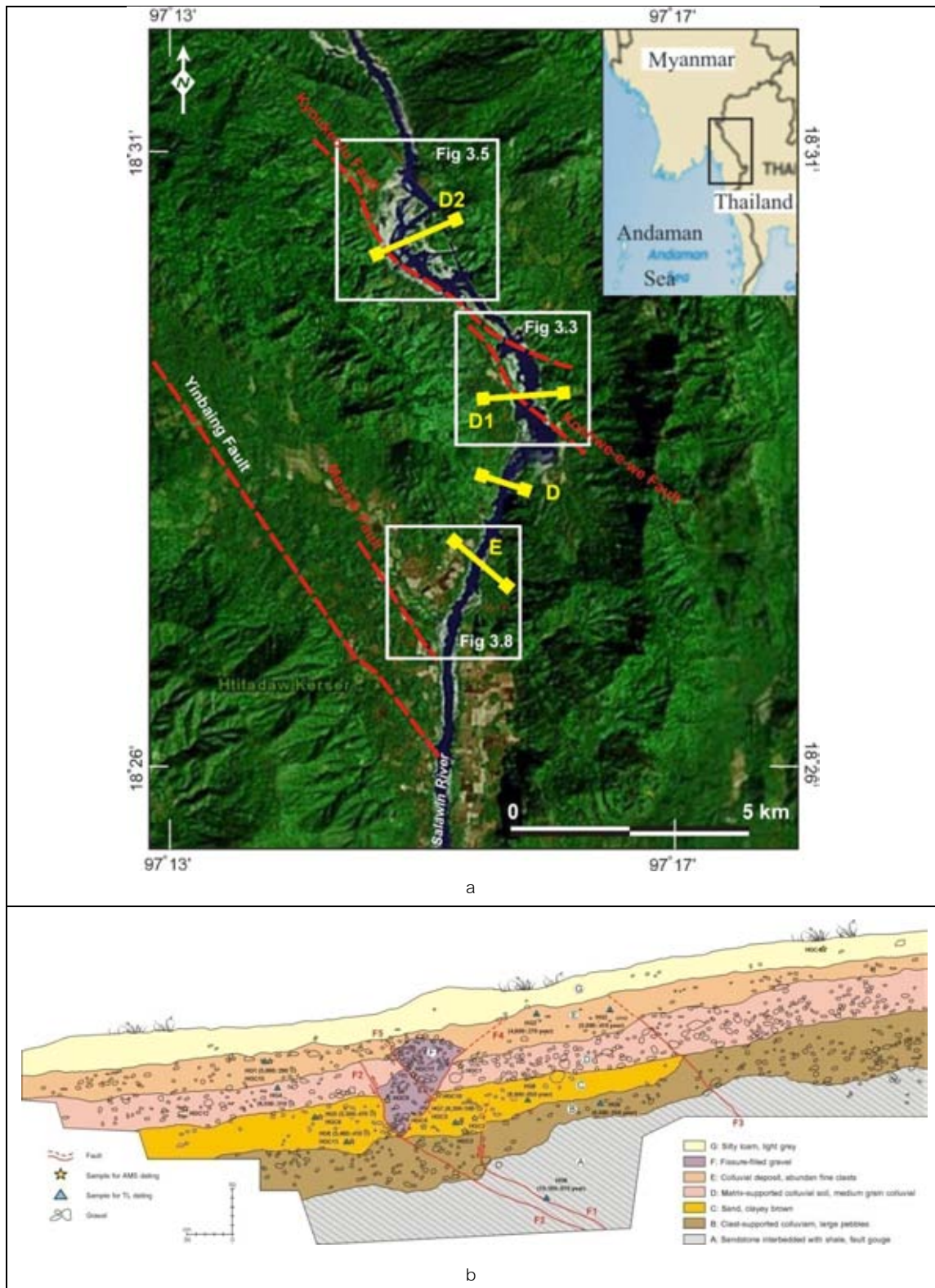


Figure 1.15 a) IKONOS satellite image showing locations of proposed dam sites (yellow lines) along the Salawin River. Dashed red lines indicate the potential active fault, mostly trending in NW-SE direction. b) Trench-log stratigraphy showing fault orientation and TL ages of sedimentary layer, the Hutgyi dam area, the Salawin River. Lithostratigraphy compare with the age of sediment.

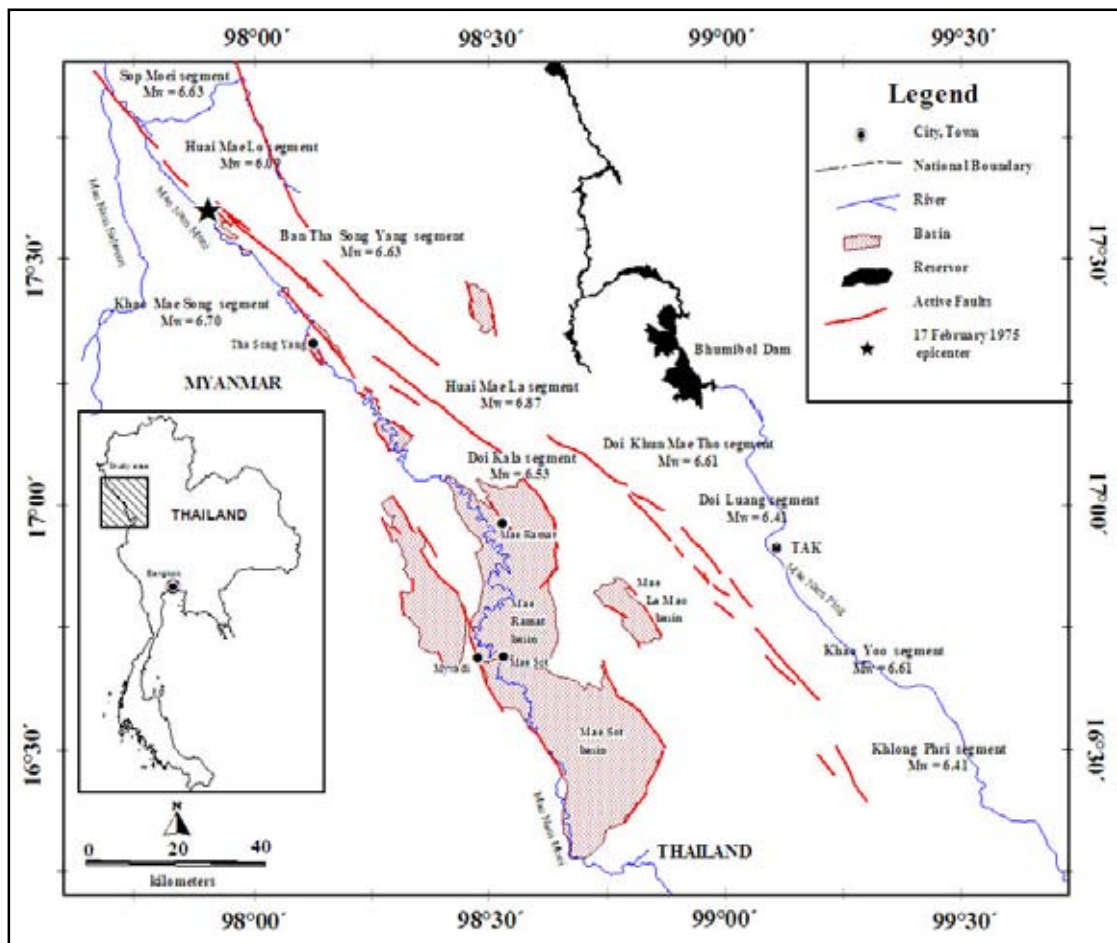


Figure 1.16 Map showing fault segments and their paleoearthquake magnitudes of the Moei-Mae Ping Fault Zone (Saithong, 2006).

CHAPTER II

LITERATURE REVIEWS

2.1 Regional Geologic setting

The regional landforms of eastern of Northern Thailand consist of mountain range and elongated basins with north to northeast strikes. The main rivers are mostly lie follow the basin shape that they are mostly controlled by regional geology and structures. The structures of study area are parallel to the main structures in the same direction. The geological map, scale 1:1,000,000 (Figure 2.1) that revised by Department of Mineral Resources (1998-1999) was used to explain the regional geology and regional structural. The preliminary of the systematic geological investigation in Nan area was performed by staff members of Department of Mineral Resources (1999), scale 1:250,000, including as Xaignbouri (NE47-4) and Changwat Nan (NE47-8). The more detailed geological map on the scales 1:50,000 include Amphoe Thung Chang (5147 I), Amphoe Pua (5147 II), Changwat Nan (5146 I), and Amphoe Sa (5146 II).

2.1.1 Geological setting

Geology of the region as depicted as a geologic map, scale 1:1,000,000 consist of several rock units that most of rock types are sedimentary rocks whose ages from Silurian to Quaternary sediment. Since this thesis does not focus on the geology of the concerned area, so only a brief geology from previous studies (Figure 2.1, 2.2).

2.1.1.1 Sedimentary and Metamorphic Rocks

Silurian-Devonian Rocks

Rocks of the Silurian to Devonian ages represent the oldest rocks in the study area. In the study area, this rock unit is dominantly observed to the western part of the study area in Nan and Phrae and further to the south at the nearby Sirikit dam. It is assigned as the Pha Som Group, which is composed of metamorphic rocks as phyllite, schist, quartzite and hornblendite (Bunopas, 1981). The rocks of the Pha Som Group are believed to deposit in the inner trench slope during the Silurian to Devonian ages.

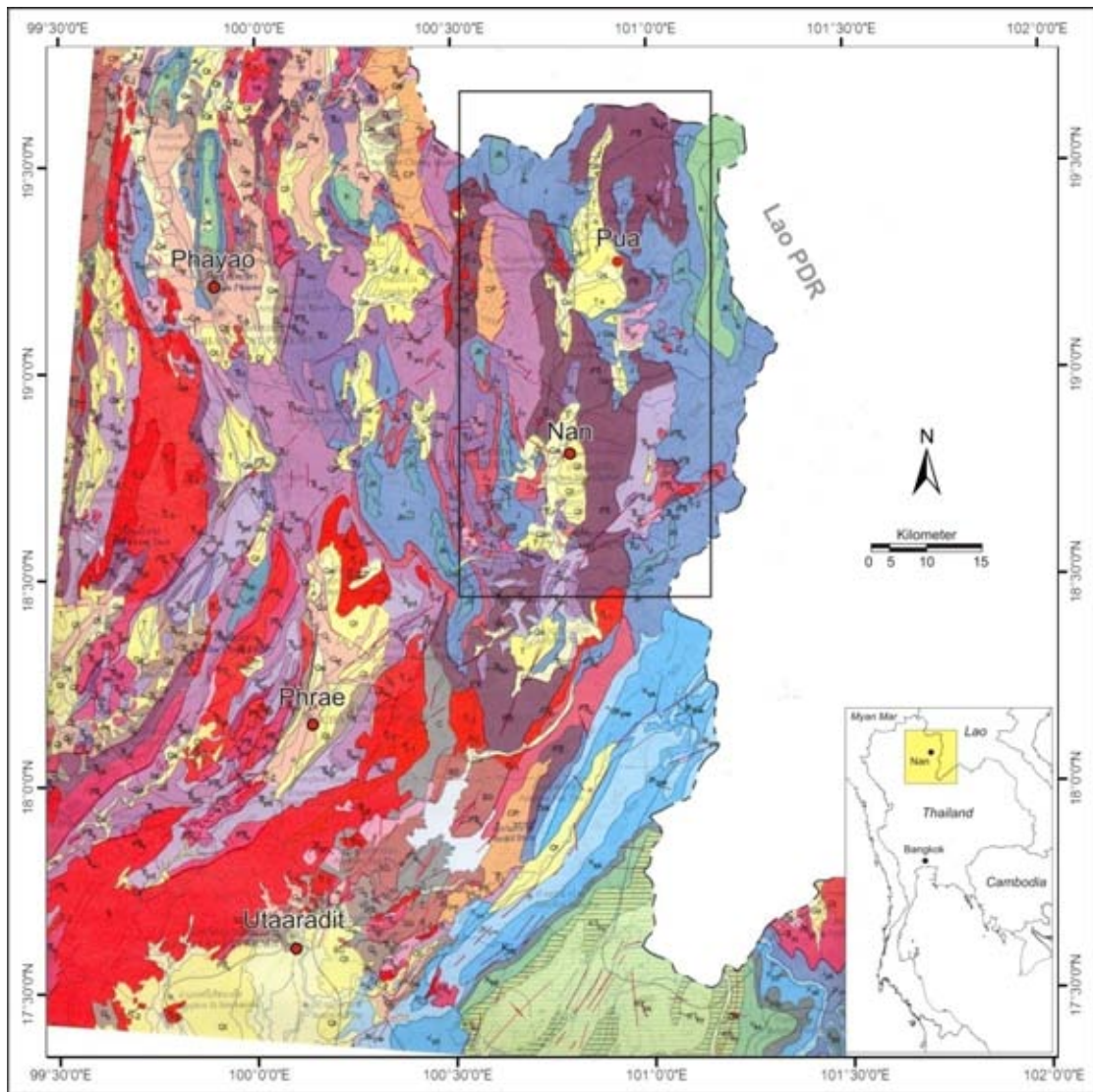


Figure 2.1 Regional geological map of the eastern part of northern Thailand (Department of Mineral Resources, 1999). Note that black box is the study area.

คำอธิบาย EXPLANATION		
อายุ AGE	หินชั้นและหินแปร SEDIMENTARY AND METAMORPHIC ROCK	
ควaternary QUATERNARY	<p>ตะกอนน้ำท่วม ชั้นน้ำขุ่น ชั้นน้ำพา ชั้นน้ำขุ่นและตะกอนโคลน</p> <p>Fluvial deposits: flood plain, silt/clay, terrace and colluvium.</p>	<p>ตะกอนชายฝั่งทะเล ชายเลน ป่าชายเลน ที่สูงที่ชื้นแฉะ</p> <p>Coastal deposits: beach, mangrove swamp, marsh and lagoon.</p>
tertiary TERTIARY	<p>หินชั้นและหินแปรที่ผ่านการแปรสภาพบางส่วนและถ่านหิน</p> <p>Mae Moh Group and Khlai Group: semiconsolidated, consolidated rocks and coal beds.</p>	<p>หินทราย หินทรายปนโคลน หินทรายและหินปูน</p> <p>Sandstone, siltstone, claystone, conglomerate and gypsum.</p>
cretaceous CRETACEOUS	<p>หินทราย และหินโคลน</p> <p>Sandstone and mudstone.</p>	<p>หินทรายและหินปูน</p> <p>Phan Phan Formation: sandstone, with interbedded shaly sandstone, cross bedded and breccia</p>
	<p>หินทรายและหินปูน</p> <p>Ankosit sandstone, conglomerate and shale</p>	<p>หินทรายและหินปูน</p> <p>Lam Thap Formation: Ankosit and white sandstone, mudstone, siltstone, cross-bedded, conglomerate and sandstone.</p>
juristic JURASSIC	<p>หินทราย หินปูน และหินโคลน</p> <p>Conglomerate, sandstone, shale and mudstone.</p>	<p>หินทรายและหินปูน</p> <p>Umpang Group: mudstone, siltstone, sandstone, and limestone</p>
	<p>หินทราย หินปูน และหินโคลน</p> <p>Conglomerate, arenite, siltstone, shale and mudstone</p>	<p>หินทรายและหินปูน</p> <p>Chabul Formation: limestone, shale and siltstone.</p>
trassic TRIASSIC	<p>หินทราย หินปูน และหินโคลน</p> <p>Conglomerate, arenite, siltstone, shale and mudstone</p>	<p>หินทรายและหินปูน</p> <p>Chabul Formation: limestone, dolomite and chert.</p>
	<p>หินทราย หินปูน และหินโคลน</p> <p>Conglomerate, arenite, siltstone, shale and mudstone</p>	<p>หินทรายและหินปูน</p> <p>Chabul Formation: limestone, dolomite and chert.</p>
perman PERMIAN	<p>หินทราย หินปูน และหินโคลน</p> <p>Conglomerate, arenite, siltstone, shale and mudstone</p>	<p>หินทรายและหินปูน</p> <p>Chabul Formation: limestone, dolomite and chert.</p>
	<p>หินทราย หินปูน และหินโคลน</p> <p>Conglomerate, arenite, siltstone, shale and mudstone</p>	<p>หินทรายและหินปูน</p> <p>Chabul Formation: limestone, dolomite and chert.</p>
carboniferous CARBONIFEROUS	<p>หินทราย หินปูน และหินโคลน</p> <p>Conglomerate, sandstone, shale, slate, chert and limestone.</p>	<p>หินทราย หินปูน และหินโคลน</p> <p>Keang Krachan Group: pebbly sandstone, pebbly mudstone, shale, sandstone, siltstone, mudstone and chert.</p>
	<p>หินทราย หินปูน และหินโคลน</p> <p>Conglomerate, sandstone, shale, slate, chert and limestone.</p>	<p>หินทราย หินปูน และหินโคลน</p> <p>Keang Krachan Group: pebbly sandstone, pebbly mudstone, shale, sandstone, siltstone, mudstone and chert.</p>
devonian DEVONIAN	<p>หินทราย หินปูน และหินโคลน</p> <p>Chert, shale, limestone and buff.</p>	<p>หินทราย หินปูน และหินโคลน</p> <p>Keang Krachan Group: pebbly sandstone, pebbly mudstone, shale, sandstone, siltstone, mudstone and chert.</p>
	<p>หินทราย หินปูน และหินโคลน</p> <p>Chert, shale, limestone and buff.</p>	<p>หินทราย หินปูน และหินโคลน</p> <p>Keang Krachan Group: pebbly sandstone, pebbly mudstone, shale, sandstone, siltstone, mudstone and chert.</p>
silurian SILURIAN	<p>หินทราย หินปูน และหินโคลน</p> <p>Chert, shale, limestone and buff.</p>	<p>หินทราย หินปูน และหินโคลน</p> <p>Keang Krachan Group: pebbly sandstone, pebbly mudstone, shale, sandstone, siltstone, mudstone and chert.</p>
	<p>หินทราย หินปูน และหินโคลน</p> <p>Chert, shale, limestone and buff.</p>	<p>หินทราย หินปูน และหินโคลน</p> <p>Keang Krachan Group: pebbly sandstone, pebbly mudstone, shale, sandstone, siltstone, mudstone and chert.</p>
ordovician ORDOVICIAN	<p>หินทราย หินปูน และหินโคลน</p> <p>Chert, shale, limestone and buff.</p>	<p>หินทราย หินปูน และหินโคลน</p> <p>Keang Krachan Group: pebbly sandstone, pebbly mudstone, shale, sandstone, siltstone, mudstone and chert.</p>
	<p>หินทราย หินปูน และหินโคลน</p> <p>Chert, shale, limestone and buff.</p>	<p>หินทราย หินปูน และหินโคลน</p> <p>Keang Krachan Group: pebbly sandstone, pebbly mudstone, shale, sandstone, siltstone, mudstone and chert.</p>
cambric CAMBRIC	<p>หินทราย หินปูน และหินโคลน</p> <p>Chert, shale, limestone and buff.</p>	<p>หินทราย หินปูน และหินโคลน</p> <p>Keang Krachan Group: pebbly sandstone, pebbly mudstone, shale, sandstone, siltstone, mudstone and chert.</p>
	<p>หินทราย หินปูน และหินโคลน</p> <p>Chert, shale, limestone and buff.</p>	<p>หินทราย หินปูน และหินโคลน</p> <p>Keang Krachan Group: pebbly sandstone, pebbly mudstone, shale, sandstone, siltstone, mudstone and chert.</p>
pre-cambrian PRE-CAMBRIAN	<p>หินทราย หินปูน และหินโคลน</p> <p>Chert, shale, limestone and buff.</p>	<p>หินทราย หินปูน และหินโคลน</p> <p>Keang Krachan Group: pebbly sandstone, pebbly mudstone, shale, sandstone, siltstone, mudstone and chert.</p>
	<p>หินทราย หินปูน และหินโคลน</p> <p>Chert, shale, limestone and buff.</p>	<p>หินทราย หินปูน และหินโคลน</p> <p>Keang Krachan Group: pebbly sandstone, pebbly mudstone, shale, sandstone, siltstone, mudstone and chert.</p>

Figure 2.2 Explanation of geological map (Department of Mineral Resources, 1999), showing in Figure 2.1.

Carboniferous Rocks

This stratigraphical unit contains marine clastic rocks of Carboniferous age, and is assigned as the Mae Tha Group. In study area, this stratigraphical unit is mainly exposed at the boundary between Changwat Nan and Phrae; and at Amphoe Thapladuk, Changwat Uttaradit. It is composed mainly of conglomerate, sandstone, shale, and slate and there are limestone and chert beds interbedded within. Upper of this sequence in study area is rhyolite, andesite, agglomerate and tuff

Carboniferous-Permian Rocks

The Carboniferous to Permian rocks of the Phrae Group (Bunopas, 1981) are unconformably underlain by rocks of the Pha Som Group. The Phrae Group rocks are well exposed at the central part of the research area; west of Amphoe Tha Wang Pha, Changwat Nan continuous to Amphoe Pong, Changwat Phayao, and west of Sirikit dam. Thickness of the Phrae Group is more than 4,000 meters and can be sub-divided into 2 units. The lower unit is composed of red chert, agglomerate, andesite and diorite, top of this sequence contains sandy shale, coarse-grain sandstone and conglomerate. The upper unit Phrae is composed of volcanic rocks, quartzitic sandstone, shale, limestone, and calcareous shale.

Permian rocks

Regionally, Permian rocks which are collectively called the Ratburi Group are also widely exposed, particularly throughout the western part of the concern area, Phrae and Changwat Lampang. This unit can be separated into 3 parts. The lower are mainly exposed in Amphoe Na Mun and Amphoe Long. It consists of sandstone, siltstone, shale, chert, conglomerate, tuff, and volcanic rocks and conformably underlain by the Carboniferous rocks. The middle part is mainly exposed in Changwat Nan and contains micaceous sandstone, shale, and well bedded limestone. The upper part is mainly exposed in east of Nan and Phrae and contains sandstone tuffaceous shale, limestone, chert, and conglomerate.

Permian-Triassic Rocks

Permo-Triassic rocks occur as a linear belt and largely exposed throughout the central part of Changwat Nan to the west of Changwat Phayao. The rock unit consisted of sandstone, tuffaceous sandstone, shale, chert, argillaceous limestone, limestone lenses, rhyolite to tuff, and meta-andesite

Mesozoic Rocks

Based on the geological map at scale of 1:1,000,000, Mesozoic rocks in the northern part of Thailand, can be separated into 2 parts, marine and non-marine sedimentary rocks.

Marine Mesozoic Rocks

In the regional study area, marine Mesozoic rocks are also widely exposed around Lampang, Phrae, Phayao, and west of Changwat Nan. This rock unit can be divided into 2 parts, the marine Triassic rocks of the Lampang Group and marine Jurassic rocks. The Lampang Group is deposited in deep sea graded to shallow water during Triassic period. Lampang Group can be divided into 7 formations (Chaodumrong, 1992), namely in ascending order, the Phra That, Pha Kan, Hong Hoi, Doin Long, Pha Daeng, Kang Pla, and Wang Chin Formations. These lithologic units are composed mostly of mudstones, limestones, greenish gray sandstone, and subordinate conglomerates totaling 5,000 meters in thickness. Marine Triassic rocks are both unconformably and conformably underlain by Permian rocks. The Marine Jurassic rocks are exposed nearby Amphoe Na Noi, Changwat Nan, and consist mainly of mudstone interbedded sandstone with marine fossils.

Non-Marine Mesozoic Rocks

This rock unit was deposited in the alluvial system during the Mesozoic period and composed of mudstone, sandstone, and conglomerate. The non-marine Mesozoic rocks are also widely exposed, particularly throughout north and central of the regional area and along Thai-Lao PDR border.

As shown in Figure 2.1, the non-marine Triassic rock unit distributed around Phayao and Amphoe Wiang Sa and Ban Luang, Changwat Nan. This rock unit contains light gray sandstone, greenish gray mudstone, and conglomerate with clasts of marine clastic rocks. The Jurassic non-marine clastic rocks are conformably underlain by Triassic rocks and the Jurassic rocks unit is cropped out in northeast of Changwat Phrae which consists of red conglomerate, light gray arkose, red sandstone interbedded with shale, conglomerate, and mudstone.

On the other hand, non-marine Jurassic rocks of the Khorat Group Outcrop are observed along southern part of Nan and Uttaradit boundary through the border into Lao PDR. The lowest of Khorat group in this area is Phu Kradung

Formation (Ward and Bunnag, 1964) is the oldest formation, contains mostly maroon siltstone, claystone, sandstone, and conglomerate. Based on fossils found, the formation ranges in age from Lower to Upper Jurassic. Phra Wihan formation has conformable contact with the underlying Phu Kradung and overlying Sao Khua Formation. Phra Wihan formation comprises yellowish white, fine- to medium-grained, well-sorted and well round quartzitic sandstone, siltstone, thin-bedded claystone and conglomerate. Based on stratigraphic correlation and fossils, the Phra Wihan Formation ranges in age from Upper Jurassic to Lower Cretaceous (Meesook, 2000). The Sao Khua Formation consists of various cycles of reddish brown silty claystones interbedded with siltstones, sandstone and conglomerate, and caliches. The Sao Khua Formation is overlain conformably by the Phu Phan Formation which ranges in age from Upper Jurassic to Lower Cretaceous (Meesook, 2000). Most of the Phu Phan Formation consists of pale gray, thick-bedded, planar and trough-cross-bedded, well-rounded, poorly-sorted, medium- to coarse-grained, conglomeratic sandstone. Based on fossil assemblages and stratigraphic correlation, this rock unit is overlain by Khok Kruat Formation; the formation is defined to Lower Cretaceous age and is interpreted to be deposited by braided and occasional meandering (Meesook, 2000). Khok Kruat Formation has conformable lower contact with Phu Phan Formation but has unconformable upper contact with Maha Sarakham Formation. This rock unit contains reddish brown to maroon sandstone, siltstone, claystone and conglomerate. Based on vertebrate fossils, is interpreted in deposited by the meander river system in semi-arid to arid paleoclimate (Meesook, 2000) during the Lower Cretaceous time (Capetta, et al., 1990). Maha Sarakham Formation is unconformably underlain by the Khok Kruat Formation and conformably overlain by Khao Ya Puk Formation (Sattayarak et al., 1991). The Lower Cretaceous age given for the formation on the basis of polynomorphs (Sattayarak et al., 1991) and this rock unit is deposited by the saline water in lake or pond in the arid condition (Meesook, 2000). Khao Ya Puk Formation is well exposed at Chat Trakan National park and is conformably underlain by Maha Sarakham Formation. The formation consists of brick red, thick bedded sandstone, maroon siltstone, and conglomerate. Age of the formation is in the period of Cretaceous-Tertiary time that is based on the stratigraphic ground and is interpreted to be deposited by meandering river and by wind in semi-arid conditions. Phu Khat Formation is the upper most of Khorat Group of thesis area. The formation is

unconformably underlain by Khao Ya Puk Formation, consisting of brown to maroon, fine- to medium-grained, well-sorted, calcareous sandstone interbedded with siltstone and claystone. Based on the stratigraphic correlation, the formation has same age as the Cretaceous-Tertiary Khao Ya Puk Formation and deposited by meandering river and alluvial fan in the semi-arid paleoclimate.

Tertiary Rocks

Tertiary rocks in northern Thailand are important as sources of coal and clay minerals. These rocks have deposited in the intermontane and rift basins. The basins are grabens or half grabens, typically bounded by north to northwest-striking normal faults (Polachan et al., 1991; Lorenzetti et al., 1994). There are several significant Tertiary basins in the study area, such as Pua, Nan, Phrae, Phayao, Ngao, Chiang Muan and Mae Moh basins. The Tertiary rocks have been deposited in these basins consist mainly of semi-consolidated clastic sediments as claystone, siltstone, sandstone, and conglomerate. Based on several kinds of fossils including plants, bivalves, gastropod, and vertebrates, they indicated the age of Tertiary. In the satellite images the tertiary rocks are shown as low-relief and gentle slopes as compared with those of the older rocks.

Quaternary Sediments

The Quaternary sediments in northern Thailand were chiefly deposited in the intermontane basin. They are deposited by colluvial and alluvial processes and well exposed at foot hills and along the main rivers such as Ping, Wang, Yom, and Nan River, respectively. The processes of rivers developed broad flood plain and river terraces, in the higher elevation which is undulated terrains covering with colluviums and alluvial fan sediments. These alluvial and colluvial processes are also related to the tectonic evolution of this region. The Quaternary sediments are deposited in this area, characterized by unconsolidated sediment such as sands, silts, clays, and gravels. Based on stratigraphic correlation, the sediments in terrace area assign in Pleistocene age, while the flood plains and the sediments on the upper of alluvial deposits are Holocene age.

2.1.1.2 Igneous Rocks

Plutonic Rocks

Most plutonic rocks in the thesis area are granitic rocks belonging to Granite Belt of Thailand (Charusiri, 2002). Based on the stratigraphic correlation and dating results, the granite rocks can be divided into 2 categories, Permo-Triassic Granite and Triassic Granite, however both are of I-type. The Permo-Triassic granite is well exposed in the east of the study area, particularly at Amphoe Chiang Kan and Amphoe Muang, Changwat Loei. It is composed of micro granite and quartz-monzonite, granodiorite, and plagiogranite. The Triassic granite is mainly characterized by biotite granites, tourmaline granites, granodiorites, biotite-muscovite granites, and biotite-tourmaline granites. This granite is well exposed in the central and east of the study area, especially at Amphoe Tha Pla, Changwat Uttaradit and Amphoe Pua, Changwat Nan.

Volcanic rocks

In northern Thailand, volcanic rocks occur as small, semicircular and elongated shapes. These volcanic rocks can be separated into 3 suites based on their age. Permo-Triassic Volcanic, consisting of rhyolite, andesite, agglomerate, rhyolitic tuff, and andesitic tuff, They are exposed at Changwat Phrae and east of Changwat Lampang. 2) Jurassic volcanic rocks are exposed along Phayao and Chiang Rai border and Changwat Nan; the volcanic rocks are composed of andesite and rhyolite. And 3) Cenozoic basalt or the so called Denchai basalt is well exposed in the west of Amphoe Denchai, Changwat Phrae. This basalt flowed over the older sedimentary rocks and can be separated into 7 recognizable layers (Barr and Macdonald, 1979). The other Cenozoic basalt occurs as small hills along the Nan River near the Sirikit Dam.

2.1.2 Structural Setting

In the study area, the major structure can be well recognized in satellite images is the faults and fractures. The major faults and fractures are in the northeast-southwest and north-south directions. Two important faults are Northern Thailand Fault Zone (NTFZ) and the Nan-Uttaradit Fault Zone (UFZ) (Figure 2.3). They are considered to tectonically control regional attitudes of the above-mentioned rock units. Not only the major NE-SW trending fault but also there are the other important

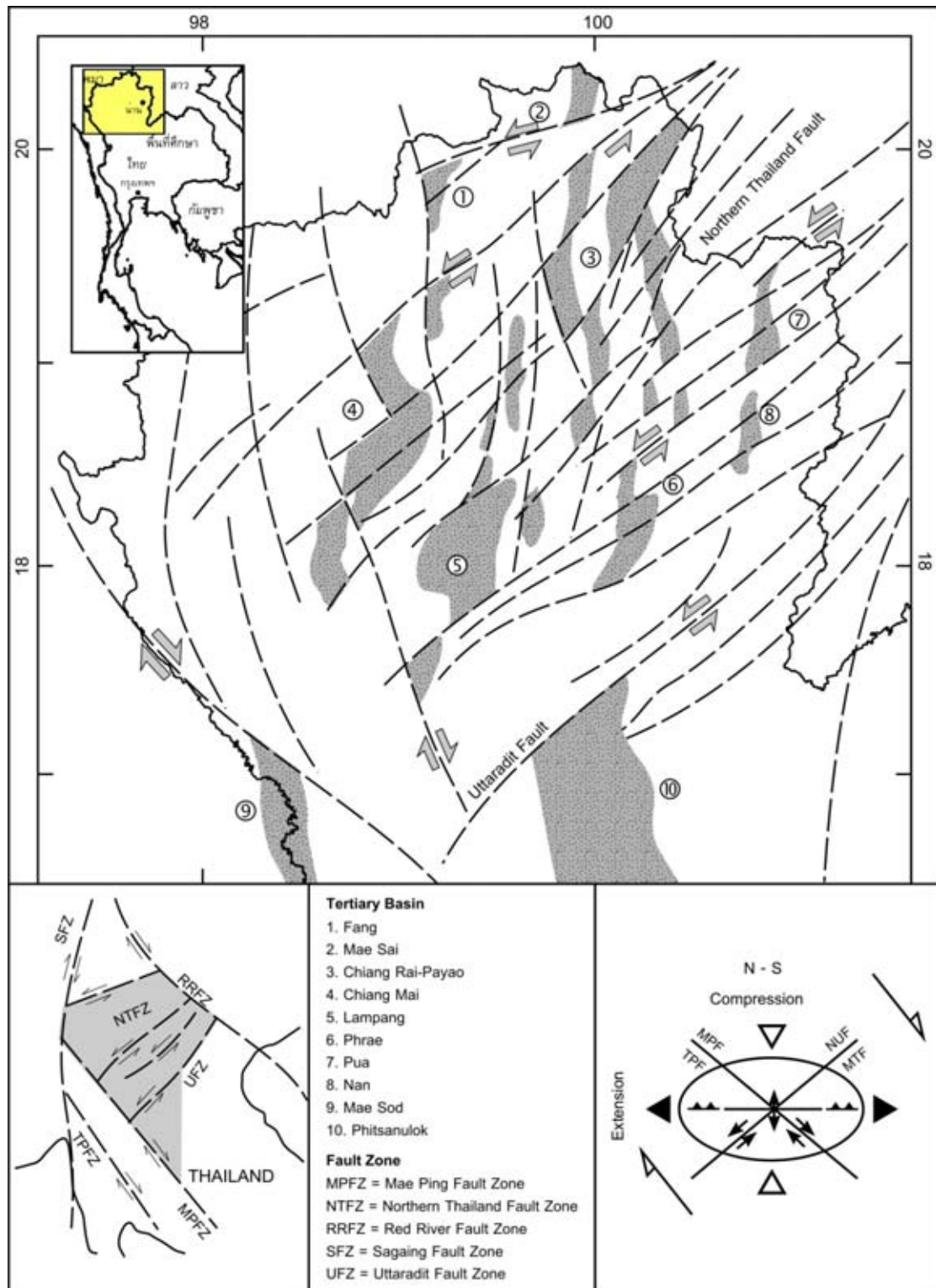


Figure 2.3 Structural map of Northern Thailand showing relationship between conjugate strike-slip faults and the development of N-S trending pull-apart basins (after Polachan and Sattayarak, 1989).

faults in the north to north-northeast strike, including Pua Fault (Fenton et al., 1997), Mae Tha Fault, Phayao Fault, Phrae Fault. Parts of these faults cut through the Tertiary and Quaternary sedimentary unit as well. They also represent the contact zone of sediments deposited in the Tertiary basins.

2.2 Tectonic Setting

2.2.1 Tectonic evolution during Cenozoic in the Sunda shelf and Northern Thailand

Deformation of the South East Asia (SE Asia) throughout Tertiary period is a consequence of the collision between the Indo-Australian and Eurasian plates and researchers was referring to (Tapponnier et al., 1982, 1986; Daly et al., 1991; Dewey et al., 1989; Rangin et al., 1990; Lee and Lawver, 1995; Hall, 1996; Packham, 1996; and Matthews et al., 1997). The propagation collision model (Tapponnier et al., 1982) that has a free boundary to the south and east is widely accepted (Figure 2.4).

The experiments with plasticine of Tapponnier et al., (1982) are shown in Figure 2.5. They indicated many similarities between the results of their experiments and those of the geology of the Southeast Asia. For instance, they proposed that the F2 fault in the experiment corresponds to the Altyn Tagh Fault, and the F1 one corresponds to the Red River Fault. The tectonics of eastern Asia would thus reflect the succession in time of two major phases of the continental extrusion. The gap between block 2 and block 1, which are compared to the southern China and the Indochina respectively; (Figure 2.5), would be analogous to the South China Sea, whereas the gap A, between the rigid block and block 1, corresponds to the Andaman Sea. The principal tectonic units are shown in the Figure 2.5. According to Molnar and Tapponnier (1975), the Himalayan Thrust Fold belt was plane between the conjugate faults of the sinistral Quetta Chaman Fault in the west and the dextral Sittang Fault, Sagiang, in the east. These strike-slip faults mark the margins of the Indo-Australian plate indent which has been driven northward into the Eurasian plate. The action forced the N-S thrusting in the Himalayas (Molnar and Tapponnier, 1975; Ni and York, 1978).

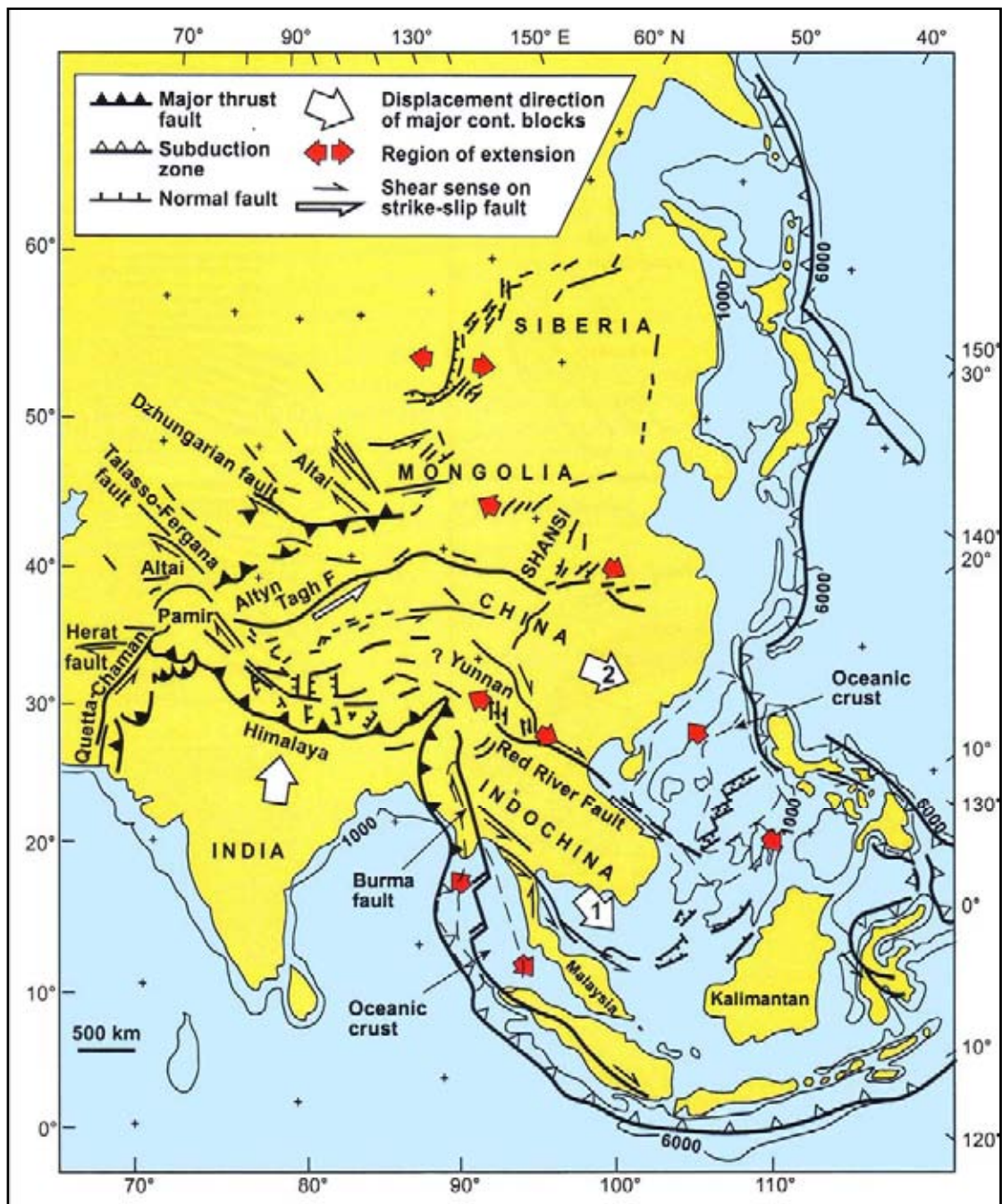


Figure 2.4 Tectonic map of central-east Asia illustrating 'extrusion' model and its relationship with Cenozoic structures in the region. Numbers in white arrows indicate the relative order in which certain continental blocks were extruded toward the southeast (after Tapponnier et al., 1982).

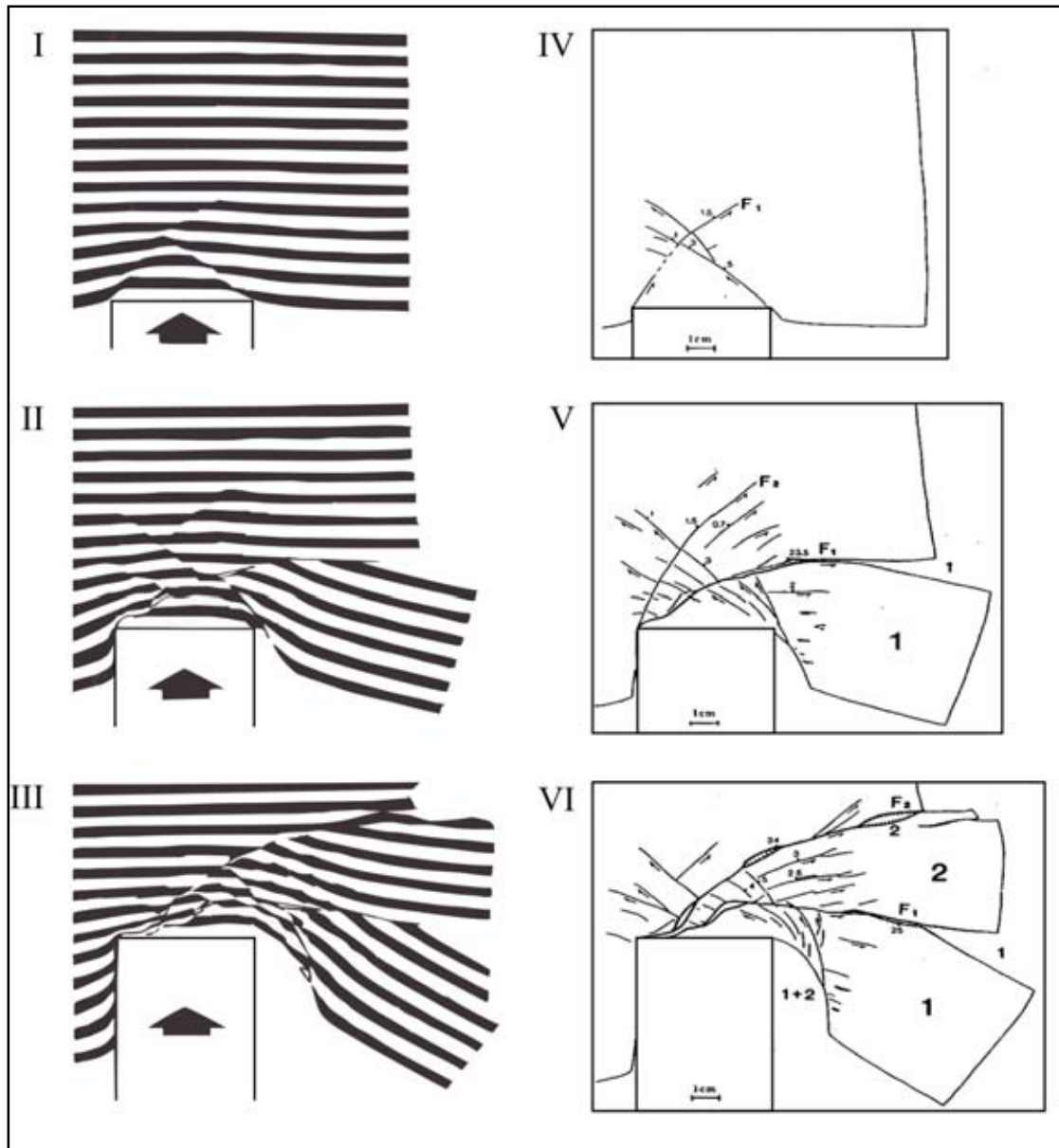


Figure 2.5 Three successive stages (I to III and IV to VI are in interpretation) of extrusional model experiment with plasticine (plain view). In unilaterally confined experiment, two major faults (F1 and F2) guide successive extrusion of two blocks. In stage VI, blocks 1 and 2 can be compared to Indochina and southern China, and open gap 1, 1+2, 2 to South China Sea, Andaman Sea, and northeastern China, respectively (after Tapponnier et al., 1982).

A large number of the NE-SW left-lateral strike-slip faults and the NW-SE right-lateral displacements can be observed (Ni and York, 1978). It also induced the Tibetan Plateau and developed various N-S trending basins since the Late Cenozoic (Molnar and Tapponnier, 1977; Ni and York, 1978). The outcome of N-S shortening by the penetration of the Indo-Australian Plate into the Eurasian Plate yielded the E-W lateral flow of crustal materials from Tibet to South China which moved eastward away from the path of India (Molnar and Tapponnier, 1975). Molnar and Deng (1984) proposed the at least half of the present-day northward convergence between India and Asia is accommodated by crustal thickening. These are the results of their studies of the seismic deformation in Central Asia.

The early collision between Indo-Australian and Eurasian plates was commenced through Late Palaeocene until Middle Eocene (58-44 Ma), whilst hard collision started in the Middle Eocene (44 Ma) (Lee and Lawver, 1995). The Cenozoic tectonic evolution of this region can be separated into four stages, related to the northward movement of the Indo-Australian plate relative to the Eurasian plate. The eastern syntaxis, the right corner of the Indo-Australian plate (Lacassin et al., 1997), has penetrated through the Eurasian plate and has resulted in changing stress patterns of the region through times. The changing stress fields have controlled the opening of the sedimentary basins in this region and the South China Sea as well as the sense of movement of the major strike-slip faults (Huchon et al., 1994).

Srisuwan (2002) postulated the Cenozoic tectonic evolution of South East Asia region. It can be discussed in four stages as follows.

Stages I: Early Eocene to Early Oligocene (50 to 32 Ma): the South China Sea margin extension commenced earlier than the collision of Indo-Australian with Eurasian and the supposed time of initiation of the Red River Fault. The more extensive rifting in the South China Sea is noted and the first time rifling in the West Natuna Basin area is also mentioned to commence at this stage. The Malay, Mekong Delta, and parts of Gulf of Thailand had been opening at 40-35 Ma.

Stages II: Early Oligocene to Early Miocene (32 to 23 Ma): end of left lateral Mae Ping Fault was approximately 30 Ma. Simultaneously, the beginning of widespread extension of the Gulf of Thailand, Malay and West Natuna Sea Basins started during Late Oligocene. The Mergui Basin and Andaman Sea, are thought to be

formed during Late Oligocene, and continued to Early Miocene. The Northern Thailand basins and ranges probably developed in this stage. The Mae Ping and Three Pagodas Faults changed sense of movement to right-lateral movement whereas the Mae Chan, Uttaradit, and Phrae- Thoen Faults became left-lateral movement.

Stages III: Early to Middle Miocene (23 to 15 Ma): clockwise rotation of the whole of Greater Sunda Block and increasing in the convergence rate along the Sunda Arc. North Sumatra Basin and Central Thailand Basins continue to be extended. During 20 Ma to 15 Ma, clockwise rotation of Southern Thailand and counter-clockwise rotation of Malay Peninsula and Sumatra were reported. Inversion in the Malay and West Natuna Basins, most Cenozoic basins in the Gulf of Thailand and onshore Thailand experienced uplift and erosion that corresponded to a pervasive Middle-Miocene unconformity.

Stages IV: Middle Miocene to Recent (15 to 0 Ma): the clockwise rotation of Borneo still continued while rotation of the Thai-Malay Peninsula and Sumatra ceased, and continued northward moving of Australia. North Sumatra had rotated counter-clockwise with south Malaya and the rotation proceeded the orientation of the Sumatran margin became less oblique to the Indo-Australian plate motion vector. This caused the right-lateral Sumatran strike-slip system, and extension in the Andaman region. Extension occurred in the Gulf of Thailand and inversion in the Malay and West Natuna Basins, whereas the Andaman Sea continued opening toward its present extent. All NW trending strike-slip fault zones in the Sunda region were right-lateral. The inversion and uplift episode, the structural activity in the Cenozoic basins of the Sunda region slowed down toward quiescence around 10 to 5 Ma, during which period regional subsidence occurred and was probably induced by post-rift thermal re-equilibrium. This late-stage subsidence has continued to the recent time (Figure 2.6).

2.2.2 Development of Tertiary Basins in Northern Thailand

The tectonic evolution of Thailand, and Southeast Asia throughout the Cenozoic period, are a result of collision of India plate with Eurasia plate. Collision began about 50 Ma (Middle Eocene) and has resulted in 2,000 to 3,000 km of the Himalayan orogeny (Peltzer and Tapponnier, 1988). As a result of India drove into the southern margin of Eurasia, Indochina was rotated clockwise about 25° and

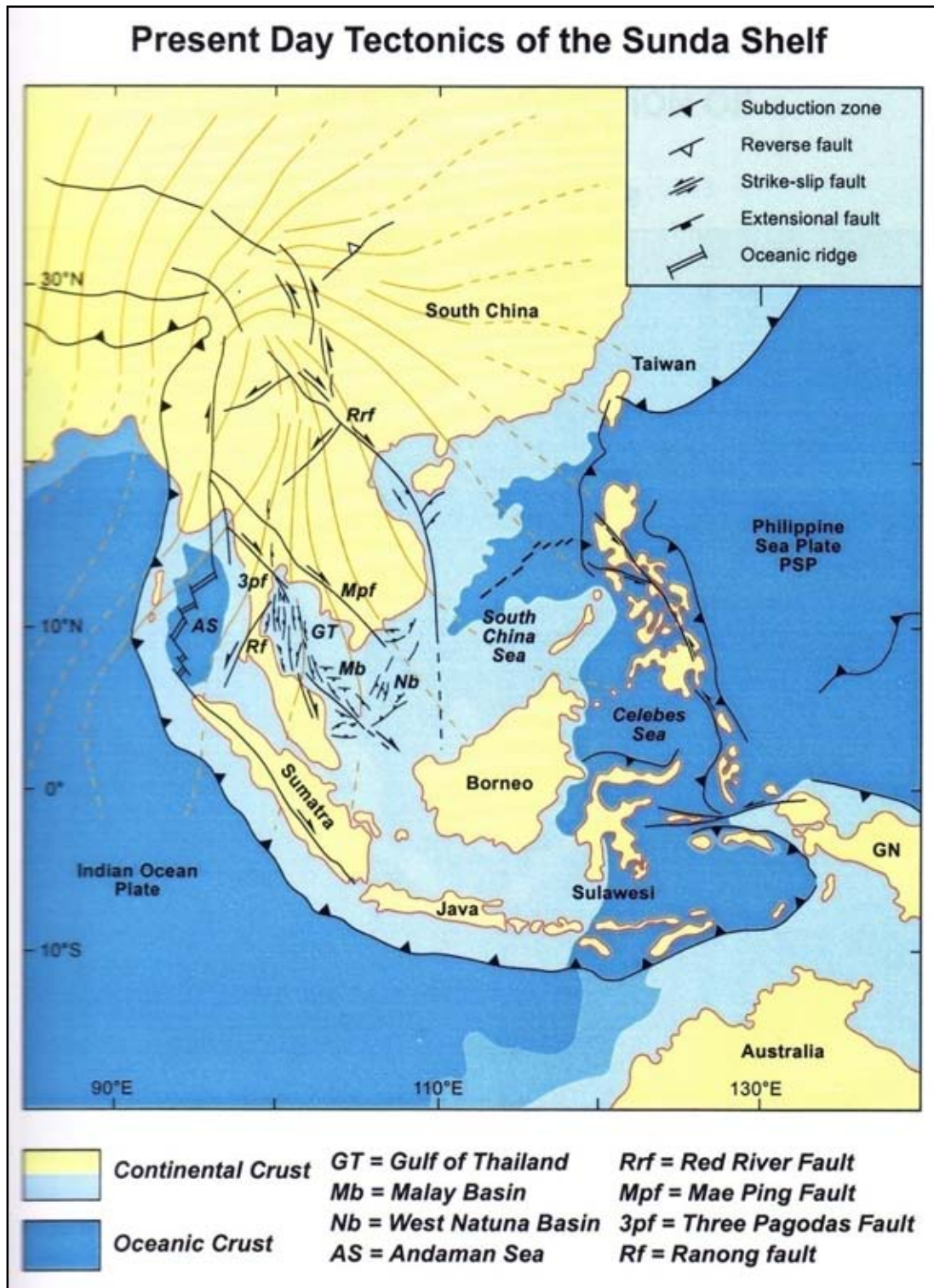


Figure 2.6 Tectonic map of Southeast Asia showing major structural elements in relation to direction of present maximum horizontal stress (after Srisuwan, 2002).

toward to the southeast by approximately 800 km along the Red River and Wang Chao-Three Pagodas fault zones through the first 20-30 million years of collision (Peltzer and Tapponnier, 1988). Extrusion migrated northwards onto the Altyn Tagh Fault as collision progressed. Rotation of Indochina continued and reversing the sense of motion of the Red River Fault from left-lateral to right-lateral (Allen et al., 1984; Peltzer and Tapponnier, 1988). Differential slip between the main strike-slip faults, from north to south, the Red River, Mae Ping, Three Pagodas, and Sumatra fault zones (Figure 2.4), created a transtensional regime that consequence in the opening of the Tertiary basins in Southeast Asia (Ducrocq et al., 1992).

The most Tertiary basins in the northern of Thailand are grabens or half grabens, typically bounded by normal faults, oriented in north to northwest direction (Polachan et al., 1991; Lorenzetti et al., 1994). The location and geometry of the basins are controlled by the north-south structure in pre-Triassic rocks and pre-existing northwest-striking, strike-slip faults (O'Leary and Hill, 1989). Basin evolution during Thailand follows a roughly similar sequence of events. The main phase of strike-slip faults were resulting in rapid extension, with widespread fluvial sedimentation (Oligocene-Early Miocene), was followed by lacustrine sedimentation as basins became increasingly isolated (Early-Middle Miocene). Lacustrine sedimentation ended, and there was an influx of coarse terrigenous clastics suggesting a period of rapid, localized uplift (Middle- Late Miocene). Finally, following a brief period of basin inversion that resulted in a widely recognized Late Miocene unconformity, fluvial sedimentation, generally coarsening upward, resumed (Late Miocene-Recent) (Polachan et al., 1991; Remus et al., 1993; Alderson et al., 1994). The climax of extensional process is the eruption of Late Tertiary and Early to Middle Quaternary alkaline basalts (Hoke and Campbell, 1995). Paleomagnetic data, showing localized rotations during the Tertiary, indicates that the opening of these basins appears to have been fairly complex (McCabe et al., 1988, 1993; Richter et al., 1993).

2.3 Seismicity in Northern Thailand and Nan area

Earthquake in Northern Thailand have been recognized for long time since the past historical period till present day but these earthquakes are just small to moderate levels (Figure 1.1). Although in this region great earthquakes have not been

recorded, most of strong earthquakes have been reported frequently in Myanmar Andaman-Sumatra belt.

Northern Thailand region is assigned into the Northern Basin and Range Province (Figure 2.7), on account of its tectonics similar to the Basin and Range Province of the Western United States (Fenton et al., 1997), a region of extended crust, forming basin and range topography (MacDonald et al., 1993). According Bott et al. (1997), both historical and instrumentally earthquake records in northern Thailand and adjacent areas have been collected and revised from various agencies. Based on the historical records, there are 17 significant historical earthquakes of maximum intensity MM VI or $M_L 5$ and greater reported in the study area since 1360 (Figure 2.8). The first historical record was Sukhothai earthquake, occurred in 1362 with approximately maximum intensity MM VI. After that, there were three significant earthquakes occurred in Changwat Chiang Mai in 1482, 1545, and 1715 with intensity MM VI, VII, and VI respectively. The earthquake in 1545 had harmed Great Pagoda in Chiang Mai, and in 1715, the earthquake occurred in Amphoe Chiang Saen, Changwat Chiang Rai damaged temples and pagodas in this area.

In Nan area, based on the antecedents of Nan, there are six significant earthquakes have been recognized in this area since 1560 to 1879 (Charusiri et al., 2000). The earthquake events destroyed Pagodas, temples, and man-made establishment, such as the earthquake event in 1793, 1801 and 1820, the peak of Maha That Phu Piang Chae Haeng was broken down (Charusiri et al., 2000), at Ban Nawong, Amphoe Pua, Phra That Din Wai was shaken by an earthquake occurred in 1827 (Academic Center of Khun Ngang School Group, 2003).

Based on the instrumental record, Gutenberg and Richter (1954) mentioned that in December 22, 1925 and February 12, 1934. There are two earthquake epicenters with $M_L 6$ in Lao PDR, approximately 150 km from Nan city. On 28 and 30 September 1989, there are two earthquake events occurred in Myanmar, west-northwest of Changwat Chiang Rai with the same magnitude of $M_w 5.8$, and caused damages in Northern Thailand. September 11, 1994 earthquake event reported with epicenter close to Mae Suai, Changwat Chiang Rai with $M_b 5.1$. The earthquake was felt across Changwat Chiang Rai and Amphoe Phan, and it also caused some damages Phan hospital, 30 temples, and 21 schools were reported to be moderate to strongly damage. Landslide at Doi Mok was also reported in response to this event.

The earthquake on December 21, 1995, the magnitude of M_L 5.2 is located near Amphoe Phrae, Changwat Chiang Mai. Felt report was also in Changwat Chiang Rai, Phayao, Lamphun, Lampang, and Mae Hong Son with minor damages in Chiang Mai.

In Nan area and nearby, the moderate to large earthquakes frequently (Figure 2.8) were reported, such as earthquakes in 1925 and 1934 as mention above. Gutenberg and Richter (1954) mentioned that the largest earthquake in Northern Thailand located with M_L 6.5 that occurred on May 13, 1925 and is located to west of Amphoe Thung Chang, Changwat Nan. Additionally, there are lot of earthquakes occurred around Nan area. For instance, during 1980 to 1983, earthquake swarms occurred south of Changwat Phrae and approximately 100 km from Nan city. First record of the swarm occurred on December 19, 1980 and the largest event have reported on December 22, 1981 and December 23, 1981 with M_L 4.0 and 4.2 respectively. On 9 December 1995, a M_L 5.1 (M_b 4.7) earthquake occurred near Amphoe Rong Kwang at the northeastern end of Phrae basin, approximately 50 km from Nan city.

Based on earthquake data in Thailand focal mechanisms (Bott et al., 1997) of western and northern Thailand can be computed (Figure 2.9). The focal mechanisms indicated the compression in the north-south direction and extension in the east-west direction which is approximately perpendicular to many of the north-south-striking Cenozoic basin-bounding faults in northern Thailand.

2.4 Active faults in Thailand

2.4.1 Definition of active faults

The definition of active faults varies widely. Willis (1923) defined an active fault as the one on which a slip is likely to occur and a dead fault as the one on which no movement may be expected. Albee and Smith (1966) proposed a definition of an active fault in a geologic sense as a fault which has moved in the past and will eventually break again. The activeness of a fault is not just a single state that depends on the degree of activity. An active fault in the definition of Wood (1915) refers to historic movement that shows evidence of recent surface movement known as the trace phenomena. Cluff and Bolt (1969) said that a fault should be considered active if it has displaced recent alluvium or other recently formed deposits, whose surface effects have not been modified to an appreciable extent by erosion. Allen et al. (1965)

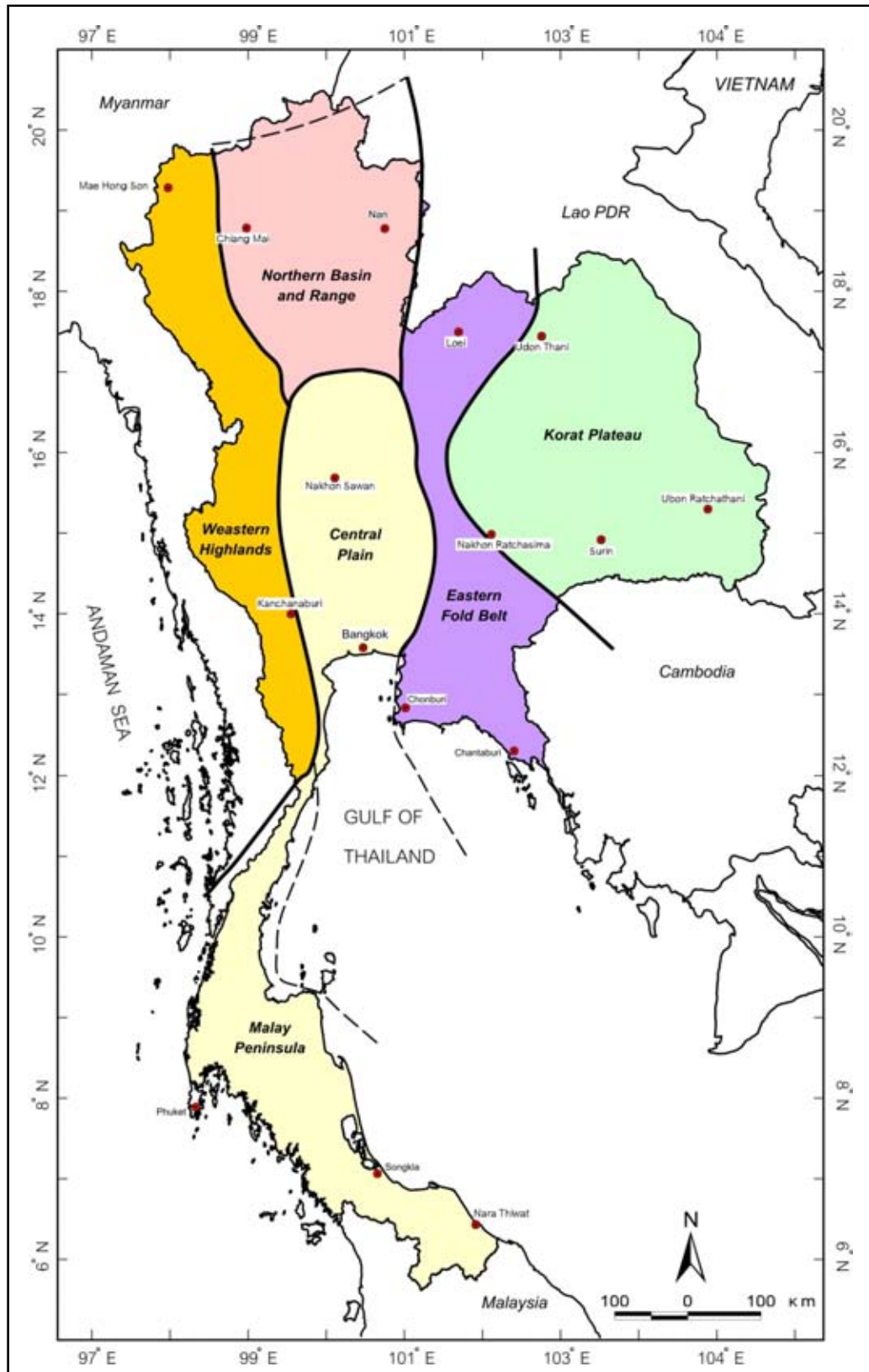


Figure 2.7 Seismotectonic provinces in Thailand (after Woodward-Clyde Federal Services, 1996).

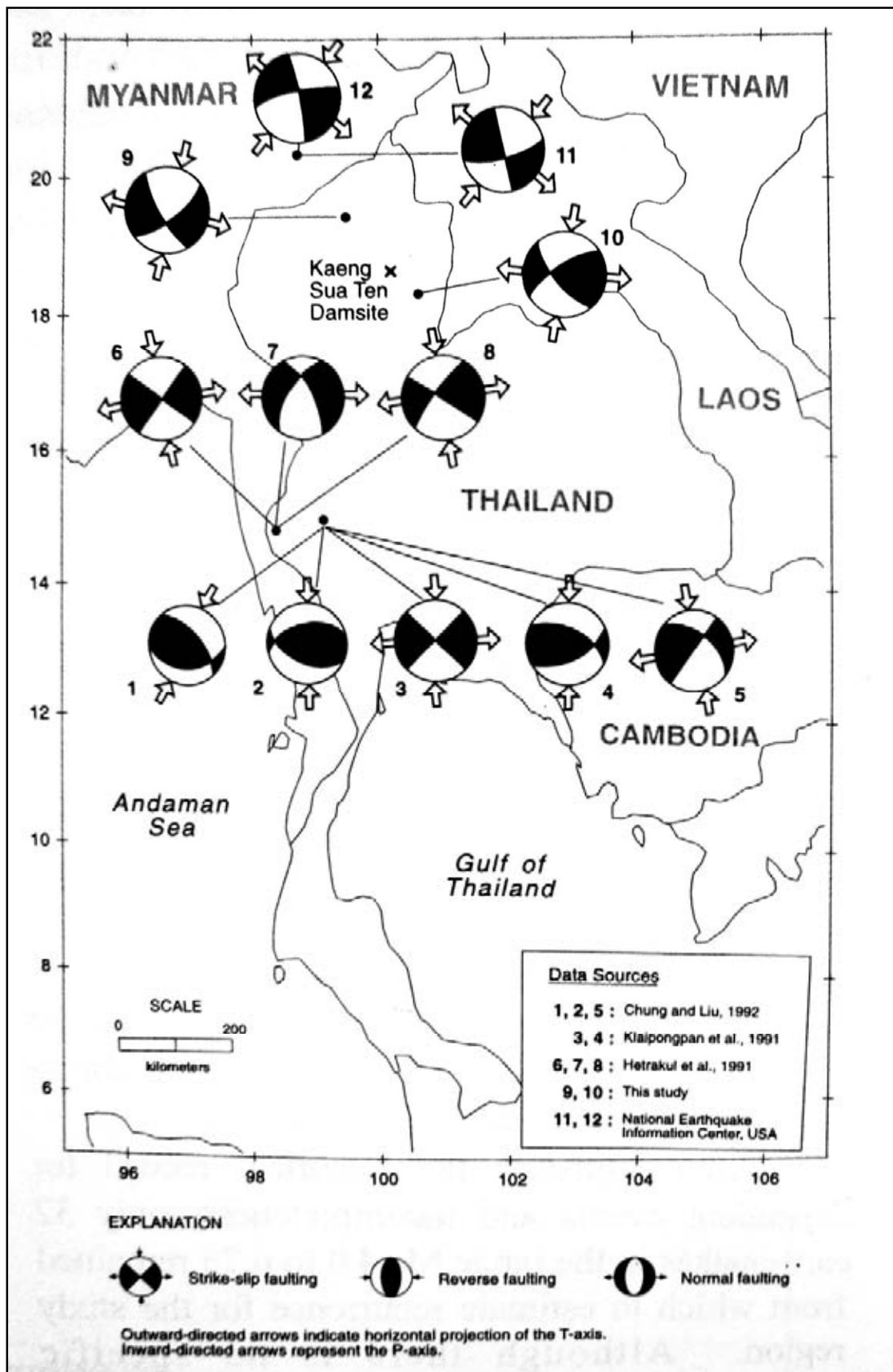


Figure 2.9 Schematic focal mechanisms of Thailand and adjacent regions (Bott et al., 1997).

stated that faults that have had sufficiently recent movement to displace the ground surface are usually considered active by geologists simply because the ground surface is a very young and ephemeral feature. If stream offsets and scarps in alluvium are to be the criteria for activity of faults, then the term "active" must be applied to events dating back into the Pleistocene Epoch, perhaps as much as 100,000 years.

In engineering designation, fault activity is restricted to fault movement during the last 10,000 years, to the Holocene Epoch. This study adopted the definition proposed by the United States Bureau of Reclamation that an active fault is the fault that has a relative displacement within the past 100,000 years.

At present, methods for estimating future hazards of faults are deficient. The designation of a fault merely as active provides an inadequate indication of the attendant hazard. Restricting of the definition of active faults to those having had displacement within a defined past period of time, such as 10,000 or 100,000 years, provides little assessment of the hazard. In addition, the adoption of different restricted definitions by different agencies has caused confusion. An accurate expression of the probability of occurrence of future displacement, of earthquakes generated, and of the size of such events is needed in evaluating the hazards of active faults (Wallace, 1980).

The active fault, as used by U.S. Geological Survey, is a fault that is likely to have another earthquake some times in the future. Faults are commonly considered to be active if they have moved one or more times in the last 10,000 years.

The active fault based on International Committee on Large Dam (ICOLD, 1989), is a fault reasonably identified and located, known to have produced historical fault movements or showing geologic evidence of Holocene, around 11,000 years, displacements and which, because of its present tectonic setting, can undergo movement during the anticipated life of man-made structures

The Western States Seismic Policy Council (WSSPC, 1997) recommends that the following guidelines be used in defining active faults in the Basin and Range physiographic province. Active faults can be categorized into three types, recognizing that all degrees of fault activity exist and that it is the prerogative of the user to decide the degree of anticipated risk and what degree of fault activity is considered "dangerous". They are: 1) Holocene Active Fault - a fault that has moved

within the last 10,000 years; 2) Late Quaternary Active Fault - a fault that has moved within the last 130,000 years; and 3) Quaternary Active Fault - a fault that has moved within the last 1,600,000 years.

It should be emphasized in this thesis that more than half of the historic magnitude 6.5 or greater earthquakes in the Basin and Range province have occurred on faults that did not have Holocene activity, furthermore, earthquakes in the province will occur on faults in all three categories.

Site investigations for foundations of nuclear power plants and research reactors (IAEA, 1988 and 1992; U.S. Nuclear Regulatory Commission, 1982.) states that a capable fault is a fault which has exhibited one or more of the following characteristics: 1) Movement at or near the ground surface at least once within the past 35,000 years or movement of a recurring nature within the past 500,000 years; 2) Macro-seismicity instrumentally was determined with records of sufficient precision to demonstrate a direct relationship with the fault; and 3) A structural relationship to a capable fault according to characteristics (1) or (2) such that movement on one could be reasonably expected to be accompanied by movement on the other.

2.4.3 Active Faults in Thailand

Hinthong (1995, 1997) reviewed the present status of the study of active faults program in Thailand (see Figure 1.7). Apart from the knowledge of the importance of understanding of active faults, the various basic concepts, principles or even the implications have been laid out for refining. Approaches towards refining their definitions and classifications, as well as their criteria for recognition of active faults have been compiled from various sources. The importance of active fault evaluation to society is that it provides the basis for design, siting, zoning, communication, and response to earthquake hazards. It is necessary for all types of major engineering structures in order to reduce potential loss of life, injury, or damage.

According to various authors and researchers, three approaches to define active faults can be distinguished and applied. These three definitions are characterized as general technical definition, engineering definition, and regulatory definition. Those three applications of definitions were discussed, based primarily on its original definition which was proposed in the context of a two-fold classification

of "dead" and "alive" or "active" faults, and with respect to their potential for future renewal or recurrence of displacement or offset.

In consideration that based upon available data, and with the exclusion of the tentatively inactive and inactive classifications, fault activity can be classified as three classes: active, potentially active, and tentatively active. Basically, there are three major criteria for recognition of active faults, namely, geologic, historic, and seismologic criteria.

In order to cope with the problem of the study of active faults in Thailand, the adoption of active fault classifications, specifically for the benefit of the utilization only in Thailand, four classes have been proposed, namely, potentially active, historically and seismologically active, neotectonically active, and tentatively active faults and fault zones.

Consequently, with the restriction, deficiency of necessary data, and the lack of various seismologic, geodetic, geophysical, and other subsurface methods of analysis, but only supported by some thermoluminescence age dating, the inventory of twenty-two preliminary active faults in Thailand have been outlined. The related purpose was to lay out major faults/fault zones for the preparation of preliminary active faults map of Thailand, scale 1:1,000,000.

Charusiri et al. (2001), therefore, ranked the active faults, based upon historic, geologic, and seismologic data (Table 2.1). Since Thailand is not the main site for present-day large earthquakes as compared with those of the nearby countries, the best definition used herein is from the combination and modification of those above - mentioned definitions. Additionally, the age of the fault is also essential in their justification, it is proposed (Table 2.2) that the fault becomes "active" if it displays a slip movement in the ground at least once in the past 35,000 years or a series of quakes within 100,000 years. If the fault shows only one movement within 100,000 years, it would be defined as "potentially active". Furthermore, if only once in the past 500,000 years, it would be become "tentatively active". All of these faults are expected to occur within a future time span of concern to society. The fault becomes "neotectonic" if it occurred in Pliocene or Late Tertiary, and it is regarded as "(paleo-) tectonic" or "inactive" if it occurred before Pliocene.

Table 2.1 Active fault rank, criteria, and examples in Thailand (after Charusiri et al., 2001).

Rank	Historic	Geologic	Seismologic	Examples
Active (AF):				
<i>Tectonic fault which displays a history of strong earthquake or surface faulting in the past 35,000 yrs, or a series of quakes during 100,000 yrs, and is expected to occur within a future time span of concern to human society.</i>				
		Surface faulting and assoc. strong quakes, also with geodetic evidence.		
		<i>Young Quaternary deposits cut by fault,</i>		
		<i>distinct youthful geomorphic features.</i>		
			Epicenters along that fault.	
				<i>Mae Chan, Phrae, Thoen, Pua.</i>
Potentially Active (PAF):				
<i>A tectonic fault without historic surface offset, but with a recurrence interval sufficient to human concern, and with an earthquake within 100,000 yrs.</i>				
		Surface faulting unclear.		
		<i>Subdued & eroded geomorphic features,</i>		
		<i>faults not known to cut young alluviums,</i>		
		<i>but offset older Quaternary deposits.</i>		
			Alignment of epicenters but with low confidence of assigned locations.	
				<i>Mae Tha, Mae Hong Son,</i>
				<i>Srisawat, Three - Pagoda.</i>
Tentatively Active (TAF):				
<i>A fault with insufficient data to define past activity and its recurrence interval is relatively very long or poorly defined, or displaying an earthquake within 500,000 yrs.</i>				
		Data indicate fault evidences, but evidences may not be definitive.		
		<i>Traced clearly by remote-sensing data with some hot springs.</i>		
			Scarce and low seismicity.	
				<i>Payao, Nam Pat,</i>
				<i>Ranong, Klong Marui,</i>
				<i>Klong Thom, Southern Peninsula.</i>

Table 2.2 Activity of faults in Thailand based upon age-dating data (after Charusiri et al., 2001).

Era	Period	Epoch	Yrs before	Fault activity
C E N O Z O I C	Quaternary	Holocene	0	Active fault is categorized within one of these events: 1) Active - if one quake within 35,000 yrs, or several within 100,000 yrs. 2) Potentially active - if one quake within 100,000 yrs 3) Tentatively active – if one quake within 500,000 yrs Neotectonic fault (difficult to determine-active or inactive)
			11,000	
	Pleistocene			
	Tertiary	Pliocene	160,000	
		Pre-Pleiocene	350,000	(Paleo-)Tectonic fault (or inactive)
			650,000,00	
Pre-Cenozoic				

2.4.4 Pua Fault

Fenton et al. (1997, 2003) investigated the recent paleoseismicities in northern and western Thailand using the evidences of neotectonic geomorphology, seismicity and compared to previous active fault studies in the investigation area. Based on the result of their study, Pua Fault was considered as the active fault. The Pua Fault is a normal fault bounding the eastern margin of the Tertiary Pua Basin. Fault orientation is mainly in the north-south direction with west dip. The 68 km-length (Figure 2.10) lead Fenton et al. (2003) to estimate moment magnitude as M 7 from empirical relationships among rupture length and magnitude (Wells and Coppersmith, 1994). Remote-sensing interpretation reveals that the fault forms a very prominent west-facing scarp. According to their study, the Pua Fault can be divided into three distinct segments, the linear northern Thung Chang Segment, the concave-west central Pua Segment, and the linear southern Santisuk Segment (Figure 2.10).

The most distinct neotectonic geomorphology observed along the Thung Chang Segment is marked by a linear escarpment, comprising triangular faceted spurs, low-angle (about 10 to 15°) scarps (Figure 2.11), and wine-glass canyons.

The 24 km long Pua Segment is concave to the west (Figure 2.10). The central part of this fault segment displays the highest and steepest triangular facets found along the Pua Fault, and also displays some of the best-developed wine-glass canyons in Northern Thailand (Figure 2.12).

The Santisuk Segment comprises the most subdued topography along the Pua Fault, although the fault escarpment displays the same geomorphic features indicative of active faulting. Further evidence for Holocene movement on the Santisuk segment is the exposure of a 30 m wide fault zone offsetting young soil horizons developed in a sequence of alluvial gravels and lacustrine clays in a gravel pit at Ban Hua Na (Figure 2.13). The offset soil horizon is considered to be Holocene in age on account of its lack of reddening and poorly developed rubification (Woodward-Clyde Federal Services, 1996) that means these faults are not older than Holocene period. The most southern part of Santisuk Segment shows small scarp which is about 6 m high. This small scarp is uniformly well developed along the entire Santisuk Segment. The age of alluvial surfaces offset by this scarp is unknown;

however, the lack of incision and preservation of these surfaces suggests that they are likely to be Holocene in age. Assuming that scarp has formed during the Holocene, this 6 m offset implies a minimum vertical displacement rate of about 0.6 mm/yr.

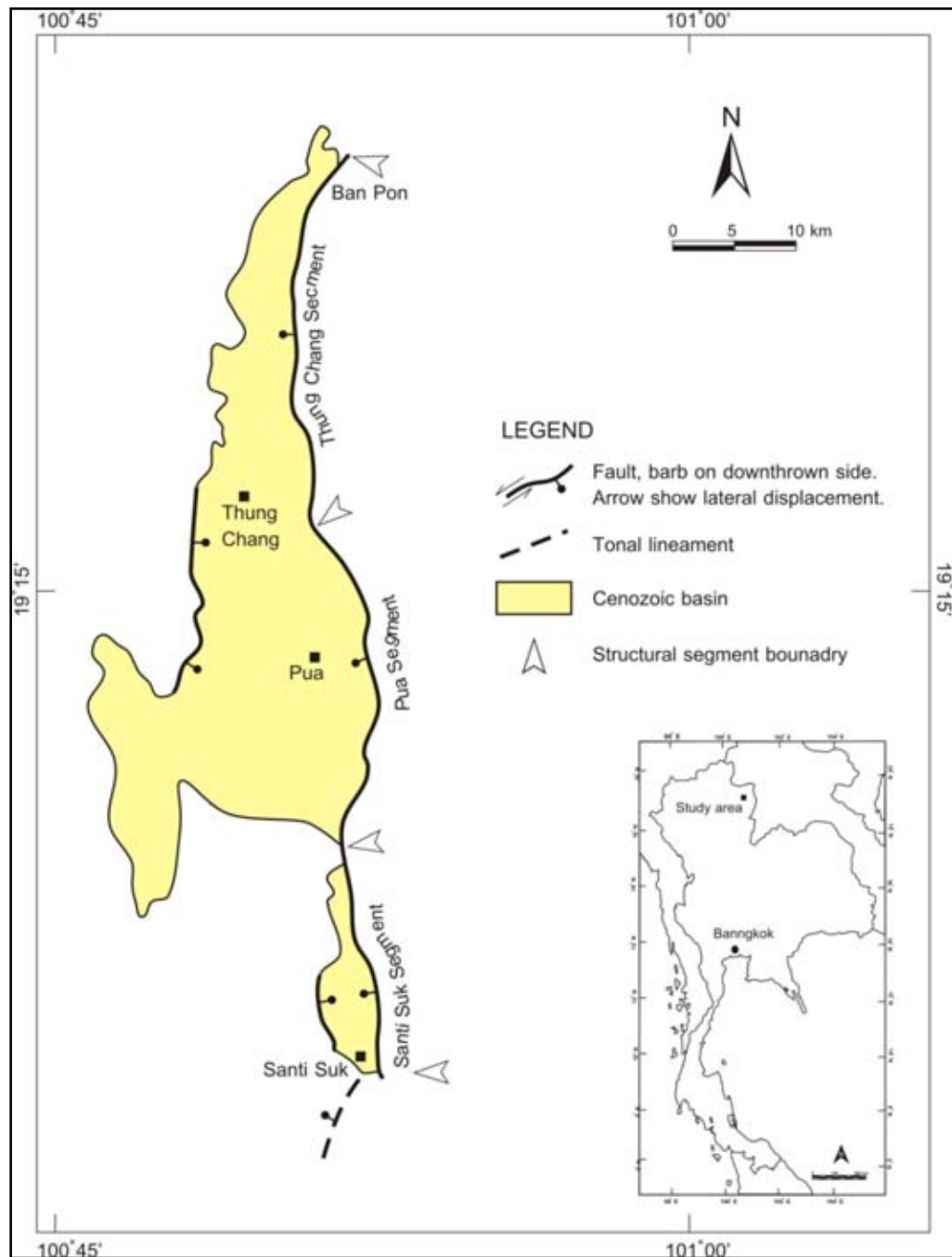


Figure 2.10 Simplified map of the Pua Fault System showing fault segments and localities mentioned in the text (Fenton, 2003).



Figure 2.11 Low angle fault scarp on surface of Late Quaternary alluvial fan, Thung Chang Segment, Pua Fault (Fenton et al., 2003).



Figure 2.12 Wine-glass canyon developed where the Nam Khun crosses the Pua Fault (Fenton et al., 2003).

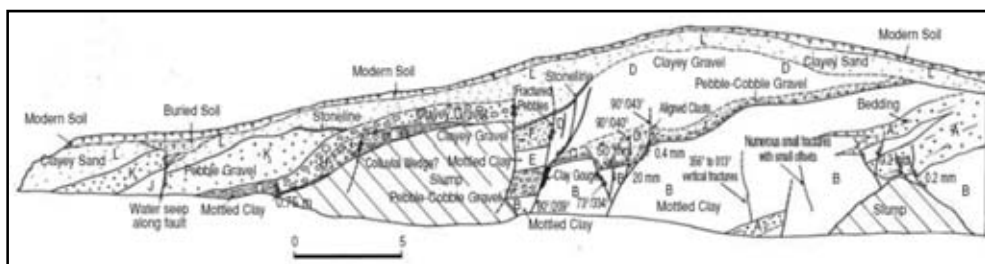


Figure 2.13 Exposure of faulted alluvial gravels and lacustrine clays at the southern end of the Pua fault overall sense of displacement is down-to-the-west (Fenton et al., 2003).

CHAPTER III

REMOTE-SENSING INTERPRETATION

In this thesis chapter, description is divided into three sections. The first section is supposed to investigate geological lineaments and Cenozoic basins interpretation in a regional scale using Landsat 7 ETM⁺, ASTER, and SRTM DEM imageries. The second section describes fault segmentation of the Pua Fault and criteria used. The last section is focused on the detailed study of tectonic geomorphology and results on morphotectonic interpretation of individual selected segments. In addition, morphotectonic maps, which include fault branches and neotectonic evidence of fault movements, are also shown in this chapter.

3.1 Results from satellite images interpretation

The author applied remote-sensing data for analyzing and interpreting geology and structures in a regional scale using Landsat 7 ETM⁺ and ASTER imageries. The area under investigation lies within the latitudes 17° 45' to 20° 00' N and longitudes 99° 50' to 101° 50' (see Figure 1.3). The purpose is to investigate whether or not the studied faults in the area can be linked to the so-called “Pua Fault” which is considered to be ‘active’ in northern Thailand. This step is required for the next step-paleoseismic trenching and TL dating sampling.

3.1.1 Satellite image acquisition

The satellite images are used widely as fundamental knowledge for land planning, land use, infrastructure design, and geological investigation. Nowadays, satellite images are essential to study earthquake geology. Basic concept of space-borne image is to collect data from objects or landscape features (Figure 3.1) with measured electromagnetic radiation with any wavelengths (Figure 3.2) that reflected or emitted from the objects or terrain and convert electromagnetic signal to an image. Any objects on earth can be reflected or emitted the electromagnetic radiation with vary wavelengths called “spectral signature” (<http://rst.gsfc.nasa.gov>). These spectral signatures are important property to identify differential of each material type as shown in the Figure 3.3, sand material can be reflected more energy than green vegetation but at other wavelengths it absorbs more (= reflects less) than does the vegetation. In

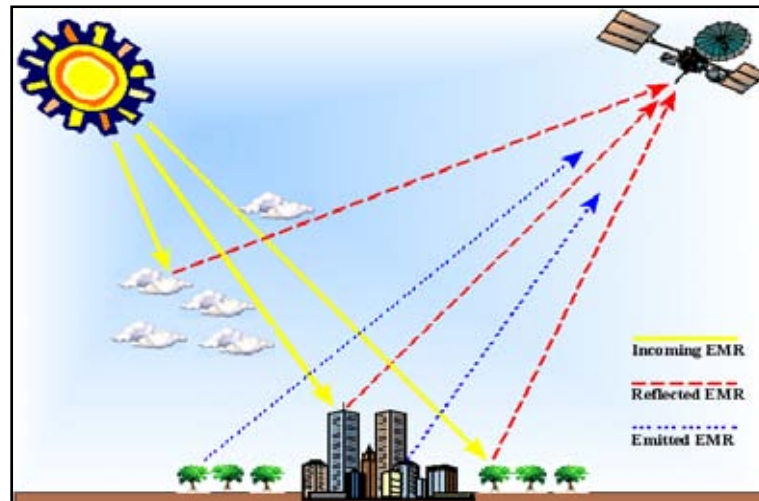


Figure 3.1 Electromagnetic radiation (or EMR) spread from sun impact to earth and reflex to atmosphere. Satellite can be detected these electromagnetic wave and convert to image. (www.ellie.cla.sc.edu)

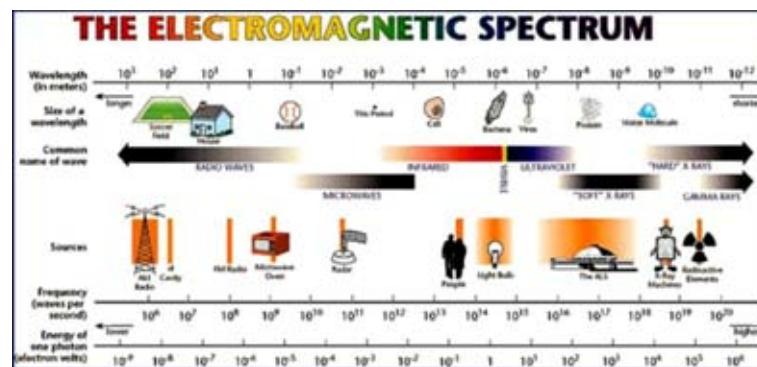


Figure 3.2 Electromagnetic wavelength with low frequency to high frequency, such as radio wave, microwave, visible wave, ultraviolet wave and grammar ray (<http://www.nasa.gov>).

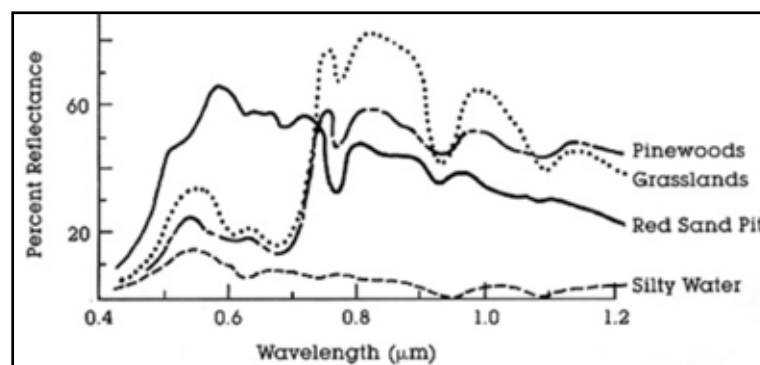


Figure 3.3 The reflection of electromagnetic wave of each object on earth (<http://www.nasa.gov>)

principle, we can recognize various kinds of surface materials and distinguish them from each other by these differences in reflectance. These concepts are useful to separate the geological materials and geological structures in the study area.

3.1.1.1 Landsat 7 ETM⁺ Imagery

The Landsat 7 satellite was successfully launched from Vandenburg Air Force based on April 15, 1999. A satellite image scene covers a land area approximately 185 kilometers (across-track) by 180 kilometers (along-track). The Landsat 7 system is designed to collect 8 spectral bands or channels of reflected electromagnetic radiation, Visible wavelength is consist of band 1-3, Infrared wavelength is consist of band 4, 5 and 7. Band 6 for thermal infrared wavelength and band 8 for panchromatic as shown below.

Band No.	Wavelength Interval (μm)	Spectral Response	Resolution (m)
1	0.45 - 0.52	Blue-Green	30
2	0.52 - 0.60	Green	30
3	0.63 - 0.69	Red	30
4	0.76 - 0.90	Near IR	30
5	1.55 - 1.75	Mid-IR	30
6	10.40 - 12.50	Thermal IR	120
7	2.08 - 2.35	Mid-IR	30
8	0.52-0.92	Panchromatic	15

The Landsat 7 ETM⁺ images are used for this thesis supported by The Global Land Cover Facility's website (<http://glcf.umiacs.umd.edu>). The study area covers Landsat 7 ETM⁺ scene for 6 scenes including as shown below.

	Path/Row	Data of Acquisition	Spectral Bands (no.)	Spatial Resolution (m)
1.	129/46	2-11-2000	7	30 m (MX), 60 m (TI)
2.	129/47	2-11-2000	7	30 m (MX), 60 m (TI)
3.	129/48	2-11-2000	7	30 m (MX), 60 m (TI)
4.	130/46	25-12-1999	7	30 m (MX), 60 m (TI)
5.	130/47	25-12-1999	7	30 m (MX), 60 m (TI)
6.	130/48	14-3-2000	7	30 m (MX), 60 m (TI)

3.1.1.2 ASTER Imagery

The ASTER (Advanced Space Borne Thermal Emission and Reflection Radiometer) image is taken from Terra satellite that launched in October, 1999 and each image scene covers an area of approximately 60 kilometers (across-track) by 60 kilometers (along-track). The ASTER image consists of electromagnetic signals in several wavelengths from Visible Wavelength to Thermal Infrared similar to those of Landsat 7 satellite, but ASTER image contains more separated spectral bands. A total of 14 bands with resolution ranging from 15 m to 90 m as shown below.

Subsystem	Band No.	Spectral Range (μm)	Spatial Resolution	Signal Quantization Levels
VNIR	1	0.52 - 0.60	15 m	8 bits
	2	0.63 - 0.69		
	3N	0.78 - 0.86		
	3B	0.78 - 0.86		
SWIR	4	1.600 - 1.700	30 m	8 bits
	5	2.145 - 2.185		
	6	2.185 - 2.225		
	7	2.235 - 2.285		
	8	2.295 - 2.365		
TIR	9	2.360 - 2.430	90 m	12 bits
	10	8.125 - 8.475		
	11	8.475 - 8.825		
	12	8.925 - 9.275		
	13	10.25 - 10.95		
	14	10.95 - 11.65		

The ASTER images for interpretation in this thesis are supported by Earth Remote Sensing Data Analysis Center (ERSDAC), Japan. The amount of ASTER image scene is 3 scenes as follow.

	Scene No.	Data of Acquisition	Spectral Bands (no.)
1.	ASTL1B0412310353050501140927	31-12-2004	14
2.	ASTL1B0412310353140501140928	31-12-2004	14
3.	ASTL1B0412310353230501140929	31-12-2004	14

3.1.1.3 SRTM DEM and ASTER DEM data

DEM or Digital Elevation Model is represented to the topography on earth surface. The DEM data for the structural interpretation in this thesis is composed of SRTM DEM and ASTER DEM. The SRTM DEM data can be detected by

spacecraft under SRTM (Shuttle Radar Topography Mission) project. It can be downloading from USGS website (<http://srtm.usgs.gov>). The study covers 2 scenes of SRTM DEM as follow

	Band No.	Data of Acquisition	Spatial Resolution
1.	srtm_56_09	25-6-2004	90 m
2.	srtm_57_09	25-6-2004	90 m

The ASTER DEM data are detected by Terra satellite under ASTER project supported from ERSDAC. The study area covers 3 scenes of ASTER DEM including

	Scene No.	Data of Acquisition	Spatial Resolution
1.	AST3A1 0103010411160308050653	1-3-2001	15 m, 30m, 90m
2.	AST3A1 0103010411250308050654	1-3-2001	15 m, 30m, 90m
3.	AST3A10103010411340308050703	1-3-2001	15 m, 30m, 90m

3.1.2 Result from Landsat 7 ETM⁺ images and SRTM DEM interpretation

Satellite and space-borne images for geomorphotectonic investigation in this research are integrated data from LANDSAT 7 ETM⁺ and DEM data acquired during 1999-2004. All of satellite data are collected in digital platform and using ENVI software for image enhancement and identification. In this study, lineaments and Cenozoic basins were performed by visual justification with the assistance of ArcGis software. For the image processing and enhancement, the author used methods, such as false-coloured composite, principle component, band ratio, contrast stretching, and topographic modeling. These methods are helpful with the best image appearance and useful for delineation of major structures and Cenozoic basins.

3.1.2.1 Lineaments

In an attempt to understand regional characteristics and patterns of geological lineaments in the study area and nearby, Landsat 7 ETM⁺ imageries and SRTM DEM data were conducted for lineament interpretation approach. The Landsat 7 ETM⁺ image with scale 1: 250,000 is a false-coloured composite, bands 4, 5, and 7 represented in red, green, and blue (Figure 3.4), respectively The other is false-coloured composite of spectral band 6 (red), band ratio 3/2 (green), and band ratio 4/5 (blue) (Figure 3.5). In addition, SRTM DEM data was taken on June 25, 2004 and were used for creating a hill shade image or virtual terrain model as shown in Figure

3.6. Those images as mentioned above covers the eastern part of northern Thailand and nearby areas.

The interpretation result from both enhanced Landsat 7 ETM⁺ images and SRTM DEM for neotectonic evidence is displayed in Figure 3.7. The false-colored composite (red, green, and blue) are digitally added to the image data. Practically, hill shade image interpretation is used to assist in delineating large scale neotectonic features and to define orientations and directions of the investigated fault segments (McCalpin, 1996). The result shows the appearance of several neotectonic features including fault scarps, triangular facets, offset streams, and shutter ridges. Based upon Landsat and DEM interpretation, there exists a series of faults trending in the northeast, northwest, and north directions (Figure 3.8). The major lineaments or fault lines are in the northeast direction and extend from northern Thailand including the surveyed area through Thailand – Lao border to the western part of Lao PDR. In Thailand, northeast striking lineament is part of The Northern Thailand and Uttaradit Fault. Zones Earlier works (such as Polachan, 1988) considered these fault zones caused the opening of Cenozoic basins. And the two minor trends of lineaments and faults lie in north to north-northeast and northwest direction with short length than major trend. As shown in Figure 3.7, most of lineaments which oriented in northeast-southwest and northwest-southeast direction situate in the area of base rocks, whereas the lineaments in north-south direction situate along basin boundary such Pua, Santisuk and Nan Basin.

3.1.2.2 Cenozoic basins

Based on Landsat images and DEM data interpretation, the study region contains many of Cenozoic basins as Lampang, Phayao, Phare, Pua, and Nan Basin and lot of small basins both in Thai and Lao PDR side (Figure 3.7). They are well recognized in remote sensing images by relatively low-relief and gentle slopes to flat-lying areas (see Figure 3.4) when compared with those of the older rocks (mountainous area). Most of the basins have elongate shape and oriented in the north-south direction or following the main structure.

The important basins in the study area are Pua and Nan basins. Pua Basin is about 40 km north of Nan area near Thai-Lao PDR border and is obviously seen in satellite and DEM images because most basins are bounded by fault lines (see Figure 3.12).

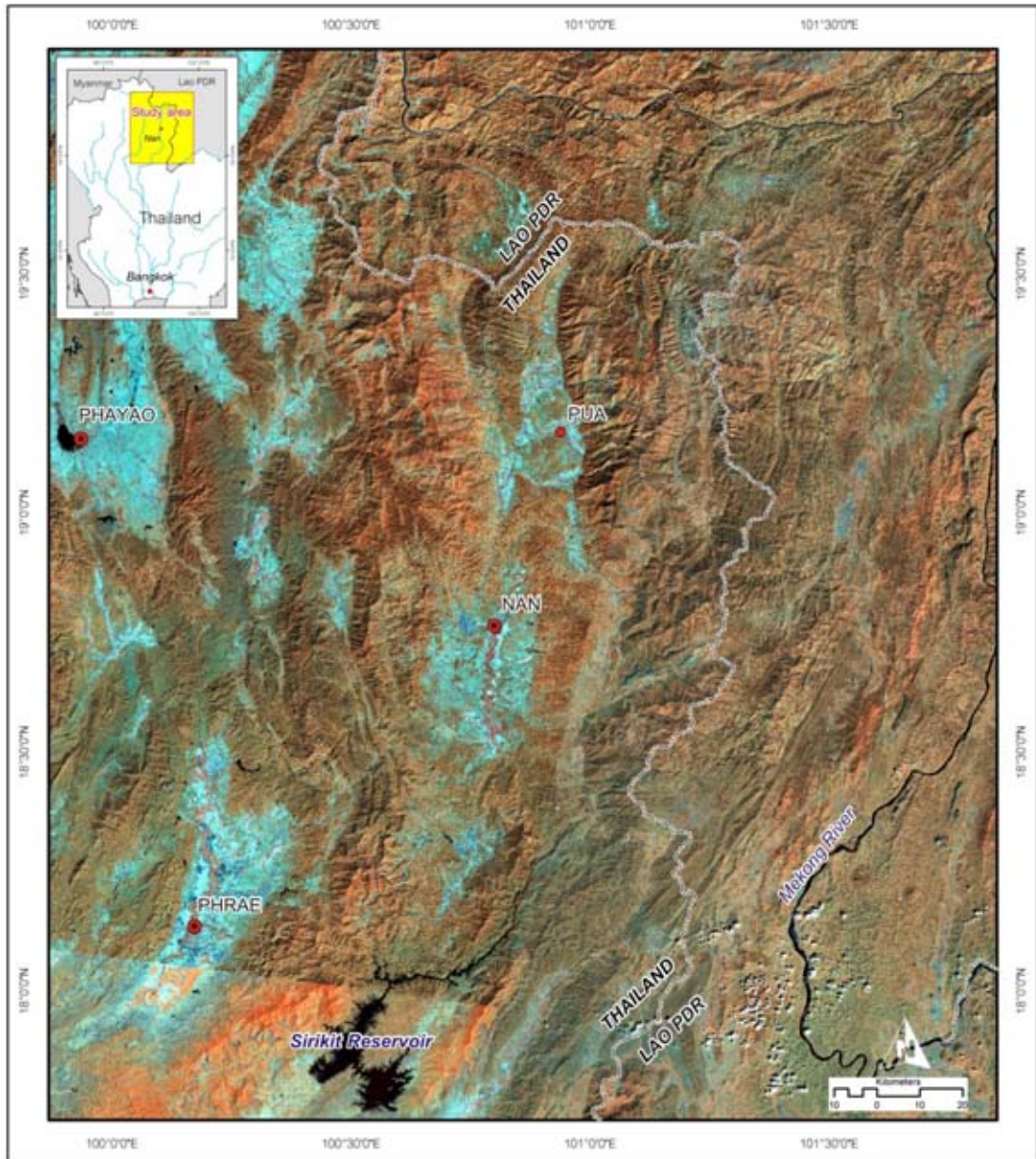


Figure 3.4 Enhanced Landsat 7 ETM⁺ by using the false-colored composite image data of bands 4 (red), 5 (green), and 7 (blue) showing physiographic features of the study area covered the eastern part of northern Thailand and western part of Lao PDR. Note that there exists some contrasting structural features between eastern and western blocks of the roughly N-trending Pua-Nan-Sirikit Reservoir zone, suggesting the difference in tectonic regime between the two blocks.

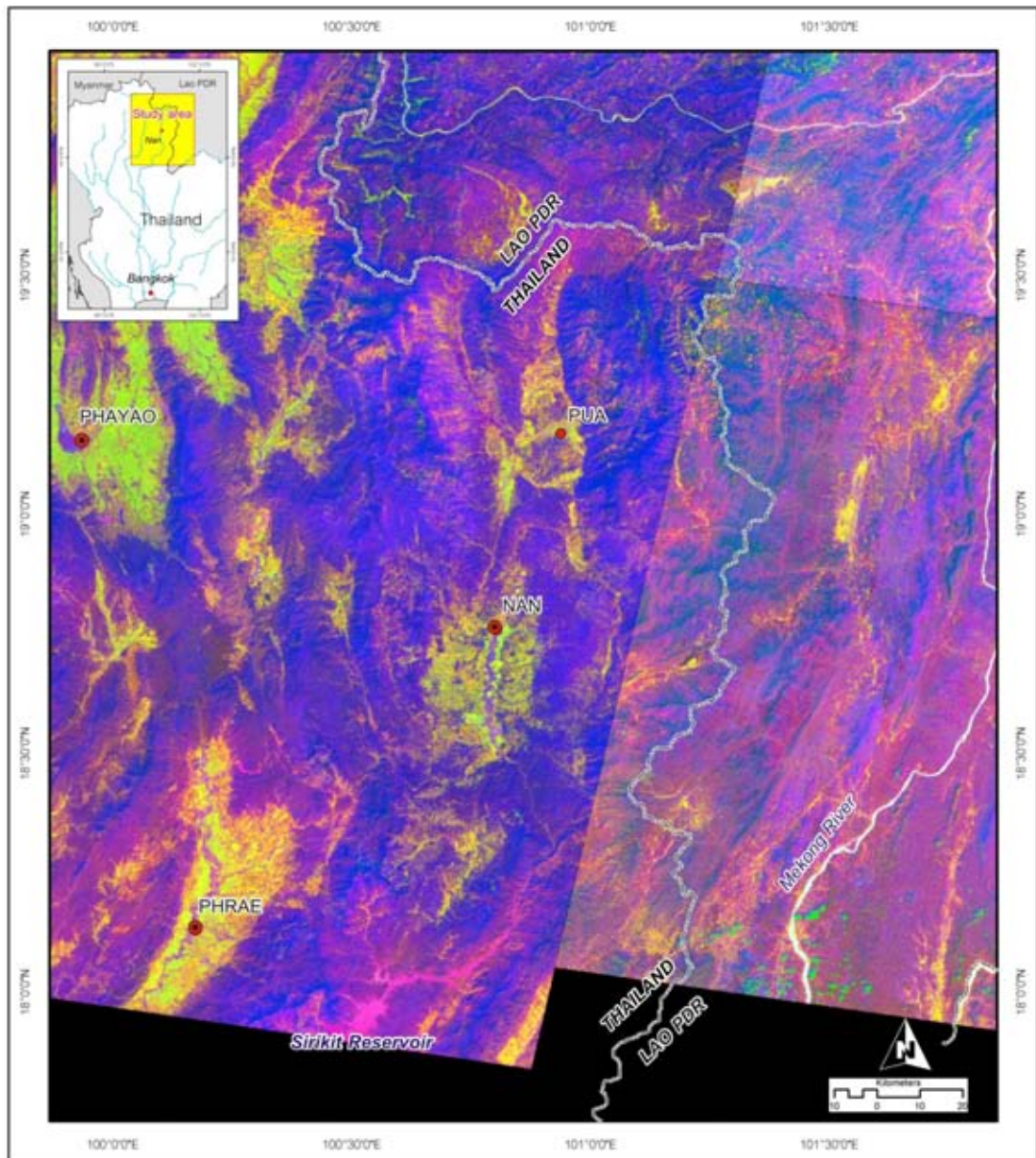


Figure 3.5 Enhanced Landsat 7 ETM⁺ by using the false-colored composite image data of bands 6 (red), band ratio 3/2 (green), and band ratio 4/5 (blue) showing physiographic features of the study area covered the eastern part of northern Thailand and some part of Lao PDR. Note that identification of Cenozoic basins (shown herein as yellow-coloured) can be done easily after the enhancement process, and that a sharp lineament in the north-northeast trend connecting the Pua and the Nan basins. Interpreted result is shown in Figure 3.8.

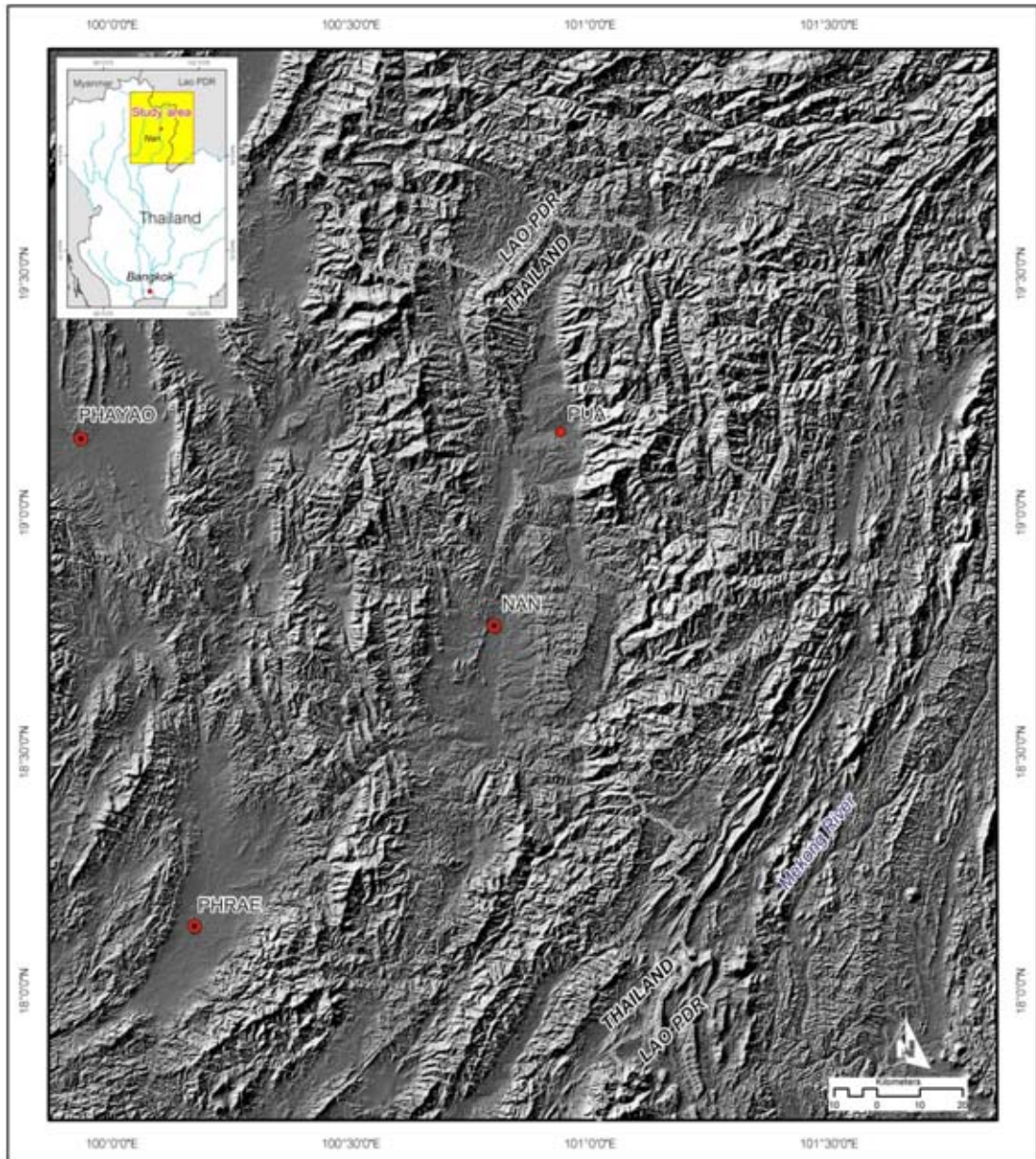


Figure 3.6 Shade relief image from SRTM DEM data taken on February 11, 2000 showing contrasting hard-rock geology and structures between western and eastern blocks of the Pua-Nan-Sirikit Reservoir zone. Note that not many Cenozoic Basins occur in east of the Pua-Nan-Sirikit Reservoir zone. Also shown is a series of the ENE-trending faults in the eastern block that is quite distinct and non-cut the major structures and lithologies. See also Figure 3.7 for interpretation.

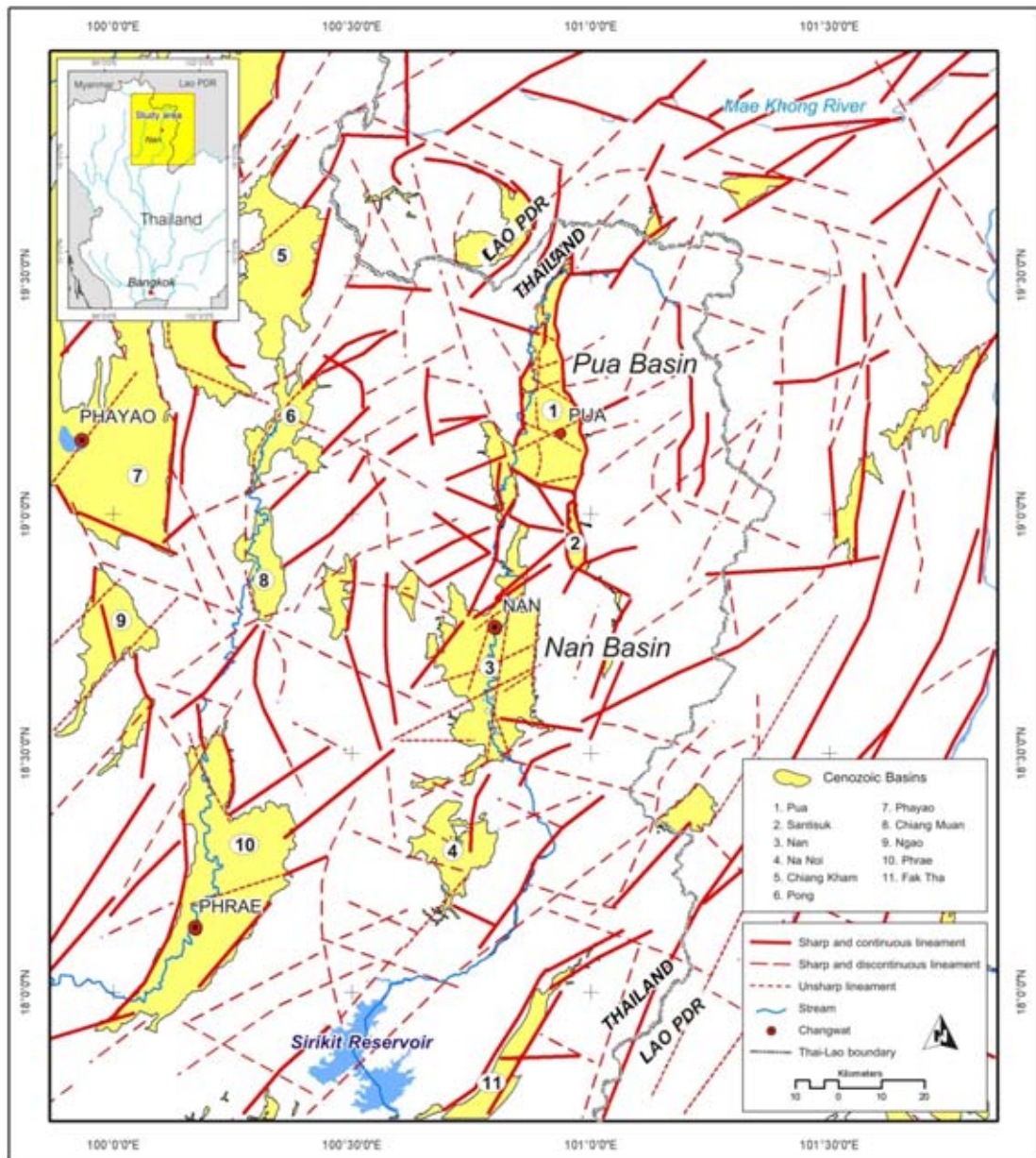


Figure 3.7 Map of the study region showing distribution of lineaments and Cenozoic basins interpreted using the enhanced Landsat 7 ETM⁺ image and SRTM DEM data in Figures 3.5 and 3.6. Note that Pua Basin contains more distinct sharp lineaments than those of Nan Basin.

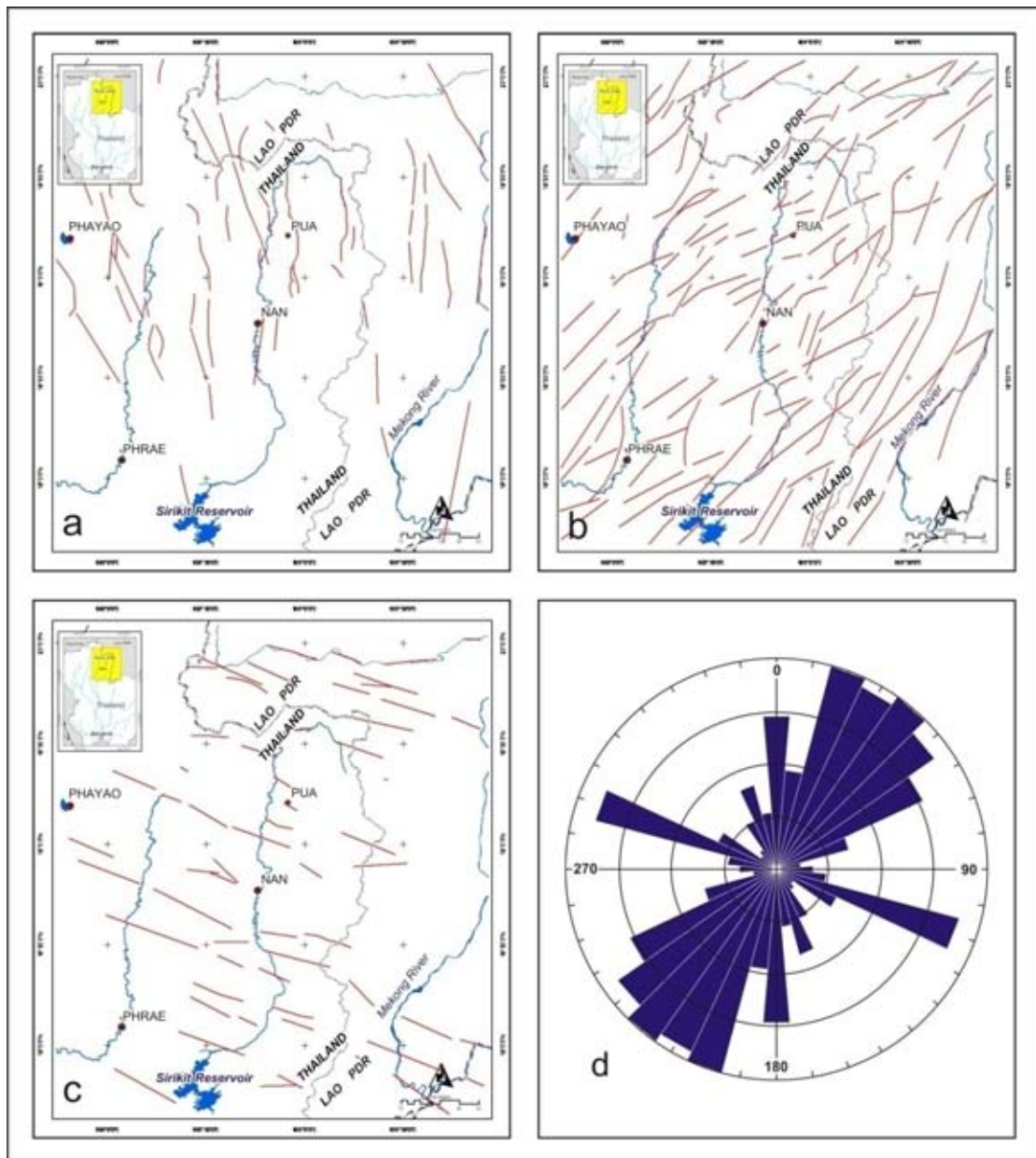


Figure 3.8 Lineament maps after filtering process of enhancement showing a) the north-south-trending with 45 lineaments, b) the northeast-southwest-trending with 119 lineaments, c) the northwest-southeast-trending with 224 lineaments. d) Rose diagram based on 224 points with the majority of the lineaments in the northeast-southwest direction.

The basin orients in north-south direction, the upper part of the basin is narrow (about 5 km) and the lower part is much wider (about 20 km). The western and eastern boundaries of Pua Basin are fault bounding and well recognized in satellite images. On the other hand, Nan Basin located southward of Pua Basin and the geometry of Nan Basin is shorter than Pua Basin but more widely. The width of the Nan Basin is about 25 km and the length is about 60 km. If compare to Pua Basin, Nan Basin has low relief and morphotectonic evidences are occurred in this area is not sharp as the Pua Basin.

3.1.3 Result from ASTER images interpretation

The author applied ASTER high resolution image with the resolution of 15 x 15 m. for analyzing and interpreting geology and structures in a large scale. The area under investigation covers both Pua and Nan basins and lies within the latitudes 18° 24' to 19° 38' N and longitudes 100° 32' to 101° 9' (Figure 3.9). The purpose is to investigate in more detail for neotectonic evidence, lineaments or fault lines and lithological classification. In the ASTER interpretation false-coloured composite method with bands 3, 2, and 1 represented in red, green, and blue (Figure 3.9), respectively, and another one is false-coloured composite of spectral band 6 (red), 3 (green), and 1 (blue) (Figure 3.10). In addition, ASTER DEM data is used for creating a hill shade image showing realistic topographical model (Figure 3.11). The images as mention above covering most of Changwat Nan and adjacent areas were applied for analysis as well (Figure 3.9 -3.11). Identification of lineaments was performed by visual justification. Traceable lines are applied to the GIS database using the ArcGis program.

3.1.3.1 Lineaments

The study area covers the whole parts of Pua, Santisuk, and Nan basins with the Nan River as a major channel, flowing from the north to the south (Figure 3.12). Results from ASTER images enhanced by ENVI software indicate that most major lineaments or fault lines are in the northeast-southwest trend and two minor in the north-south and northeast-southwest trends. Those major lineaments are with 2-40 km-long and parallel to the main structures similar to those of the Landsat image. Most lineaments occur in base rocks on both west and east of the study area (Figure 3.13). The minor north-south trending faults are well recognized in the middle part of

the study area. On the remote sensing images, north-south striking faults obviously occurred at the contact boundary of the basin and the mountainous area. However the faults in the basin are not well observed. The important north striking fault is basin-bounding fault at the eastern flank of Pua Basin and extends continuously to Santisuk basin called “Pua Fault”. The Pua fault is proposed by Fenton et al. (1997). However both Fenton et al. (1997) and Charusiri et al. (2001) considered this fault as the active fault (Figure 3.12). In Nan Basin, as observed in Figure 3.9, 3.10 and 3.11, we can observe faults in the north-south direction similar to those of Pua Basin but the occurrence of faults are not as clear as those found in Pua Basin. Based on remote sensing interpretation, several geomorphotectonic evidences, such as triangular facets, fault scarps and offset streams are well recognized along the basin-bounding faults. Additionally, the other minor lineaments with the northwest-southeast trend are observed, however, most of them appear in the base rocks area (Figure 3.13).

3.1.3.2 Lithological classification

The lithological classification is based largely on ASTER images interpretation integrated with ground-truth survey and fundamental geological map at a scale of 1:50,000. Concentration or more detailed work is placed on investigating action of young sediments in Pua, Santisuk and Nan basins; the result of study was presented as detailed geological map (Figure 3.12). Sediments and rocks occurring in the study area are herein grouped into 5 units. They are summarized in an ascending sequence from the oldest to the youngest, as shown below.

The unit 1: Base rocks

Base-rock unit was designed as the lowermost unit present in the study area. Rocks of this unit are exposed both in Thailand and Lao PDR. They are (meta-) sedimentary rocks and volcanic rocks with minor granitic rocks. Based mainly on the previous work investigation, the rocks in this unit were deposited from Permian throughout Cretaceous age.

Most faults occurring in the base rocks are mainly “old” or “inactive” faults, however some are considered as “active”. Major base rocks are marine clastic rocks of Permo-Triassic ages, including sandstone and shale with minor tuffaceous rocks, were cut by the in active, northwest- and northeast-trending fractures and faults. However some are in the contact with Quaternary alluvial deposits by the

north-trending active faults, such as those found in the east of Ban Thung Ao, Ban Tuad and Ban Ngob Nao villages. The other base rocks are the non-marine clastic rocks of Mesozoic age. These base rocks are cut by the northwest-trending inactive faults, such as Ban Don Sop Pua village. Nonetheless, some rocks are found with the boundary contact with the Permo-Triassic rocks with the prominent sharp fault contact, such as to the west of Ban Sop Yao village. In the north of Santisuk Basin, the granite base rocks of Triassic age are in contact with the Quaternary sediments by the active fault of the Santisuk segment, such as those found at Ban Thung Hao, Ban Rai Pattana and Ban Nam Yao.

Unit 2: Tertiary semi-consolidated sediment

This unit is well recognized in satellite images (Figure 3.10), as dark pink colour) with relatively gentle-slope topography and undulating terrain with low resistance as compared with those of the base rocks. In the study area, this unit is dominantly presented in the central part of Pua Basin and the northern and southern parts of Nan Basin. Most of Tertiary sediments exhibit semi-consolidated nature and are mainly gravels, sands, silts, and clays. In several areas, particularly north of Thung Chang District (Ban Thung Ao and Ban Thung Sun villages), Tertiary rocks are interpreted to represent the alluvial fan deposits which were dissected by the neotectonic faults of the Thung Ao segment.

Unit 3: Upper terrace and colluvium deposit

In the ASTER images (Figures 3.9, 3.10 and 3.11), the unit 3 shows more bright colour and has lower relief than Unit 2. This unit is well exposed along main river valley and on slope close to mountain foot. The unit 3 is poorly sorted and consists mainly of the large angular rock fragments, as observed in exploratory trench and open pits. This unit always contains semi-consolidated to unconsolidated bed like Tertiary deposits. Based on the sedimentological characteristic this unit should be deposited on mountain slopes with short transportation.

In some places, such as Ban Mai Samaki, the unit was observed to be cross-cut by the northeast-trending. However, at the area between Ban Tin Tok and Ban Taud, the northwest-trending fault cut the unit with the right sense of movement.

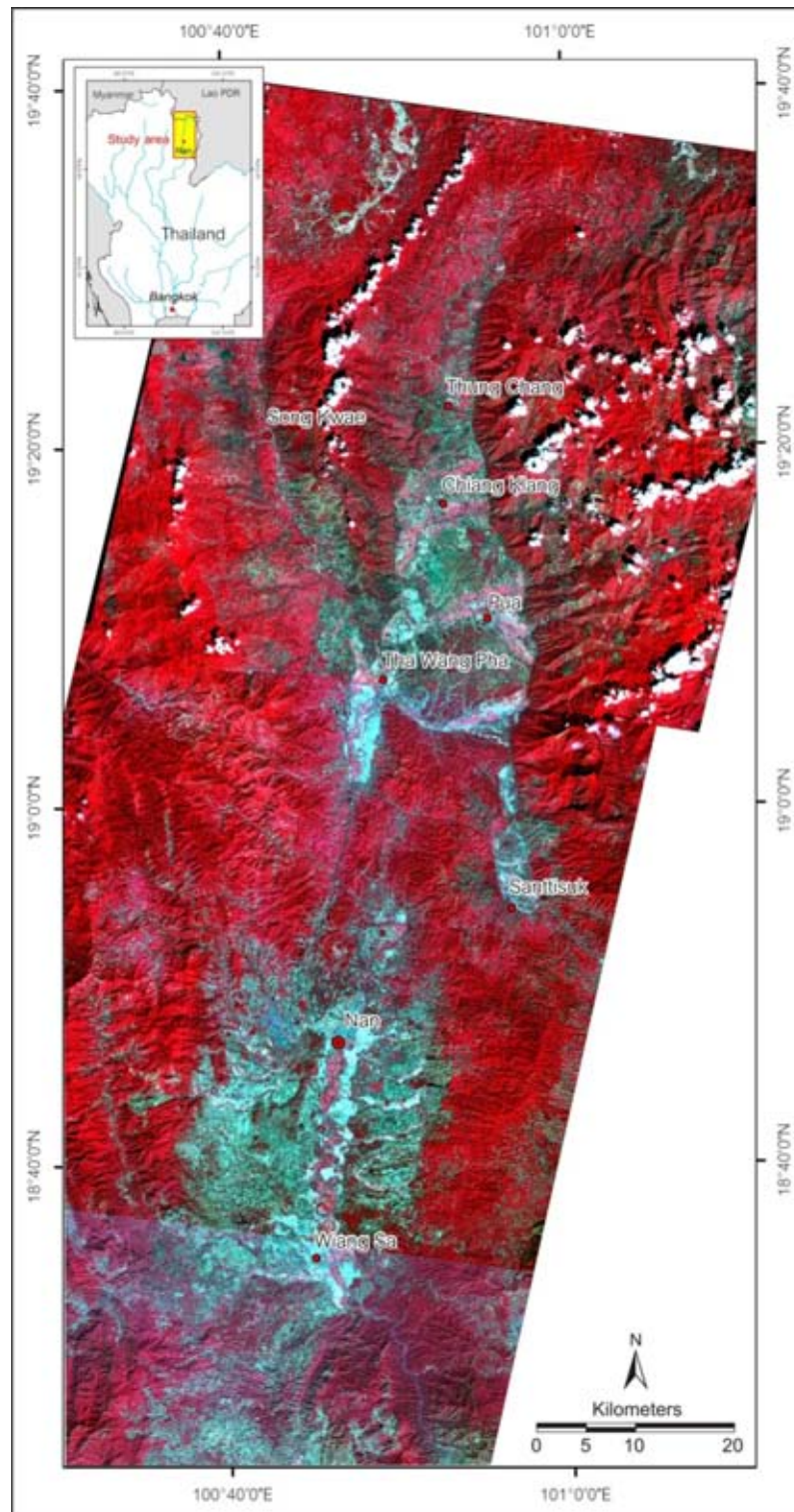


Figure 3.9 Enhanced Aster image by using the false-colored composite image data of band 3 (red), band 2 (green), and band 1 (blue) showing physiographic features of the study area covered. Note that eastern edge (blue/red boundary) of the Pua Basin is quite prominent. There exists the cross structure into the basin in the NE direction from Tha Wang Pha to Pua District. Similar situation also shown at north of Chiang Klang. The Nan Basin shows more subtle features.

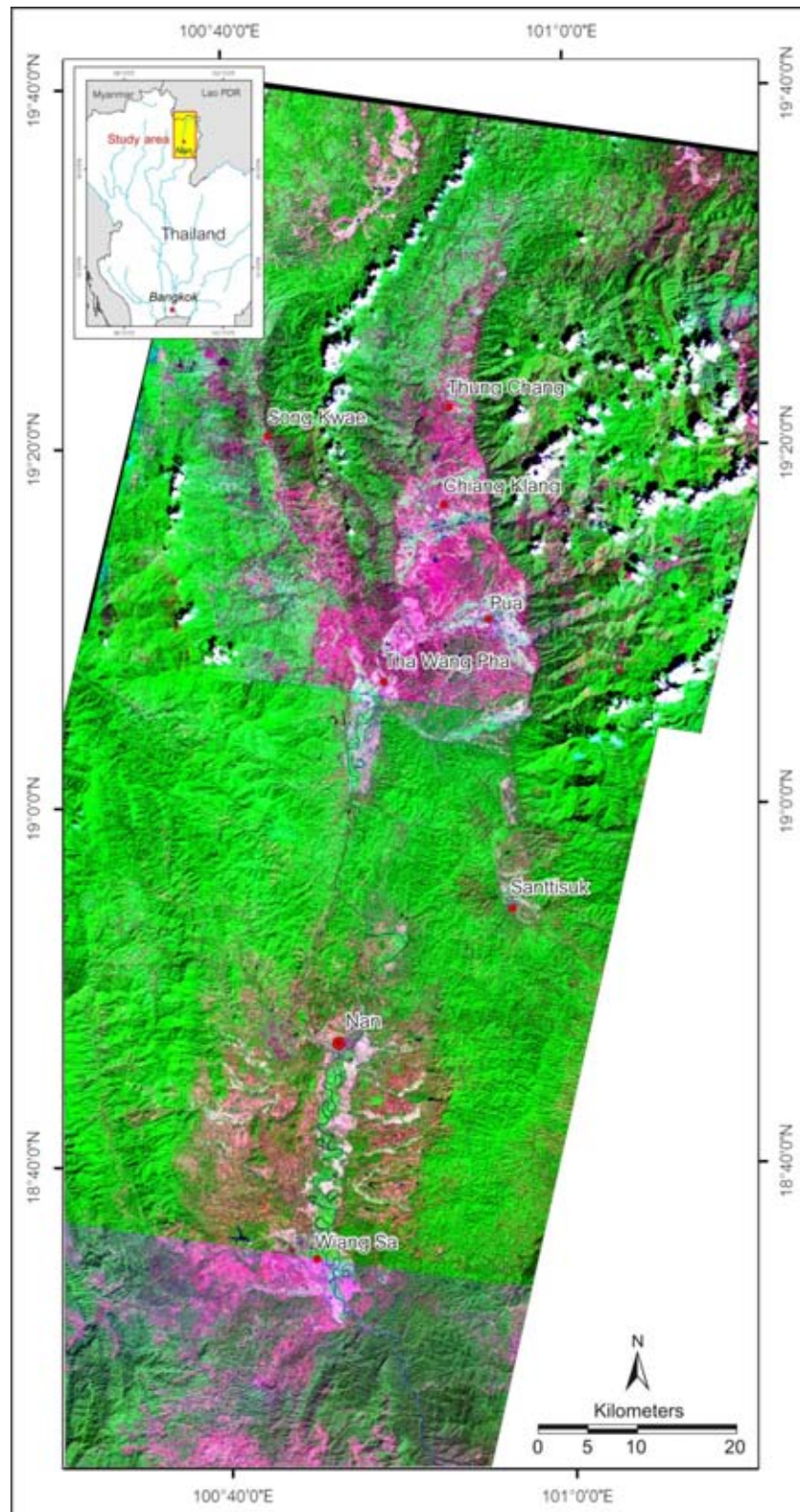


Figure 3.10 Enhanced Aster image by using the false-colored composite image data of bands 6 (red), band 3 (green), and band 1 (blue) showing physiographic features. Cenozoic basins are shown in pink and white and most hard-rock geology is depicted in green. Note that cross structures are clear. Linear features connecting the Pua and Nan basins are also distinct (Interpreted result is shown in Figure 3.12).

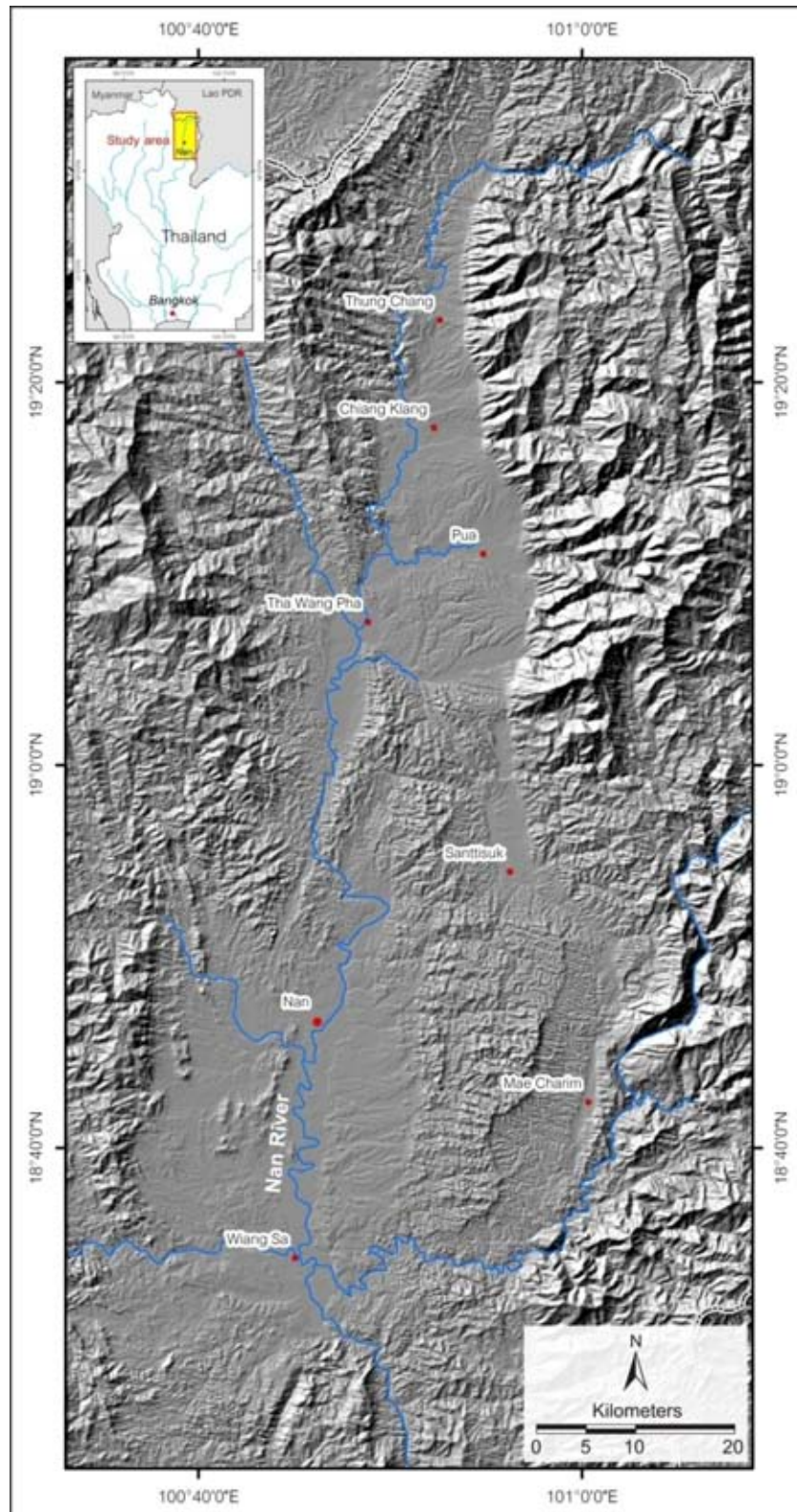


Figure 3.11 Shade relief image from ASTER DEM data showing several morphotectonic landforms of the Nan-Pua study area. Note that the basins are shown as flat terrain or very low relief features whereas the mountainous areas are mainly with high-relief tonation. The interpreted result is shown in Figure 3.12.

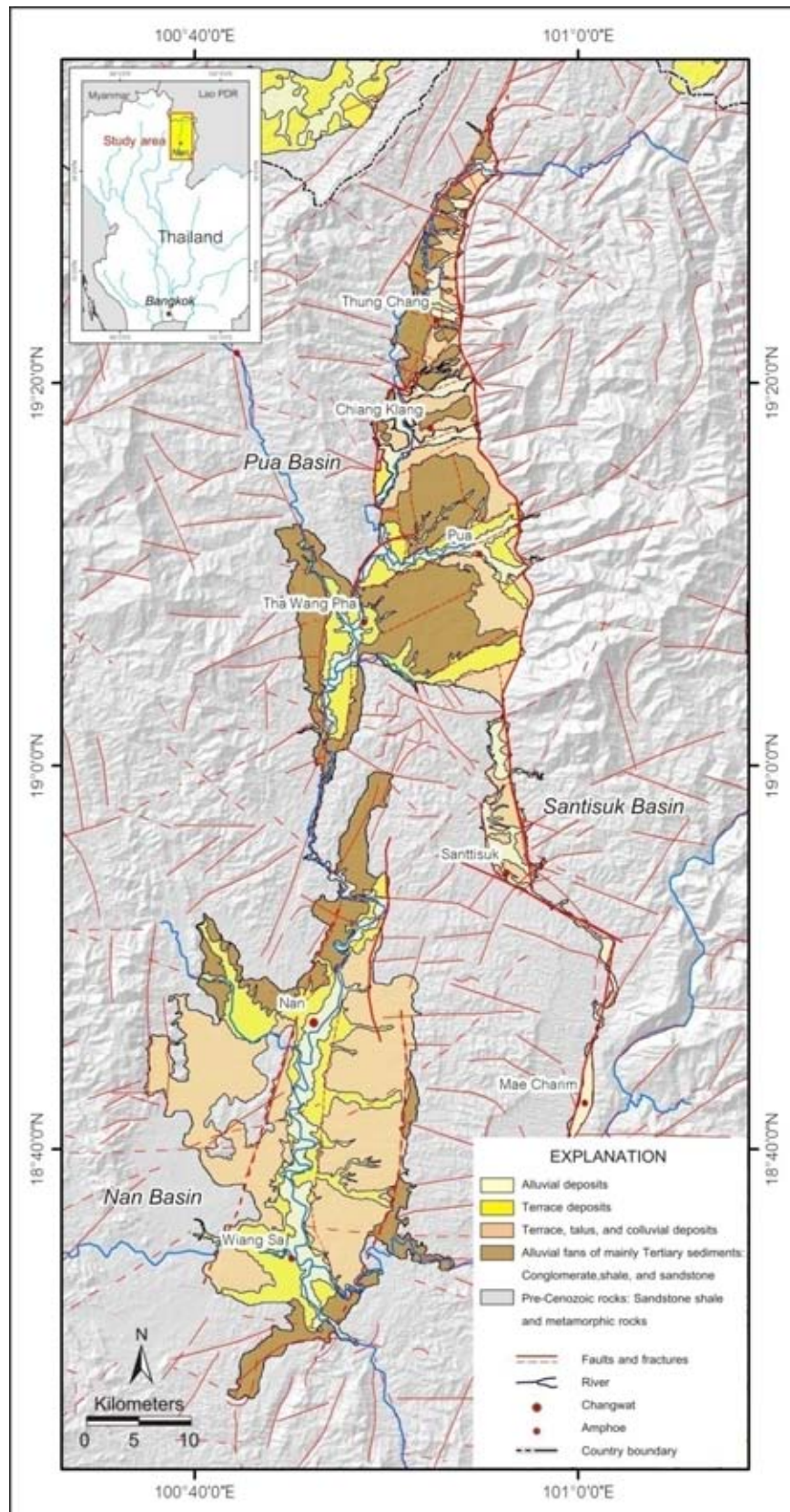


Figure 3.12 Interpretation map using the enhanced Aster images and Aster DEM data in Figures 3.9-3.11 shows major geology of the Cenozoic basin and the essential lineament features. Note that some lineaments cross cut the basins.

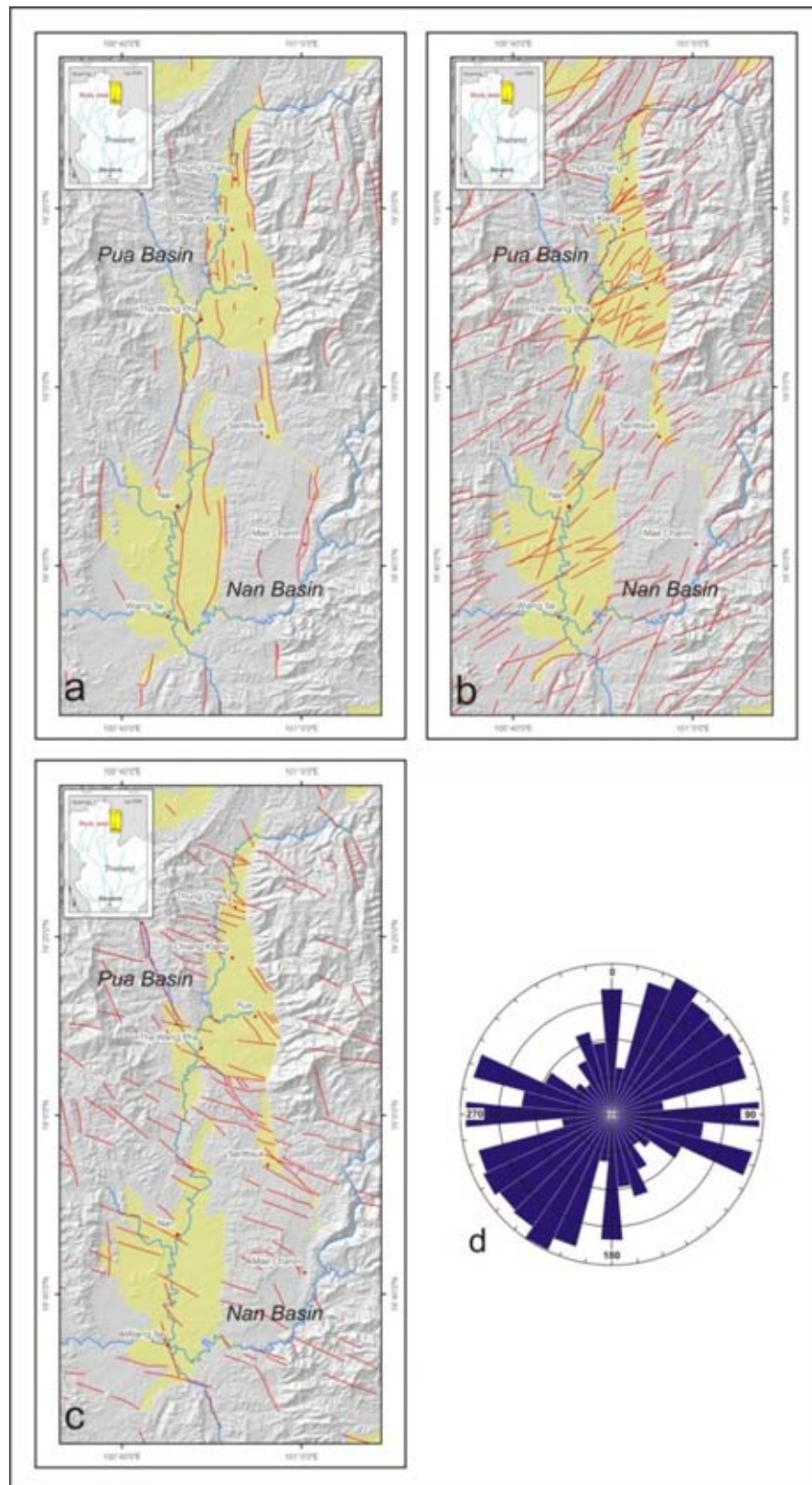


Figure 3.13 Lineament maps after enhancement in the DEM format showing a) the north-trending with 99 lineaments, b) the northeast to east-northeast-trending with 314 lineament c) the northwest-trending with 214 lineaments. d) Rose diagram based on 627 points with the majority of the lineaments in the northeast-southwest direction.

Unit 4: Lower terrace deposit

Lower terrace deposit can be found along the main active stream channels. In the ASTER images (Figures 3.9-3.10), this unit shows bright or white colour because the areas belonging to this unit have no long-life trees. In general, this unit has lower relief than Unit 3. The unit 4 is composed largely of gravel, sand, silt and clay. Satellite image data advocate that they are the unit is flat-lying area with gentle slope angles. In area of Ban Muang Luang village, the northwest-trending fault cut across unit and also the base rocks.

Unit 5: Meandering and flood plain deposit

This unit is well recognized on satellite images with bright colour. The geometry of this unit is banded shape follow the channel line. The unit 5 can be observed both banks of the Nan River and major channels. Especially in Nan Basin, meandering and flood plain sediment is widely exposed along the Nan River (Figure 3.12). This sedimentary unit is composed of sand, silt and gravel layer (see detail in the trench explanation). The thickness of these sediment layers have been varied along the river channels. In the western part of the Pua Basin, particularly in the north of Ban Son Pua, the active stream channel was dissected by the Sob Pua fault segment.

3.2 Fault segmentation

3.2.1 Concept of fault segmentation

Concept of fault segmentation is elucidated by the fact that historical surface rupture triggered by earthquakes along the long faults seldom occurred throughout the entire length, and just only one or two segments became ruptures during large earthquake (McCalpin, 1996). For instance, the San Andreas Fault zone of California was divided into four segments based on difference of historical surface rupture (Allen, 1968). The long fault trace is composed of numerous discrete segments (Segall and Pollard, 1980). The segmentation of fault systems is related to the identification of individual fault segments, based on continuity, character and orientation. It is recommended that a segment can rupture as a unit (Slemmons, 1982). Aki (1984) suggested that the delineation of segments is related to the identification of discontinuities in the fault system. Discontinuity can be divided into two main

groups: geometric and inhomogeneous group. Note that this statement has borrowed from seismologists who have used these terms for asperities and barrier. In addition, it is believed that fault may be segmented at a variety of scale that is from a few meters to several tens of kilometers in length (Schwartz, 1989).

All fault segments have their own boundaries. The segment boundary is a portion of a fault where at least two preferable successive rupture zones have ends (Wheeler, 1989). There are several geomorphic features related to fault boundary or termination. For example, releasing bends and steps, restraining bends, branch and cross-cutting structures, and change in sense of slips are commonly observed at segment termination of strike-slip fault (Knuepfer, 1989). For normal and reverse faults, geomorphic features for definition segment endpoints are not clear (McCalpin, 1996).

Since late 1970s, many workers have found that not all faults have historical rupture records along their fault zone. Thus numbers of criteria have been conducted in order to work on fault segmentation approach such as geometric, structural, geophysical, and geological criteria. McCalpin (1996) had summarized criteria for fault segmentation into five types (Table 3.1). According to new criteria of fault segmentation have arisen, one fault has been segmented by various authors depending upon different criteria. For example, the San Andreas Fault was divided into segments by at least four authors (Table 3.2).

In Thailand, the term “fault segmentation” was first introduced by Fenton et al. (1997) and at least two geologists who show the supporting evidence for fault segmentation, that are - Won-in (1999) and Kosuwan et al. (1999). According to Fenton et al. (1997), two active faults in northern basin and range provinces of Thailand are recognized by fault segmentation, including the Thoen Fault in Changwat Lampang and the Pua Fault in Changwat Nan. Criteria used for segmentation comprise geomorphic feature, structural style, and sense of offset.

Won-in (1999) divided the Three-Pagoda fault in western Thailand into five segments based on structural, geologic, and geometric criteria. Kosuwan et al. (1999) divided the Mae Chan fault zone in Changwat Chiang Rai into four segments based on similar criteria to those of Won-in (1999). According to Udchachon (2002), the study area in the Phare basin, based on remote-sensing, seismicity and field data,

Table 3.1 Types of fault segments and criteria used for active fault in this study mainly following McCalpin (1996).

Type of Segment ^a	characteristics used to define the segment ^a	Likelihood of being An earthquake segment ^b
1. Earthquake	Historic rupture limits.	By definition, 100% ^c
2. Behavioral	1) Prehistoric rupture limits defined by multiple, well-dated paleoearthquakes. 2) Segment bonded by changes in slip rates, recurrence intervals, elapsed times, sense of displacement, creeping versus locked behavior, fault complexity.	High Mod. (26%)
3. Structural	Segment bounded by fault branches, or intersections with other faults, folds, or cross-structures.	Mod.-High (31%)
4. Geologic	1) Bounded by Quaternary basins or volcanic fields. 2) Restricted to a single basement or geologic terrain.	Variable ^d (39%)
5. Geometric	3) Bounded by geophysical anomalies. 4) Geomorphic indicators such as range-front morphology, crest elevation. Segments defined by changes in fault orientation, stepovers, separations, or gaps in faulting.	Low-Mod. (18%)

^a Classification following the segment boundary types of dePolo et al. (1989, 1991) and Knuepfer (1989).

^b Percentages = percent of cases where historic ruptures have ended at this type of boundary, as opposed to rupturing through it (Knuepfer, 1989, Table 3).

^c However, restriction of a single historic rupture to the segment does not mean that all future ruptures will be similarly restricted.

^d Small number of observations, accuracy questionable (Knuepfer, 1989, Table 3).

Table 3.2 Comparison between the Pua Faults from this study and the important active faults as compiled by McCalpin (1996).

Fault name	Type ^a	Number of segments	Total fault length (km)	Mean segment length (km)	Modal segment length (km)	Criteria used for recognition ^b
1. Wasatch fault zone ^c	N	10	343	33	35	B,P,S,G,M
2. NE Basin and Range, >100 kmc	N	10	-	25	20-25	B,P,S,G,M
3. NE Basin and Range, <100 kmc	N	20	-	20	10-20	B,P,S,G,M
4. Idaho ^d	N	20	280	22	20-25	B,P,S,G,M
5. North-central Nevada ^e	N	70	-	10	10	M
6. San Andreas ^f	S	4	980	245	15-175?	B,S,G,M
6. San Andreas ^g	S	7	980	140	300?	B,P,S,M
6. San Andreas ^h	S	784	980	1.2	1	M
6. San Andreas ⁱ	S	68	980	14	12	M
7. San Jacinto ^j	S	20	250	12	10-15	M
8. Elsinore ^k	S	7	337	48	-	M,P
9. Xianshuihel ^l	S	1	220	220	-	M
10. Transverse Ranges ^m	R	-	-	20-30	-	M
11. Oued Fodda, Algerian ⁿ	R	3	32	11	11-12	B,P,S,M
12. Pua	N	14	285	19	6-39	B,P,S,G,M

^aN,normal; S,strike-slip; R,reverse.

^bB,behavioral; P,paleoseismic;
S,structure; G,geological; M,geometric.

^cMachette et al. (1992a).

^dCrone and Haller (1991).

^eWallace (1989).

^fAllen (1968).

^gWallace (1970).

^hWallace (1973).

ⁱBilham and King (1989).

^jSanders (1989).

^kRockwell (1989).

^lAllen et al. (1989).

^lAllen et al. (1989).

^mZiony and Yerkes (1985).

ⁿKing and Yielding (1983).

at least four fault segments within the Phrae fault system have been discovered, namely, the Southwestern, Western, Southeastern, and Northeastern segments. According to Saithong (2006) separated Moei-Mae Ping fault into 10 segments based on similar criteria as the other research.

3.2.2 Results of Fault Segmentation

In 1997 Fenton et al. investigated late Quaternary faulting in northern Thailand, based upon neotectonic geomorphology. They proposed Pua Fault as an active fault, which bounded the western rim of the Pua Basin and is continuous southward to Santisuk basin. The Pua fault is separated into 3 segments, Thung Chang segment, Pua segment, and Santisuk Segment. This thesis is the continuous study after Fenton et al. (1997) as mentioned above. The study has more detail in the remote sensing interpretation and covers the whole area of Pua, Santisuk, and Nan basins.

In this study we use three criteria for fault segmentation which are structural, geological and geometric applied following those purposed by McCalpin (1996). Lineament interpretation using enhancement of Landsat, ASTER and DEM images in previous section plays an important role not only for locating and delineating the fault but also for segmenting fault. Based on the results of fault segmentation integrated with the previous study (Fenton et al., 1997, 2003). The Pua fault system can be divided into 14 fault segments and, viz. Thung Ao (22 km), Ban Doo (9), Den Phana (13 km), Tin Tok (12 km), Santisuk (19 km), Sri Bunruang (17 km), Na Bua (21 km), Nam Ngaen (29 km), Huai Muen (12 km), Sob Pua (10 km), Nam Tuan (20 km), Chom Chan (35 km), Phu Kaeo (39 km), and Wiang Song (6 km). These names are taken from the places along fault zone, such as village or Amphoe (district).

As shown in Figure 3.14, Thung Ao segment is a northern most of basin-bounding fault in the eastern rim of Pua Basin, not too far from Thung Chang Distric. The next segment southward is north-trending Ban Doo segment located to the east of Chiang Klang District. The continuous segment toward the south is Den Phana segment which situated on the east of Pua district and followed by the Tin Tok segment. This segment is the southernmost segment of Pua Basin's eastern rim. Santisuk segment which is bounded the eastern rim of Santisuk basin. Sri Bunruang Segment extends from Santisuk segment southward, but Sri Bunruang segment orients in the northwest-southeast direction. This segment connects Na Bua fault

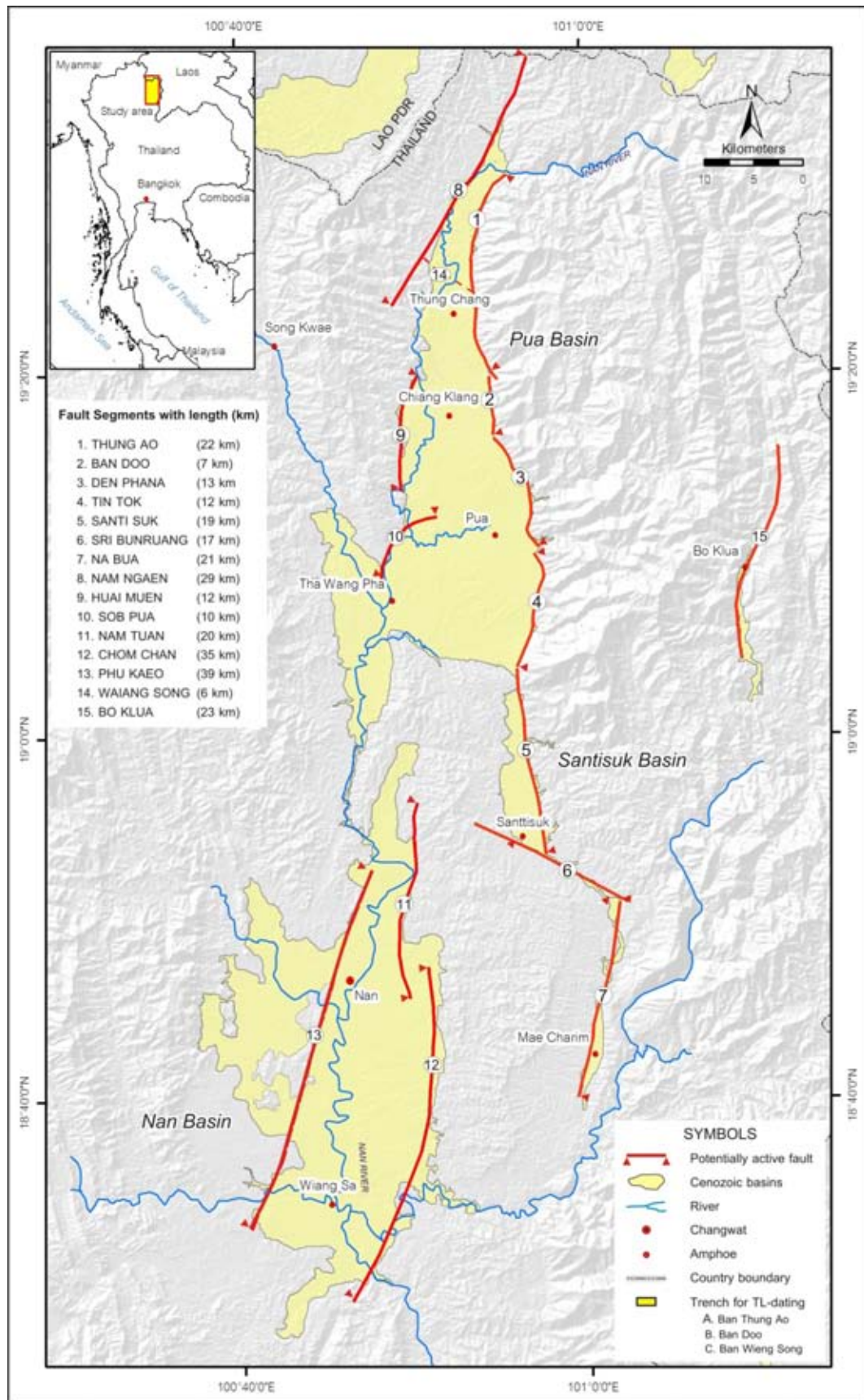


Figure 3.14 Map of the study area displaying locations of the Pua Faults (red line) and its major 14 inferred active fault segments with their length.

segment. The latter is the north-northeast- trending segment. Along the western rims of the Nan-Pua basins, fault segments show different characteristics. They are not continuous and some of which are arcuate-shape. The most prominent is the northeast-trending Nam Ngaen segment which located on the northernmost of western rim of Pua Basin, and the fault segment next to Nam Ngaen segment southward is Huai Muen and Sob Pua segments. The later is more arcuate and shorter than the former. In Nan Basin there are three fault segments, the north-trending Nam Tuan and Chom Chan segments which are located on the eastern rim of Nan Basin but whereas the north-northeast-trending Phu Kaeo is the longest segment located on the western flank of Nan Basin.

Thung Chang Segment of Fenton et al. (1997)'s displays a better-defined continuous lineament, as seen from the satellite image data in this study. Based upon geometrical relationship, it is therefore divisible into 3 fault traces (segments) which show almost discontinuity to one another, including Thung Ao and Ban Doo Segments. Pua Segment can also be separated into 2 segments, Den Phana and Tin Tok segments (Figure 22).

3.3 Neotectonic Evidences and Faulting

3.3.1 Introduction to tectonic geomorphology

In this section, basic concepts of tectonic geomorphology related to three types of faults; strike-slip, normal, and reverse faults, are briefly explained. The description commences with backgrounds criteria used and ends up with the result.

Accordingly, structures associated with an idealized strike-slip fault model constructed by Christie-Blick and Biddle (1985), suggested that these fault branches should be the component of shear zone, which are synthetic, secondary synthetic, and antithetic shears (Figure 3.15). All of these shear zone features are accommodated in principal displacement zone (PDZ).

According to strike-slip fault zone, a variety of structure and landforms can be originated by simple shear including fractures, folds, normal faults, thrust faults, and reverse faults as illustrated in Figure 3.16 (Christie-Blick and Biddle, 1985). Naturally, within a broad shear zone, different generations of motion have produced various kinds of these structures, all of which can be superimposed and

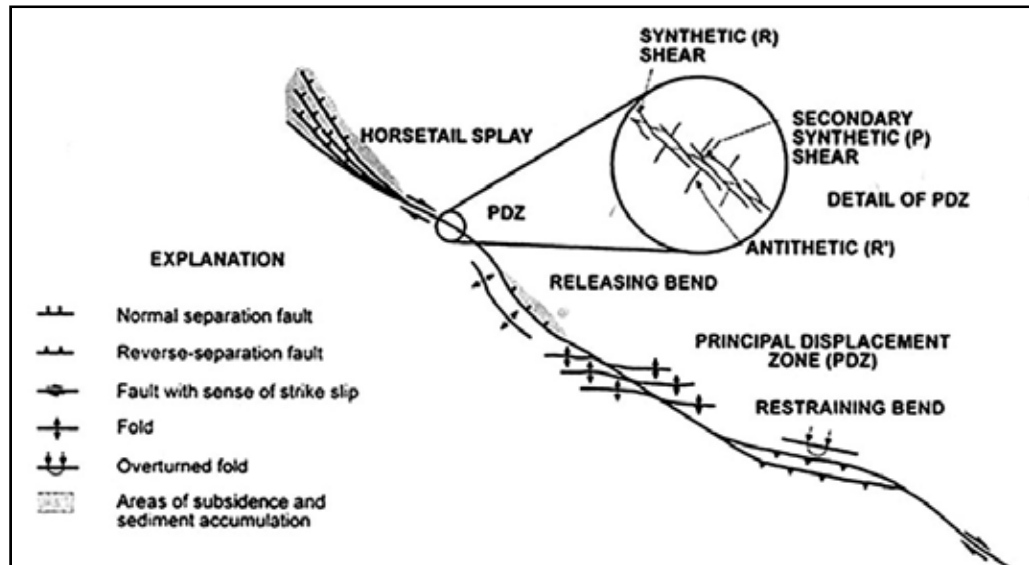


Figure 3.15 Plan view of structures associated with an idealized strike-slip fault (after Christie-Blick and Biddle, 1985).

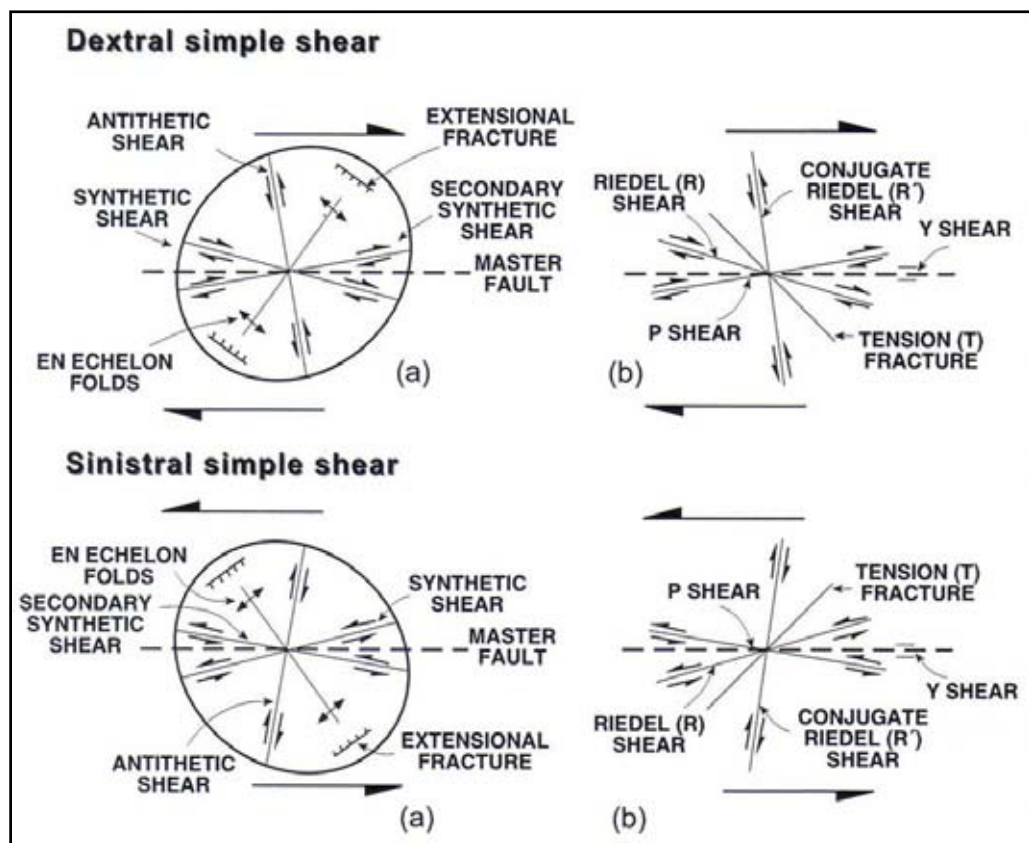


Figure 3.16 Simple shear models associated with strike-slip fault (a) and producing contraction and extensional features (b), used in this study following the work done by Christie-Blick and Biddle (1985).

showed array of structural complexity (Sylvester, 1988). In many strike-slip faults, bending fault trace can be observed at overlapping areas among the adjacent blocks. Therefore, fault movement can create both compressive and tensile stresses into the curve of fault segments. For instance, as shown in Figure 3.17, releasing bend and restraining bend can cause pull-apart basins and uplift features related to tension and compression stresses, respectively (Biddle and Christie-Brick, 1985). In many cases, both pull-apart basins and uplift highs may be explained in term of step-over in which two fault segments have ended up, and both showing the same sense of movements.

In conclusion, there are many features of tectonic geomorphology produced by strike slip movement. As shown in Figure 3.18, these features are linear valleys, offset or deflected streams, shutter ridges, sag ponds, pressure ridges, benches, scarps, and small horsts and grabens (Keller and Pinter, 1996). Noteworthy, fluvial terraces, offset-stream channels, and alluvial fans are typical features used to reconstruct paleoearthquakes offset history (Weldon et al., 1996).

Besides, based on simple shear model illustrating in Figure 3.19, normal fault trace should be formed perpendicular to the direction of maximum elongation and maximum extension stress. Figure 3.19 shows an idealized cross-section of extension tectonic environments. Master fault has bounded the main on the right, accompanied by minor synthetic and antithetic faults. Other structures commonly found in an extension regime are horsts and grabens showing on the left. Depending on tectonic geomorphology on ground surface, typical indicator of normal faulting is a fault scarp (McCalpin, 1996) (Figure 3.20), which can be developed to form triangular facets when proper condition, such as erosion and repetition of active fault movement has reached (Figure 3.31). In addition, other evidence of extension environments includes linear-range fronts, escarpments, volcanic flows and cones, rift valleys, and axial rifts of oceanic ridge systems (Keller and Pinter, 1996).

Lastly, tectonic landforms associated with reverse faulting include belts of active folding and faulting, steep mountain fronts, and fault scarps. The elongated axis of these structures is usually found lied perpendicular to the direction of maximum compressive stress axis as shows in figure 3.17. The most common geomorphic evidence of compression tectonism in continent is fault scarp (Carver and McCalpin, 1996). Based on historical surface ruptures in Armenia, 1988 earthquake, seven types of thrust fault scarp morphology have been reported by Phillip et al. (1992) (Figure 3.21).

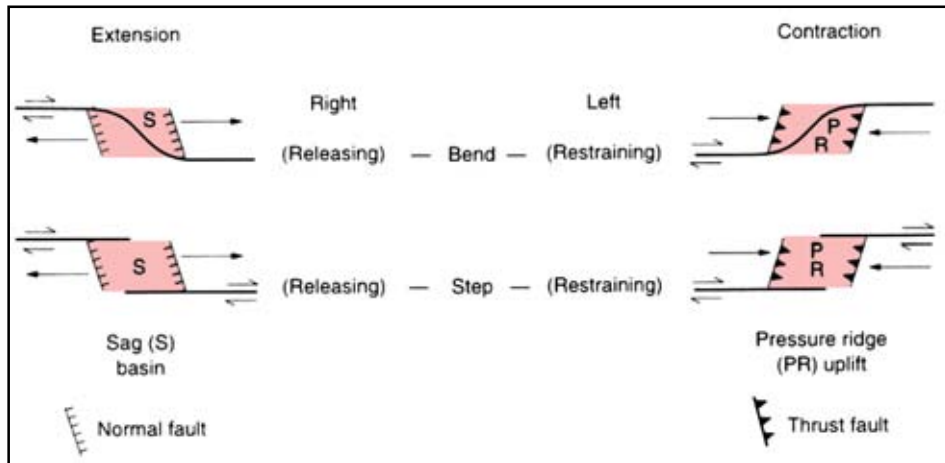


Figure 3.17 Sags and pressure ridges associated with bends and steps along strike-slip faults (after Keller and Pinter, 1996).

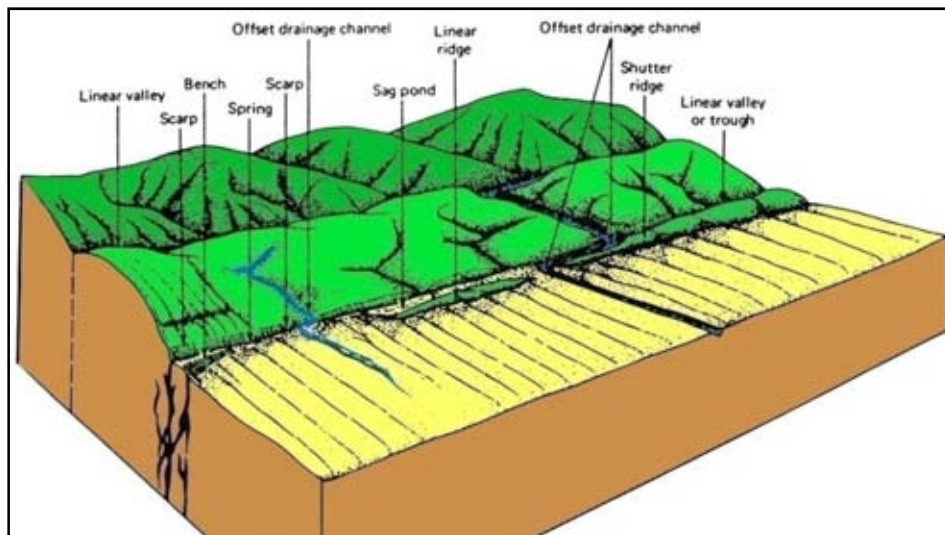


Figure 3.18 Assemblage of landform associated with active tectonic strike-slip faulting (after Burbank and Anderson, 2001).

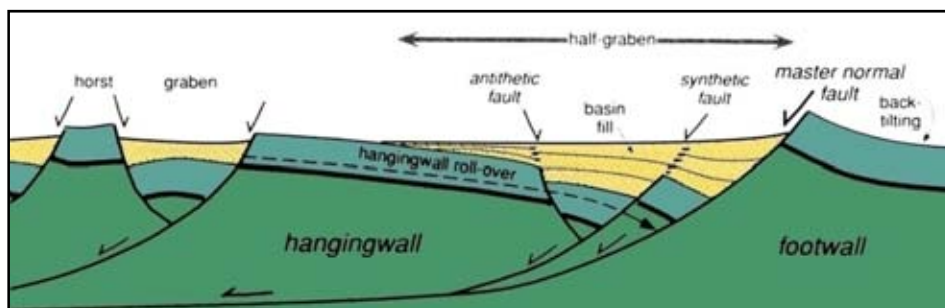


Figure 3.19 Idealized cross-section of extension tectonic environments (after Burbank and Anderson, 2001).

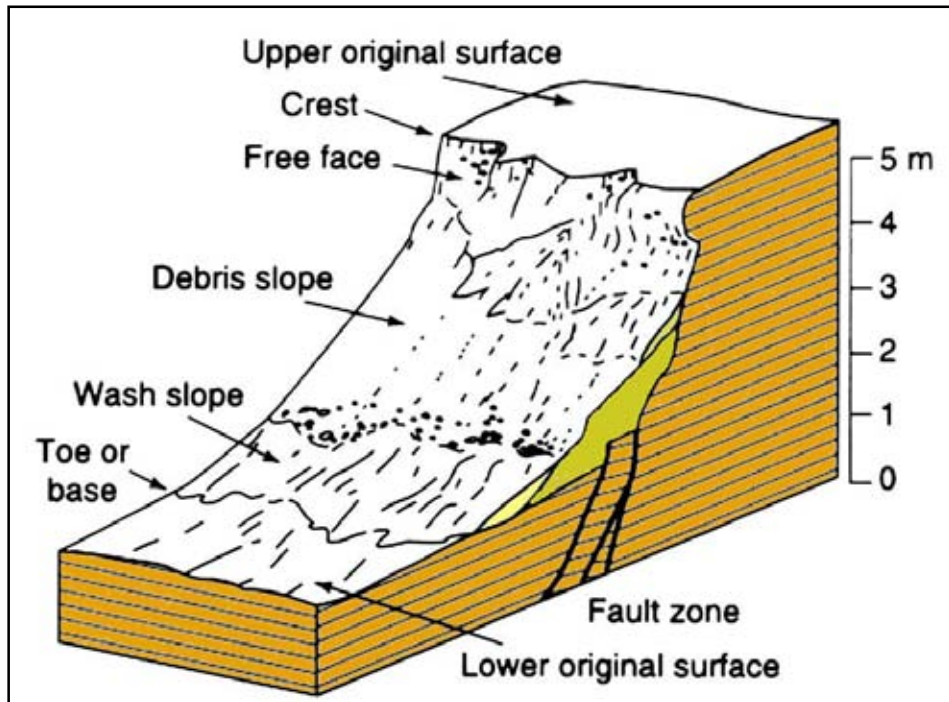


Figure 3.20 Basic slope elements that may be present on a fault scarp (after McCalpin, 1996).

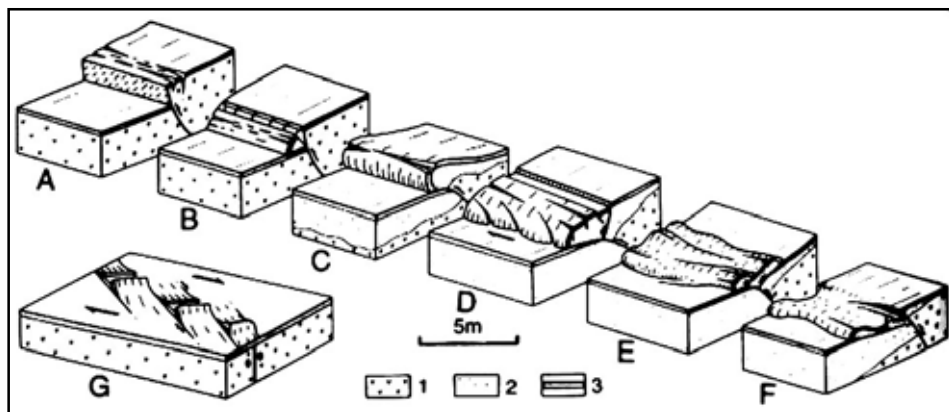


Figure 3.21 Types of reverse fault scarps. (A) Simple reverse (or thrust) scarp. (B) Hanging-wall collapse scarp. (C) Simple pressure ridge. (D) Dextral pressure ridge. (E) Back-thrust pressure ridge. (F) Low-angle ridge. (G) En-echelon pressure ridge. 1, bed rock; 2, soft Quaternary sediments; 3, turf (after Phillip et al., 1992).

Fenton et al. (1997) revealed several tectonic geomorphologies found along seven faults in northern basin and range province of Thailand. These morphologies include linear-range fronts, triangular facets, offset drainages, stream knick points, wine-glass canyons, and scarps. Won-in (1999) mentioned that fault scarps, triangular facets, offset stream channels, shutter ridges, beheaded streams, pressure ridges, fault trace cutting terraces, basin development, parallel ridges, and uplift river gravel deposit are observed along the Three-Pagoda fault zone. Kosuwan et al. (1999) stated that several tectonic geomorphologies, such as offset streams, sag ponds, shutter ridges, and benches, and river terraces on young alluviums/colluviums, were observed along the Mae Chan fault zone.

3.3.2 Result from Aerial photo and IKONOS images interpretation

Based on results of lineament analysis by satellite images, several selected areas for the more detailed study is air-photographic and IKONOS image with the resolution of 1 x 1 m. that provided by www.pointasia.com for locating the studied faults more precisely. Regarding the result of air-photo and high resolution satellite images interpretation, the most interested fault segments align in the north-south direction. The author found several morphotectonic evidence that are recognized along the interesting segment. There are at least six interesting areas namely; Ban Thung Ao, Ban Doo, Ban Tin Tok, Ban Thung Hao, Ban Sob Pua, and Ban Muang Luang (Figure 3.22).

3.3.2.1 Area 1: *Ban Thung Ao, Amphoe Thung Chang, Changwat Nan*

Ban Thung Ao Area is situated in the north of Pua Basin near Thai-Lao PDR boundary. Topography in this area of both eastern and western sides is mountainous and high-relief. In the central part the area is undulating terrain with small hills alternated with narrow flood plain area. The Nan River is the main river flowing southward but its branches flow in several directions, however most of them flow in the east-west direction. Based on the geological map, scales 1:50,000 Amphoe Thung Chang and geological map of Thailand, scale 1:1,000,000 (DMR, 1999), the mountainous area is underlain by the succession of Permo-Triassic rocks which comprises mainly sandstone interbedded with siltstone and shale, partly metamorphosed to quartzite and schist. The younger units, including Mesozoic and

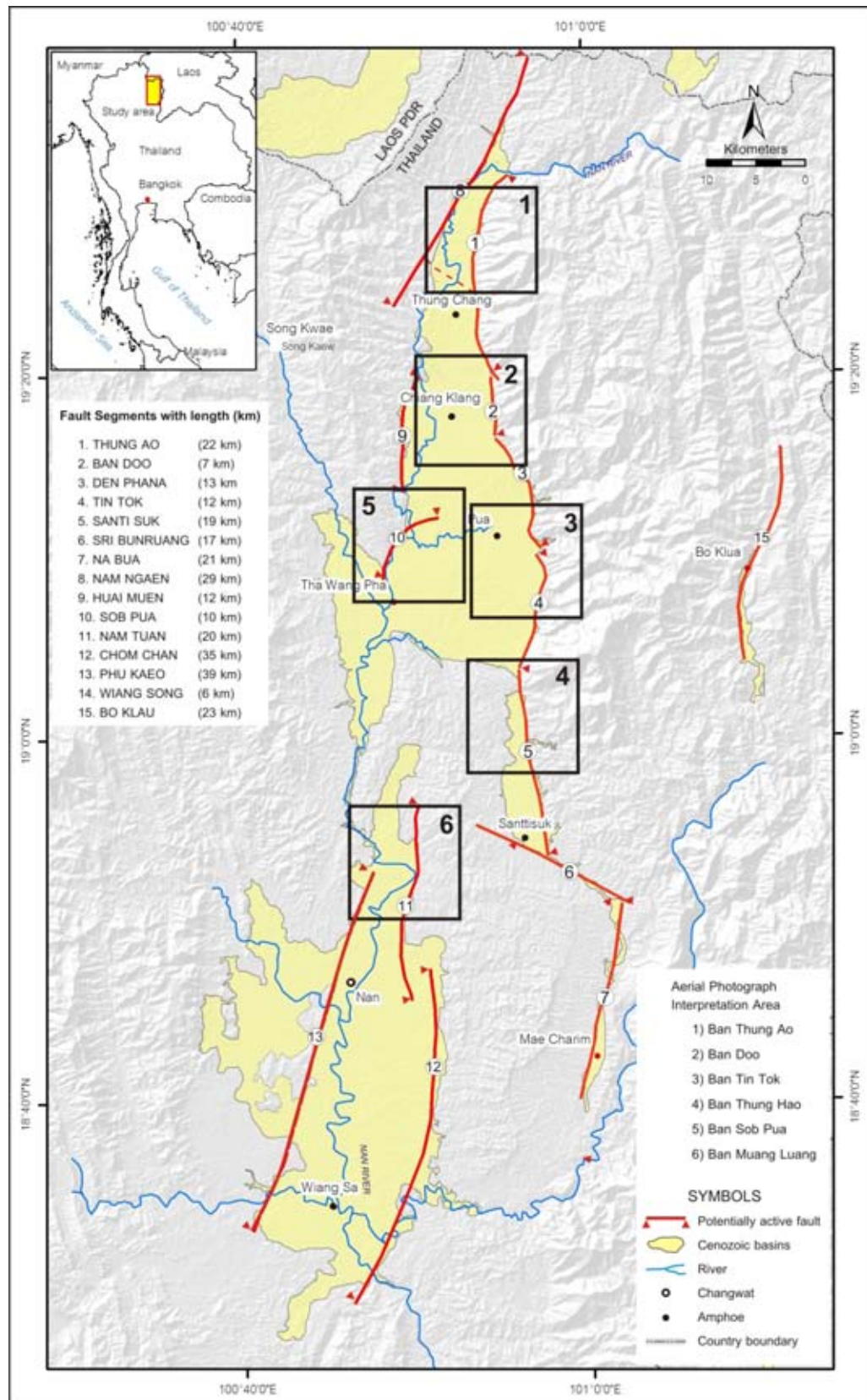


Figure 3.22 Map showing locations of the Pua Fault Zone (red line) and its major inferred active fault segments. Boxes with numbers indicate selected areas for remote-sensing and aerial photographic interpretations for detailed paleoseismic studies.

Tertiary sediments are unconformably underlain by the Permo-Triassic sequence. The Tertiary unit contains semi-consolidated sediments of intercalated gravels, silts and sands. As shown in Figure 3.23, the areas west of Thung Ao village, 3 alluvial fans are recognized with the well-defined fan shape. These fan deposits were controlled by the earlier, north-south trending fault segment situated immediately at Ban Nam Lar to Ban Thung Ao. The recent Quaternary sediments is the uppermost unit, it can be separated into two units, one is terrace deposits consisting of gravel, sand, silt and clay; and the other unit is sand and clay of alluvial deposits.

Both satellite image and DEM data indicate that the fault trace is quite continuous and align in the north-south direction with concave to the east. The total length of the fault is estimated at about 22 km. Based on the high resolution images (aerial photograph and IKONOS image) interpretation at the Ban Thung Ao area. Several types of morphotectonic evidences are recognized, such as offset streams, triangular facets, shuttle ridges, and linear valleys (Figure 3.23). The triangular facets are important neotectonic geomorphologic features developed in the Permo-Triassic sandstone. Triangular facets were clearly observed at Doi Khun Huai Nam Ao Mountain. A set of triangular facets consists of at least 13 facets with dipping angle of about 50°-60° to the west. Their geometry is about 200-350 m at base width and about 40-60 m in height (Figure 3.24).

Figure 3.25 shows an area in the eastern part of Ban Thung Ao close to mountain foot. Sets of small streams and hill ridges of at least 3 sets have been offset southward by Thung Ao segment and each set is parallel to one another in the same direction. Length of offset stream is about 50-60 m. Offset ridges have also been found along Thung Ao Fault (Figure 3.26). This confirms that the Thung Ao segment have been laterally-moved several times. On the other hand, the nearby north-south trending shutter ridge with the average base width of about 200 m and the average height of about 25 m has been confirmed. Based on neotectonic evidence along Thung Ao segment there are the west-dipping normal faults with left-lateral displacement of approximately 50-70 m, possibly suggesting the faults have ever been moved at least 4 times in the past.

3.3.2.2 Area 2: Ban Doo, Amphoe Chiang Klang, Changwat Nan

The mapped area extends continuously from Ban Nam Oh through Ban Doo to Ban Don Tan. Based on the geological map, scale 1:50,000 Amphoe Thung Chang,

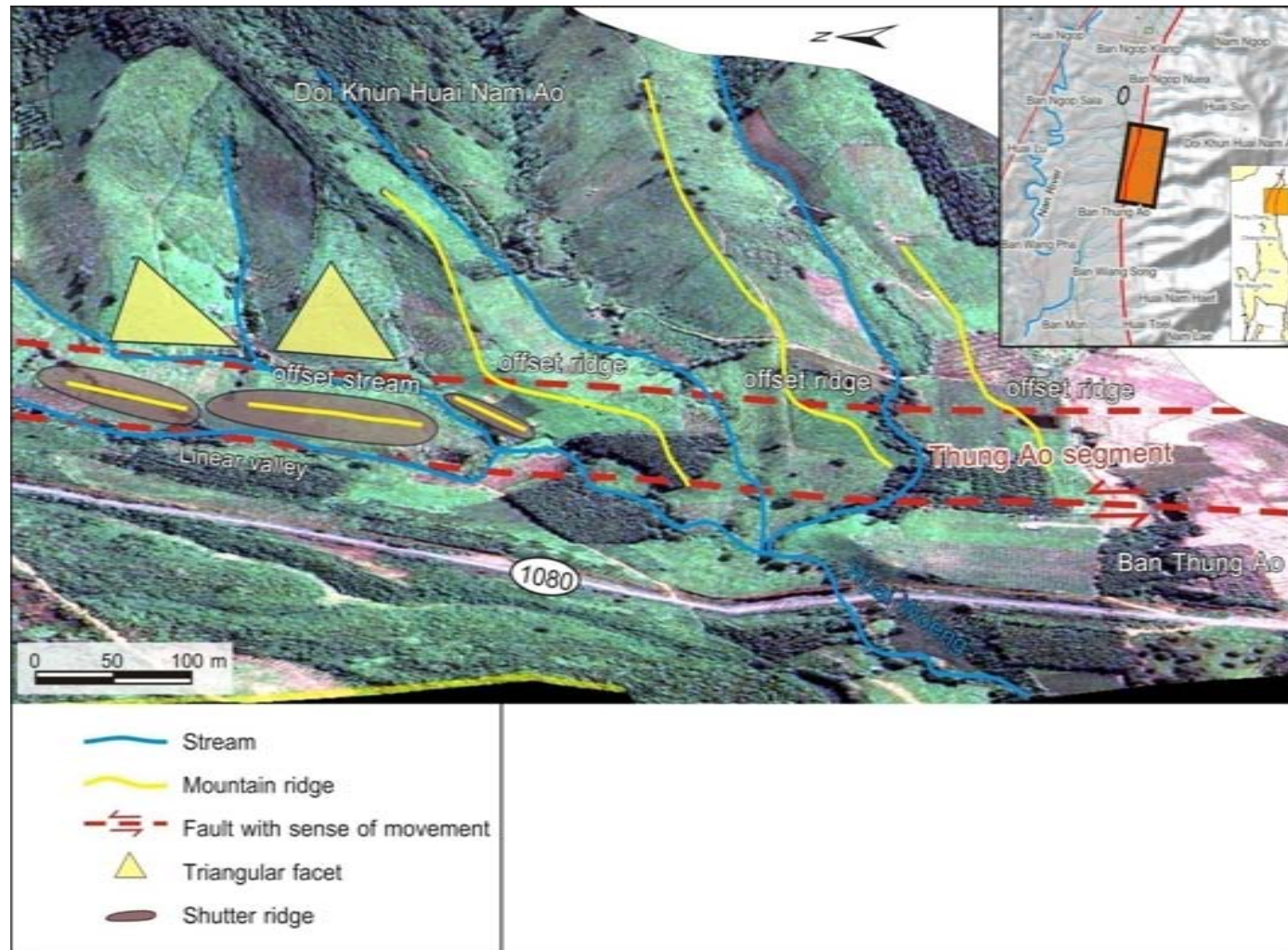


Figure 3.24 The 3D model of IKONOS image (www.pointasia.com) at Ban Thung Ao area, Nan showing landform developed by fault (red lines) such as triangular facet (t), small fault scarp (s), offset stream (0) and linear valley (v).

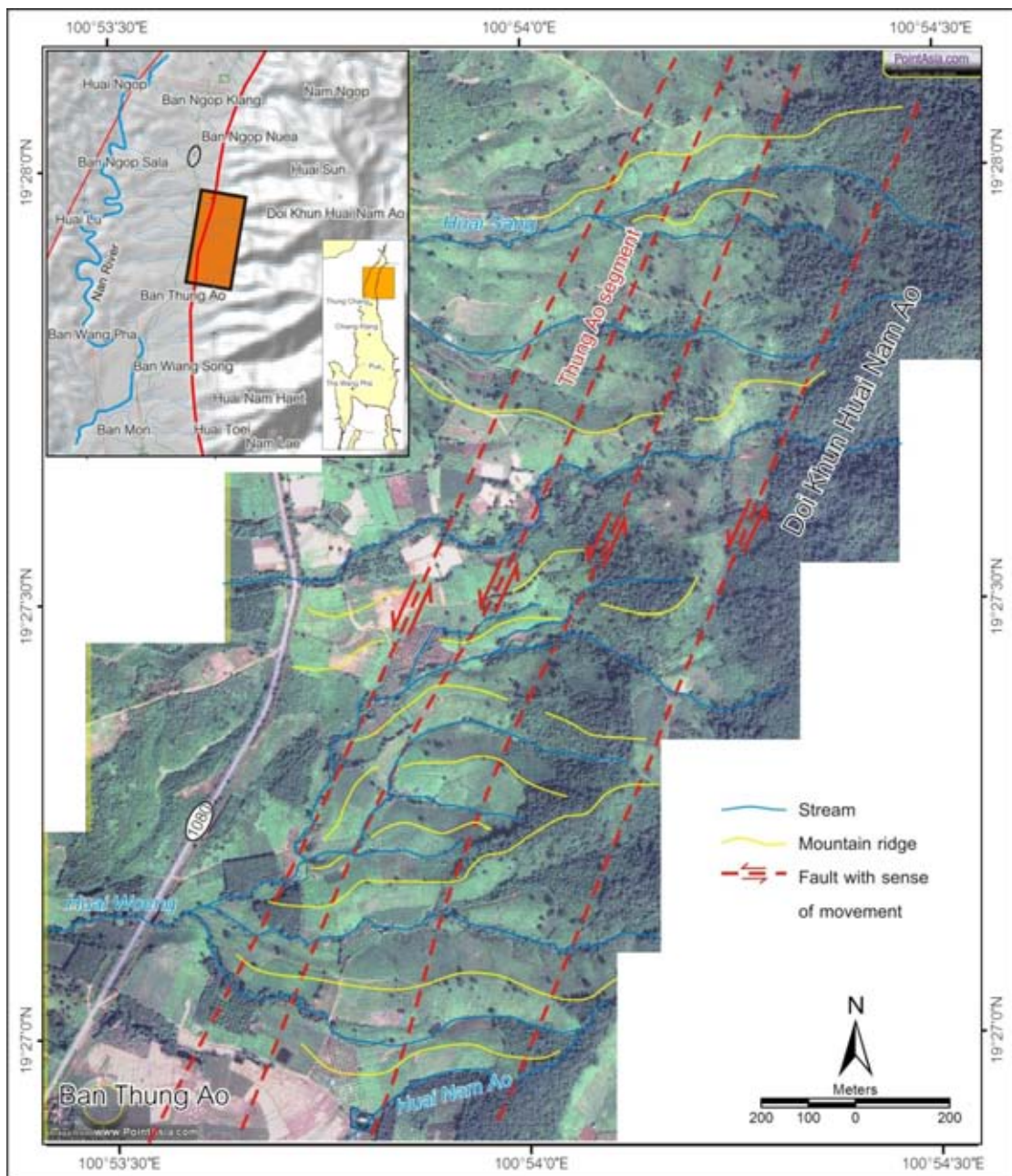
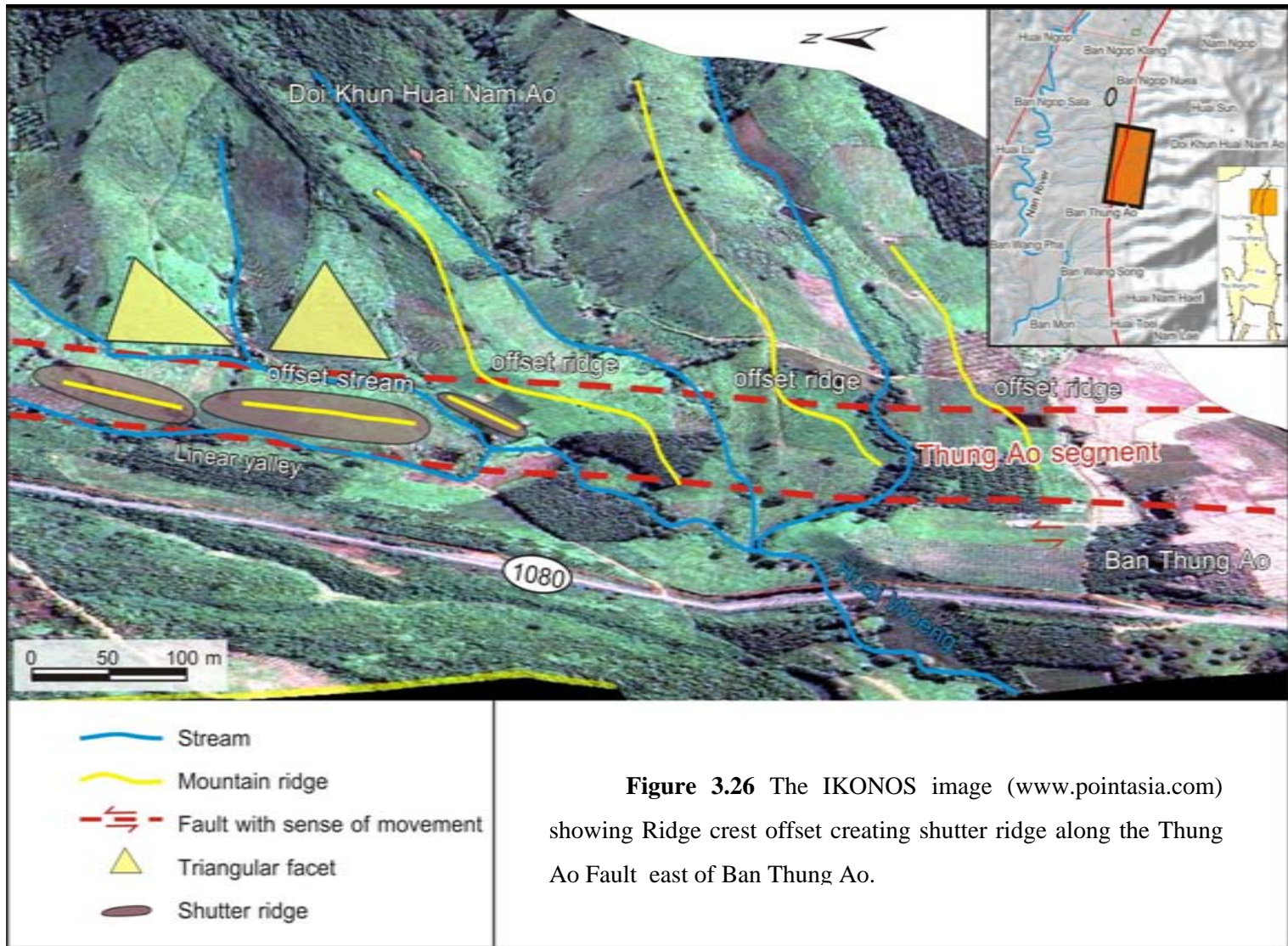


Figure 3.25 The IKONOS image (www.pointasia.com) showing the orientation of the Thung Ao fault segment (dashed lines) in the north-northeast direction and offset spurs with the left lateral sense of movement.



the study area consists of Permo-Triassic successions in the mountainous area and Cenozoic sediments in the low land. The Permo-Triassic rocks comprise mainly sandstone interbedded with siltstone and shale, partly with quartzite and schist. Alluvial fan / old colluvial sediments of possibly late Tertiary age are underlain by Permo-Triassic sediments and contain semi-consolidated conglomerates, siltstones and sandstones. Areas to the north and south of Ban Klang (northcentral part of the concerned study area, see Figure 3.27) are considered to have been formed by alluvial fan system. The northern part (Af1 of Figure 3.27) shows the well-defined fan-shape feature. The southern part (Af2 of Figure 3.27), the fan deposit was observed by subsequent (old) colluvial deposit. These fans however were once controlled by the late tectonic fault system in the northwest –trend. The two upper units are undifferentiated terrace deposits of gravel, sand, silt and clay and the younger Quaternary unit comprising sand and clay of alluvial deposit unit.

In the area east of Ban Doo village, aerial-photographic analysis reveals several features of morphotectonic evidence along the Ban Doo segment with the length of about 7 km (Figure 3.27). Major supporting features include offset streams, triangular facets, wine-glass canyon, scarplets (or small scarps). Many of the streams show offsetting feature. The outstanding offset stream observed in this area is the Huai Ngoi, Nam Prue and small streams nearby. At Ban Paruak, the stream is shifted about 50-70 m to the south, suggesting a left-lateral movement. However, in the southern part of Ban Doo segment (Figure 3.28a) at north of Ban Doo, a stream is deflected to the north approximately 60 m, possibly supporting right-lateral displacement. However, this can be reinterpreted as shown in Figure 3.28b that the right-lateral movement along the Ban Doo segment may be fictitious and misinterpreted. We consider that due to the steep slope angle headward erosion of the northern stream must be high so as to make the piracy of southern stream in response to the left-lateral movement.

Seventeen triangular facets (Figure 3.28a), were observed along the fault line. The facets have approximately 150-250 m base width 60-80 m height and facing to west with dipping angle 60° (Figure 3.29). Over much of its length, the Ban Doo segment comprises a series of faceted spurs interrupted by several steps of erosional pediment remnants (Figure 3.30). Our interpretation is similar to that of Hamblin (1976) as shown in Figure 3.31 that such facet spurs were the result of

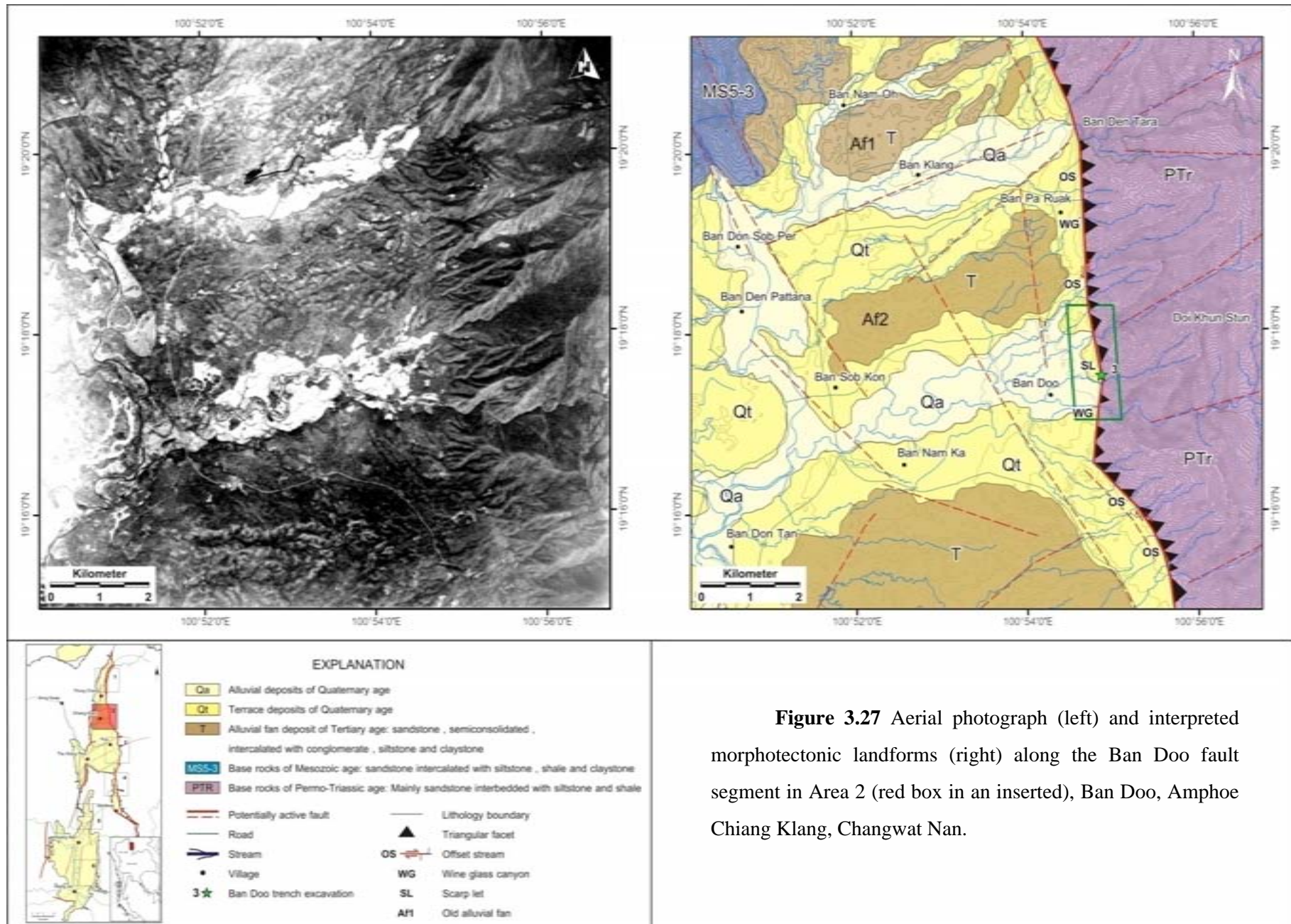


Figure 3.27 Aerial photograph (left) and interpreted morphotectonic landforms (right) along the Ban Doo fault segment in Area 2 (red box in an inserted), Ban Doo, Amphoe Chiang Klang, Changwat Nan.

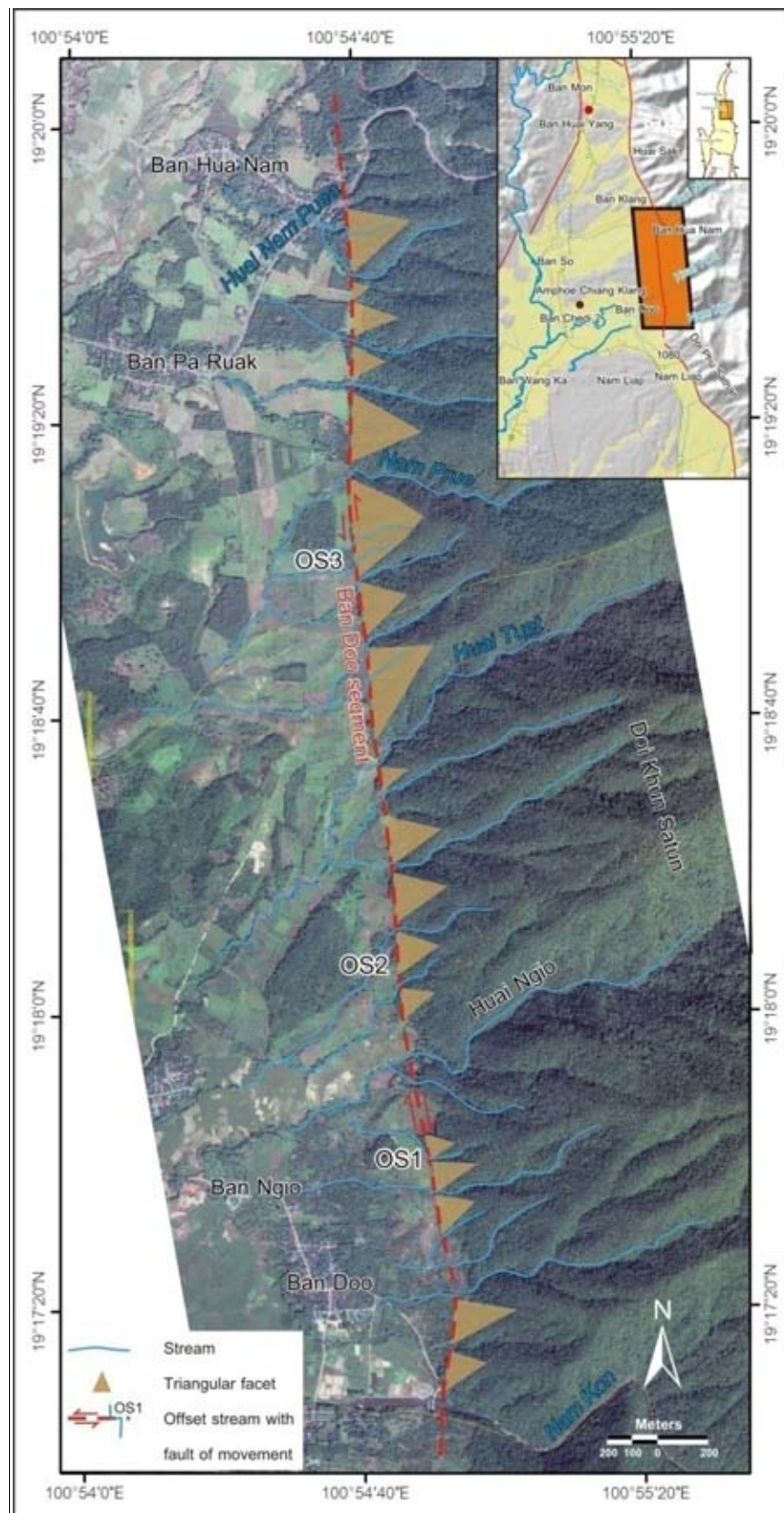


Figure 3.28a The IKONOS image (www.pointasia.com) showing of Ban Doo area showing location of the Ban Doo fault segment with a series of triangular facets and offset stream with the left-lateral sense of movement.

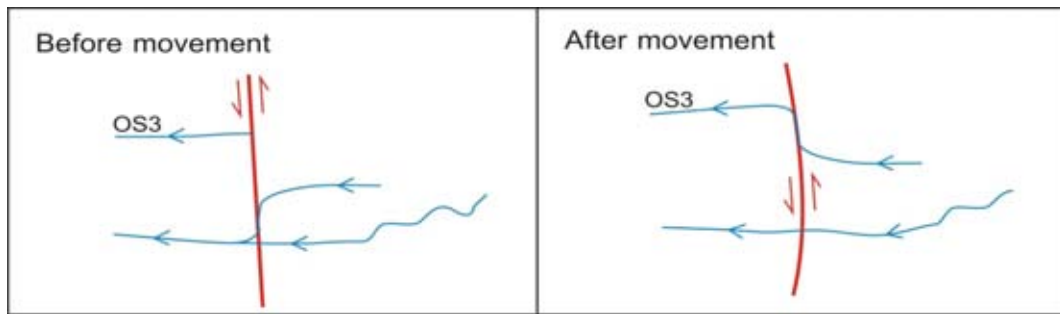


Figure 3.28b Development of pseudo-right lateral movement

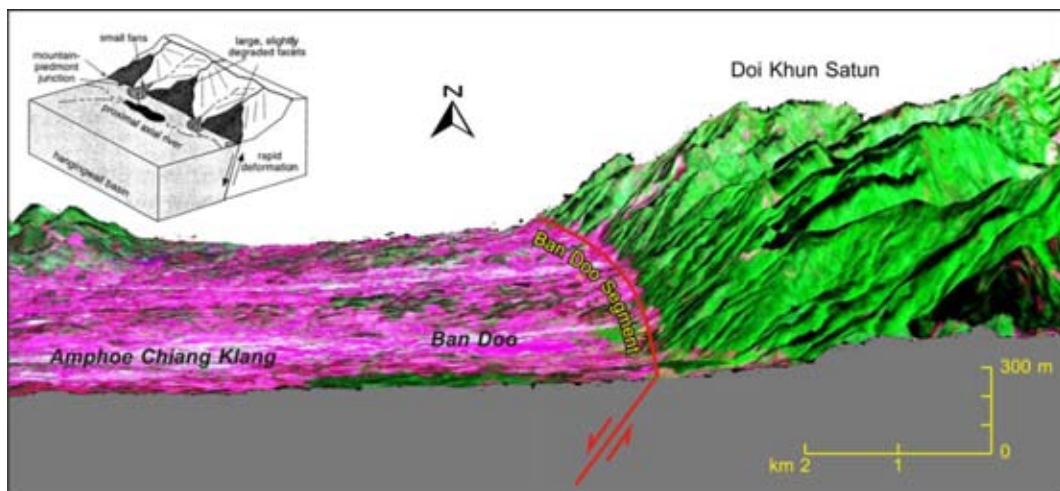


Figure 3.29 The 3D model of ASTER image at Ban Doo area in Nan province showing geographic features, such as linear range front, steep drainage and large triangular facet with steep slopes dipping westward to the Pua Basin, indicating normal fault movement with rapid hanging wall subsidence and foot wall uplift.

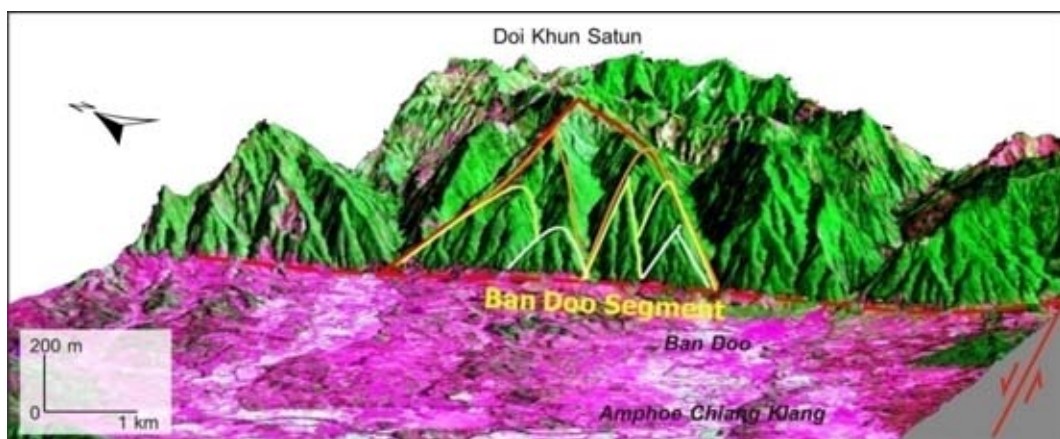


Figure 3.30 The 3D model of ASTER image at Ban Doo area showing a series of triangular faceted spurs along the Ban Doo segment (red dashed line). The over steepened base and the development of several erosional benches along the escarpment including at least 4 times of fault movement in the Ban Doo area, Nan province.

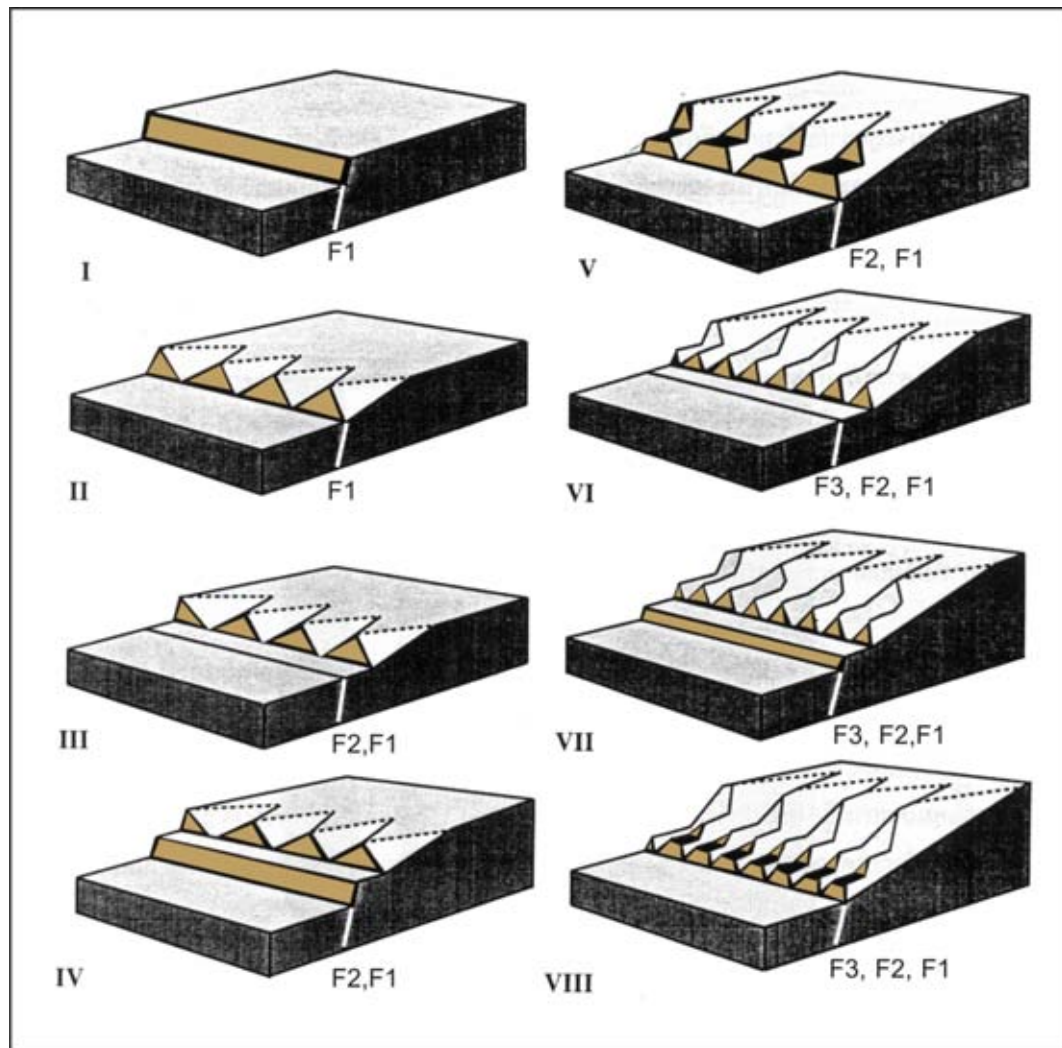


Figure 3.31 Development of faceted spurs produced by episodic vertical tectonic movement (after Hamblin, 1976).

- I - undissected fault scarp.
- II - development of faceted spurs by streams cutting across the fault scarp (F1).
- III - period of tectonic quiescence with slope retreat, and development of a narrow pediment.
- IV - renewed fault movement (F2).
- V - dissection of the new fault scarp by major streams and streams developed on the faces of the faceted spurs developed at stage II.
- VI - a new period of tectonic quiescence, with the development of another narrow pediment within the footwall block at the base of the range front.
- VII - renewed fault movement (F3).
- VIII - dissection of the fault scarp produced at stage VII resulting in a line of small faceted spurs at the base of the range front. Remnants of narrow pediments (benches) are preserved at the apices of each set of faceted spurs. Progressive slope retreat is accompanied by a decrease in the slope angle of the faceted spurs.

episodic fault movement. The facets may have formed during periods of vertical (or dip-slip) fault movement and the benches may have been created during periods of tectonic stability of when, erosional processes and fault scarps retreated.

3.3.2.3 Area 3: *Ban Tin Tok, Amphoe Pua, Changwat Nan*

The study area is located in southernmost part of Pua Basin, east of Amphoe Pua; its geology is similar to that of the Ban Doo area. The mountainous area belongs to Permo-Triassic which is characterized by (meta-) sandstone interbedded with (meta-) siltstone and shale. Lower area belongs to Cenozoic sediment deposit and unconformably underlain by Permo-Triassic unit. The Cenozoic sediment is divided into three units, lower unit of Tertiary sediments containing semi-consolidated alluvial fan / old colluvial. The second unit of terrace deposits comprises gravels, sands, silts and clays. The uppermost unit is Quaternary alluvial deposit of mainly sand and clay (Figure 3.32).

The result from aerial-photographic interpretation at the area of Ban Tin Tok along the west-concave north-south trending Tin Tok segment is shown in Figure 3.32. Important tectonic geomorphologic features are sets of triangular facets, fault scarps, and wine-glass canyons. In the study area, there are 2 sets of triangular facets. The first set consists of six triangular facets with the about 400 m average base width, and about 60-80 m average height and 60° dipping slope angle. The second set comprises four triangular facets with the 0.3-1 km base width, about 80-200 m average height and 60-75° dipping slope angle. These facet spurs have their slope angles dipping to the west direction.

In the southern part of Tin Tok Segment at Ban Hua Nam, there is a significant neotectonic feature, i.e. wine-glass canyon. As shown in Figure 3.33, the 3D model displays the highest and steepest triangular facets along fault segment and also displays where Huai Nam Khun crosses the Tin Tok segment and developed deep canyon which becomes wider in the upper part and narrower at bottom. The wine-glass canyon is considered to have formed by renewed uplift or an increased rate of uplift of the footwall in a normal fault system (Figure 3.34).

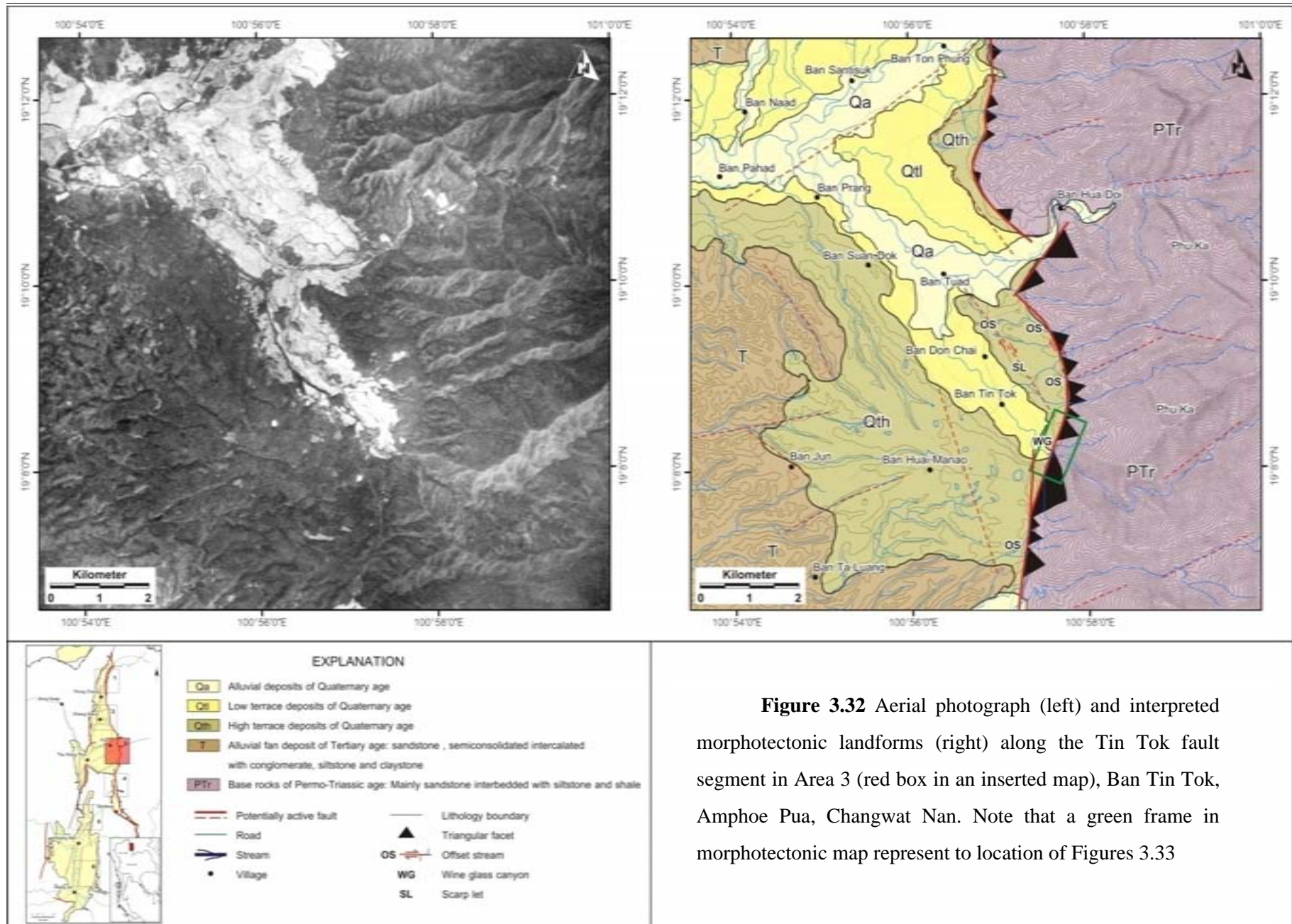


Figure 3.32 Aerial photograph (left) and interpreted morphotectonic landforms (right) along the Tin Tok fault segment in Area 3 (red box in an inserted map), Ban Tin Tok, Amphoe Pua, Changwat Nan. Note that a green frame in morphotectonic map represent to location of Figures 3.33

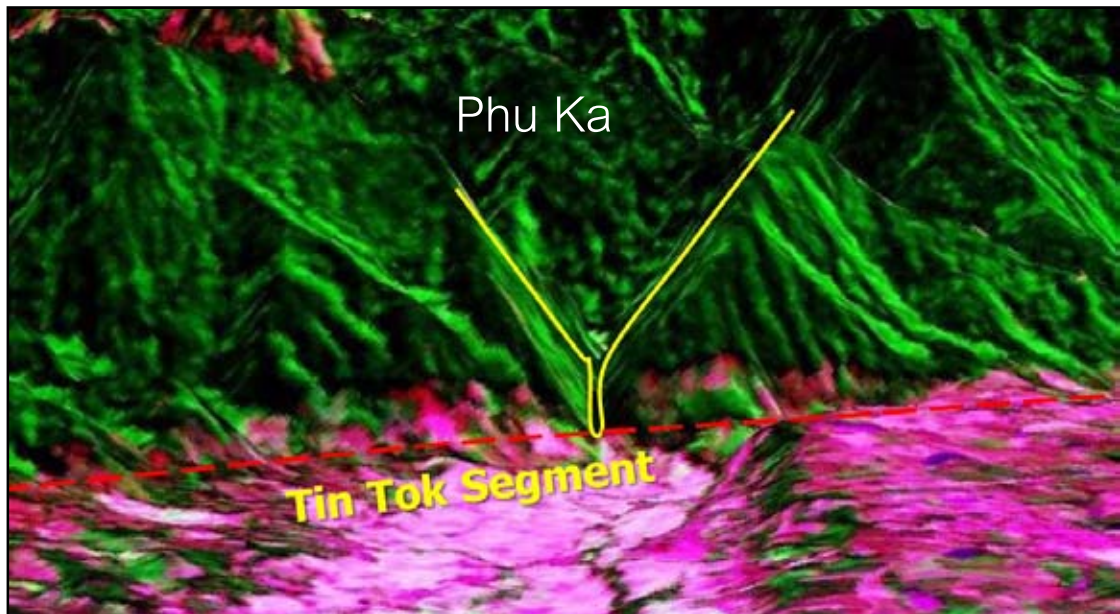


Figure 3.33 The 3D model of ASTER image showing a series of triangular facets and the v-shape valley with narrow canyon called “wine-glass canyon” at the base of Phu Ka Mountain at Ban Tin Tok, east of Amphoe Pua normal fault movement.

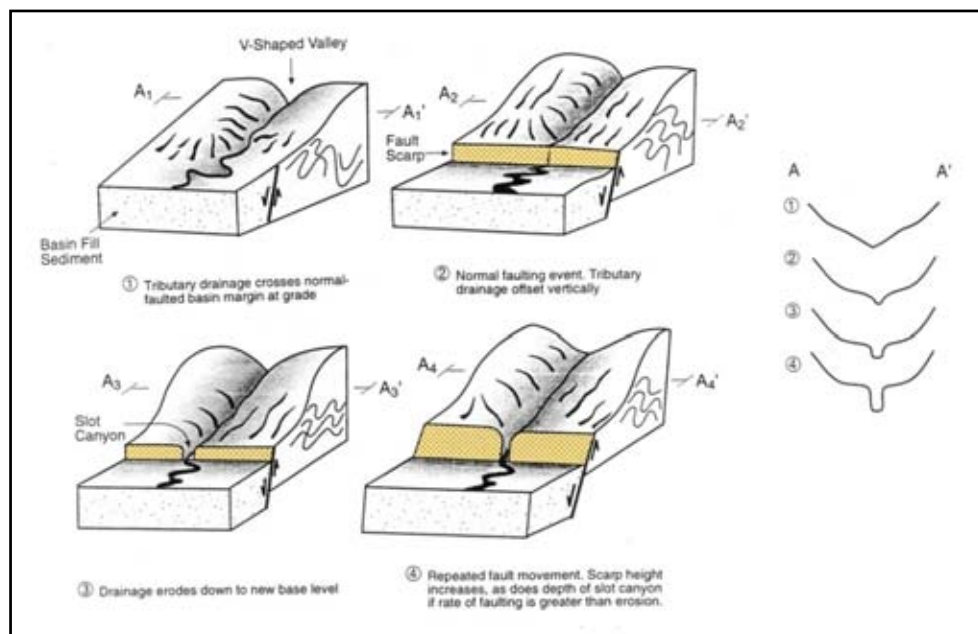


Figure 3.34 Formation of a wine-glass canyon seen in Figure 3.3 based on the interpretation reported earlier by Woodward-Clyde Federal Services (1996) at Ban Tin Tok. 1 - Tributary drainage crosses normal faulted basin margin at grade. 2 - Normal faulting event. Tributary drainage offset vertically. 3 - Drainage erodes down to a new base level. 4 - Repeated fault movement. Scarp height increases, as does depth of slot canyon if rate of faulting is greater than erosion.

3.3.2.4 Area 4: *Ban Thung Hao, Amphoe Pua, Changwat Nan*

Ban Thung Hao area in the northern flank of Santisuk basin is controlled mainly by the upper part of Santisuk Segment. Both satellite image and DEM data indicate that the fault trace is quite continuous and align in the north-south direction. The total length of the fault segment is estimated at about 19 km (Figure 3.35). Based on the geological map at scale 1:50,000, the base rocks in the study and neighboring areas are Permo-Triassic clastic successions mainly in the west and the south and including Triassic granite rocks in the east. Tertiary and Quaternary deposits are limited in the river valley. The terrace deposits show a sharp fault contact with base rocks. The recent Quaternary sediment seems to be restricting only as a flood plain of the Mai Pattana village.

Based on the result from aerial-photographic interpretation, Ban Thung Hao area is the sub-basin of Santisuk basin (called Thung Hao Sub-basin). Both eastern and western rims of the sub-basin are normal (dip-slip) faults. The western rim has the well-developed 12 triangular facets and a linear valley. A set of triangular facets have dipping angle about 40°-50° to the east and vary in geometry from 400 to 600 m. in at base and from 100 to 150 m in height (Figure 3.35). As mentioned above, the Thung Hao Sub-basin is a normal fault-bounding basin (Figure 3.36) it is likely that the formation of this basin is a result of undergoing east-west extension as shown in Figure 3.37. Additionally, a scarplet is found west of Ban Kok (Figure 3.35), indicating the latest fault displacement.

3.3.2.5 Area 5: *Ban Sob Pua, Amphoe Pua, Changwat Nan*

Ban Sob Pua situated on the western rim of Pua Basin is in the vicinity of Amphoe Pua (Figure 3.38). Based on the current investigation, the base rocks of the study area are mainly Permo-Triassic marine clastic rocks which are overlain unconformably by Tertiary semi-consolidated deposits. The flat area is characterized by these terrace deposits and recent sediments of alluvial deposit. These Tertiary sediments, which are mainly observed in the east are considered as part of the two large alluvial fan system situated in the northwestern and southwestern parts of the Pua district (Amphoe Pua). These Tertiary sequences were subsequently dissected by the arcuate normal fault, giving rise to alluvial sedimentation in the Quaternary age.

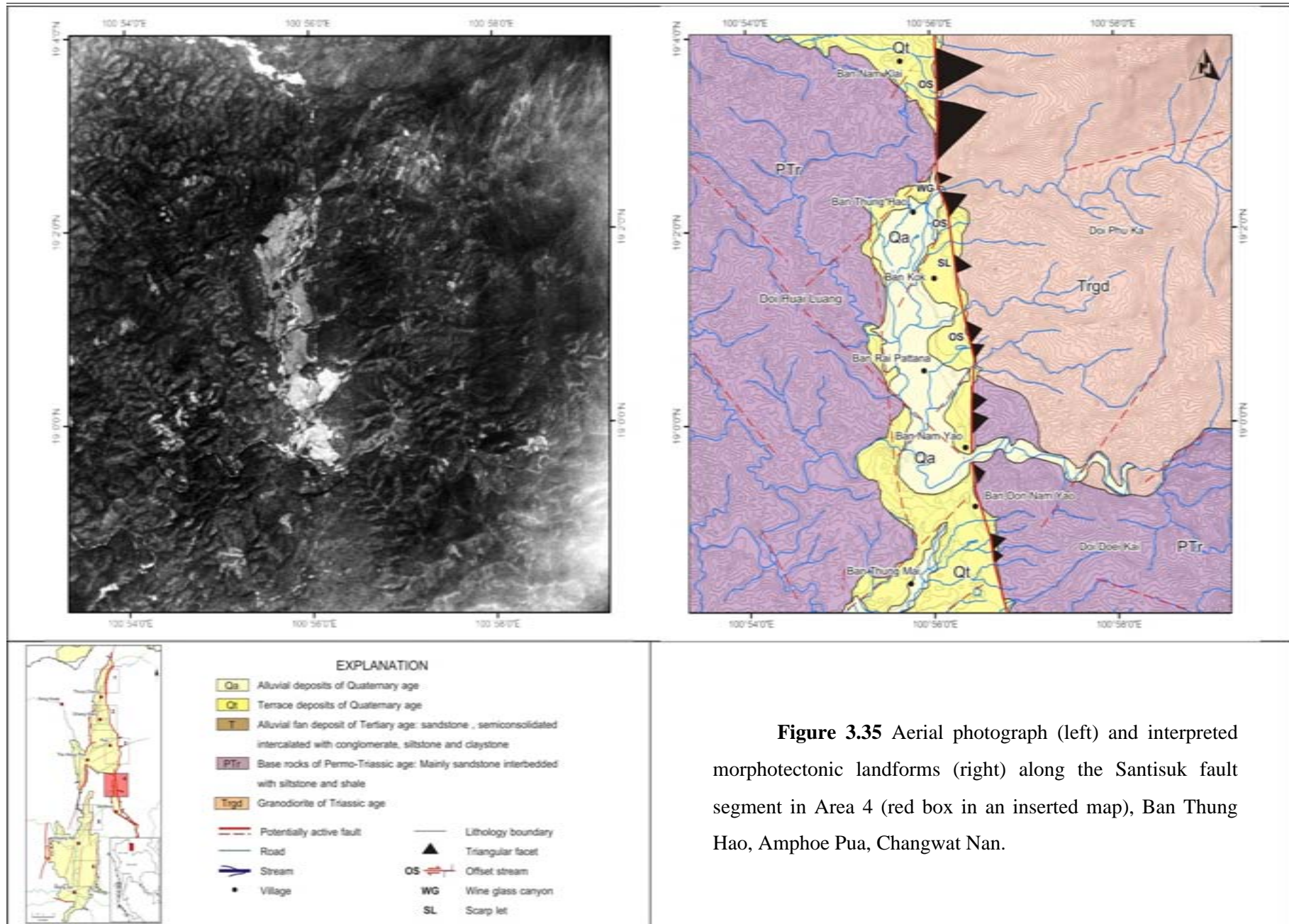


Figure 3.35 Aerial photograph (left) and interpreted morphotectonic landforms (right) along the Santisuk fault segment in Area 4 (red box in an inserted map), Ban Thung Hao, Amphoe Pua, Changwat Nan.

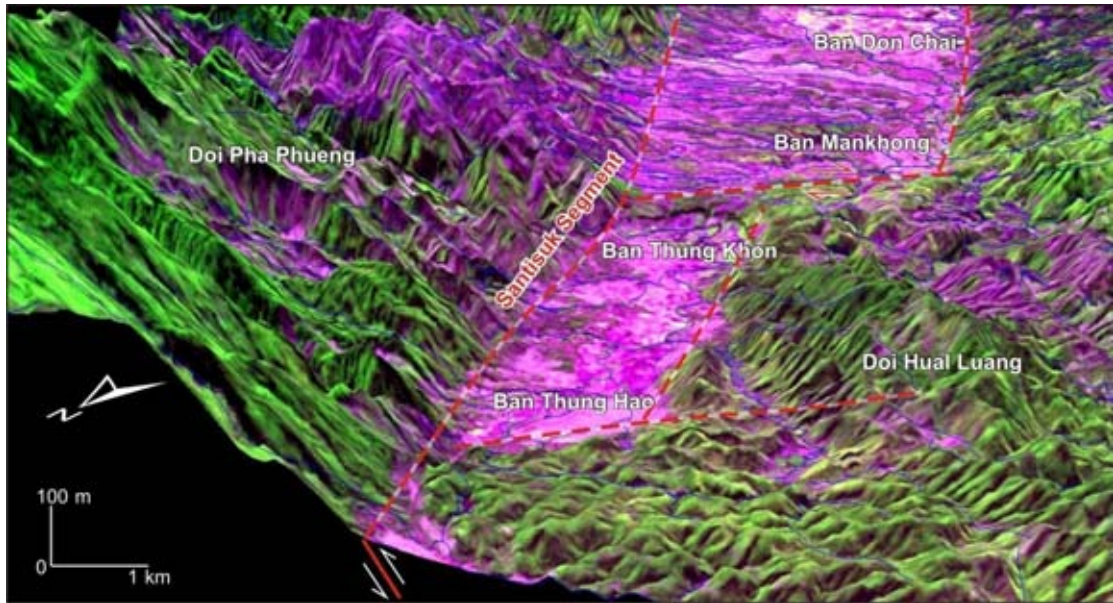


Figure 3.36 The 3D model of ASTER image showing the development sub-basin in the upper part of the Santisuk basin bounded by normal faults probably in an extensional (rift) basin (see also Figure 3.37)

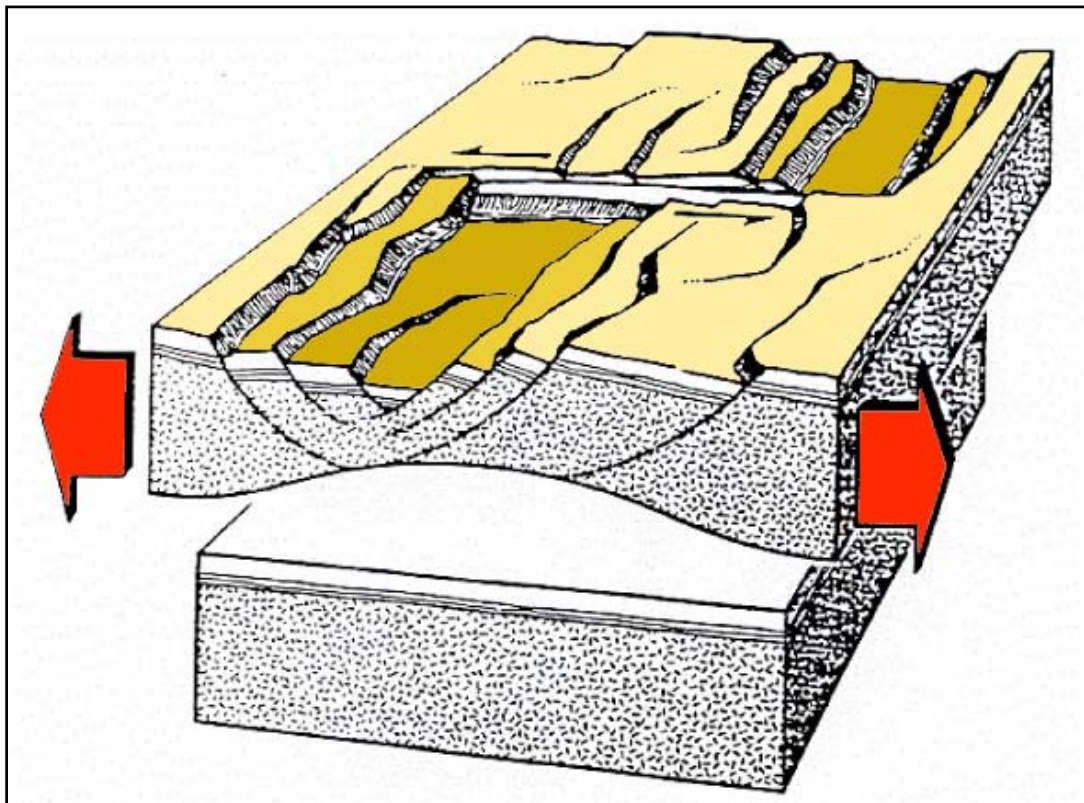


Figure 3.37 Extensional (rift) basin formation with the associated normal fault blocks caused by the strike-slip movement (after Koop and Stonely, 1982).

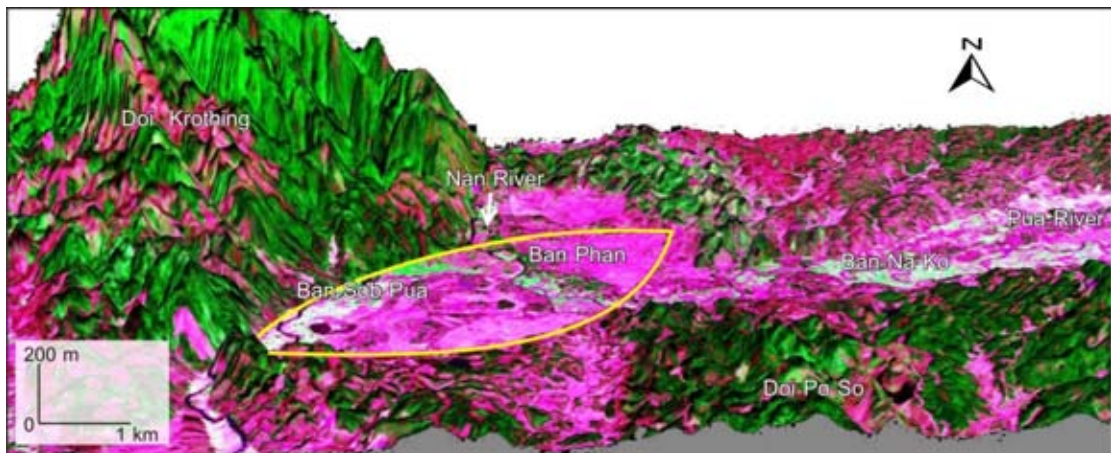


Figure 3.39 The 3D Model of ASTER image at Ban Sob Pua, west of Pua Basin showing eye-shape sub-basin as a result of the depression zone of the strike-slip movement.

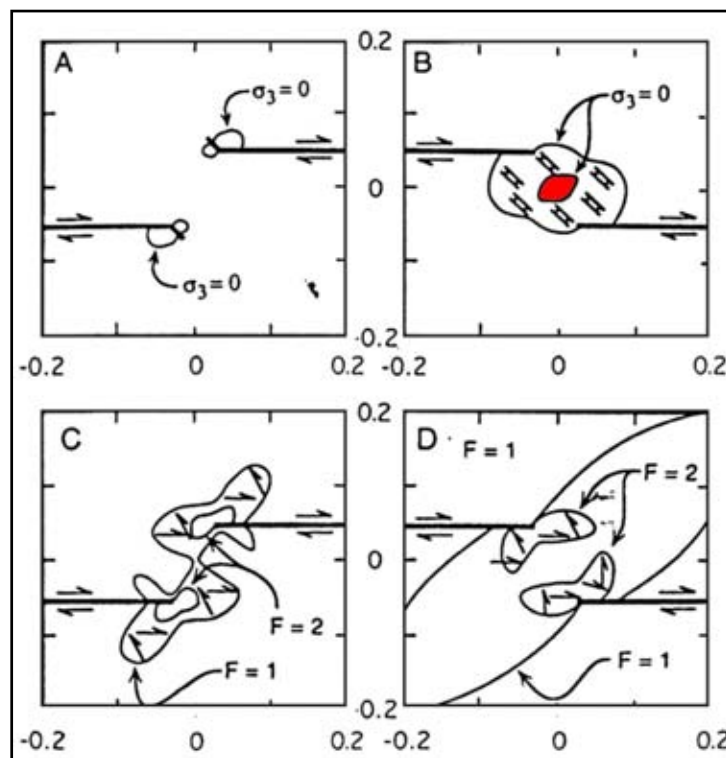


Figure 3.40 Physical modeling of stresses produced at contractional and dilational step-overs along strike-slip faults suggesting plausible locations and orientations of secondary structures. Contours show where $\sigma_3 = 0$ outline region of tensile stress and zone of potential tensile fracturing for (A) a contraction step and (B) a dilational step. Representative tensile fractures (ladder-like symbols) are drawn perpendicular to local σ_3 . In (C) and (D), contours show shear-failure condition, F , for contraction step and dilational step, respectively. Potential shear-fractures are oriented at 30° to locate direction of maximum compression. Redrawn and modified from Segall and Pollard (1980).

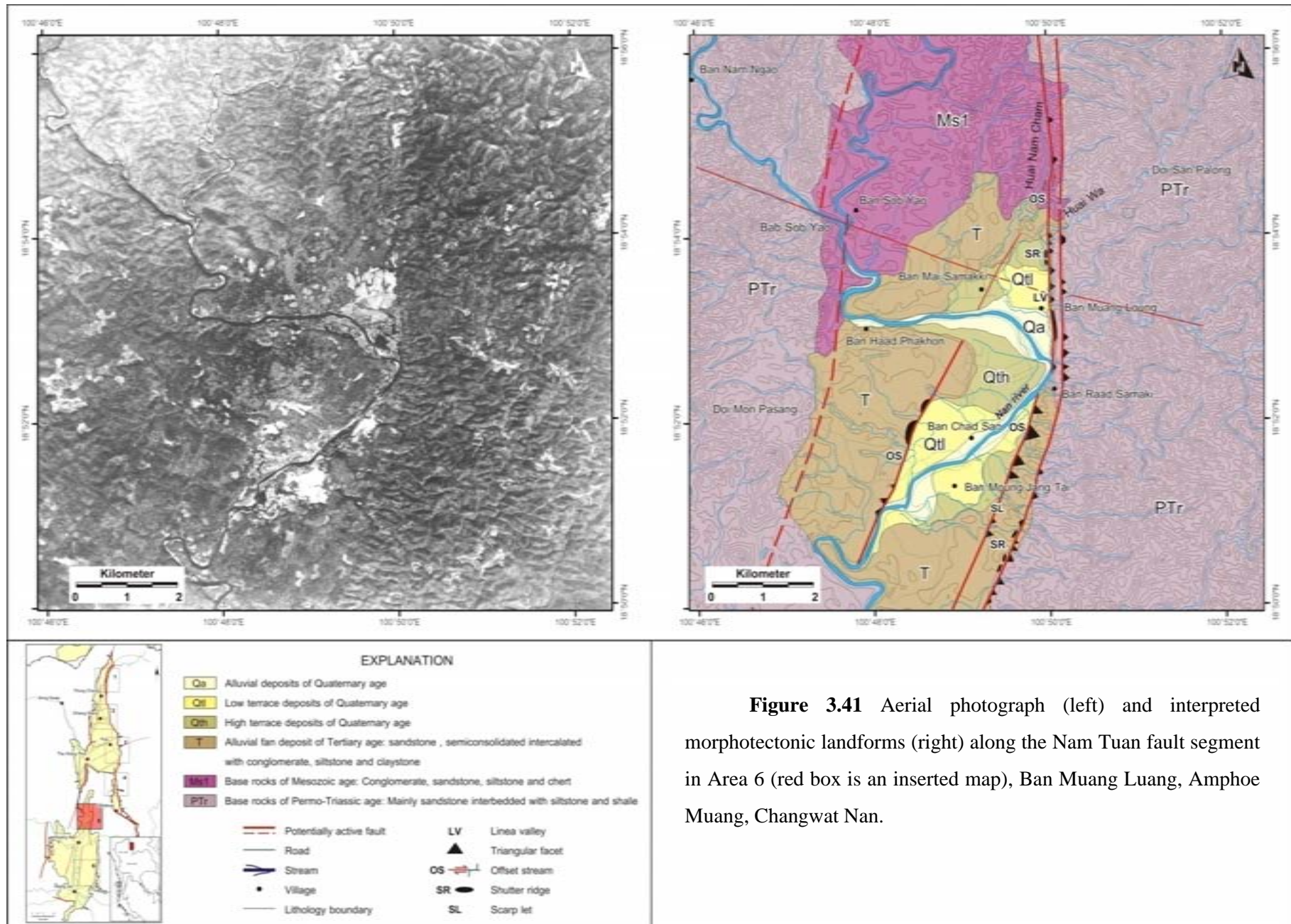
Based on the aerial-photographic analysis reveals several features of morphotectonic evidences along the 10 km-long Sob Pua segment. The strike of the fault orients in the northeast-southwest direction and concave to the southeast. Important tectonic geomorphologic features are sets of triangular facets and many offset streams. The first set consists of four triangular facets which have the average base width of about 500 m, the average height of about 70 m, and the surface slope of 60°. The second set comprises four triangular facets, with the 350-400 m base width, the 80 m average height and the 40° dipping surface (Figure 3.38).

Ban Sob Pua area is a sub-basin of Pua Basin. The geometry of the basin looks like an eye shape with the long axis in the northeast direction. In general the area is mainly covered by Quaternary alluvial and terrace deposits and rimmed at both southeastern and northwestern sides by the arcuate fault. It is interpreted that the oval-shaped (or the eye-shaped) basin may have occurred as result of stresses produced at the contractional and dilational step-overs along the strike-slip faults. This phenomenon is similar to the physical modeling of stresses proposed by Segal and Pollard (1980), as shown in Figure 3.40. Particularly interested is showing in Figure 3.40b, whereby, a dilatational step is influenced by tensile fractures (ladder-like symbols) and occurred the depression zone in central part which its form like eye-shape. Such depression may have caused widespread denudation of the higher-altitude surrounding area and alluvial deposition in the lower depression area. It is further considered that after strike-slip motion, perhaps in the late Tertiary, the Ban Sop Pua area is tectonically tilted northwestward and may have cause the alluvial deposition till present. This has been confirmed by the appearance of a set of triangular facet and the active meandering behavior to the western part of the basinal area.

3.3.2.6 Area 6: Ban Muang Luang, Amphoe Pua, Changwat Nan

The Ban Muang Luang area is the only selected study area in Nan Basin where the neotectonic landforms are not clear in comparison with the northern basin. Remote sensing result shows two subparallel fault traces bounds the Nan Basin to form the large river valley with higher relief largely occupied by the Mesozoic non-marine sediments and the lower relief mainly occupied by the Cenozoic alluvial sediments.

The result from space-borne data interpretation indicates the major trend of lineaments and faults along the basin boundary in the north to north-northeast direction. Nam Tuan Segment is a basin-bounding fault and is well recognized and more prominent on the eastern flank of the basin. Aerial-photographic analysis reveals several features of morphotectonic evidence along the fault segment (Figure 3.41). Supporting features include the triangular facets, offset streams, shutter ridges, linear valleys, and scarplets. The set of thirteen subdue triangular facets can be delineated. The average base width is about 50-200 m and the average height is about 60-80 m from the base with 40°-50° faceted spurs dipping to the west direction. The outstanding offset stream observed along the foot hill where stream cut across fault at the Ban Sob Yao and eastward of Ban Raad Samaki. Its flow direction changes to northward before joining the Nan River. A right-lateral movement caused about 50 m stream shift (Figure 3.42b). The occurrence of the north-south trending shutter ridge with the 50 m average base width and about 15 m height indicate the vertical slip movement. The linear valley, Huai Wa and Huai Nam Cham, trend is parallel to the main fault and directly flows to the Nan River at Ban Hat Khet (Figure 3.42a).



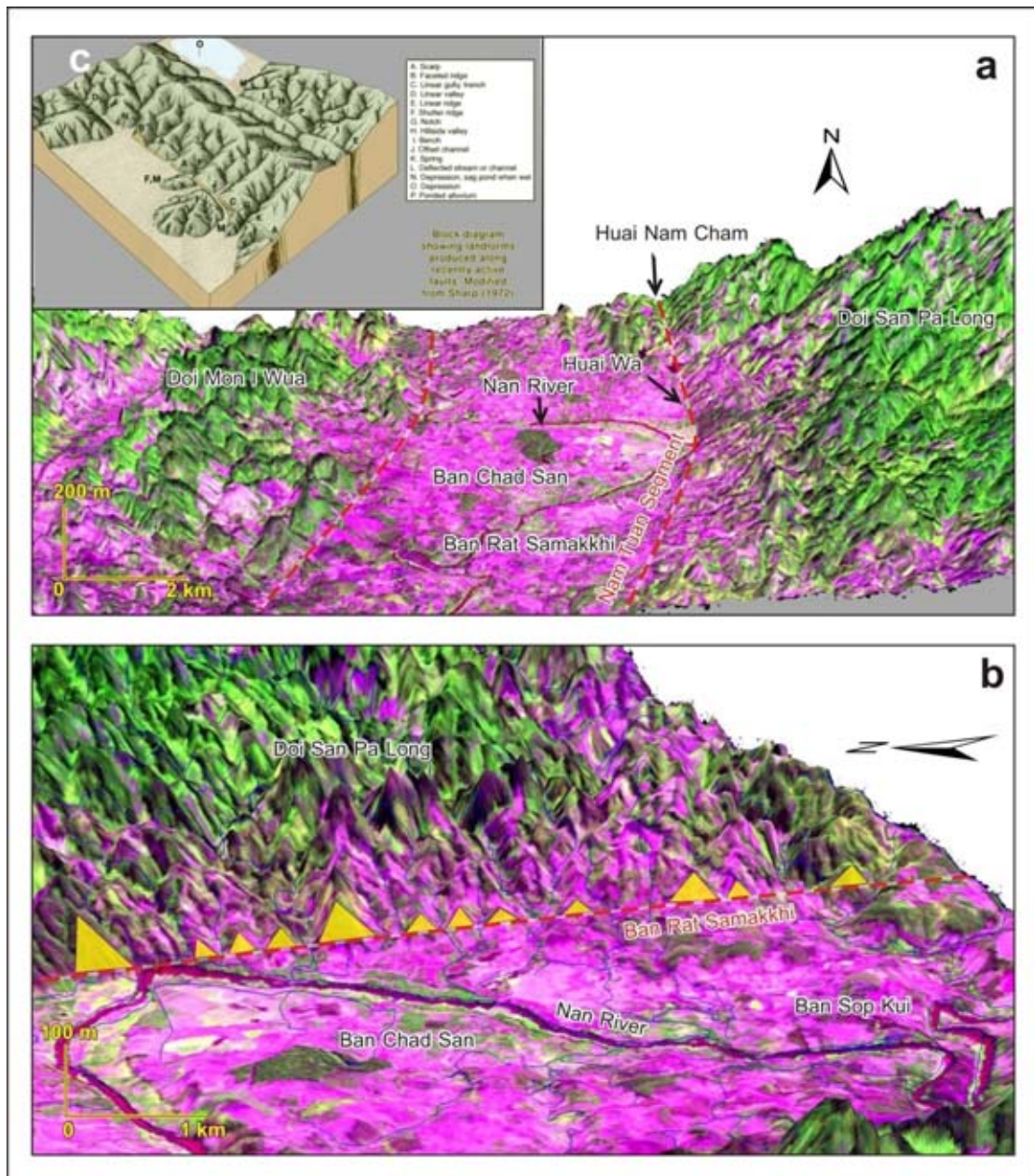


Figure 3.42 The 3D model of ASTER image at Ban Muang Luang, north of Nan Basin showing Nam Tuan Segment (red dashed lines) and the neotectonic features, such as linear valley (a) and triangular facet with steep slopes (b), in comparison with landforms produced along recently active fault proposed by Sharp (1972).

CHAPTER IV

FIELD INVESTIGATIONS

Two main outputs were assigned for the field investigation. One is the field checking for remote sensing image interpretation. Special emphasis was placed on landforms or morphotectonic evidence relating to active faults, and evaluation of the morphotectonic study. The other outcome is to assign the detailed field investigation in the particular area, including the exploratory trenching for paleoseismic and geochronological studies.

4.1 Field evidences of tectonic geomorphology

4.1.1 Area 1: Ban Thung Ao, Amphoe Thung Chang

The study area is situated in the north of Pua basin near Thai-Laos and border and the area can also be accessed by asphalt roads in all seasons. Topography in this area, both east and west sides, belong to mountainous, Doi Khun Huai Nam Ao is an important mountain located on the eastern flank of basin. The central part of this area comprises mainly the undulating terrain with small hills alternate with the narrow flood plain area. The Nan River is main channel, and it flows southward but the branches flow in the different direction, however most of them flow in the east-west direction (Figure 4.1).

We found that all morphotectonic features interpreted from satellite images are clearly observed in the field. However, there are some features which can be found in the field. For instance, at a quarry in Ban Ngop Nuea the author observed outcrops of Tertiary semi-consolidated rocks consisting of sandy clay and plant remain with overlain by sand and gravel bed. These Tertiary sediments have been cut by normal fault dipping into the basin (Figure 4.2). Based on air-borne images, triangular facets are well recognized along the Thung Ao segment. In the field at Ban Thung Ao appears a set of west dipping triangular facets appears immediately at flood plain. The facet set was developed in the north trend along the Doi Khun Nam Ao range, suggesting a fault running parallel to the mountain front (Figure 4.3). In Figure 4.4, the appearance of triangular facets along the Thung Ao segment is well developed as series of facet spurs. Perhaps this indicates that the fault show several movements. At the foot hill, east of Ban Thung Ao (Figures 4.5) there are significant morphotectonic evidences

including a stream course as linear valley feature parallel to fault line. A small shutter ridge and a compress ridge are oriented parallel to fault trace in the north-south direction. Besides, the hill ridges and many streams were offset in same direction, i.e., southward, the shortest offset length is approximately 60 meter.

According to field investigation result of Ban Thung Ao area, several morphotectonic evidences indicate that the Thung Ao segment has a potential to be the active fault faults and its movement is normal sense together with the left-lateral movement.

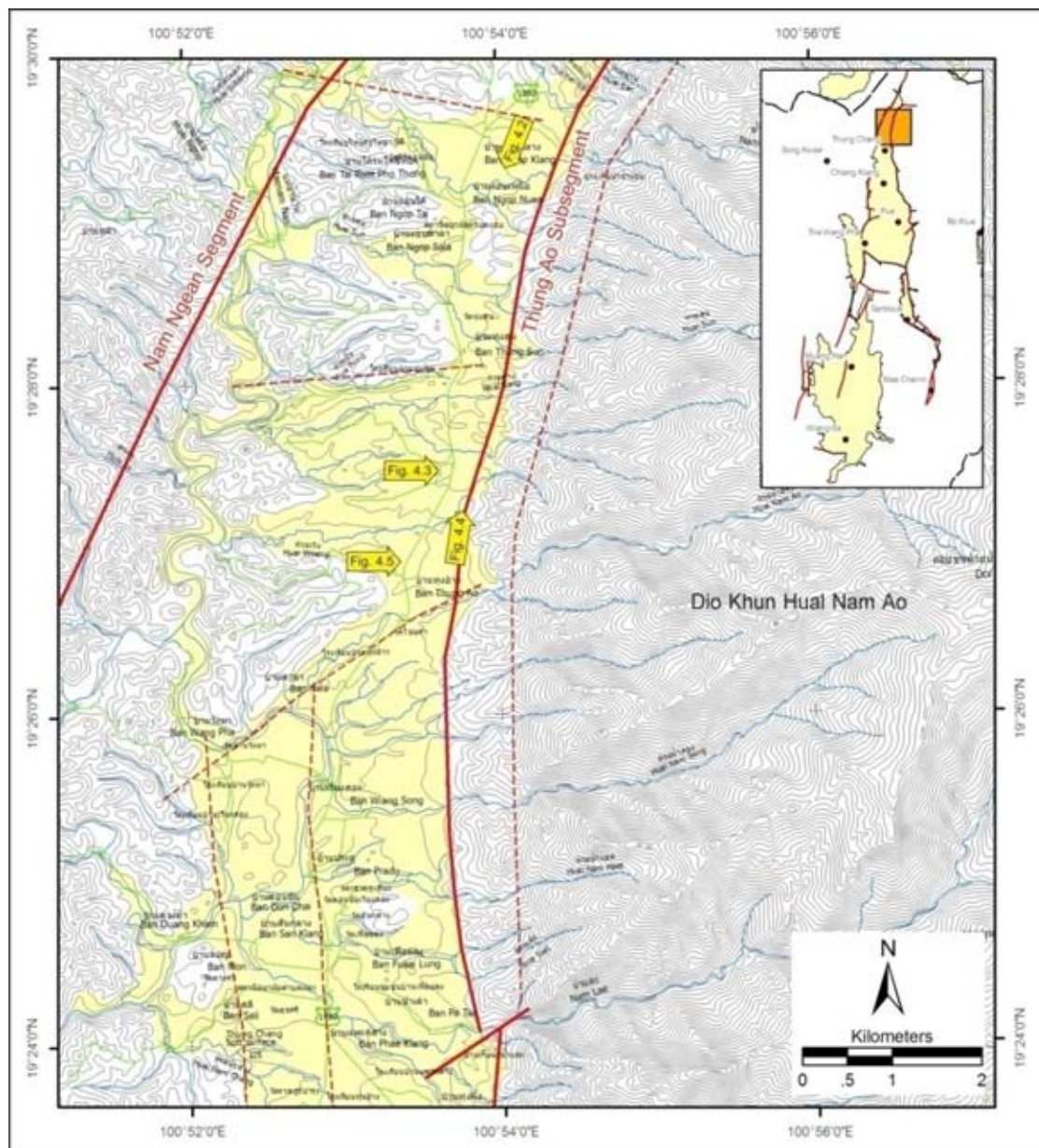


Figure 4.1 Topographic map of Ban Thung Ao area, showing the location of the Thung Ao segment. Note that the yellow arrows represent the areas of photographs taken from field investigation.

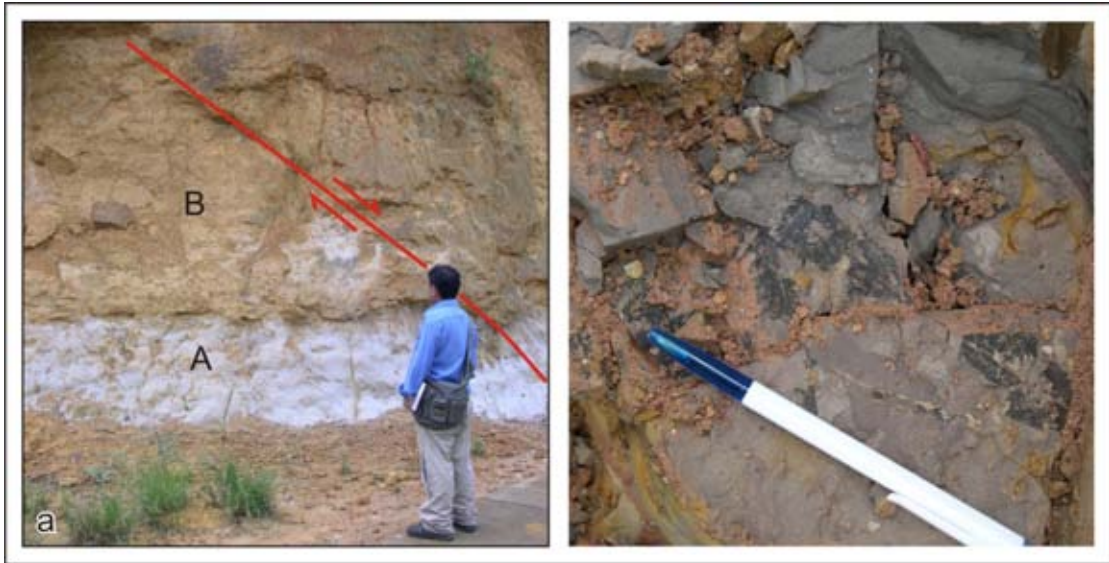


Figure 4.2 a) Semi-consolidated alluvial deposits at Ban Ngop Nuea consisting of silty mud overlain by gravel beds which were cut by normal fault dipping to west (the author –Kitti Khaowiset- is to scale). b) A close-up view of plant fossils (dark coloured) in (grey) silty mud indicated Tertiary age (view looking to south at 699238 E / 2155615 N).



Figure 4.3 A panorama of the north-trending Doi Khun Huai Nam Ao mountain range, north of BanThung Ao, showing the west-dipping triangular facet covered mostly by corn field (A) in the lower part of the fault step (B) (view looking to west at 698473E/2151683N).

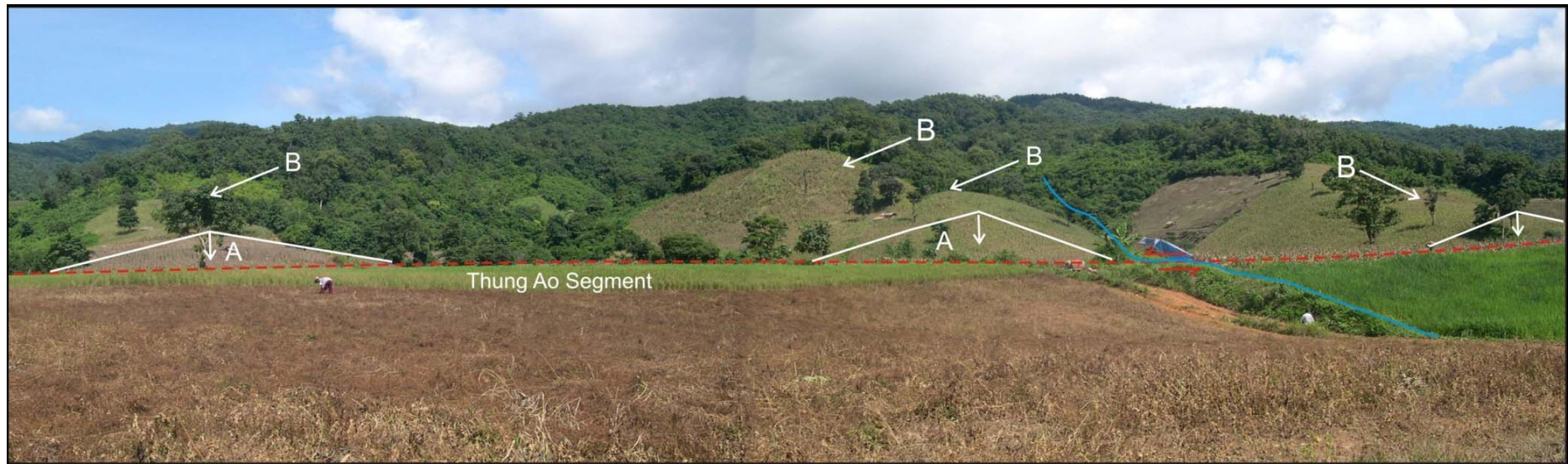


Figure 4.4 A panoramic view of set of triangular facets (A) and facet spur (B) of the Thung Ao fault segment, and its north-trending, north of Ban Thung Ao, Amphoe Thung Chang, Changwat Nan (view looking to east at 699177E/2152622N).

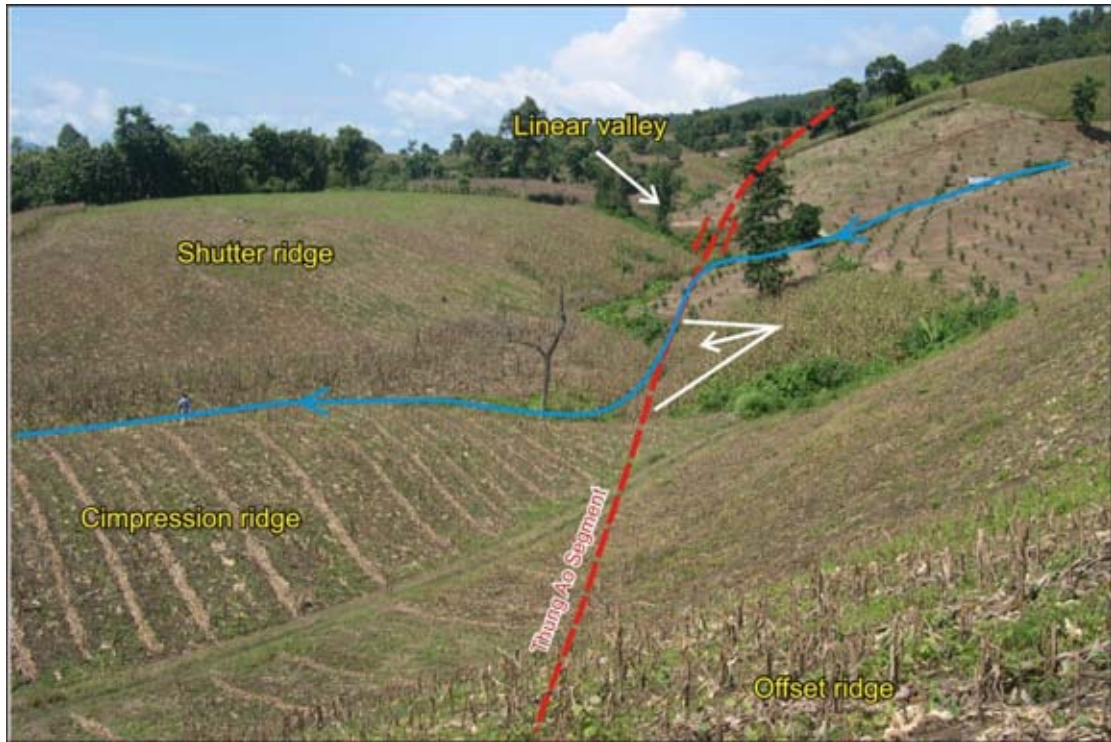


Figure 4.5 A physiographic feature showing the obvious geomorphotectonic evidences such as north-northeast-trending offset stream, small scarp, shutter ridge, compression ridge and offset ridge, suggesting the normal-oblique fault with a sinistral movement (view looking to NNE at 699051E/2152079N).

4.1.2 Area 2: Ban Doo, Amphoe Chiang Klang

This study area is manifested by the flat plain bounded to the east by the north-south trending mountain range (i.e., Doi Khun Setun) with a straight flank (Figure 4.6). Channels in this area are branches of the Nan River and most of them flow to the west.

The result from aerial-photographic interpretation around Ban Doo area along the north-south trending Ban Doo segment is shown in Figure 4.6. Based on the field investigation, important geomorphologic features and landforms investigated are triangular facets. The triangular facets have about 200-350 m and the height of about 60-80 m and the slope of about 45° to west (Figure 4.7). At basement of some triangular facet east of Ban Doo we can observe the offset streams and scarplets or small fault scarps. The scarplet trends N-S almost parallel to the fault with height of 3-4 m (Figure 4.8), and is nearby the trench Ban Doo. The offset stream is nearby the

scarplet which is offset to the north approximately 20 meters (Figure 4.9). Outcrops of meta-sandstone interbedded shale are on the triangular facet of Doi Phu Sathan (Figure 4.10) showing rock cleavages dipping to the west following the facet. On the other hand, the fault trace with the northeast strike in the southern part belonging to the Den Phana segment. This segment reveals at least seven triangular facets with steeply (60°) dipping to the southwest direction (Figure 4.11). This is the important evidence for the series of facet spurs produced by episodic vertical tectonic movements as illustrated in Figure 3.3. Series of facet spurs show at least 5 steps which assume that the Den Phana fault have been moved 5 times.

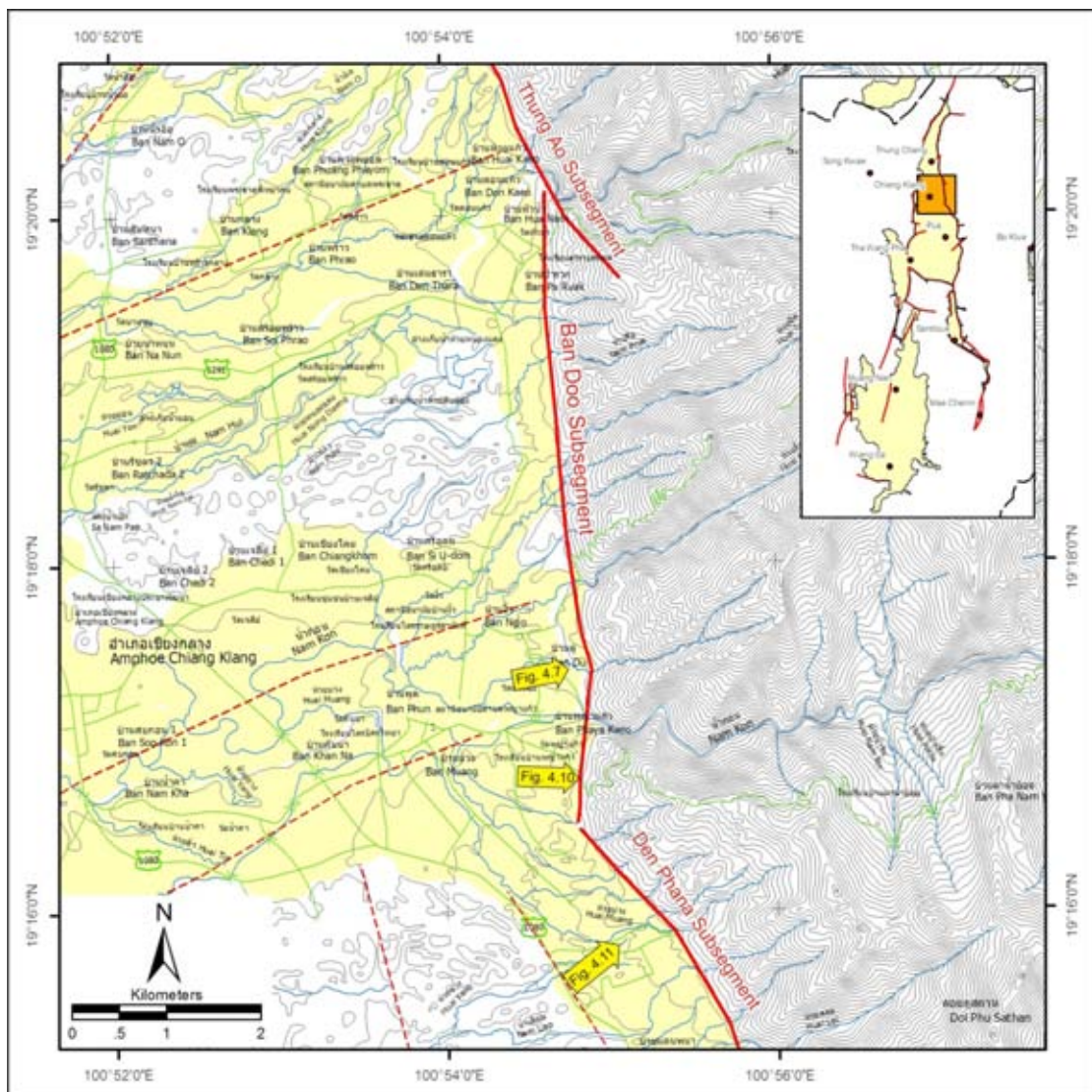


Figure 4.6 Topographic map of Ban Doo area, showing the location of the Thung Ao segment. Note that the yellow arrows represent important tectonic geomorphic features along the fault segments.

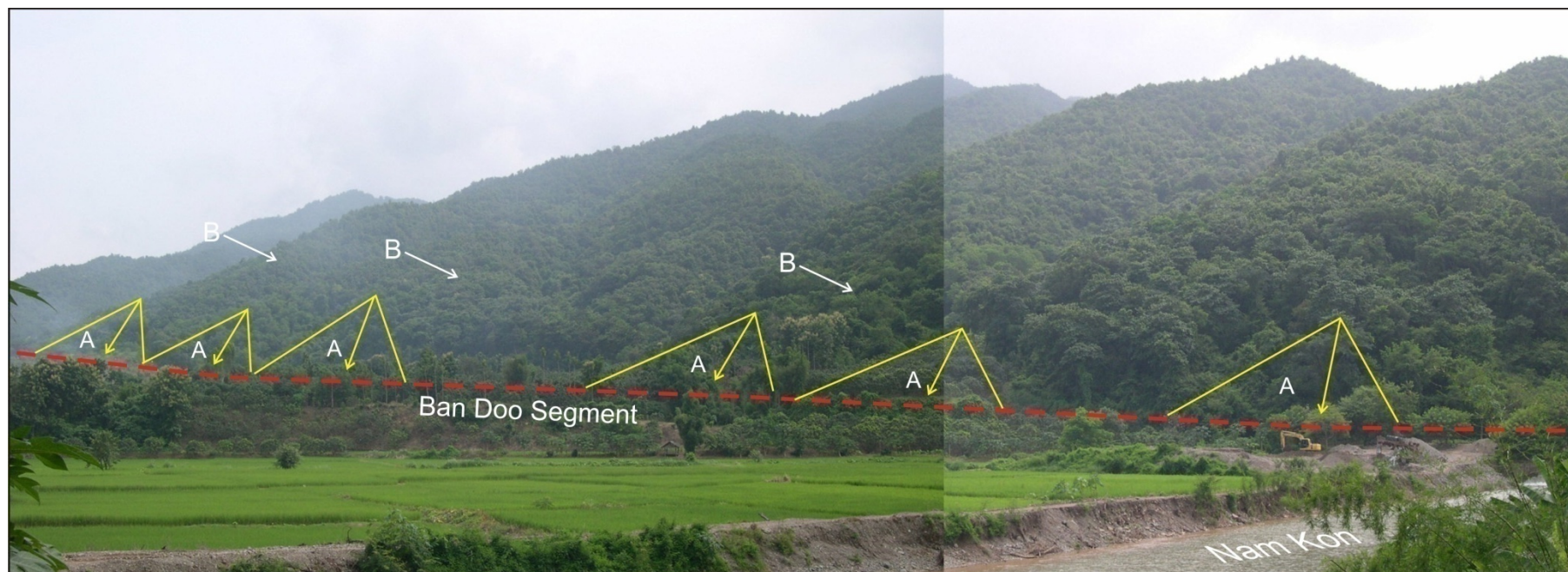


Figure 4.7 A linear front range with facet spurs (B) and triangular facets (yellow) dipping to west of the Ban Doo fault segment, Doi Khun Satun situated on the east Pua basin, Ban Doo, Amphoe Chiang Klang. Note that the Nam Kon River is on the right.



Figure 4.8 A scarplet (or small scarp) with a low-angle slope of Ban Doo segment (Pua Fault) cutting Late Quaternary alluvial deposit, Nan (located at 701177E/2134105N).



Figure 4.9 Photograph showing the NNW-trending offset stream with the dextral sense of movement (red arrowed) observed along the Ban Doo fault segment in Ban Doo area, Amphoe Chiang Klang, Changwat Nan (view looking at 701177E/2134105N to North).



Figure 4.10 Meta-shale on the west flank of Doi Phu Sathan, east of Ban Phaya Kaeo, Amphoe Chiang Klang. Cleavage is dipping to the west.

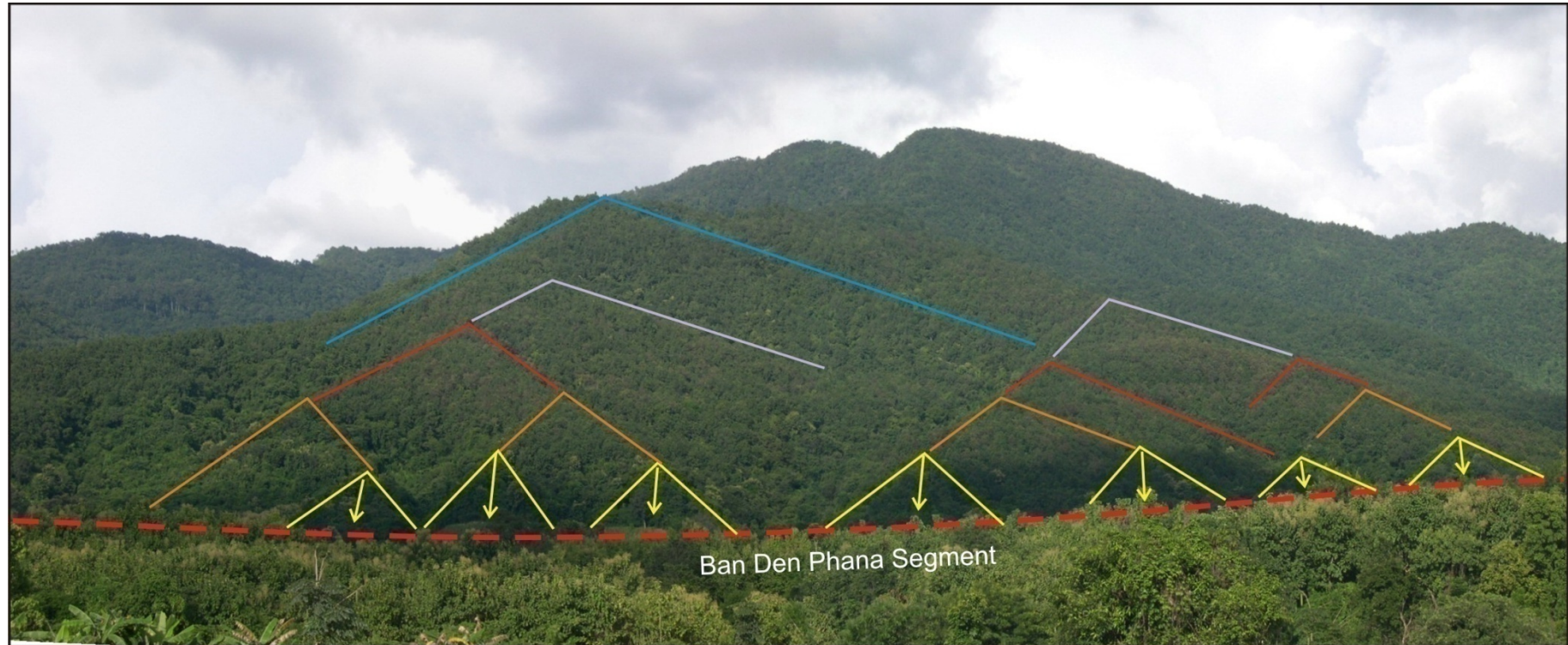


Figure 4.11 Series of triangular faceted spurs along the Den Phana segment, east of Ban Den Phana. Note that the over steepened base and the development of several erosional benches along the fault, suggesting 4 times of fault movement.

Regarding the result of field investigations and various criteria obtained at Ban Doo area, it is discovered that the north-trending Ban Doo fault and the northwest-trending Den Phana fault show sets of triangular facets, dipping at high angles to the west direction with scarplets and offset streams at facet basement. It is considered therefore that the Ban Doo and Den Phana faults are potentially active fault which have normal displacement westward and collaborated well with right lateral strike-slip movement of at least 20 meter. Series of facet spurs (at least 5 steps) imply that fault have been moved at least 5 times from the first displacement.

4.1.3 Area 3: Ban Tin Tok, Amphoe Pua

The Ban Tin Tok Su area is located south of Pua basin. Physiographically, it is characterized by Permo-Triassic sandstone mountainous of Phu Kha (600-1,000 m, msl) observed to east of the large flat area. Major streams are Pua and Nam Khwang Rivers, flowing westward to join the Nan River (Figure 4.12).

The field investigation displays several features of morphotectonic evidence along the fault segment, particularly triangular facets. The facet is produced by vertical tectonic movement. At Ban Don Keao (Figure 4.13), triangular facets are of two fold. The first set is along the Den Phana segment and shows six facets of about 200-400m average base width and about 40-60 m average height from the base with 50° dipping. The other set belonging to Tin Tok segment has five facets showing geometry similar to those of the first set. Most triangular facets in the area dip to the east direction. Figure 4.14 shows triangular facets along Tin Tok segment at Ban Don Chai. The facets are about 250-350m wide and 40-60 m high, and all of them dip to west. In most southern part of Ban Tin Tok area at Ban Hua Nam, the triangular facets along the Tin Tok segment are very high and very steep, as well as display wine-glass canyons (Figure 4.15). Basement of a wine-glass canyon is at Fai Nam Kang dam (Figure 4.16) that display outcrops of meta-sandstone cut by normal fault dipping into basin (Figure 4.16b). The Fai Nam Kang reservoir shows cryptic phenomenon because there are a lot of small air-bubbles rising up from water in the fault zone (Figure 4.16c). We interpret this feature representing the other active movement (or activity) along the fault.

Result of the field investigation in Ban Thung area indicate well-defined morphotectonic landforms, including triangular facet and wine-glass canyon.

The formation of wine-glass canyon (Woodward Clyde Federal Services, 1996) indicates vertical fault movement with the rate of faulting greater than erosion rate (see Figure 3.34). As mentioned above, Tin Tok segment is assigned as potentially active fault.

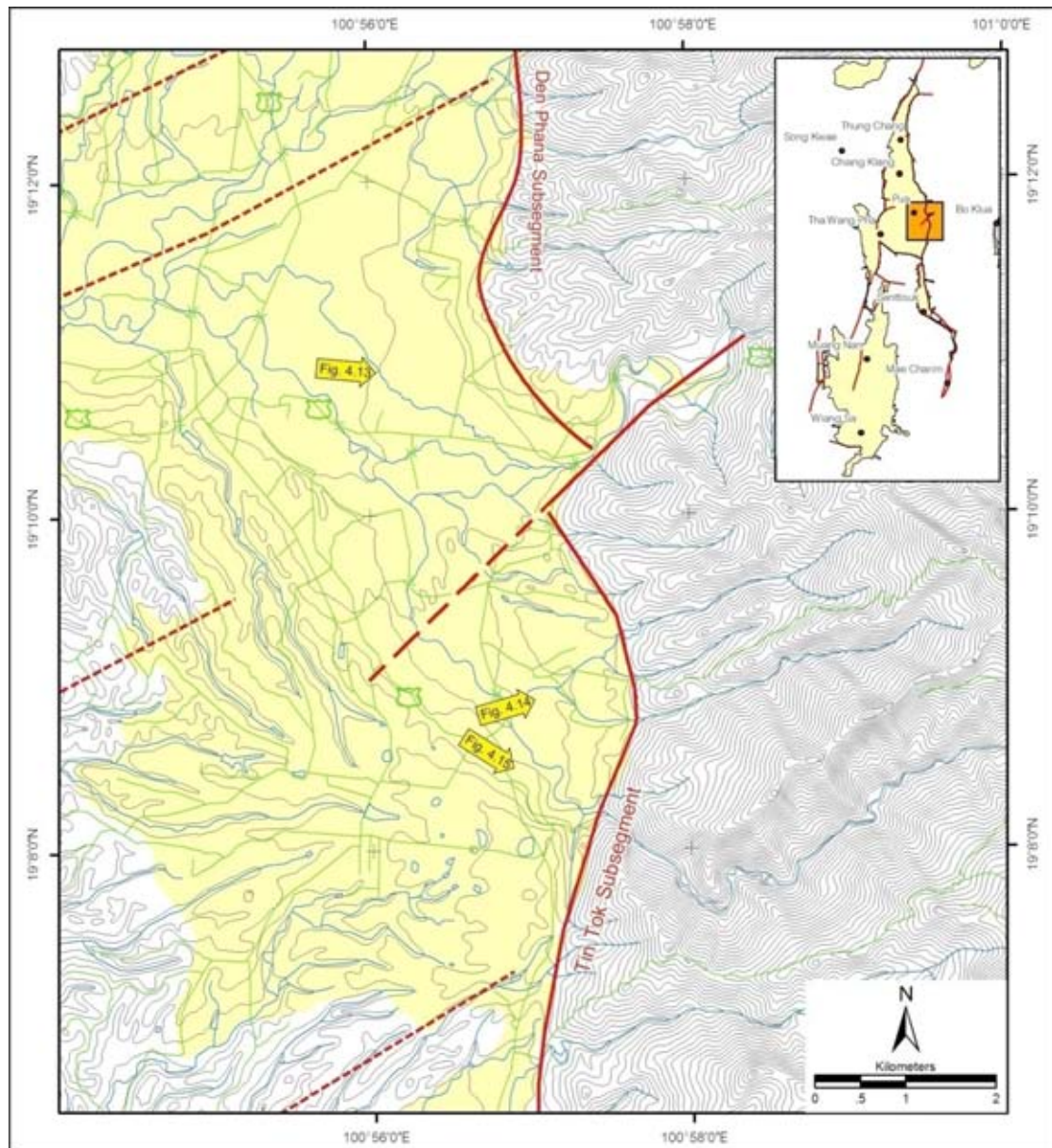


Figure 4.12 Topographic map of Ban Tin Tok area, showing location of the Tin Tok segment. Note that the yellow arrows represent the areas of photograph taken from field investigation in this area.



Figure 4.13 A panoramic view of Phu Kha showing the west dipping triangular facets along fault segment (view looking to east at 701366E/2122205N).

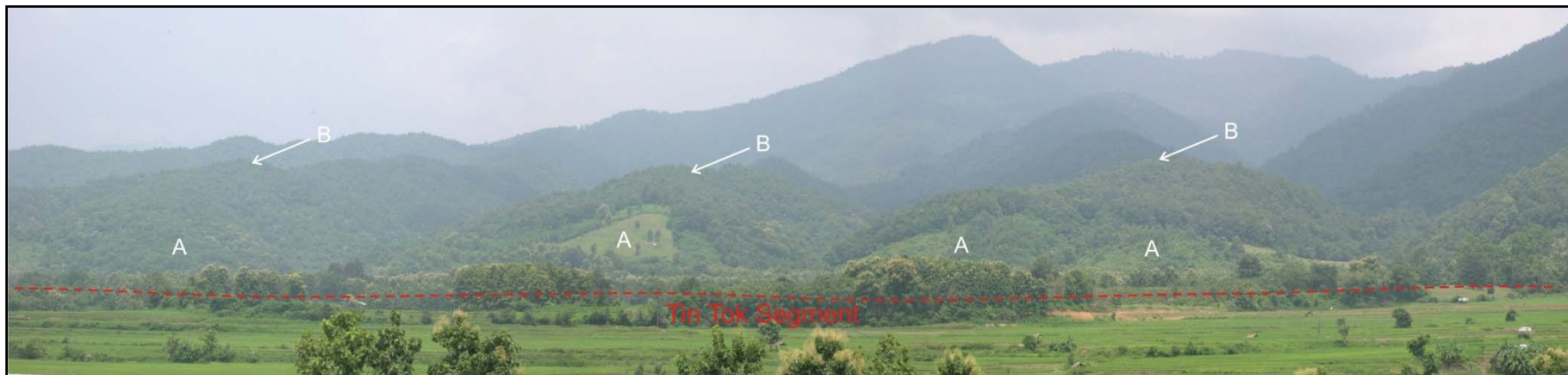


Figure 4.14 Triangular facets (A) and facet spurs (B) observed along the Tin Tok fault segment in Tin Tok area, Ban Tin Tok (view looking to NE at 704637E/2117997N).

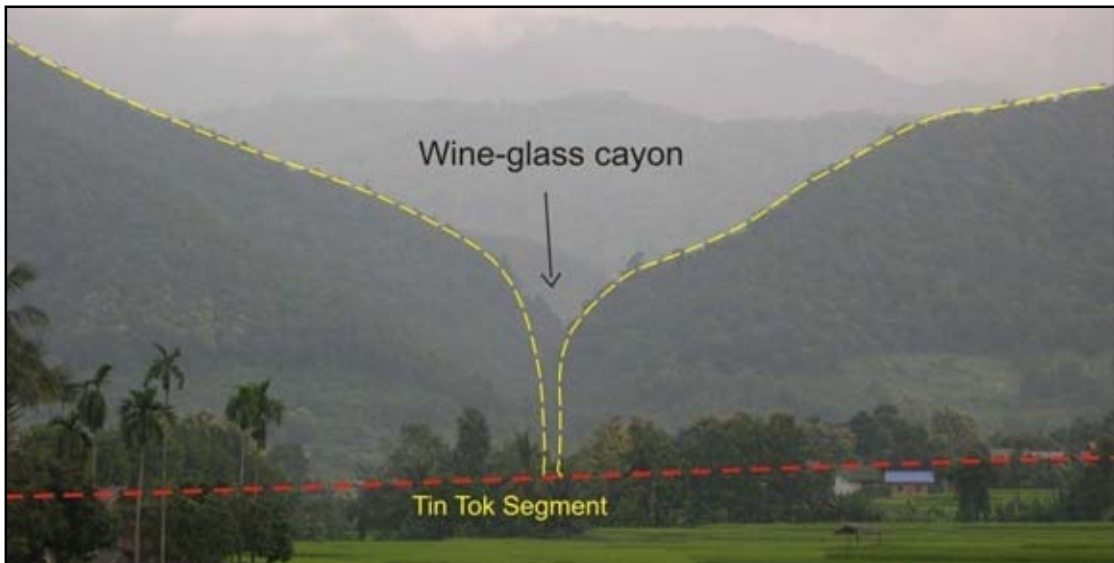


Figure 4.15 A view of wine-glass canyon developed where the Nam Khun crosses the Tin Tok segment, Pua Fault. Note that compare canyon with figure 3.34 (view looking to east at 701366E/2122205N).

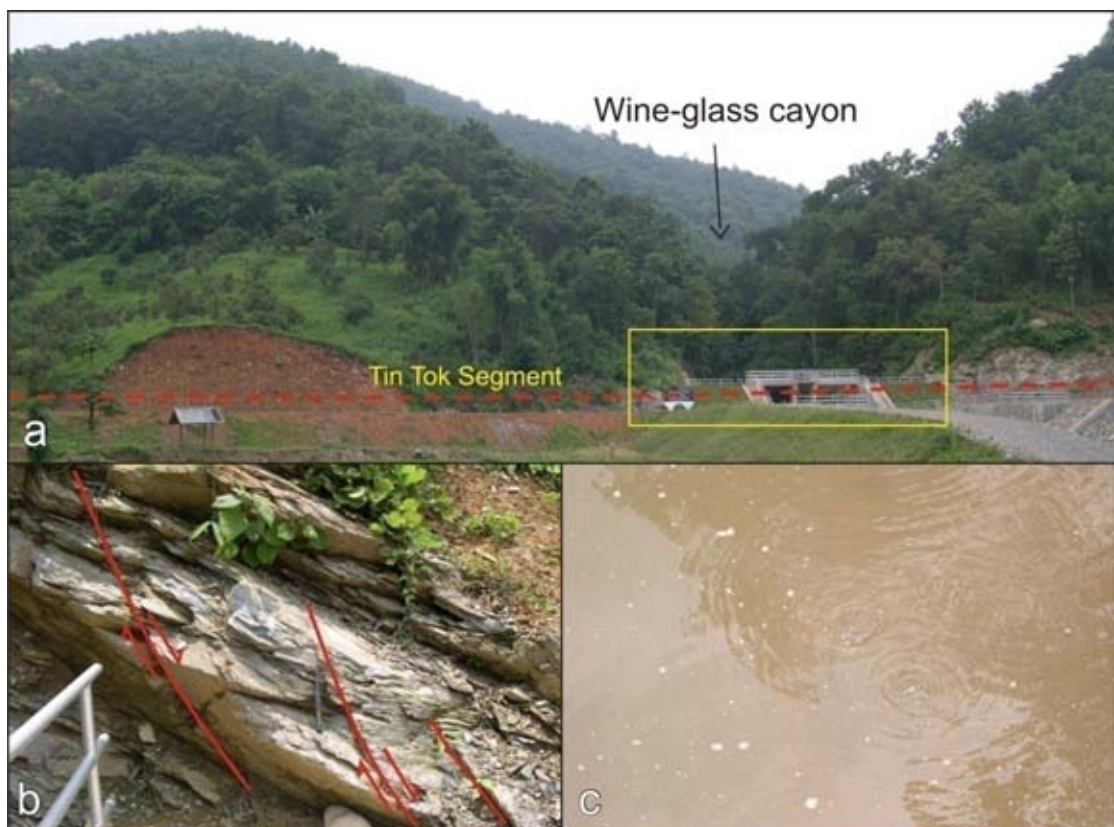


Figure 4.16 a) Foot of wine-glass canyon (figure 4.15) at Kaeng dam site, Ban Hua Nam, Nan. b) Close-up view at the foot of wine-glass canyon beside the dam showing meta sandstone cut by normal fault set. c) Small air bubbles observed at from water in the Kaeng reservoir (photo taken to southeast at 705966E/2117149N).

4.1.4 Area 4: Ban Thung Hao, Amphoe Pua

Ban Thung Hao is located in the northern part of Santisuk basin, mostly dominated by the mountainous area with rolling topography. In the central part, it is flat-laying area belonging to Thung Hao sub-basin and is bounded by normal fault. Major stream is Nam Mae Uan, flowing southward along the basin shape (Figure 4.17).

In an area of the Ban Thung Hao, the Santisuk fault segment is bounding the eastern rim of Thung Hao sub-basin. Subdue triangular facets and fault

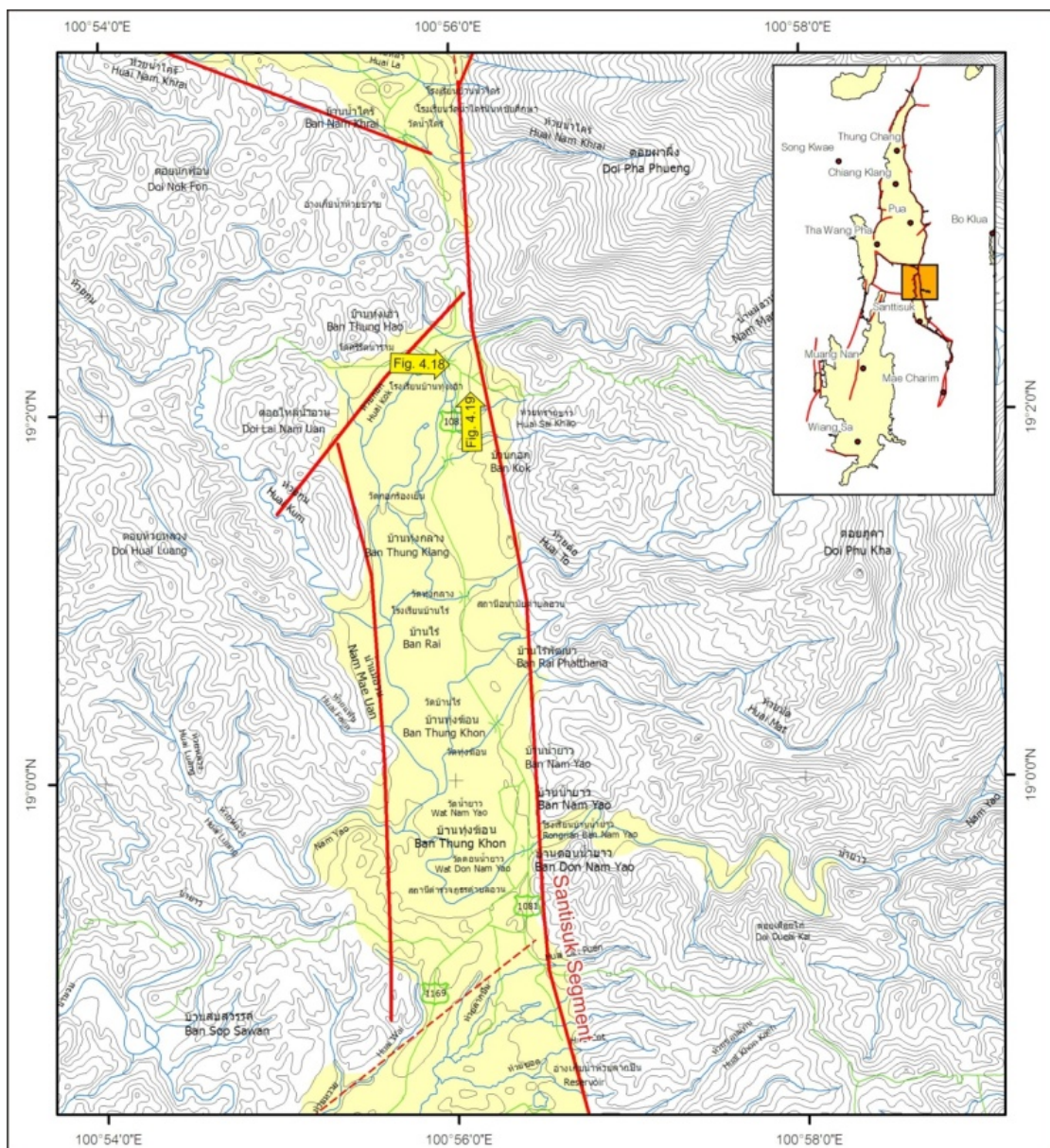


Figure 4.17 Topographic map of Ban Thung Hao area, showing the location of the Santisuk fault segment, Nan. Note that the yellow arrows represent the areas with distinct morphotectonic features.

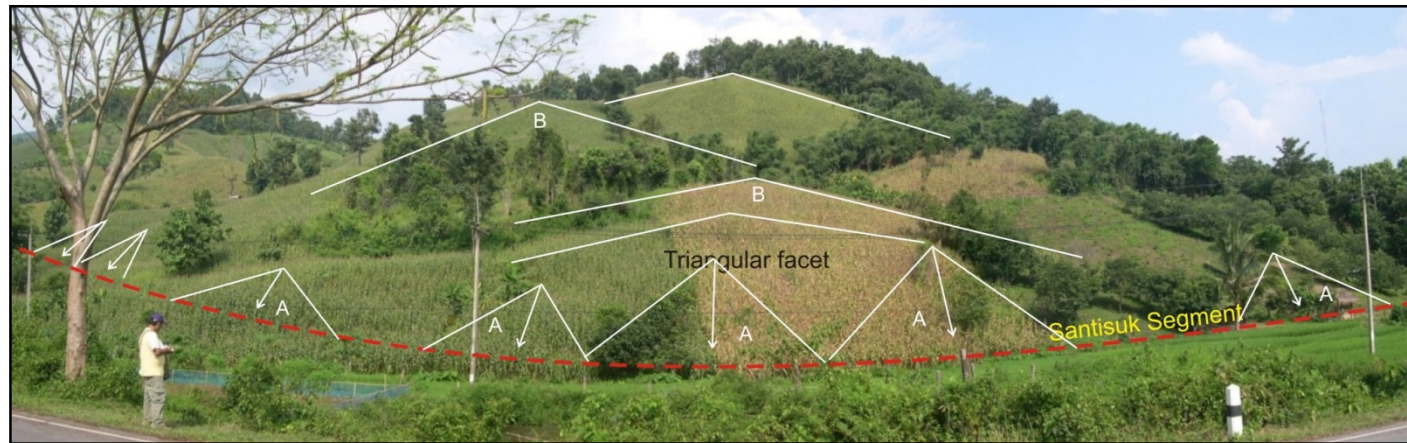


Figure 4.18 A panoramic view show set of triangular faceted (A) and fault step (B) along the Santisuk fault segment Ban Thung Hao, north of Amphoe Santisuk (view looking at 703459E/2106129N to east).

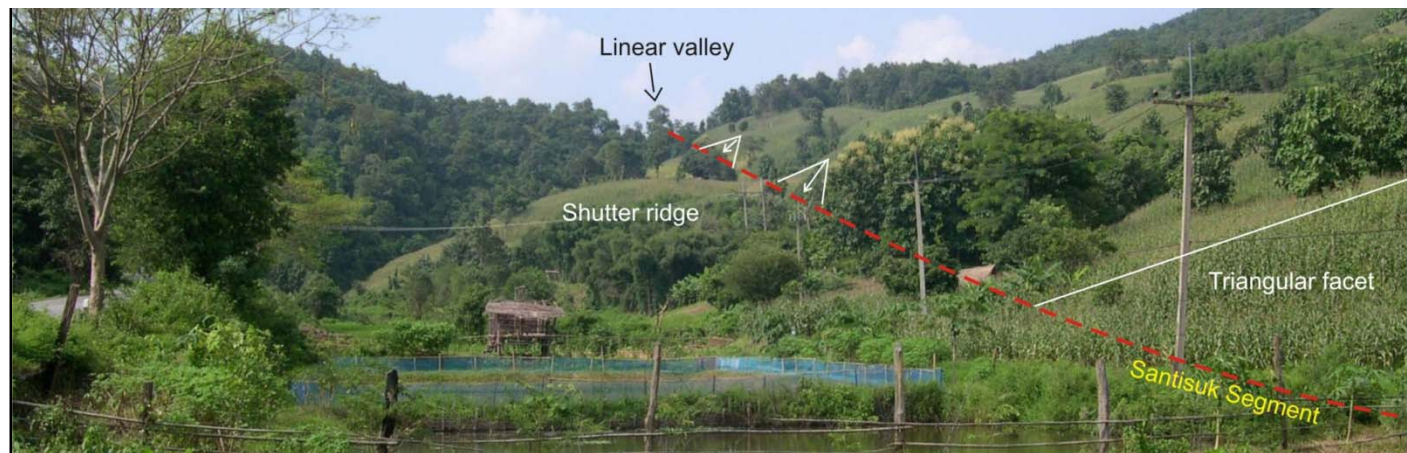


Figure 4.19 A view looking to north at Ban Thung Hao showing a set of triangular facet and linear valley. Note that the Santisuk fault segment is shown by red dashed line (703459E/2106129N).

scarps along the fault segment are observed (Figure 4.18). The facet strikes northward and dips westward, suggesting the fault orientation of the Santisuk segment. Series of facet spurs (Figure 4.18) was developed by the episodic vertical tectonic movement. Linear valley parallel to the fault line along the country road no. 1018 from Ban Thung Hao to Amphoe Santisuk, occurs in front of the triangular facets (Figure 4.19).

Several features of morphotectonic evidence are recognized, such as triangular facets and a linear valley. These suggest that the Santisuk fault segment is a normal fault with dipping into basin and become potentially active.

4.1.5 Area 5: Ban Sub Pua, Amphoe Pua

The study area shown in Figure 4.20 is situated on the western rim of Pua basin. The area can be accessed by asphalt roads which can be used in all season. The area is manifested by flood plain bounded to the west by the mountain range (Doi Koi Kok). The Nan River is the main channel, it flows southward almost following the fault. The Pua River is connected to the Nan River in this area.

At the Sob Pua area, the Sub Pua fault segment shows a continuous length of 10 km. The direction of the main fault trace as interpreted by aerial photography is in the northwest-southeast direction and concave to the southeast. The field reconnaissance survey in the Ban Sob Pua reveals that the triangular facets shows six facets with the average base width of about 300-400 m and the average height of about 60-80 m. The slope of facets is about 40°. Based on remote sensing investigation, the flood plain area is a depression zone which has been caused by the extension regime in the east-west direction. This flood plain area is well observed at Wat Sala, Ban Nawong where the Pua River is connected to Nan River (Figure 4.21). At Wat Sala, the author found that the significant evidence of historical earthquake in this area is a pagoda named “Phrathat Din Wai”, the memorial of earthquake event in 1827 (Figure 4.22).

Result of the field investigation, particularly in the study area, morphotectonic evidence along the northwest-southeast fault, triangular facets and fault scarps as well as historical earthquake data indicate that normal fault is potentially active.

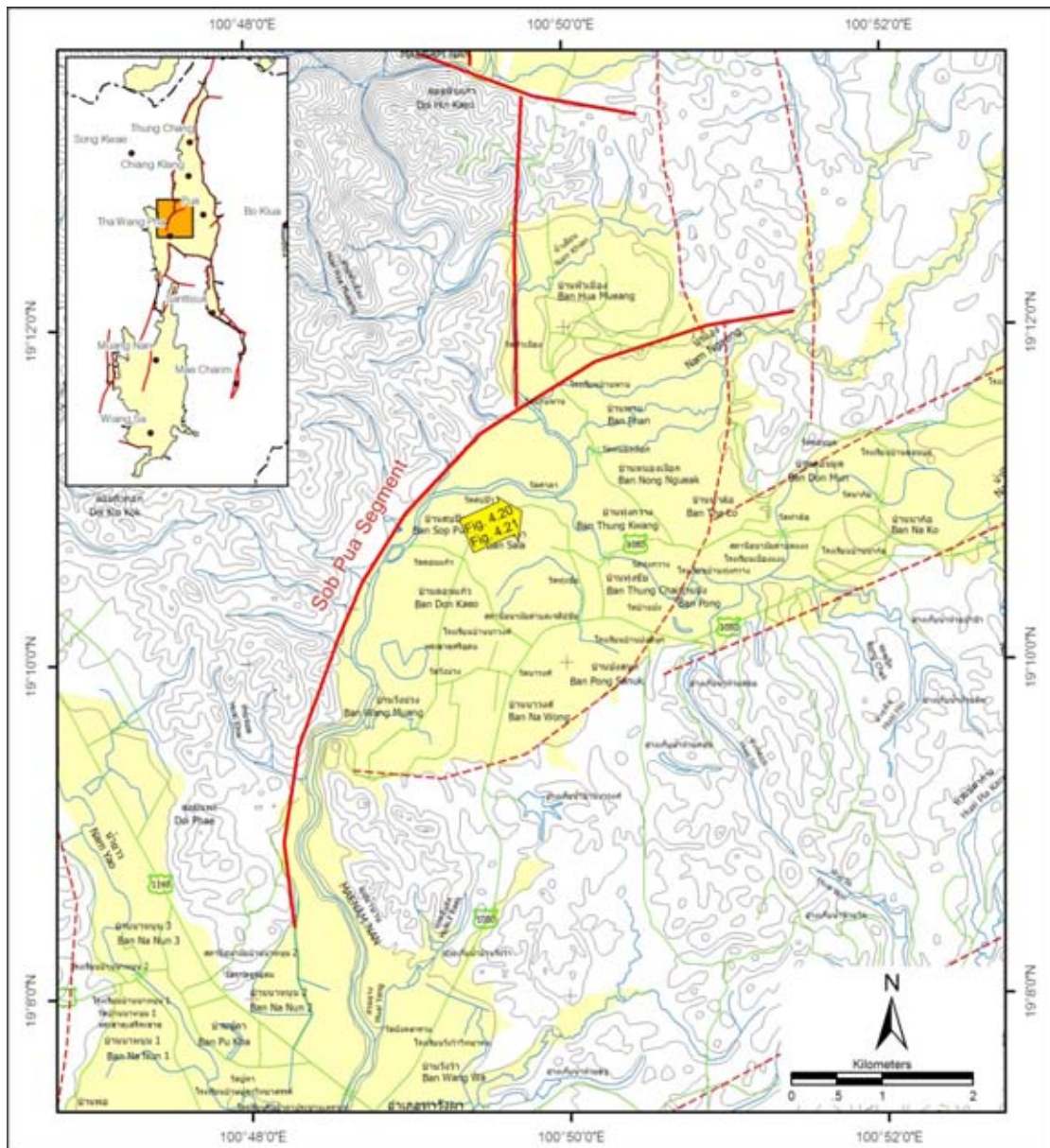


Figure 4.20 Topographic map of Ban Sob Pua area showing the location of the Sob Pua segment. Note that the yellow arrow represents the areas of photograph.



Figure 4.21 View looking northeast of the Pua river bank showing the point bar area in the west (left) and the erosional bank in the east (right) at Ban Sob Pua village (looking to east at 692366E/2122073N).



Figure 4.22 Prathat Din Whai – The Chedi at Wat Sala, Ban Nawong, Amphoe Pua was built in 1827 and named by the earthquake event on that year (locating at 692366E/ 2122073N).



Figure 4.24 Triangular facets observed along the Nam Tuan fault segment in Ban Muang Luang valley (view looking to SE at 692193E / 2086241N).

In an area of the Ban Muang Luang, the Nam Tuan fault segment (Figure 4.23) to the eastern border bounding the eastern rim of the basin. The field survey result indicates subdue triangular facets and an offset stream along the fault segment. The facet has 100 m height and strikes roughly northward and dips to the west.

Regarding the result of field investigations and various criteria obtained from the Ban Muang Luang area, it is likely that the Nam Tuan fault segment is potentially active fault which show westward normal displacement with right lateral movement (Figure 4.24).

4.2 Paleoseismic Trenching

4.2.1 Site selection for Paleoseismic Trenching

In as much as the reliable research is the supporting field evidences relevant to the fault segments concerned, it is necessity to study all the fault segment traces. Site selection of specific areas for detailed field investigation and paleoseismic trenching require some constraints to access the specified criteria. Therefore, selection of a specific area for this paleoseismic trenching covering six areas as mentioned before was conducted by compiling relevant supporting information both strength and weakness of each area for the next step. The most effective and suitable area was chosen for further detailed study and trench excavation. Nontectonically, the criteria are the accessibility since backhoe must be used for digging trench, and the ownership and authorization of the proposed area must be the second criteria.

Rating formula is shown in Table 4.1. Priority of those factors was set based on its importance and relevance to the study. Rating level 3 was set for the most important geologic factor. Those are lithology, and geomorphology. Rating level 2 is the accessibility, and the remaining factors are considered to be rating level 1.

Conclusion of rating formula is shown in table 4.2. Ban Thung Ao Area and Ban Doo area are the most effective and suitable areas to be considered as the area of study due to their highest score (29) as shown in the table.

Table 4.1 Rating criteria and priority for selection of detailed investigation area for exploration trenching (Saithong, 2006).

No.	Rating	Criteria	Rating Level
1		Lithology	3
	0	Rock	
	1	Uncosolidated homogenous sediments	
	2	Uncosolidated sediments lying over weathering rocks	
	3	Several sediment layers	
2		Geomorphologic evidence	3
	1	One geomorphologic evidence	
	2	Two geomorphologic evidence	
	3	Three geomorphologic evidence	
	4	equal or more than four geomorphologic evidences	
3		Accessibility	2
	1	Footpath, trail	
	2	Loose or hard surface, one or more lanes wide or cart tracks	
	3	Loose light surface, two or more lanes wide	
	4	Hard surface, two or more lanes wide	
4		Ownership of the land and authorization	1
	1	Unauthorized	
	2	Studying in the National Park area must be authorized by National Park, Wildlife and Plant Conservation Department	
	3	Plantation or Forest Reserve	
	4	Private area	

Note 0 = very bad;
1 = not good;
2 = fair;
3 = good; and
4 = very good.

Table 4.2 Rating of the selected areas suitable for the detailed field investigation.

Area	Lithology	Geomorphologic evidence	Accessibility	Ownership of the land and authorization	Suitability for study	Priority
Area 1	Several sediment layers	offset streams, triangular facets, shuttle ridges and linear valleys	Footpath, trail	Private area	Suitable: a corn field; in the rain season; authorized by the owner	27
	3*3	3*4	2*1	4		
Area 2	Several sediment layers	offset streams, triangular facets, wine-glass canyon, scarplets or small scarps	Loose or hard surface, one or more lanes wide or cart track	Private area	Suitable: Longan garden; authorized by the owner	29
	3*3	3*4	2*2	4		
Area 3	Homogenous sediment	triangular facets, wine-glass canyon, fault scarp	Loose light surface, two or more lanes wide that can be accessible all seasons	Private area	Suitable: Longan garden and a rice field; in the rain season; authorized by the owner	25
	3*2	3*3	2*3	4		
Area 4	Uncosolidated sediment lying over weathering rock	linear valley, triangular facet	Hard surface, two or more lanes wide can be accessible all seasons	Private area	Suitable: a rice field; in the rain season; authorized by the owner	24
	3*2	3*2	2*4	4		
Area 5	Uncosolidated sediment lying over weathering rock	offset stream, triangular facet	By boat in dry season only. Loose or hard surface, one or more lanes wide or cart track	Forest area	Unsuitable: studying in the forest area	20
	3*3	3*2	2*1	3		
Area 6	Uncosolidated sediment lying over weathered rock	offset stream and triangular facet, linear valley	Footpath, trail	Private area	Suitable: Longan garden and a rice field; in the rain season; authorized by the owner	21
	3*2	3*3	2*1	4		

4.2.2 Trench 1: Ban Thung Ao, Amphoe Thung Chang

Ban Thung Ao trench is located north of Ban Thung Ao along the country road no. 3199. Remote-sensing interpretation shows sharp lineament and geomorphology indicating offset streams, shutter ridges, linear valleys, offset ridges, and triangular facets at grid reference 0699044E /2152078N on scale 1:50,000, sheet 5147 III (Amphoe Thung Chang). The trench site is situated in the steeper slope near the offset stream, shutter ridges, offset ridge and triangular facets (Figure 4.25). The trench is excavated into the young sediments deposits, traverse perpendicularly across the fault trace. Trench geometry is 1.5 m in width, 30 m in length, and 3 m in depth.

4.2.2.1 Stratigraphic Description

As shown in Figures 4.26, 4.27, 4.28 and 4.29, it is quite clear that the Ban Thung Ao trench has relatively much more deformed stratigraphy. Trench-log stratigraphy is characterized by 6 unconsolidated sediment units. Detail of individual units is described below.

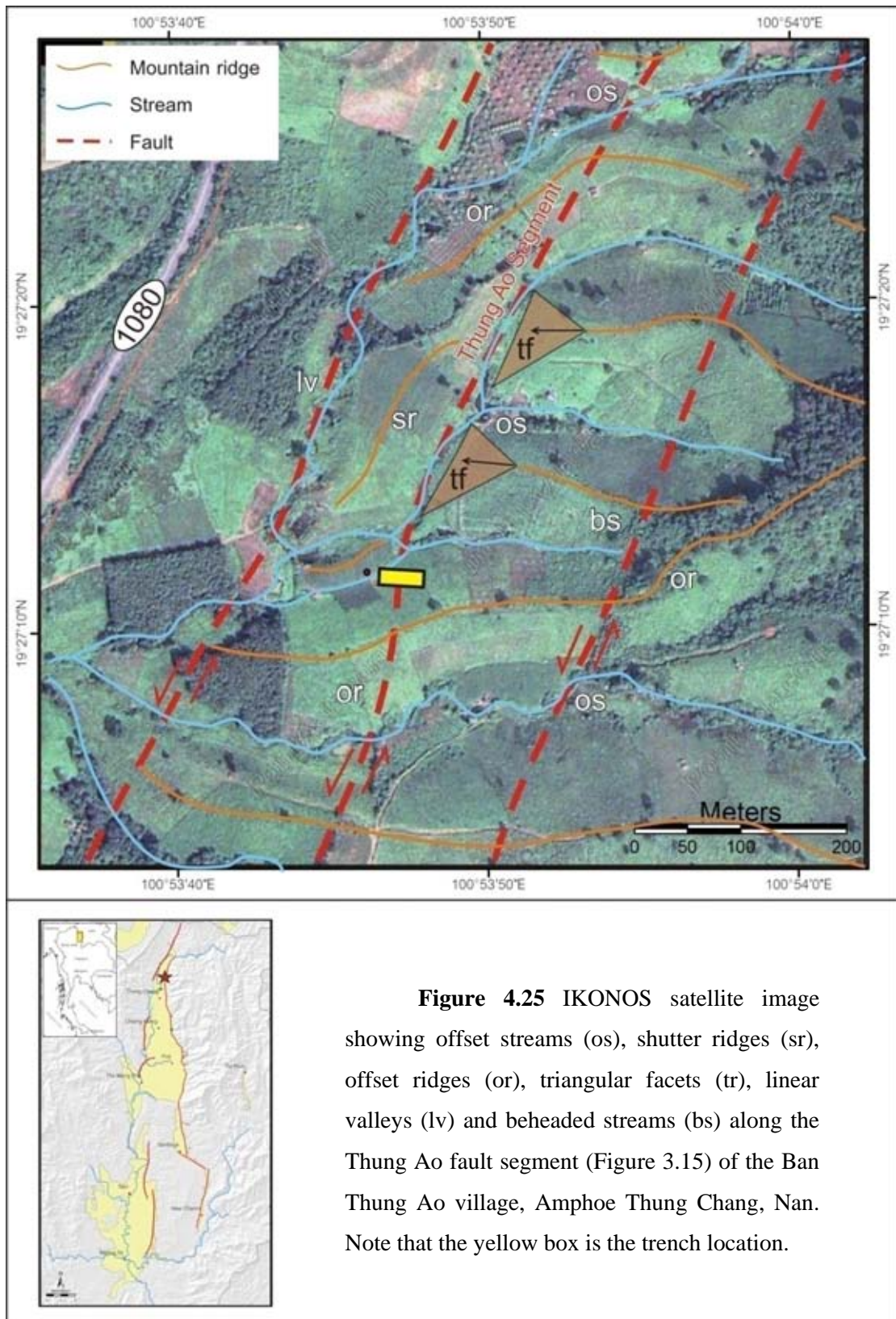
Unit A is a well-defined, light brown alluvial deposit consisting of fine- to coarse-pebble with angular to subangular shapes. The deposit is moderately-sorted and sand matrix. The thickness of this unit more than 1 meter.

Unit B is reddish brown, clayey sand layer containing sparsely distributed angular fragments of sandstone shale and iron concretion. Thickness of this unit varies significantly from 20 to 40 cm.

Unit C is well-defined, light brown colluvial deposit consisting of pebble to cobble-size sediments with angular to subangular shapes. The deposit is poorly-sorted and mainly matrix support. Its thickness ranges from 50 to 80 cm.

Unit D is characterized by light brown, clayey sand layer. Rock fragments of pebble size are also sparsely distributed in this layer. Thickness of this unit varies downhill significantly from 100 to more than 200 cm.

Unit E is characterized by light brown, fine-sand layer with some subangular sandstones and quartz pebbles (5%). The thickness varies downhill from 30 to 100 cm in the west-east direction.



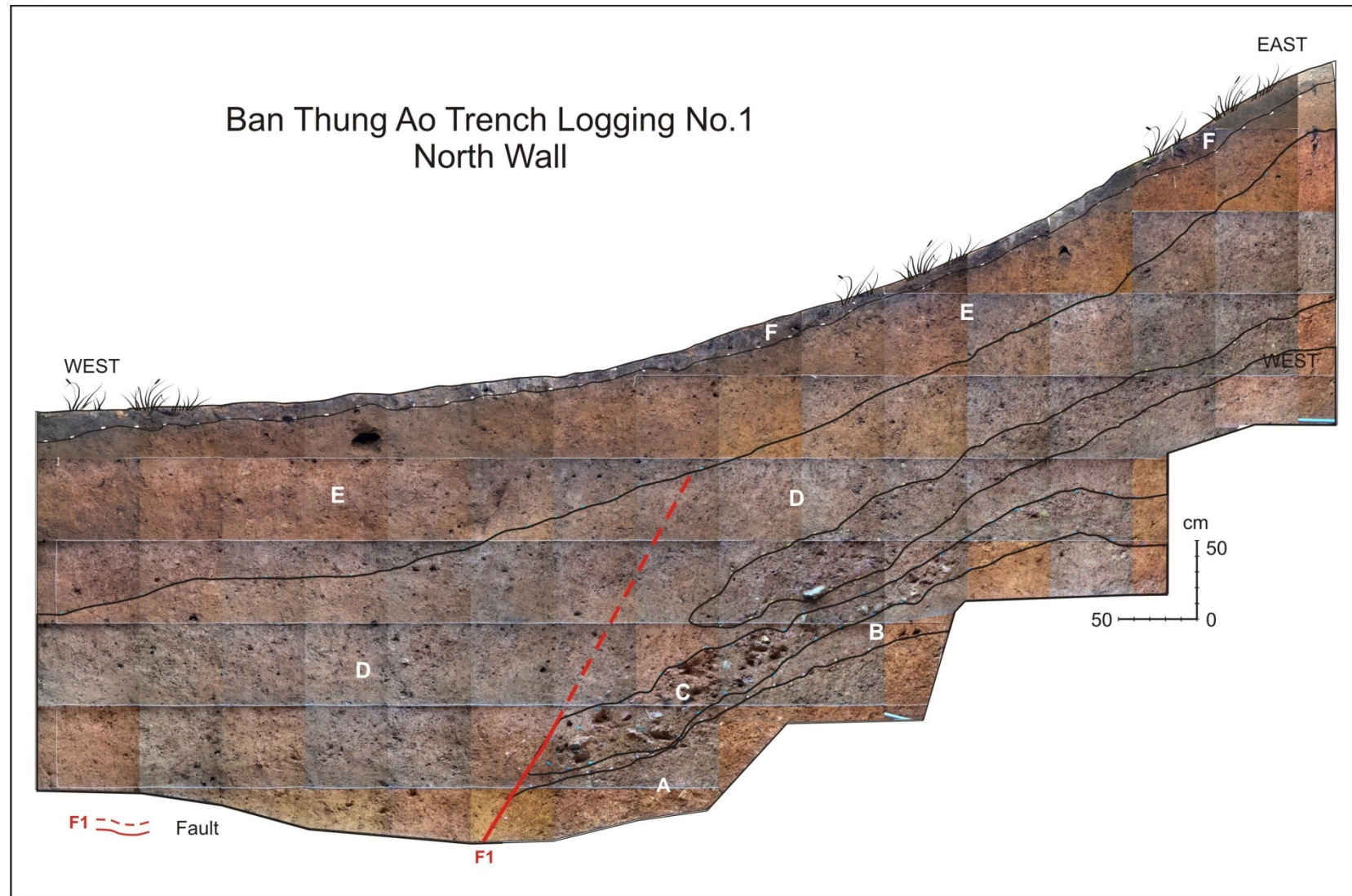


Figure 4.26 View of paleoseismic trench section (no.1) on the north wall, Ban Thung Ao village, Nan, showing Quaternary stratigraphy and fault orientation.

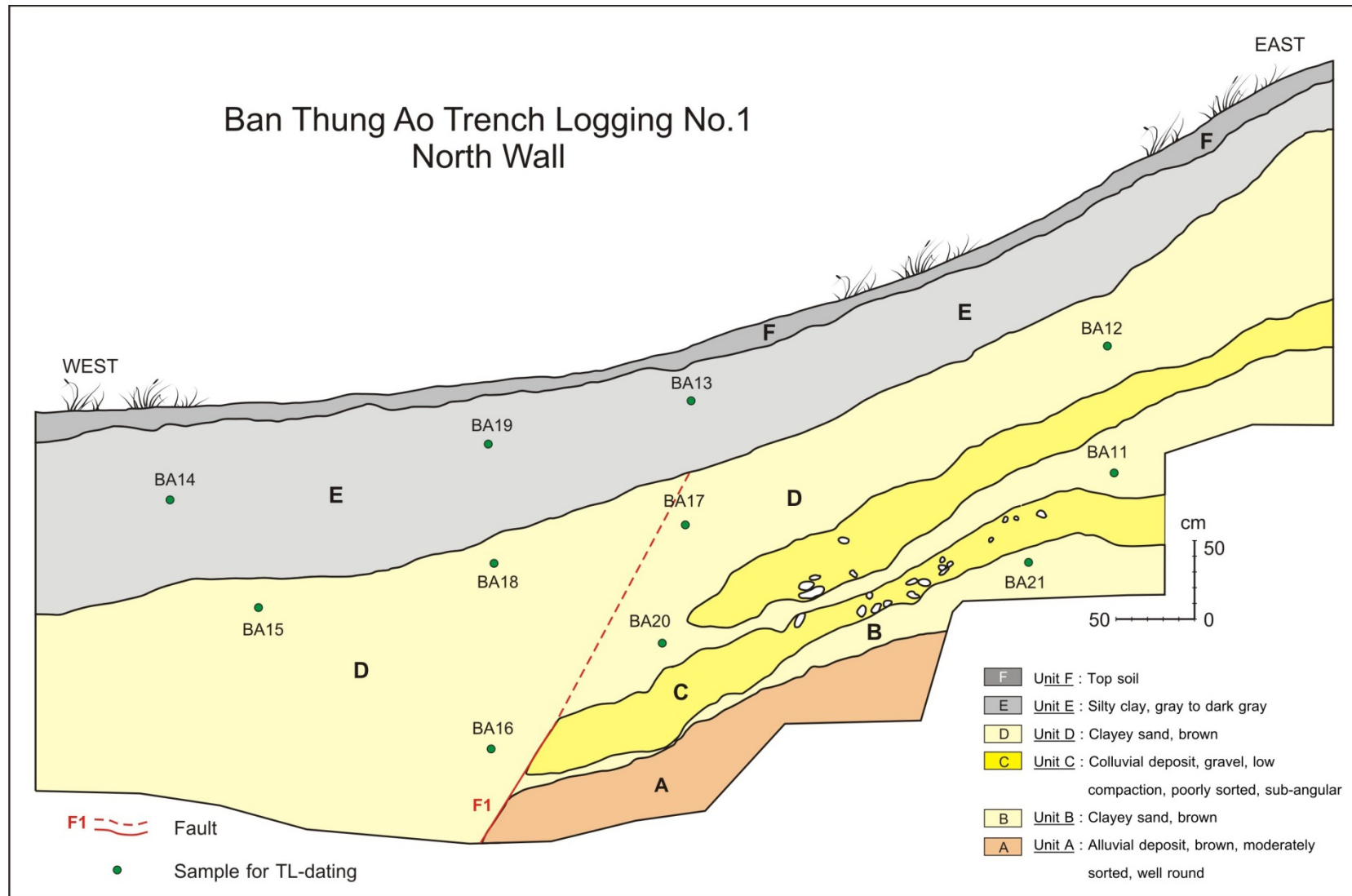


Figure 4.27 Trench-log section of the north wall of the Ban Thung Ao Trench showing principal stratigraphy, major fault, and sample location for TL dating.



Figure 4.28 View of paleoseismic trench section (no.1) on the south wall, Ban Thung Ao village, Nan, showing Quaternary stratigraphy and fault orientation.

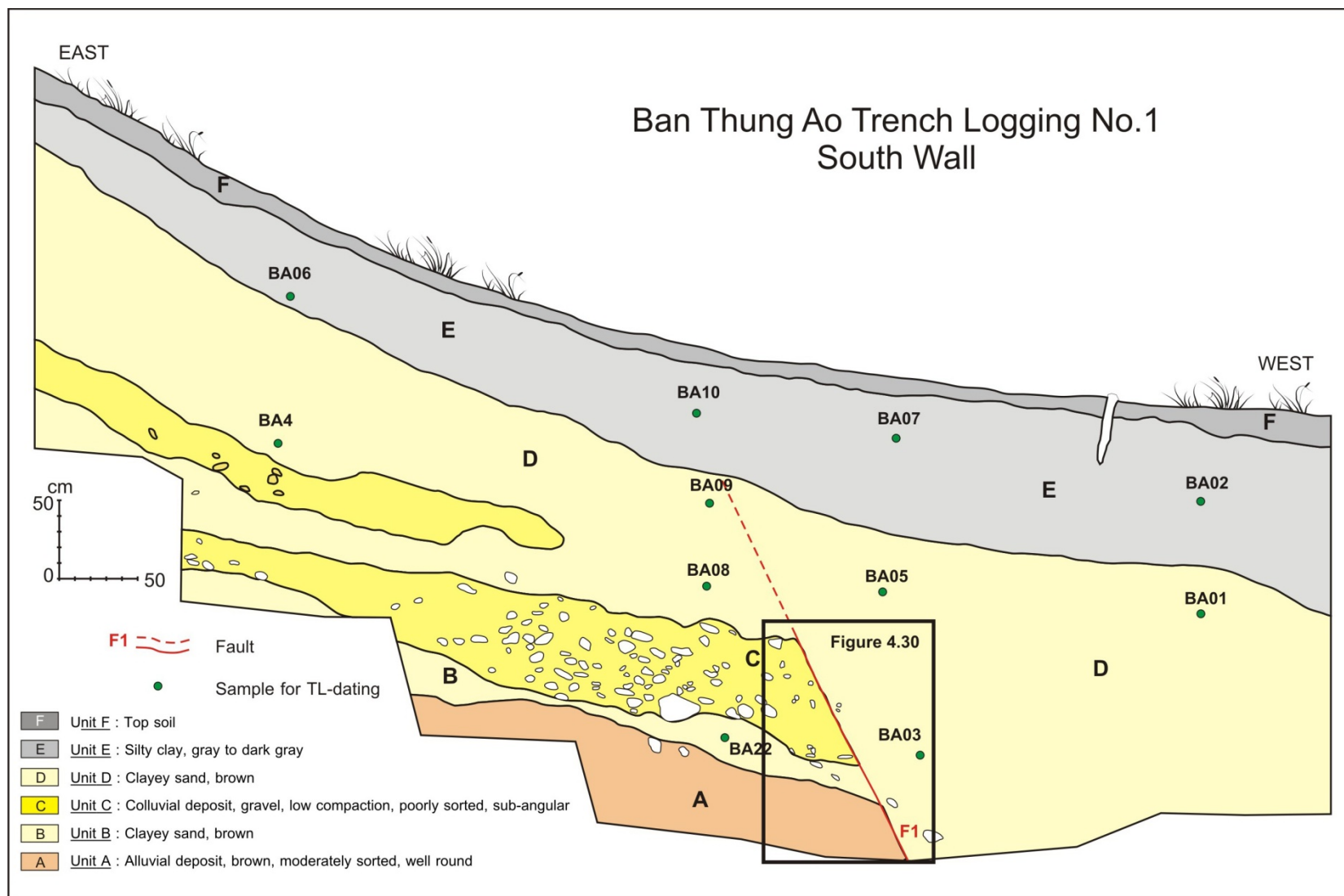


Figure 4.29 Trench-log section of the south wall of the Ban Thung Ao Trench showing principal stratigraphy, major fault, and sample location for TL dating.

Unit F is the topmost unit and consists chiefly of light grey sandy clay with bad sorting and contaminated by human activity. The upper part of the unit is the organic-rich top soil and plant debris. Thickness of the unit varies from 20 to 30 cm.

4.2.2.2 Evidence of faulting

In the excavated trench, there are several pieces of evidence regarding faulting based on trench-log stratigraphy. One fault system was recognized (F1) which cut through the sedimentary units A, B, C and D. The important fault evidence includes the discontinuity of gravel beds of units A, B and C as shown in Figures 4.27 and 4.29, the units A, B, and C are observed only at the foot wall. Unit D was observed at foot and hanging walls, but thickness of each wall is quite different. Close to the contact between unit A and unit C with unit D (Figure 4.30), the discontinuance of gravel beds are shown by a sharp contact of coarse gravels and fine sand. The other evidence is some gravels of unit C near the fault change their orientation following the west-dipping fault plane.

4.2.2.3 Structural geology

According to the fault evidence mentioned above and together with the current morphotectonic investigation, the sense of fault movement in the area is mainly normal with some left-lateral slip. At the southern wall, the fault (F1) cuts through layers A, B, C and D with a steep dip to the west. And after faulting, unit E and unit F were deposited. The true displacement of F1 is difficult to observe because the hanging wall of units A, B, and C are too deep but at least, we can estimate the fault offset by assuming the top of layer C exposed at the bottom of D (marked by [C*]). So its offset is approximately at least 1.2 m.

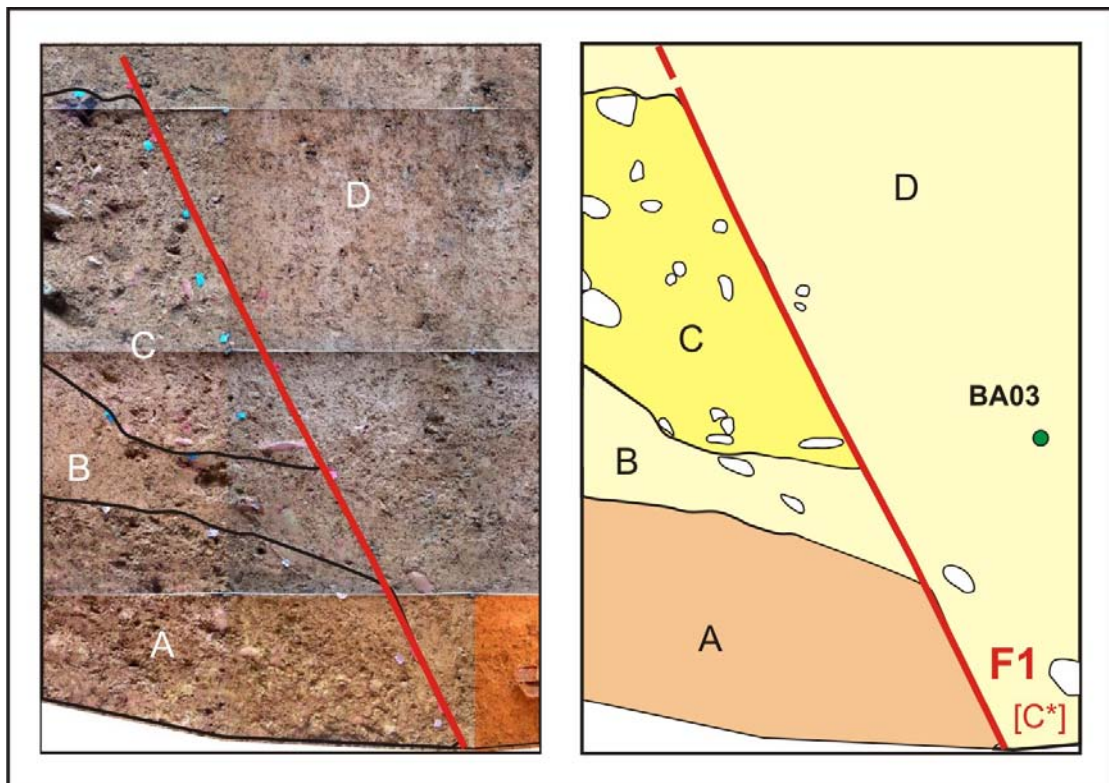


Figure 4.30 Close-up view (box in Figure 4.29) of the south wall, Ban Doo Trench, Nan, showing the west-dipping fault (F1) and location of TL dating sample. Fault (F1) cut into Layer D.

4.2.3 Trench 2: Ban Doo, Amphoe Chiang Klang

This trench is located north of Ban Doo at the northern side of the country road no. 3199. Remote-sensing interpretation shows sharp lineament and geomorphology indicates offset streams, shutter ridges, linear valleys, offset ridges, and triangular facets at grid reference 701177E / 2134105N on topographic map of Amphoe Thung Chang (5147 III). The trench was displayed on high resolution satellite image (Figure 4.31) at the hill of Doi Khun Satun and alluvial. Ban Doo trench is situated on the steeper slope near scarplet and offset stream. The excavation was done in the semi-consolidated sediments and across perpendicularly through fault line, this trench has only one wall cause the opposite wall was observed by the channel nearby. Trench geometry is 12 m in length and 5 m in depth.

4.2.3.1 Stratigraphic Description

Trench-log stratigraphy of the Ban Doo trench is characterized by 5 unconsolidated sediment units. As shown in Figures 4.32 and 4.33, it is quite clear that the Ban Doo trench has relatively much more deformed stratigraphy. Detail of individual units (units A to E) is described below.

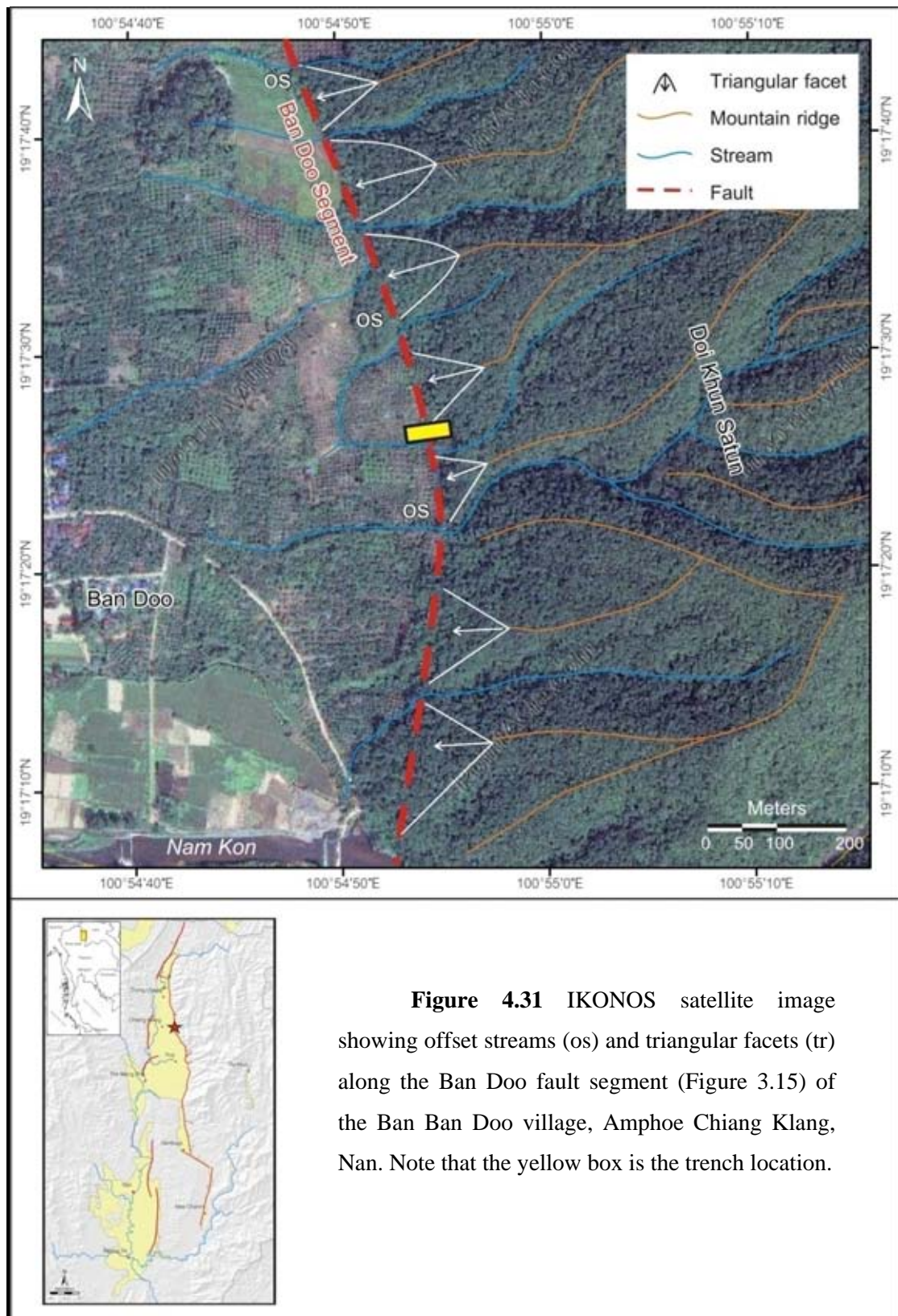
Unit A is well-defined, light brown, colluvial deposit consisting of sandstone pebble (1-3 cm in diameter), and angular to subangular sediments with sand matrix. The deposit is moderately- to well-sorted and mainly clast support. The layer is about more than 100 cm thick.

Unit B is characterized by brown, alluvial deposit with subround sandstone and quartz pebble, moderately- to poorly-sorted, mainly clast support with sand matrix and well compaction. The layer is more than 150 cm thick.

Unit C is the brown colluvial gravel layer with bad sorting. Sediment size varies from large pebble to cobble, and the maximum length of the unit is about 80 cm and the maximum width is about 30 cm. The sediments are mainly angular to subangular. Most of the fragments (>80%) are sandstone and metasandstone. This gravel layer is looser than the layer below. Thickness of this unit ranges from 100 to 150 cm.

Unit D is the debris flow which is composed essentially of light brown, sediments ranging in size from pebble to sand, poorly-sorted and mainly matrix support. Most pebbles are fragments of quartz, and quartz-rich sandstone. Thickness of this unit varies significantly from 20 cm to 4 m.

Unit E is consists chiefly of dark grey sandy clay with bad sorting. Rock fragments of pebble size are also sparsely distributed in this layer. The upper part of the unit is the organic-rich top soil and plant debris. Thickness of the unit varies from 20 to 30 cm.



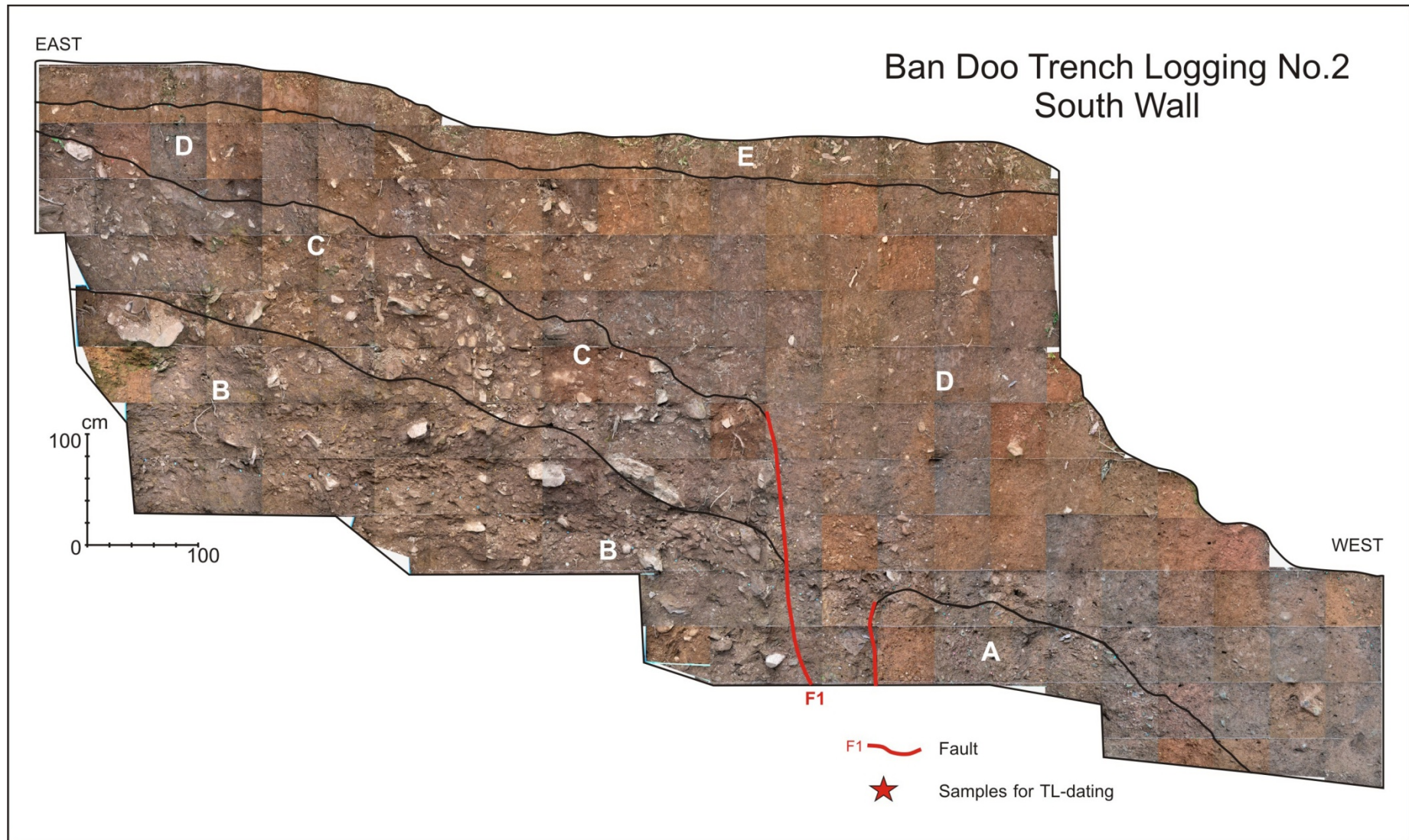


Figure 4.32 View of paleoseismic trench section (no.2) on the south wall, Ban Doo village, Nan, showing Quaternary stratigraphy and fault orientation.

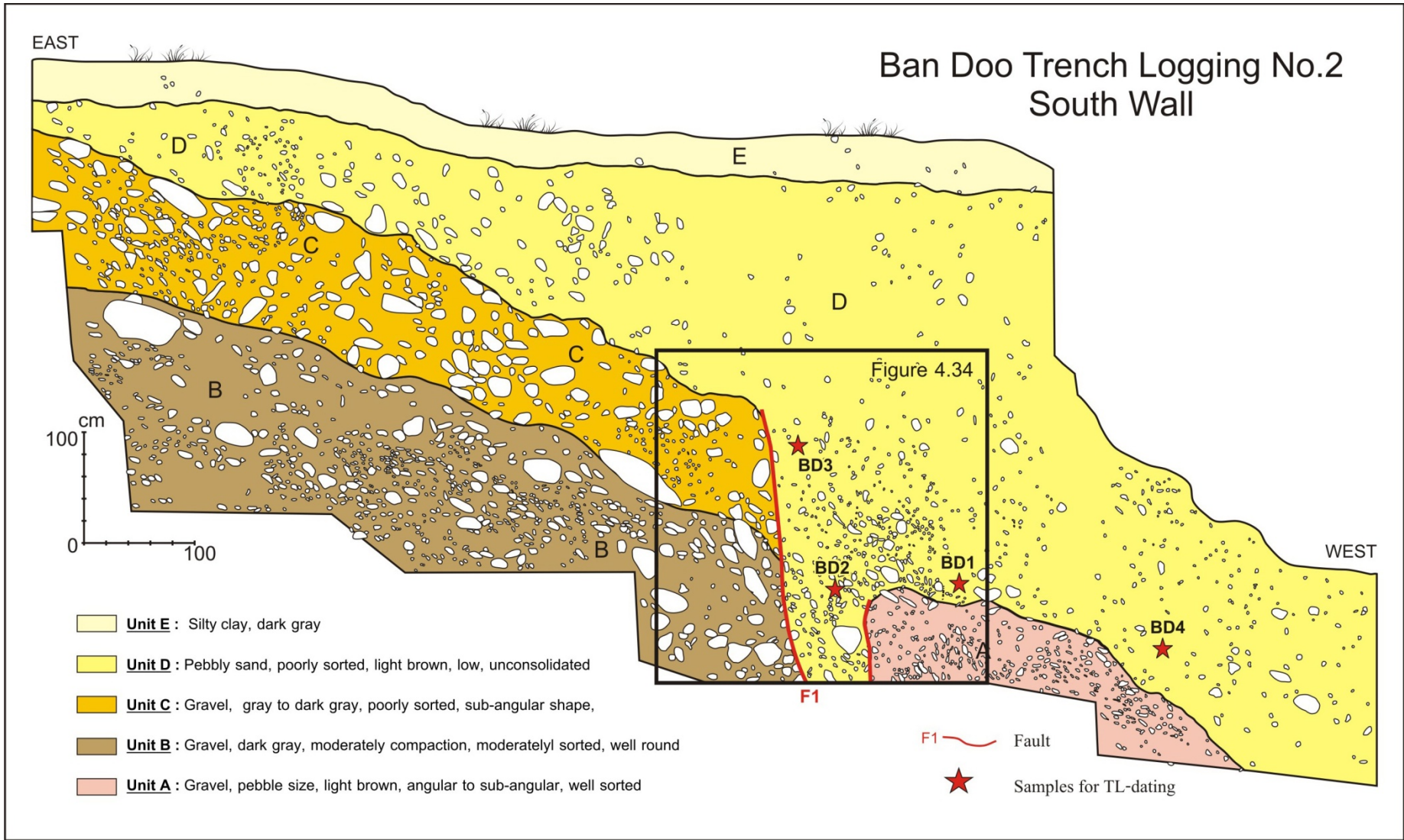


Figure 4.33 Trench-log section of the south wall of the Ban Doo Trench showing principal stratigraphy, major fault, and sample location for TL dating.

4.2.3.2 Evidence of faulting and folding

Based on trench-log stratigraphy, there are several pieces of evidence in Ban Doo trench which can indicate faulting (Figures 4.32-4.33). Fault (F1) is found from the west wall and shows one important evidence- that is the different level and type of gravel layers on each fault side. Sediments in the west side of fault belong to the unit A with fine- to medium-pebble, subangular, well-sorted, and those of the opposite side are of the units B and C with cobble to pebble size, and very poorly sorted. As mentioned above, units A and B were deposited in different environment but they are lying very close to each other. This suggests that both units A and B-C have been moved from elsewhere by a normal-oblique fault. As shown in the close-up view (Figure 4.34), gravels near the fault change their orientation following the fault plane (Figure 4.33).

4.2.2.3 Structural geology

The structure observed in the trench is a fault cutting through units A, B and C with very steep dip to the west and then an open fracture was formed due to younger fault movement and enlarged so as to develop a colluvial wedge. Then the sediment of unit D was deposited in fracture zone and covered by top soil of unit E. Based on tectonic geomorphology data such as offset stream and scarplet and stratigraphy data from trenching, the fault in this area is the normal fault with right-lateral movement.

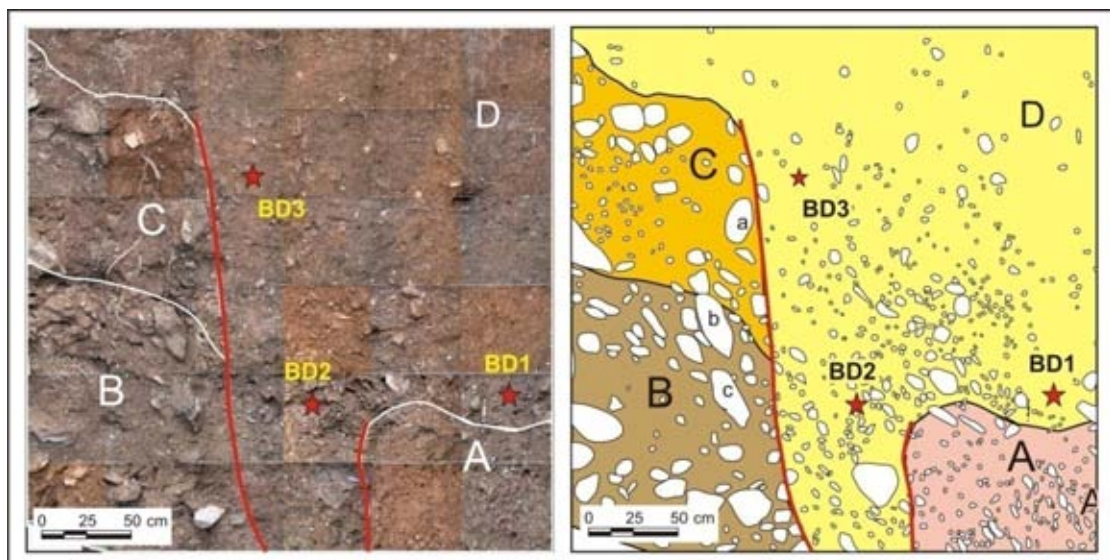


Figure 4.34 Close-up view of Figure 4.33 showing a fault contact (F1) between units C and B (left) and unit D and A (right). Note that several pebbles of units C and B showing steep dipping along the long axis.

4.2.4 Trench 3: Ban Wiang Song, Amphoe Thung Chang

Ban Wiang Song area is located at Ban Wiang Song, north of Amphoe Thung Chang at grid reference 697397E / 2148047N (Figure 4.35). This trench is an additional trench and not in our plan in the first place. It is a quarry (about 20 x 7 m) nearby road no. 1080. The quarry was fortuitous found and a sharp discontinuity of the sediment layer seems to suggest a fault movement (Figure 4.36a). Our survey team decided to excavate this quarry in a more detailed survey (Figure 4.36b). After a detailed trench excavation by workers for a few days (Figure 4.36c), the discontinuities of the sediment layer became clear that its feature was a man-made structure (probably an old ditch, see Figure 4.36d). Sedimentary layers on the trench wall were then sketched and logged for structural geology and sample collection for TL dating.

4.2.4.1 Stratigraphic Description

Trench-log stratigraphy of the Wiang Song trench is characterized by 4 unconsolidated sediment units. As shown in Figures 4.37 and 4.38, it is quite clear that the Ban Doo trench has relatively much more deformed stratigraphy. Details of individual units (units A to D) are described below.

Unit A is characterized by semi-consolidated sandy clay with some subangular sandstone, quartz pebbles and Fe- oxide interbedded with light brown alluvial deposit consisting largely of pebble, well-sorted angular to subangular sediments. Its thickness ranges from 30 to 50 cm. It is noted that the continuous alignment of pebbles is in the form of open folding.

Unit B is well-defined, reddish brown unconsolidated alluvial deposit consisting of pebble to cobble of sandstone, metasandstone and quartz, well-round sediments with coarse-sand lenses. The deposit is moderately-sorted and mainly clast support. Its thickness ranges from 2.0 to 2.5 m.

Unit C is very loose alluvial deposit (somewhat artificial fill), which is composed of coarse- to fine-sand interbedded with poorly-sorted; light brown, sediments ranging in size from pebble to sand. Most pebbles are fragments of quartz, sandstone, and the maximum length of the unit is about 80 cm and the maximum width is about 70 cm. The bottom part of unit C contains larger fragments than those of the upper part.

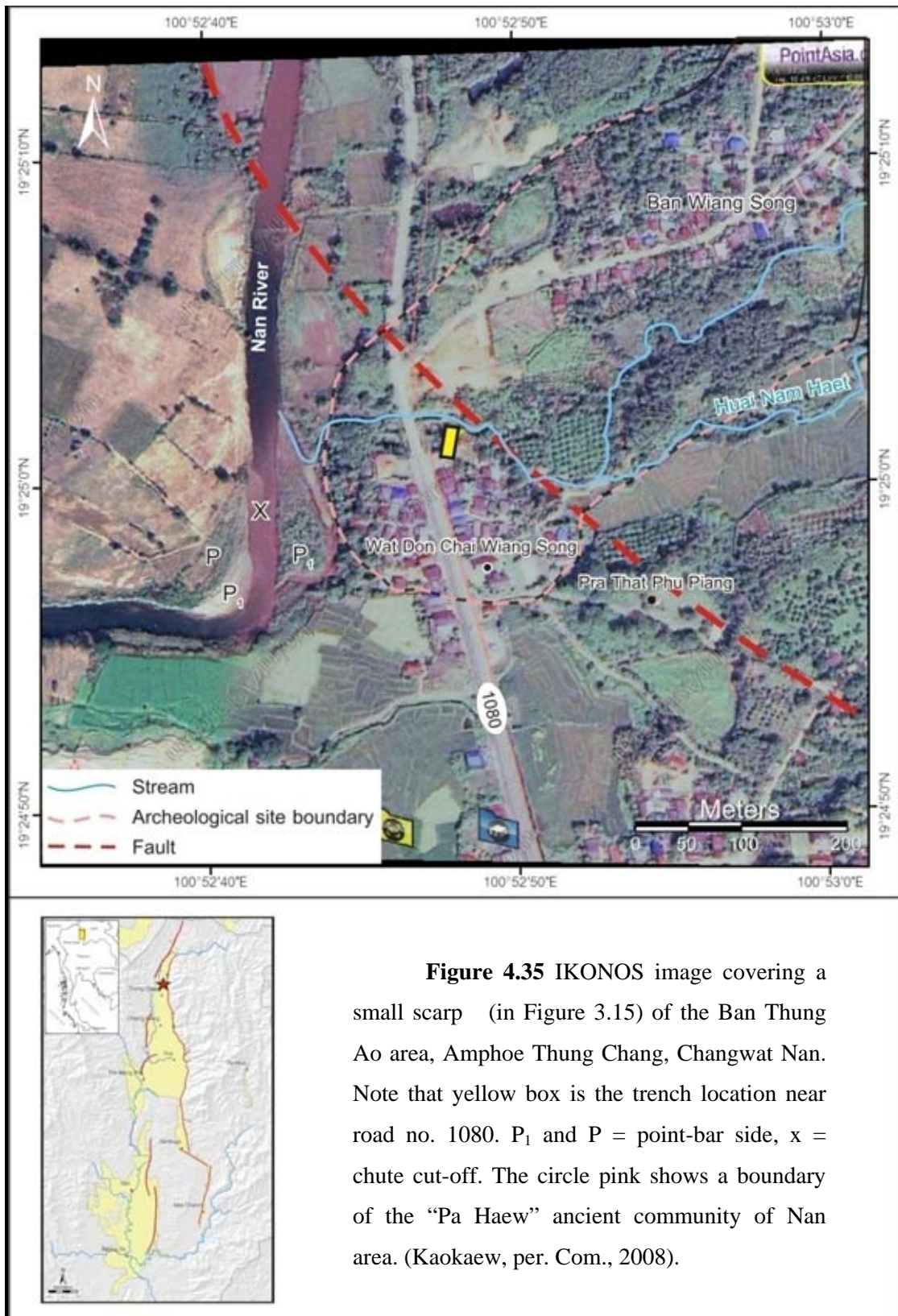


Figure 4.35 IKONOS image covering a small scarp (in Figure 3.15) of the Ban Thung Ao area, Amphoe Thung Chang, Changwat Nan. Note that yellow box is the trench location near road no. 1080. P_1 and P = point-bar side, x = chute cut-off. The circle pink shows a boundary of the “Pa Haew” ancient community of Nan area. (Kaokaew, per. Com., 2008).

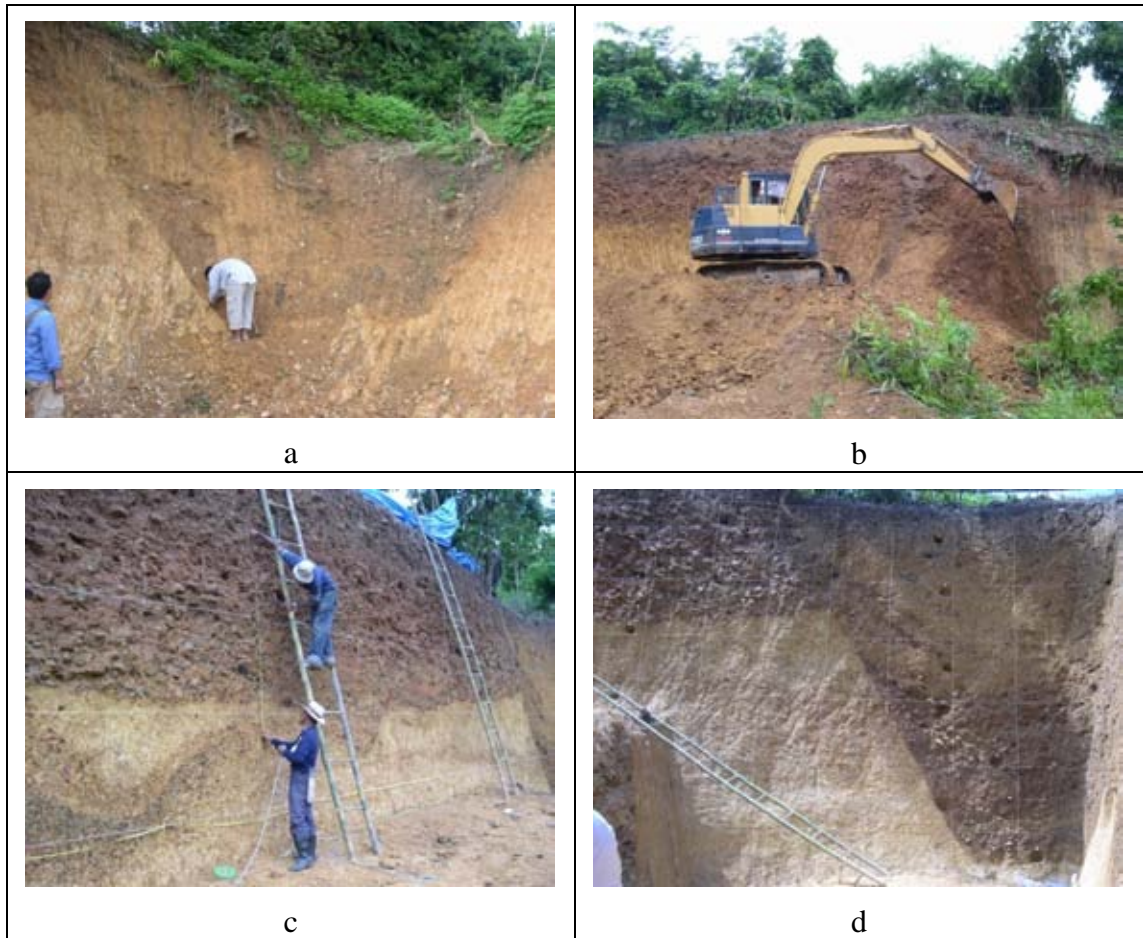


Figure 4.36 a) Quarry at Ban Wiang Song, b) Trench excavation using tractor, c) decorate trench wall by using small spade, d) show sharp contact of each unit

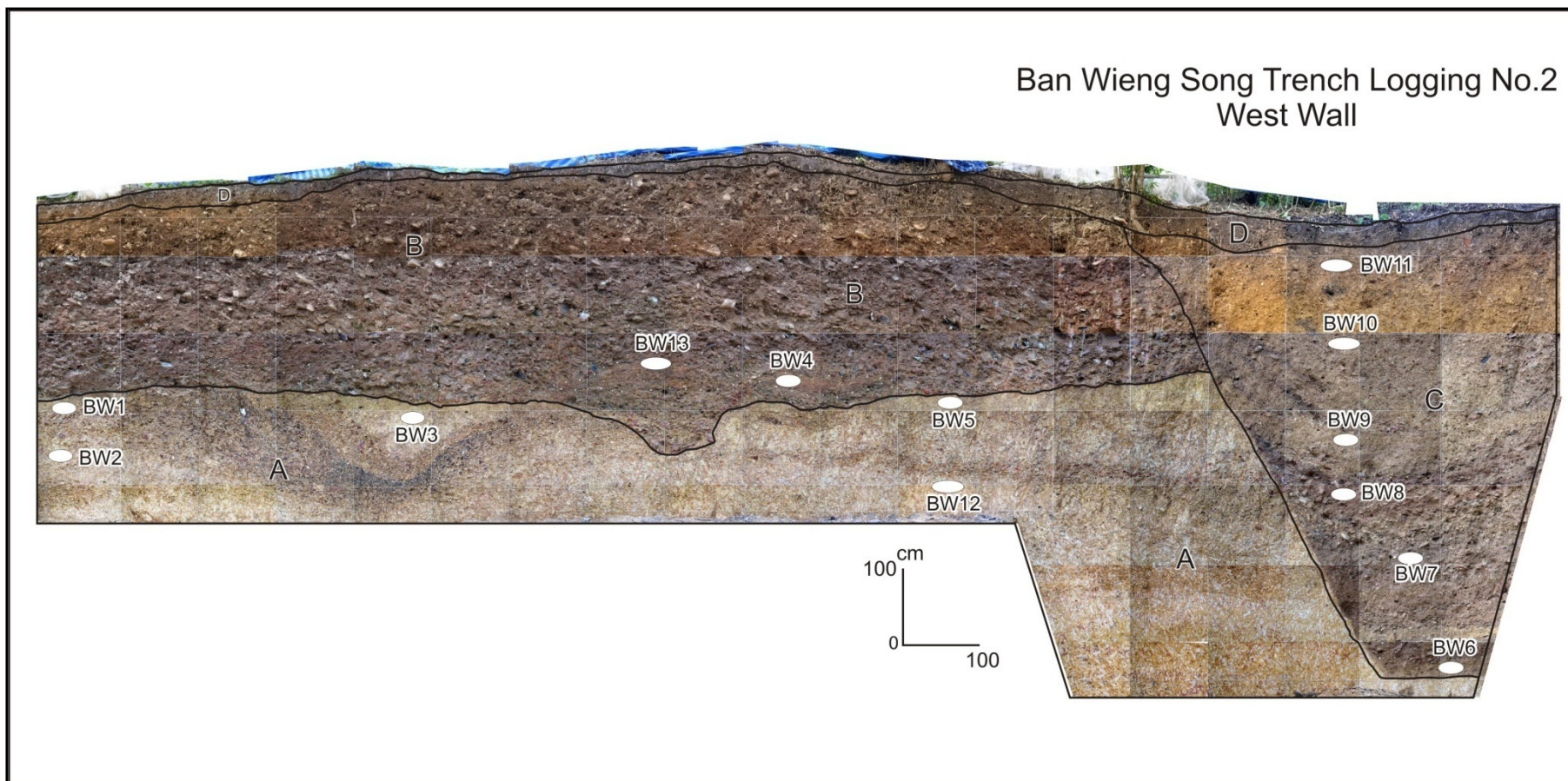


Figure 4.37 View of paleoseismic trench section (no.3) on the west wall, Ban Wieng song village, Nan, showing Quaternary stratigraphy and fold.

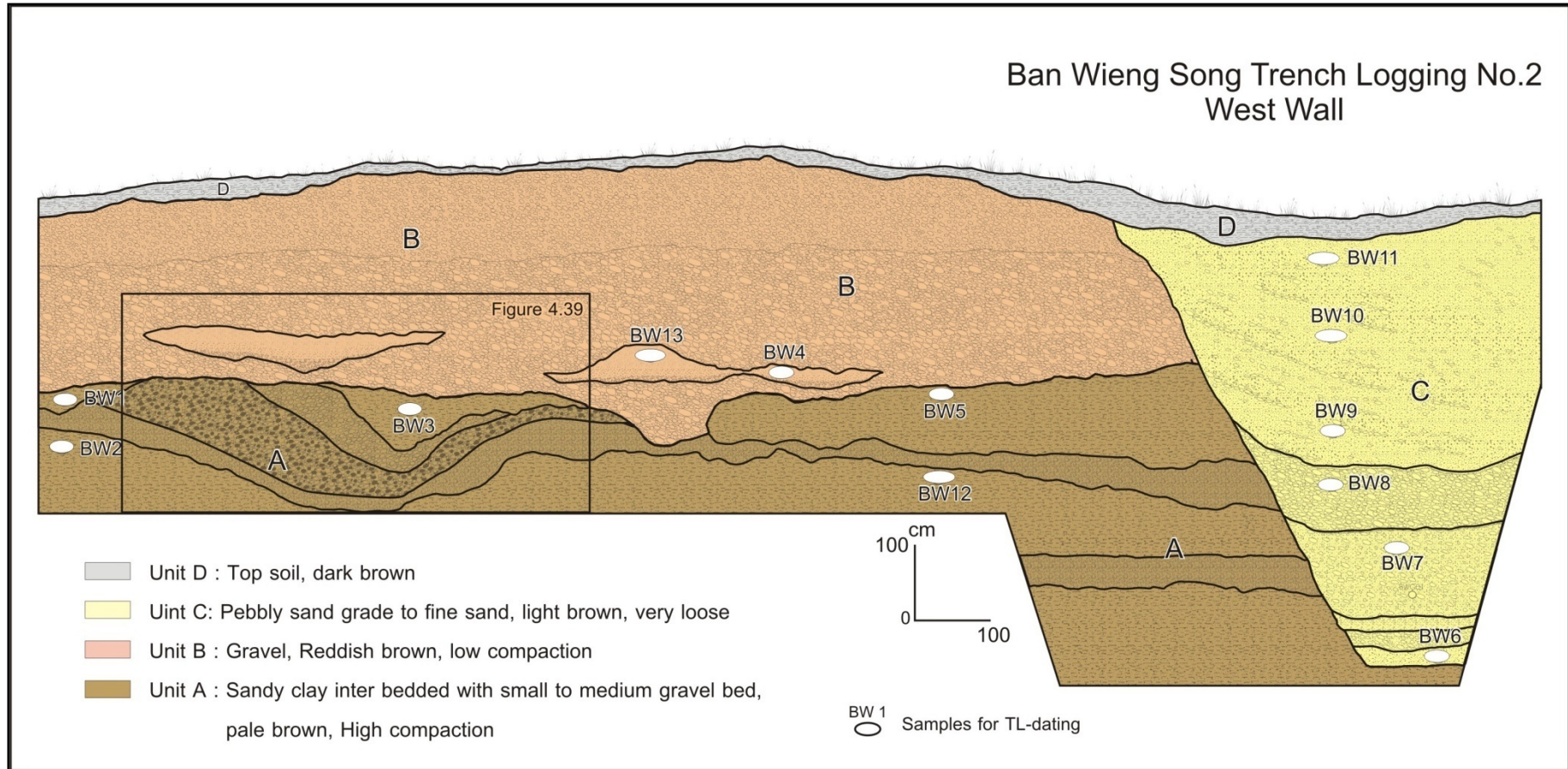


Figure 4.38 Trench-log section of the west wall of the Ban Wiang Song Trench showing principal stratigraphy, major structure, and sample location for TL dating.

Unit D consists of dark grey sandy clay with bad sorting possibly by human activity. The upper part of the unit is the organic-rich top soil and plant debris. Thickness of the unit varies from 20 to 30 cm.

4.2.4.2 Evidence of folding and faulting

Based on the lithostratigraphy data, Unit A is a folded layer and overlain unconformably by unit B. Both of units A and B have a sharp contact with unit C and all of them overlain unconformably by unit D. The folding of unit A (Figure 4.39) implies that the fault was moved nearby and effect to unit A.

As introduced above, the sharp contact of units A and B with unit C is similar to a normal fault style. So in the first idea, unit A was the same layer with unit C, and then unit C was dropdown northeastward by normal faulting. However, after a study in detail stratigraphy, unit B is quite different from unit C, so the deposition of unit C occurred after Unit B was already deposited. Based on the historical data and the data from villagers nearby as well as the personal communication with a Silpakorn University professor (Archan Chawalit Kaokaew, per. com., 2008) (<http://www.tv5.co.th/service/mod/heritage/nation/oldcity/nan7.htm>), this area is a historical site named “Ban Pa Haew” with the distinct, but complex nearby moat. As mentioned above, it is considered that the unit C is possible to be the sediment layer which was deposited in the ancient moat.

4.2.4.3 Structural geology

The evidence of faulting is found in unit A which is the alignment of pebbles as a result of compressive folding (Figure 4.39).

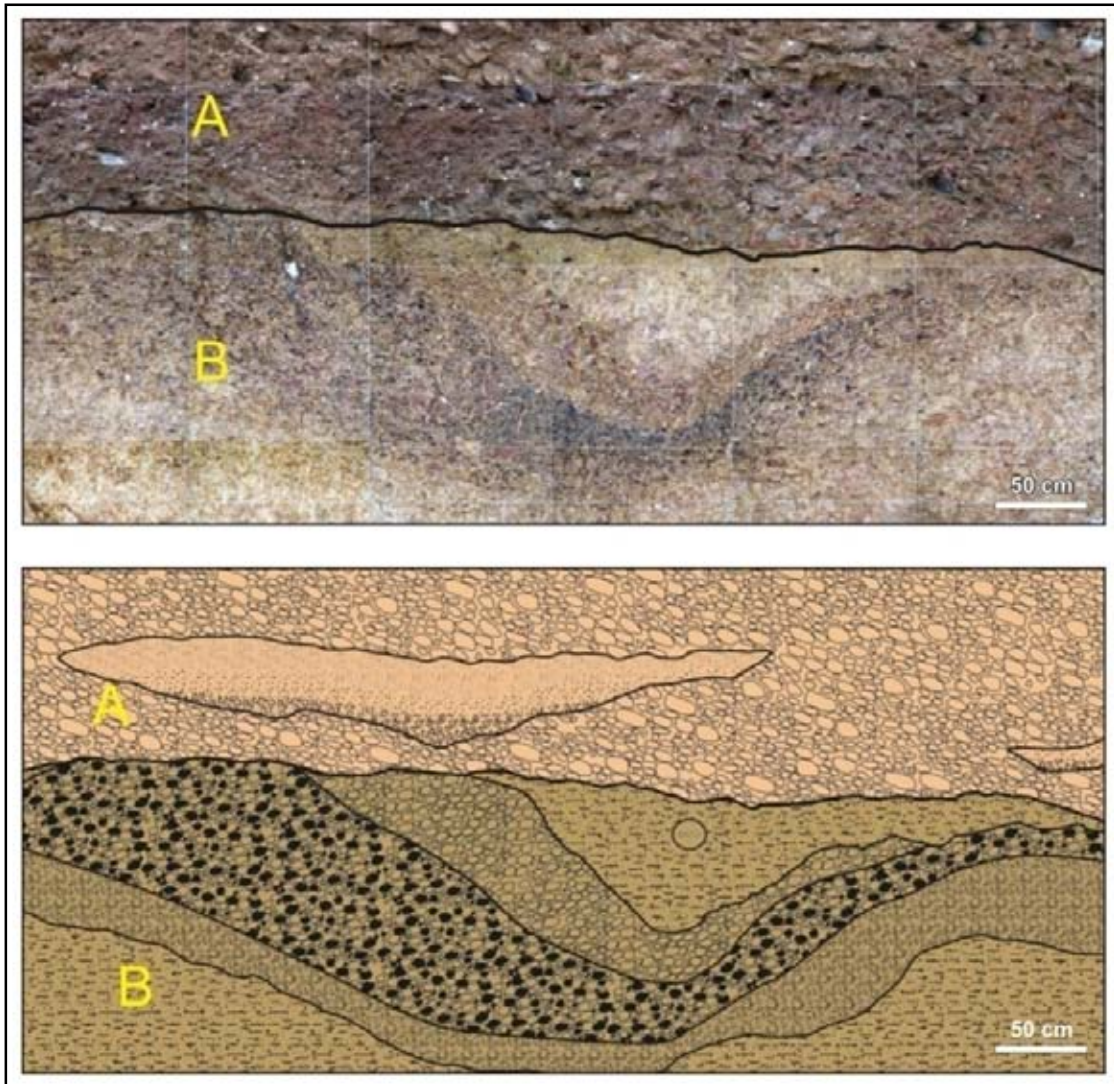


Figure 4.39 Close-up view of Figure 4.33 showing the alignment of pebbles in the forms of folding and steeply dipping features which were affected by fault nearby.

CHAPTER V

THERMOLUMINESCENCE DATING

5.1 Thermoluminescence Dating

In this section, we reported the thermoluminescence (TL) dating procedure and results. The (TL) procedure is proposed by Takashima and Honda (1989). The methodology of analysis is composed of 2 main procedures, including equivalent dose evaluation and annual dose evaluation.

5.1.1 Basic Concept

Generally, insulators such as covalence solids and glasses can generate thermoluminescence (TL-dating) signal, but metals cannot. As a result, TL-dating method can be only applied with an insulator crystal. A simple model to review on general background of TL-dating method is based on ionic crystal model, which is simplified as shown in Figure 5.1.

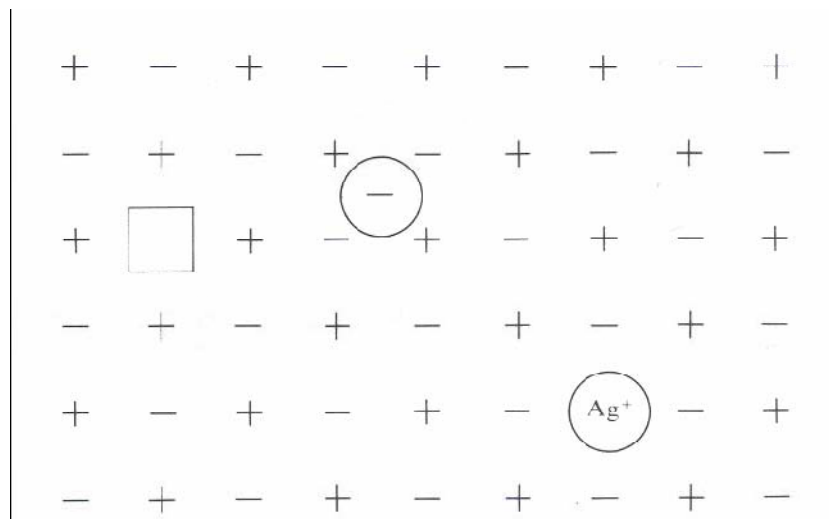


Figure 5.1 A simplified model of lattice structure of an ionic crystal showing three simple types of defect which are negative-ion vacancy on the left, negative ion interstitial at the center, and substitution impurity center on the bottom right (After Aitken, 1985).

Ionic crystals, for example calcium carbonate and sodium chloride, are composed of lattice of positive and negative ions. In this lattice, it can be defected due to at least three reasons; an impurity atom, a rapid cooling from the molten stage, and damage by nuclear radiation. The defected lattice is presented by lacking of electron from its proper place or electron vacancy, called “electron trap”, leads ionized electrons from vicinity to fill up in this trap hole. In addition, ionized electron is the result of nuclear radiation from earth materials or solar radiation. However, both nuclear radiation and solar radiation have caused much less damages to the lattice structure.

Electrons have been trapped in trap holes lasted until shaken out due to the vibration of crystal lattice. A rapid increase of temperature to high in narrow range leads this vibration to be stronger. In addition, high temperature usually upward of 400oC can evict electrons from deep electron traps to be diffused around the crystal. Note that, because of different crystals, there are different types of traps, and then optimum temperatures to evict electrons in different crystal traps are unique. However, diffused electrons can be directed into two different ways; firstly to be retrapped at different types of defect which is deeper trap, and secondly to be recombined with an ion in lattice which electrons once have previously been evicted.

According to TL-method, since it has mainly concerned only on recombination process, then the process is also reviewed in this section. Anyway, there are two types of recombination process; radiative (i.e., with light emission) or non-radiative. For this method radiative type is interested, which ions or atoms from this recombination process are called luminescence centers and the emitted light is thermoluminescence.

A simplified model of energy level to present thermoluminescence process is illustrated in Figure 5.2.

There are electron traps (T) and center of luminescence (L) located as intermediate between the valence band and the conduction band. The energy (E) is required in an optimum level to shaken out electrons from its deepest hole. In general, when electrons have already shaken out by heating, and recombination is done at the centers of luminescence, light is emitted. However, in some case which recombination has done at non-luminescence center or killer center, there is no emission of light and the energy is represented in the form of heat.

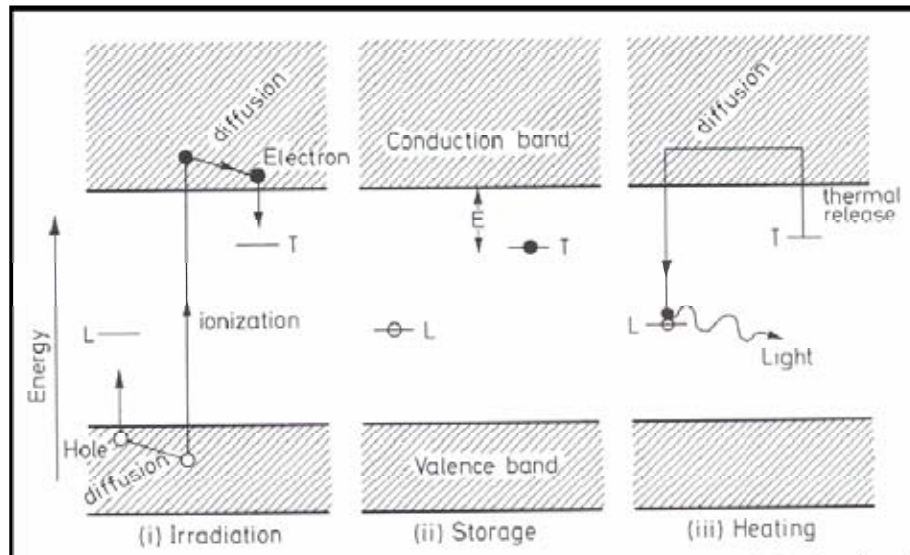


Figure 5.2 Thermoluminescence-process diagram showing energy-level related to three processes; (i) irradiation process, caused by crystal exposed to nuclear radiation, ionized electrons are trapped at hole (T); (ii) Storage stage in which electrons have been trapped, need hole deep enough for electrons (E) during geological time period of sample; and (iii) Heating process, at optimum level of temperature, electrons are released and re-combined at luminescence center (L), and then light (TL) is released (After Aitken, 1985).

In summary, thermoluminescence process can be concluded in four steps. Firstly, ionization of electrons is caused by nuclear radiation. Secondly, some of these electrons are trapped in continuous and constant rates lasted until temperature has increased. Thirdly, some of electrons are heated at the optimized temperature level to evict electrons from deep trap hole. Fourthly, some of these electrons are then reach luminescence centers and in case of recombination process has done, light emission from luminescence centers is generated. The amount of emitted light or the number of photon in this stage is depended on the number of trapped electrons, which in turn is the amount of nuclear radiative proportion or paleodose. In addition, dose rate of nuclear radiative applied to environment is called annual dose.

Ultimately, based on TL-process mentioned above, age of quartz-bearing sediments (such as those of this study) can be determined by simple equation 5.1 below;

$$\text{TL-age} = \frac{\text{Paleodose}}{\text{Annual dose}} \dots\dots\dots (5.1)$$

5.1.2 Paleodose and Annual Dose Evaluation

In this section, brief descriptions on paleodose and annual dose evaluation are provided as first and second orders, respectively. Firstly, once sediment sample has been treated to become purified quartz crystals before measurement their quantity of TL-intensity using TL-instrument. The apparatus diagram for TL-measurement is shown in Figure 5.3. However, due to further details of apparatus is out of scope, and then it was not mention herein. The output of TL-intensity from this instrument expresses in the form of grow-curve graph as shown in Figure 5.4 in which X-axis is represented temperature and Y-axis is TL-intensity. Peak of TL-intensity in this curve is used to evaluate paleodose in the next step.

5.1.3 Laboratory Analysis

TL laboratory procedure in this study is mainly followed that of Takashima and Honda (1989). The methodology of analysis is composed of 2 main procedures, including paleodose or equivalent dose evaluation and annual dose evaluation (Figure 5.5).

5.1.3.1 *Crushing and Sieving*

Upon arrival in the laboratory, TL samples normally were dried by 40-50°C baked in the dark room. Water content is also measured for all samples being dated because it is the one significant parameter for annual dose determination. The formula of water content calculation is shown in equation 5.2.

$$\text{Water content} = \frac{(\text{weight of a wet sample} - \text{weight of a dried sample}) \times 100}{\text{weight of a dried sample}} \dots\dots\dots (5.2)$$

After getting dried sample, each sediment sample was shattered by using a rubber-hammer and the material passed through sieves to isolate the grain size fraction in 2 parts. Sediments which grain size pass through 20 mesh (<841µm) were collected about 300 g and was separated to keep in plastic containers for annual dose determination. Remnant part from annual dose collection is carefully re-sieved and

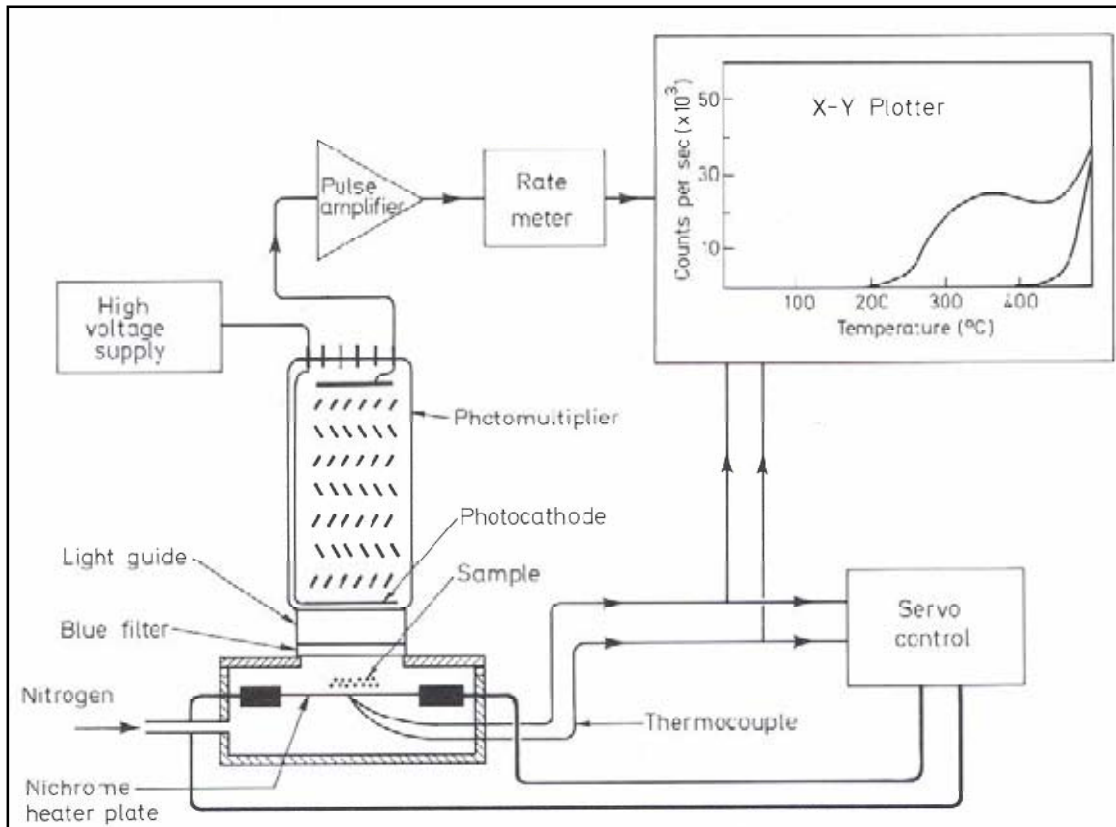


Figure 5.3 Diagram of thermoluminescence instrument (After Aitken, 1985).

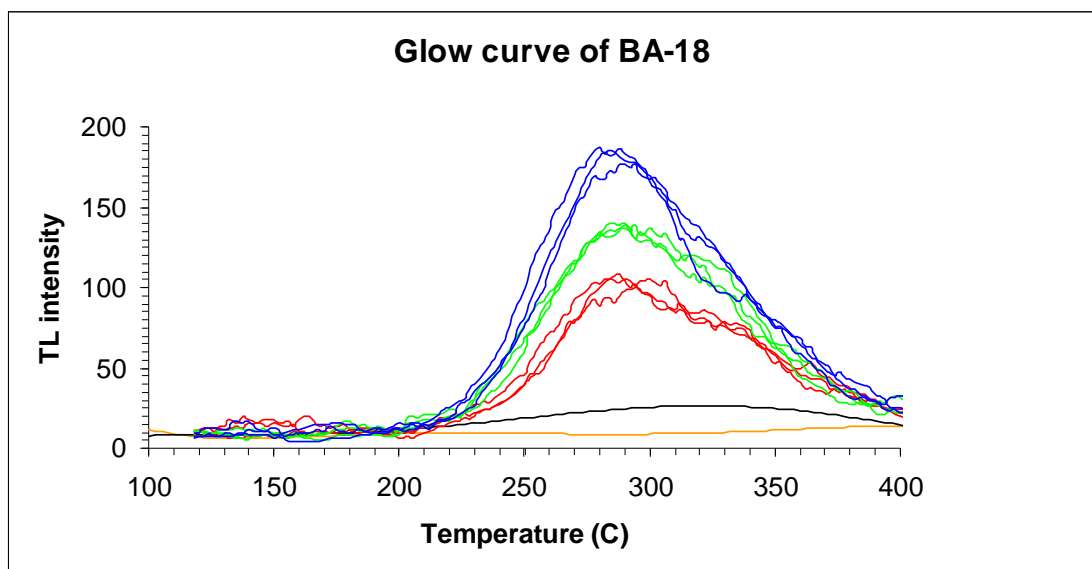


Figure 5.4 A glow curve graph shows relationship between TL intensity versus temperature.

the material passed through sieves to isolate the grain size fraction between 60-200 mesh. Both of these portions were kept in beakers for purifying quartz grain and equivalent dose determination, respectively. In the annual dose, a sample portion is ready and skips to the measurement step but in both of two portions for equivalent dose determination is necessary to participate in chemical treatment.

5.1.3.2 Paleodose or Equivalent Dose Evaluation

A) Chemical Treatment

The main objective of chemical treatment is purification of quartz mineral in TL samples from the method in order to keep off destroying the signal of sample. The detail of chemical treatment is shown below:

a) Washing the sample by distilled water 10 times for removing some organic materials and clay particles;

b) Chemically cleansed the sample in dilute 35% HCl at 50-60°C in a period of 15-30 minutes and re-washed several times with distilled water for eliminating carbonates and deep-rooted organic material;

c) Etching the sample in 24% HF at 50°-60°C for 15-30 minutes and re-washed it several times with distilled water. HF was used to dissolve the plagioclase and outer layer of quartz grains to a depth sufficient for the core remaining to have a negligible component of alpha particle dosage; and

d) After washing with water and drying in the dark room, the dried sample was then separated to remove out the dark minerals (e.g. zircon, garnet, and metallic minerals) by using an isodynamic separator (Frant'z isodynamic magnetometer)

After finishing sample treatment, it is necessary to check purity of quartz sample by XRD analysis. If the quartz-rich samples contain less than 10% of the other minerals, the samples were supposed to contain pure quartz concentrates. Then the sample was ready for determine equivalent dose in the next step.

B) Sample Preparation for Equivalent Dose Measurement

The pure quartz sample after chemical treatment is subdivided into 3 parts:

- Part 1: Natural quartz sample was used for evaluated natural sensitivities of previously acquired TL signal;

- Part 2: Sample was exposed directly with natural sunlight for 12 hours (Aitken, 1985) to effectively remove all of the previously acquired TL leaving only what is termed as the unbleachable TL signal. This part used for determining residual levels; and

- Part 3: Sample used to find out the characteristic of quartz effective with artificial irradiation that amount of radioactive irradiation (in unit Grey) is known. The gamma ray source for artificial irradiation is a Co⁶⁰ from Office of Atomic Energy for Peace (OAEP), Bangkok.

C) Equivalent Dose Measurement

Evaluation of equivalent dose commences with measurement of TL intensities on 3 sample portions: 1) natural sample portion, 2) artificial irradiation sample portion and, 3) residual sample portion (in sediment sample). About 20 mg of sample was filled in aluminum planchettes and placed on a molybdenum heater. The graph shows a relationship between TL intensity and temperature which is called “glow curve” (Aitken, 1985). The term glow curve is given to plot intensities of emitted light versus temperature (Figure 5.5). Calculation of equivalent dose can be done by extrapolating natural signal intensity and residual signal intensity with a growth curve from artificial irradiated signal intensity. The result is assumed to be proportional to the equivalent dose of equation 5.1.

Although the glow curve shown in Figure 5.5 is smooth continuum, it is really composed of stable and unstable signals. This procedure makes by comparing the shape of the natural glow-curve (i.e. the glow-curve observed from a sample which has not received any artificial irradiation in the laboratory) with the artificial glow-curve observed as a result of artificial irradiation.

Thus a constant ratio between natural and artificial glow curves gives an indication that, throughout this plateau region, there has been negligible leakage of electrons over the centuries that have elapsed since all traps were emptied in the course of the stimulation by ancient environment.

The next step is for the construction of growth curve. This can be done by the increases of TL output with known amounts of additional radiation that

induced the sample. The graph showing this relationship is called “growth curve” (Figure 5.6).

5.1.4 Regeneration Technique

In this technique, the simplest approach to the evaluation of equivalent dose is by the straight-forward procedure of measuring the natural TL intensity from a natural sample (N) and comparing it with the artificial TL intensity from the same sample that know certain dosage (artificial irradiate sample).

In this study, after heating the quartz-extracted at 320°C for 5 hrs, individual samples were liquated for 5 sub-samples (Takashima et al., 1989). For each sub-sample, artificial irradiation was added with the doses of 44, 103, 303, 723, and 1,440 Gy. The values of TL intensity (N/H+ γ) (as shown in Figure 5.6) versus temperature ranges were plotted for each sample and they are shown in Appendix.

The growth curve plot is a graph of TL ratio or TL intensity (as shown in Appendix). It should be noted herein that most graphs of the natural intensity values close to the artificially irradiated liquated (i.e., H+1,440 Gy). Therefore their paleodose can be read after curve fitting for each aliquot (Figure 5.7).

5.1.5 Residual Test

In case of sediment sample, evaluation of equivalent dose is complicated by the need to allow for the fact that the equivalent dose is composed of two components: the natural TL signal acquired since deposition and the residual signal that the sample had when it was deposited in the last time.

Many scientists (e.g. Wintle and Huntley, 1980; Tanaka et. al., 1997) proposed several methods to simulate the light source exposures. Samples were exposed to some kinds of light sources. Natural sunlight, UV-ray lamp (365 nm) and xenon lamp were the important illumination sources for bleaching experiments (Won-in, 2003).

In this research study, the naturally bleaching experiment by sunlight requires and depends significantly upon a long sunny day. For the artificial bleaching experiment, it is important to check the minimum of time that can completely bleach samples to the residual level and how much residual level in each sediment sample. The methodology of residual testing starts with bleaching sample and check TL

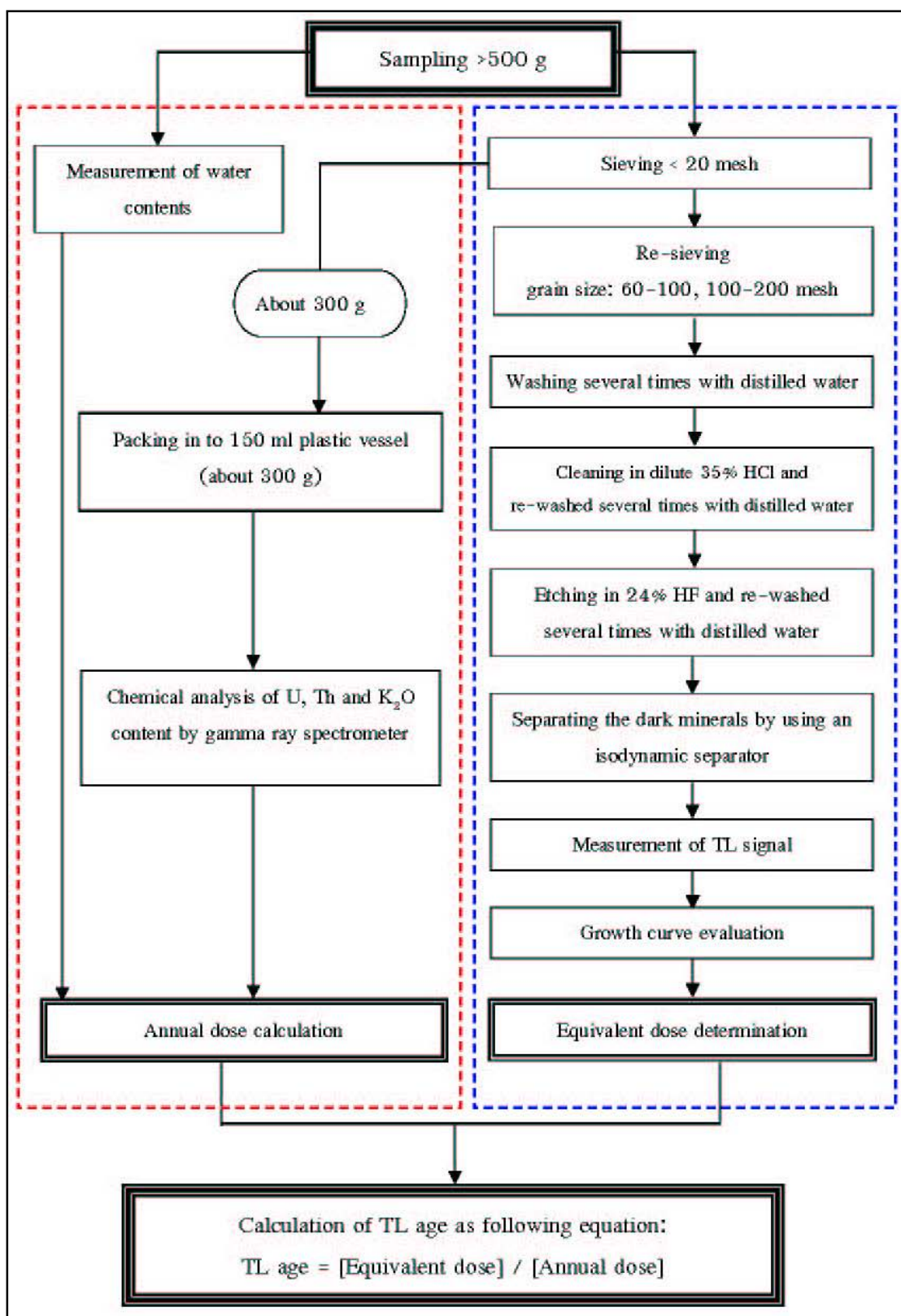


Figure 5.5 Simplified flow chart illustrating laboratory analysis used in this research study. The red dash line is the annual dose procedure and the blue dash line is the equivalent dose procedure (Modified from Takashima and Honda, 1989).

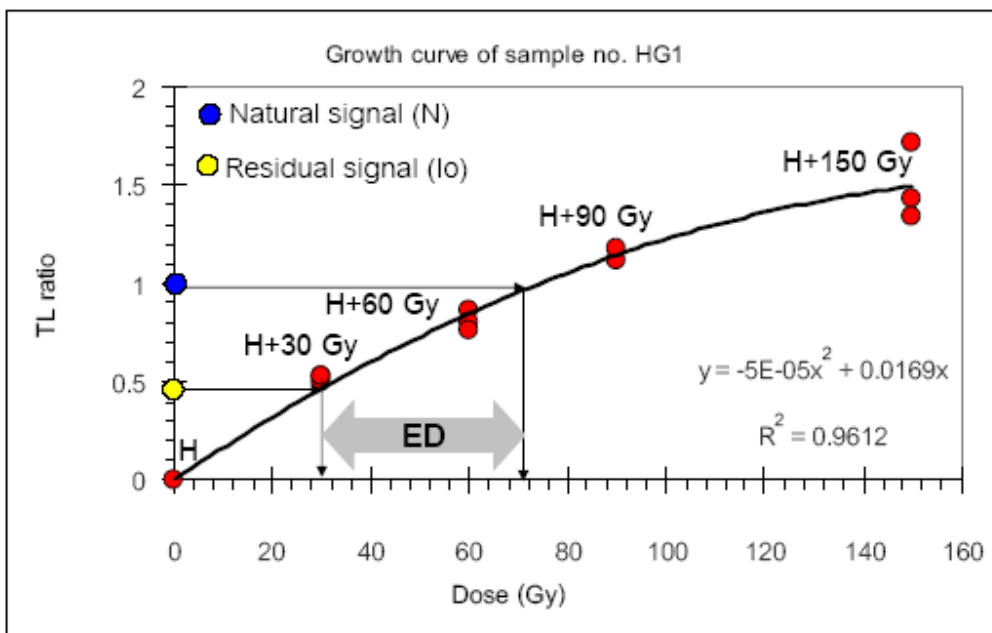


Figure 5.6 Graph showing relationship between TL ratio (artificial glow curves/natural glow curves) versus temperature (C). N is natural signal, H is heated sample at 320oC for 5 hours, and γ is known dosage that irradiated sample.

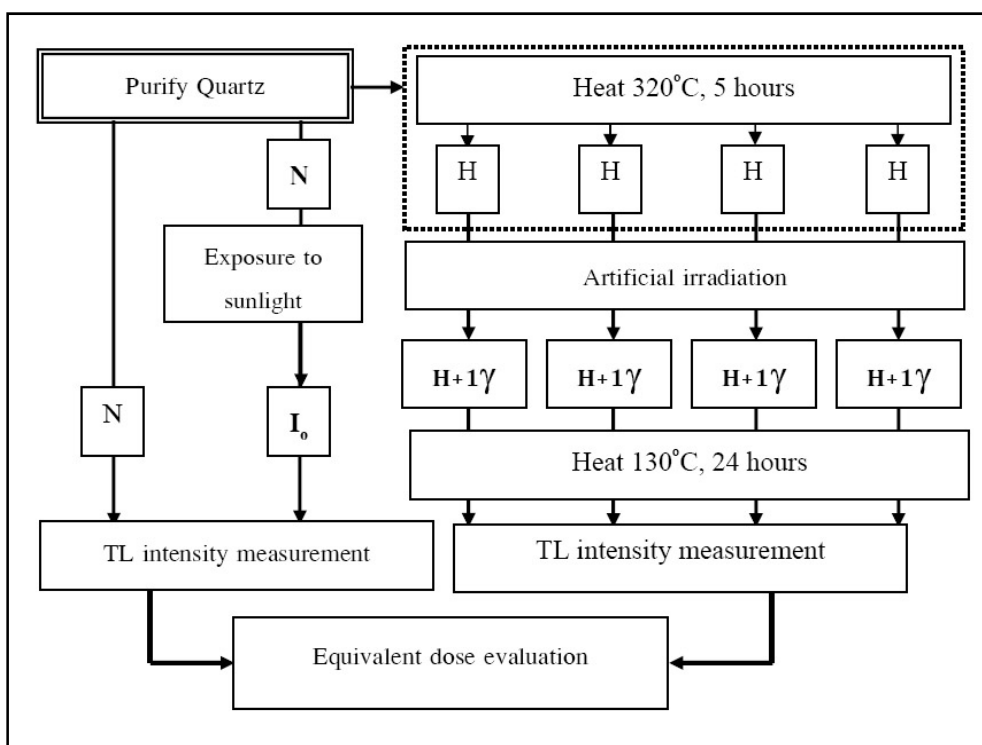


Figure 5.7 Schematic charts of regeneration technique (Takashima et. al., 1989). Note that several portions are used for measurement of the TL intensity; N is natural sample; Io is residual intensity from sample; H is 350oC heated sample; and γ is known dosage that irradiated sample.

intensity of sample in every 1 hour. Plotting graph showing a relationship between TL intensity and time used for bleaching reveal the minimum time that residual signal begin stable (unbleachable) (Figures 5.8 and 5.9).

5.1.6 Plateau Test

According to glow-curve, there are overlapping peaks that may be raised to make misinterpretation of the peak, which is the result of electron emission from deep traps not other shallow traps. Glow-curve peak, which has located in the stable region, is that of interest. The stable region is usually at 300°C or higher where electrons from deep traps are evicted near zero.

The method to recognize the stable region is a plateau test as shown in Figure 5.8. There are two glow-curves of natural sample (N) and natural + artificial sample (N+ γ) that had been plotted as solid lines in the same graph. Ratio between N and N+ γ is shown as dots. The plateau of dots is the stable region red-colour zone or band. In addition, peaks of both samples have been generated at the same temperature, and N+ γ peak is higher than N peak, it means that deep traps are deep enough to contain other electrons.

5.1.7 Annual Dose Evaluation

Generally, sediments are exposed continuously to ionizing radiation which originates from their radioactive contents, plus a small fraction from cosmic rays (Aitken, 1985). There are essentially 3 radioactive elements which contribute to the natural dose rate (annual dose) i.e. uranium (U), thorium (Th) and potassium (K). The decay of uranium and thorium results in α , β and γ radiation whereas potassium emits β and γ normally, the natural dose rates in most sediment are of the order of mGy/year.

For age determination it is necessary to evaluate the natural dose rate accurately. Several components are needed for an accurate annual dose is:

- a. Measurement of U, Th and K contents;
- b. Calculation of environmental water content in field at time of sample collection; and
- c. Cosmic ray component evaluation.

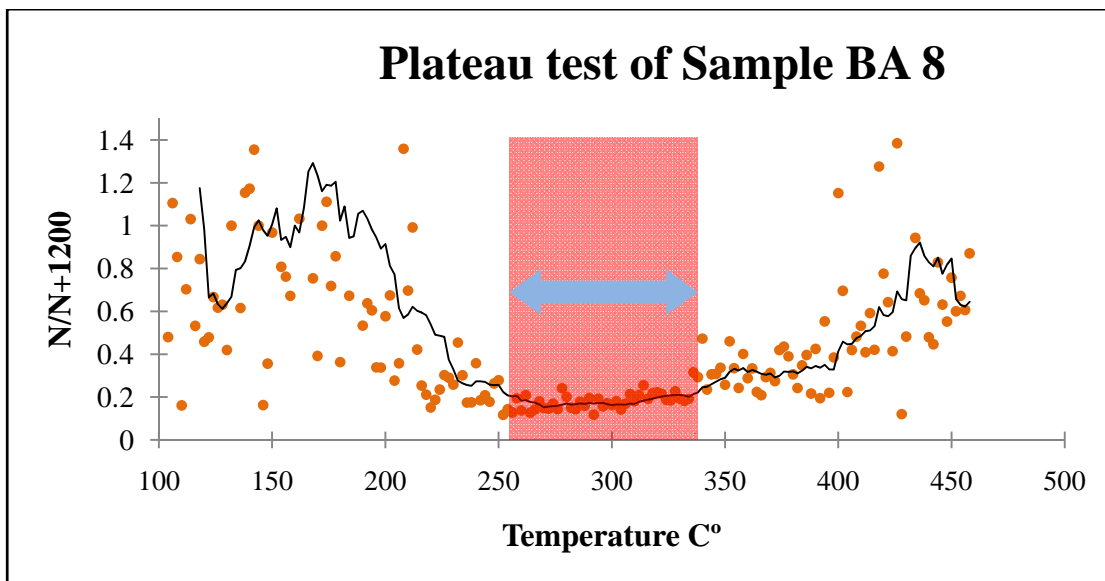


Figure 5.8 Plateau curve (solid line) is the ratio of the two glow-curves; N is represented the “natural” glow-curve and $N+1,200$ Gy is the “natural + artificial” glow-curve

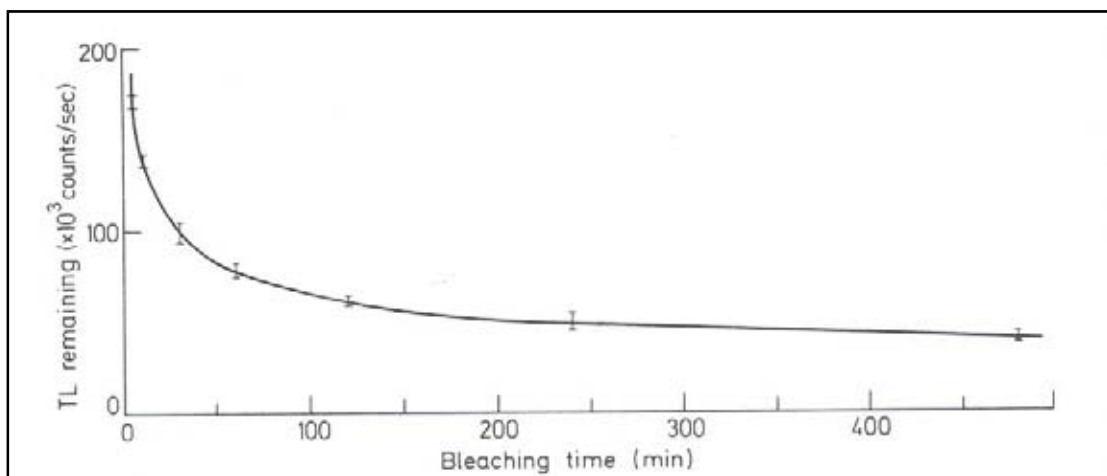


Figure 5.9 Thermoluminescence remaining after bleaching by exposes to sunlight for various time (Aitken, 1985)

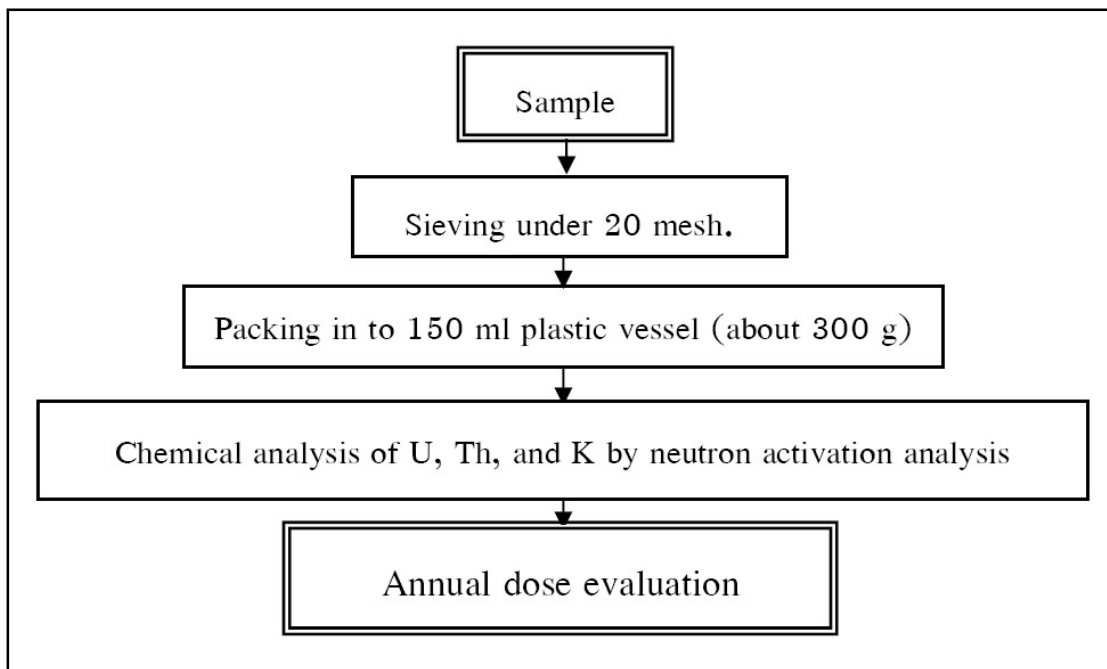


Figure 5.10 Summary of neutron activation analysis (NAA) procedures with sample preparation and annual dose determination.

The annual dose to the sample is computed from the concentrations of K, U and Th by the method described by Bell (1979) and Aitken (1985), as shown in equation 5.3.

$$\text{Annual dose} = (\text{AD}) = D_{\alpha} + D_{\beta} + D_{\gamma} + D_c \dots\dots\dots (5.3)$$

Where α = Alpha irradiation content,
 β = Beta irradiation content,
 γ = Gamma irradiation content, and
 C = Cosmic ray irradiation content.

A) Measurement of Uranium, Thorium, and Potassium Contents

Figure 5.11 shows the schematic preparation and procedure for measurement of U, Th, and K contents by neutron activation analysis (NAA). The estimated standard errors were less than 10% for U and Th, and less than 3% for K using the fixed count error calculation method (Takashima and Watanabe, 1994).

B) Annual Dose Calculation

Annual dose is calculated from chemical data of U, Th, and K contents with the equations proposed by Bell (1979) and Aitken (1985), as shown

$$\begin{aligned}
 AD = & [0.15(2.783U + 0.783Th)/(1+1.50(W/100))] \\
 & +[(0.1148BU + 0.0514BTh + 0.2492BK)/(1+1.14(W/100))] \\
 & + [(0.1462U + 0.0286Th + 0.8303K)K/(1+1.25(W/100))] \\
 & +0.15 \dots\dots\dots (5.4)
 \end{aligned}$$

Where AD = Annual dose (mGy/year),
 U = Concentration of uranium in ppm,
 Th = Concentration of thorium in ppm,
 K = Concentration of potassium oxide (%),
 B = Beta coefficient in quartz grains, and
 W = Water content (%).

5.1.8 Error Determination

Error in TL-dating result derives mainly from sample preparation and TL measuring apparatus (av. 10%), as well as standard deviation (SD) from measured values of ratio $H+\gamma / N$ on growth curve. So equation for dating errors is described as

$$\text{Error} = \text{Absolute} [(SD_{ED}^2) + (SD_{AD}^2)] \times \text{age} \dots\dots\dots (5.5)$$

Where $SD_{ED} = \text{Absolute} [(x-\bar{x})^2/N]$
 $SD_{AD} = 10 \%$

5.2 Thermoluminescence Dating Results

A total of 39 samples were selected for TL dating and their results are shown in Table 5.1. For annual dose analysis, the dated samples contain U contents varying from 1.64 to 3.33 ppm, Th contents from 6.64 to 11.30 ppm, and K contents from 0.56 to 1.78 %. In general, water contents of the dated samples are between 13.71 to 26.05. The annual dose of the date samples vary from 5 to 548 mGy/Y, and the paleodose or equivalent dose range from 3.14 to 4.70 Gy. As shown in Table 5.1 ratios of paleodose to annual dose of individual dated sample give rise to the TL dates between 2,000 to 133,000 years.

Table 5.1 TL dating results of quartz concentrates sediments for sample collected from the study area in Nan, northern Thailand.

No.	Sample	U (ppm)	Th (ppm)	K (%)	Water content (%)	Annual Dose (mGy/Y)	Paleodose (Gy)	TL Age (year)
1	BA-01	2.25	8.31	0.79	16.39	3.35	7	2,100 ± 200
2	BA-02	2.73	10.11	0.86	17.17	3.92	7	1,800 ± 500
3	BA-03	2.62	10.64	1.54	24.69	4.20	17	4,000 ± 120
4	BA-04	1.64	10.75	1.74	22.76	3.97	20	5,000 ± 330
5	BA-05	2.6	9.7	1.18	19.09	3.98	8	2,000 ± 400
6	BA-06	2.43	10.16	1.17	19.29	3.95	8	2,000 ± 50
7	BA-07	2.73	10.11	0.86	20.58	3.79	6	1,600 ± 100
8	BA-08	3.04	6.64	0.56	21.82	3.14	14	4,200 ± 90
9	BA-09	2.6	9.7	1.18	21.91	3.87	11	2,900 ± 130
10	BA-10	2.73	10.11	0.86	20.68	3.78	9	2,400 ± 50
11	BA-11	3.07	10.83	1.73	23.62	4.65	54	11,600 ± 760
12	BA-12	2.34	10.4	1.48	26.05	3.93	15	3,900 ± 100
13	BA-13	2.3	8.79	0.85	21.61	3.32	6	1,800 ± 740
14	BA-14	2.29	7.63	0.88	21.35	3.18	5	1,600 ± 400
15	BA-15	2.53	8.89	0.92	19.81	3.58	9	2,500 ± 100
16	BA-16	2.85	11.25	1.68	24.80	4.51	21	4,700 ± 160
17	BA-17	2.57	8.47	1.07	21.24	3.61	12	3,300 ± 110
18	BA-18	2.57	8.47	1.07	19.14	3.69	9	2,400 ± 150
19	BA-19	2.3	8.79	0.85	20.73	3.35	6	1,800 ± 50
20	BA-20	2.79	10.22	1.59	25.19	4.24	20	4,700 ± 20
21	BA-21	2.3	8.79	0.85	20.69	3.35	9	2,700 ± 400
22	BA-22	2.75	10.09	1.56	25.07	4.19	56	13,400 ± 3,400
23	BA-23	3.33	8.02	1.7	23.71	4.34	68	15,700 ± 2,500
24	BD-01	2.51	10.89	1.78	17.43	4.70	29	6,200 ± 240
25	BD-02	2.68	10.39	1.59	14.51	4.70	25	5,300 ± 140
26	BD-03	2.43	10.6	1.66	19.89	4.40	26	5,900 ± 120
27	BD-04	2.47	11.02	1.7	16.73	4.67	27	5,800 ± 900

Table 5.1 (con.)

No.	Sample	U (ppm)	Th (ppm)	K (%)	Water content (%)	Annual Dose (mGy/Y)	Paleodose (Gy)	TL Age (year)
28	BW-01	2.78	9.31	1.18	16.70	4.12	471	114,000 ± 1,000
29	BW-02	2.72	8.93	1.34	19.31	4.05	537	133,000 ± 2,600
30	BW-03	2.1	7.61	1.19	13.94	3.60	403	112,000 ± 1,700
31	BW-04	2.53	8.44	1.57	19.88	4.05	297	73,000 ± 100
32	BW-06	2.08	7.62	0.99	13.71	3.42	247	72,000 ± 2,000
33	BW-07	2.31	7.37	0.97	17.79	3.34	193	58,000 ± 6,800
34	BW-08	2.41	9.14	1.26	17.53	3.93	548	120,000 ± 1,500
35	BW-09	2.3	9.74	1.49	18.02	4.14	363	88,000 ± 1,200
36	BW-10	2.28	8.78	1.29	17.07	3.85	408	106,000 ± 1,100
37	BW-11	2.12	8.6	1.48	17.61	3.87	417	108,000 ± 2,900
38	BW-12	2.85	11.3	1.35	18.14	4.55	548	120,000 ± 2,200
39	BW-13	2.63	9.43	1.74	14.47	4.65	476	103,000 ± 1,800

5.3 Fault Evolution

5.3.1 Trench 1: Ban Thung Ao, Amphoe Thung Chang

5.3.1.1 Age of stratigraphic units

Based up on the result of stratigraphic trench logging and TL age determination on the samples, the ages of individual layers are show below.

Unit B which is brown clayey sand lies over unit A, light brown pebble. The TL date obtained from the Unit B is about 15,000 years.

Unit D, which overlies continuously with the unit C and unit B. The unit D, which is light brown, clayey sand, has the TL age of about 10,000 to 3,000 years.

Unit E is light brown, fine-sand and underlain by unit D. The TL dating result indicate the dates of unit E range from 1,500 to 2,000 years. The overall lithostratigraphy with TL-dated sediment samples as shown in Figures 5.11 and 5.12

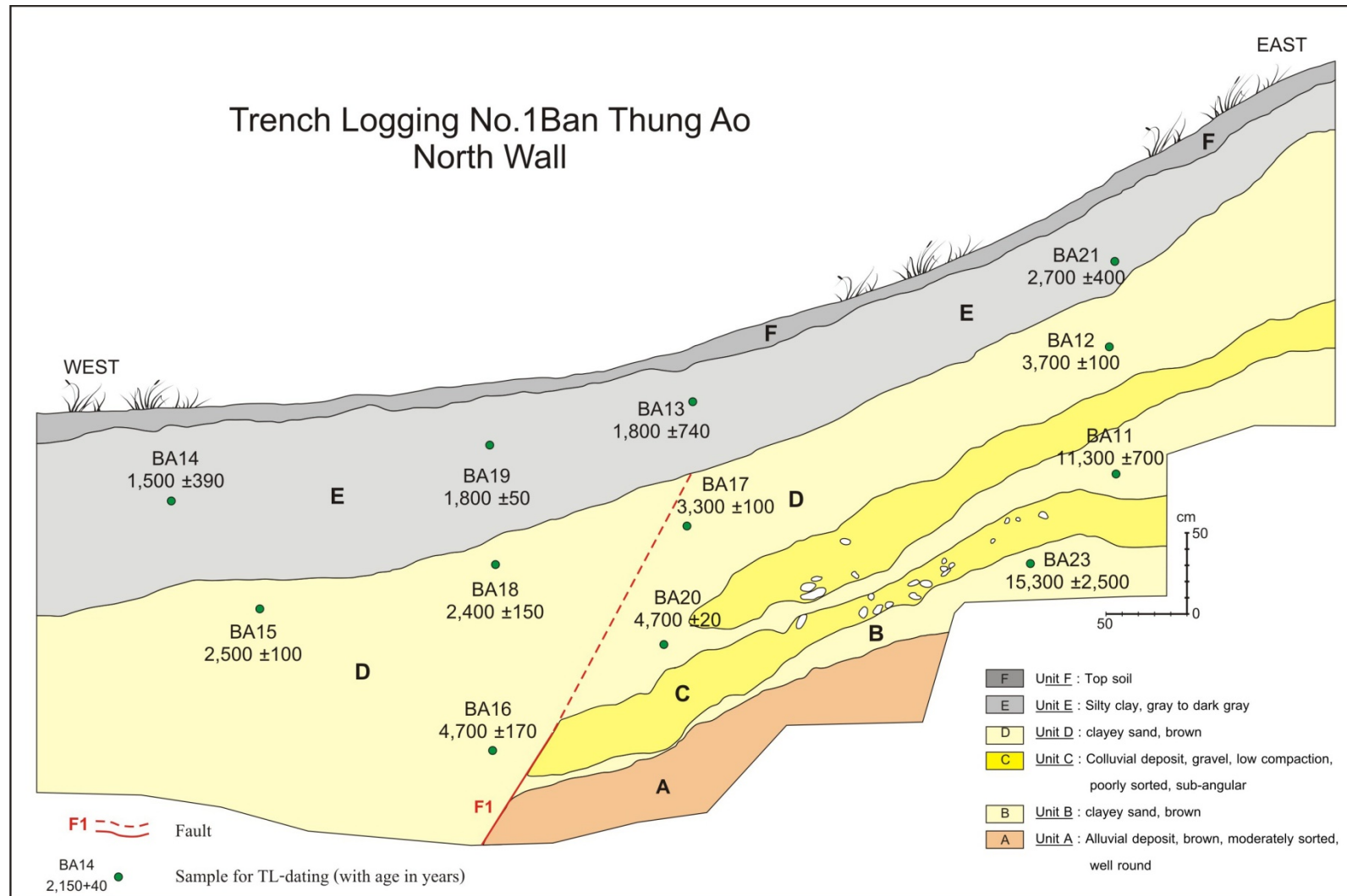


Figure 5.11 Trench-log stratigraphy showing fault orientation (F1), lithostratigraphy, and TL ages of sedimentary layer, on north wall, Ban Thung Ao trench.

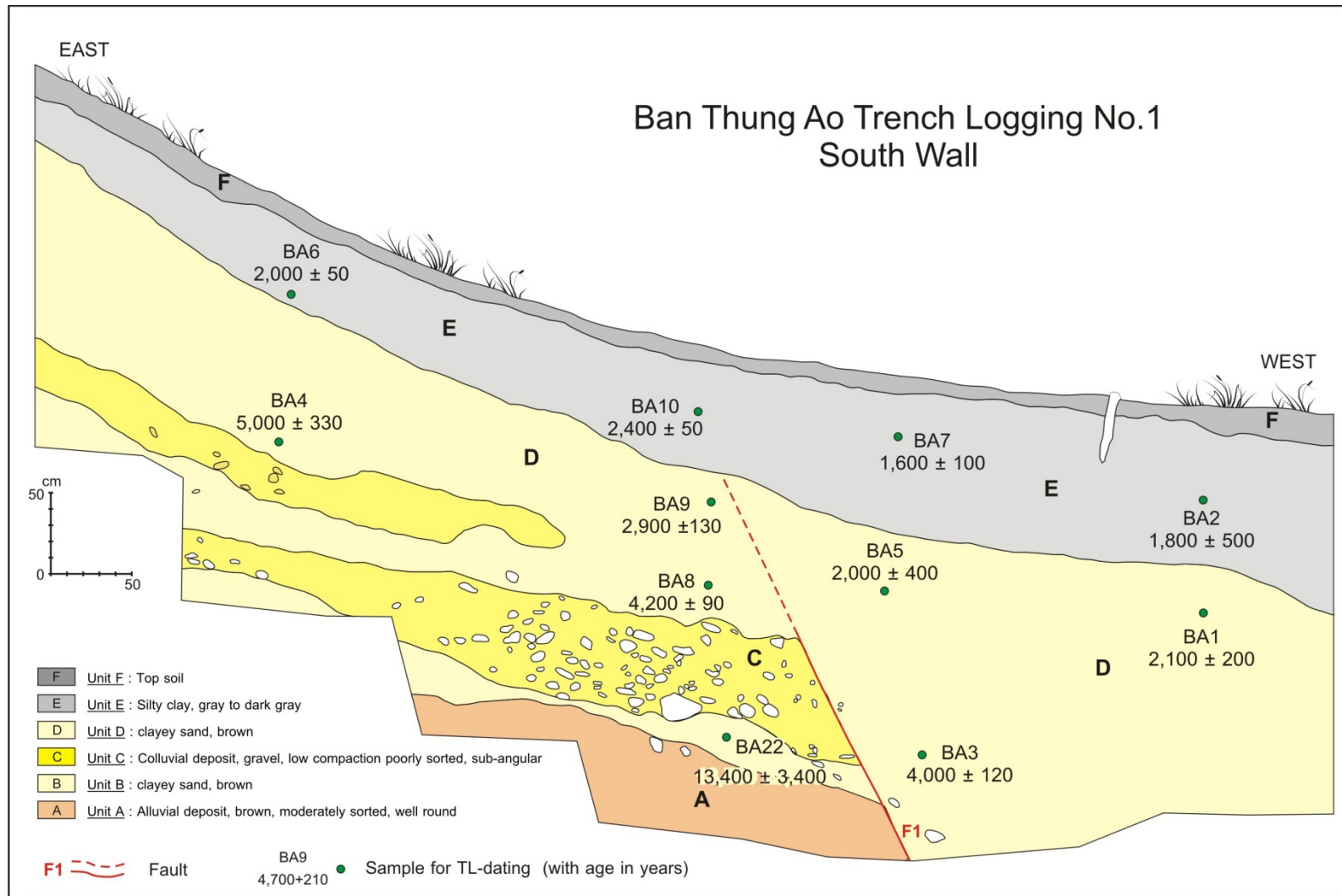


Figure 5.12 Trench-log stratigraphy showing fault orientation, lithostratigraphy, and TL ages of sedimentary layer on south wall, Ban Thung Ao trench.

5.3.1.2 Evolution of sedimentation and faulting

Judging from the overall result, it is visualized that the paleoseismic event may have occurred at approximately 2,000 years ago when the fault (F1) cut through the gravel beds of the Unit A to unit D. After that the unit E and unit F was deposited, respectively about 2,000 to recent. The evolutionary model for sediment deposition and faulting events is illustrated in Figure 5.13.

5.3.2 Trench 2: Ban Doo, Amphoe Chiang Klang

5.3.2.1 Age of stratigraphic units

Based on the stratigraphical data from Ban Doo trench and TL age determination on the samples, the ages of individual layers are shown below.

Unit D, which lies over units A and C, is the matrix supported colluvial deposit. The TL date obtained from the Unit D is about 6,200-5,300 years. The youngest unit is the gray silty loam of unit E which is younger than 5,000 years to recent years. The overall lithostratigraphy with TL-dated sediment samples is shown in Figure 5.14.

5.3.2.2 Evolution of sedimentation and faulting

As described earlier in the previous chapters, a fault in the Ban Doo area is a normal-oblique fault (F1). Based on results were observed in Ban Doo trench. The fault cut through sediments of Unit A, B, and C. Since then, the unit D rapidly deposited over the three units below (unit A, B, and C). There are some of unit D fill up in fault-related open fissure in the lower units and we took the fissure-filled sediments for TL dating. The TL dates is approximately 6,200-5,300 year and imply that fault cut through Units A, B, and C at ca. 5,000 year ago. The evolutionary model for sediment deposition and faulting events is illustrated in Figure 5.15.

5.3.3 Trench 3: Ban Wiang Song, Amphoe Thung Chang

5.3.3.1 Age of stratigraphic units

Based on the result of stratigraphic trench logging and the sediments dating data, the ages of individual layers are shown in Figure 5.14.

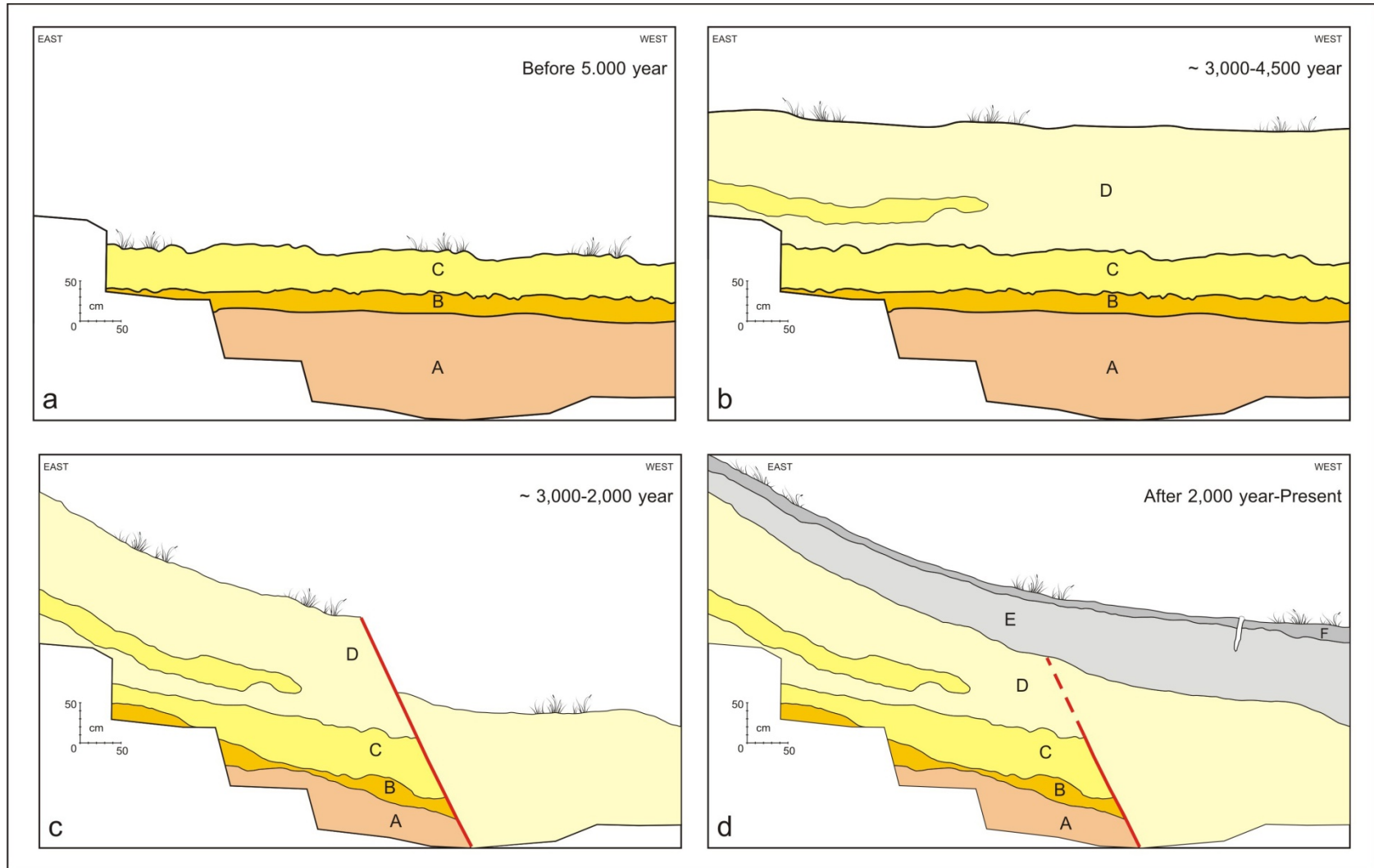


Figure 5.13 Evolution of faulting associated with sediment deposition in Ban Thung Ao trench from 5,000 year to present.

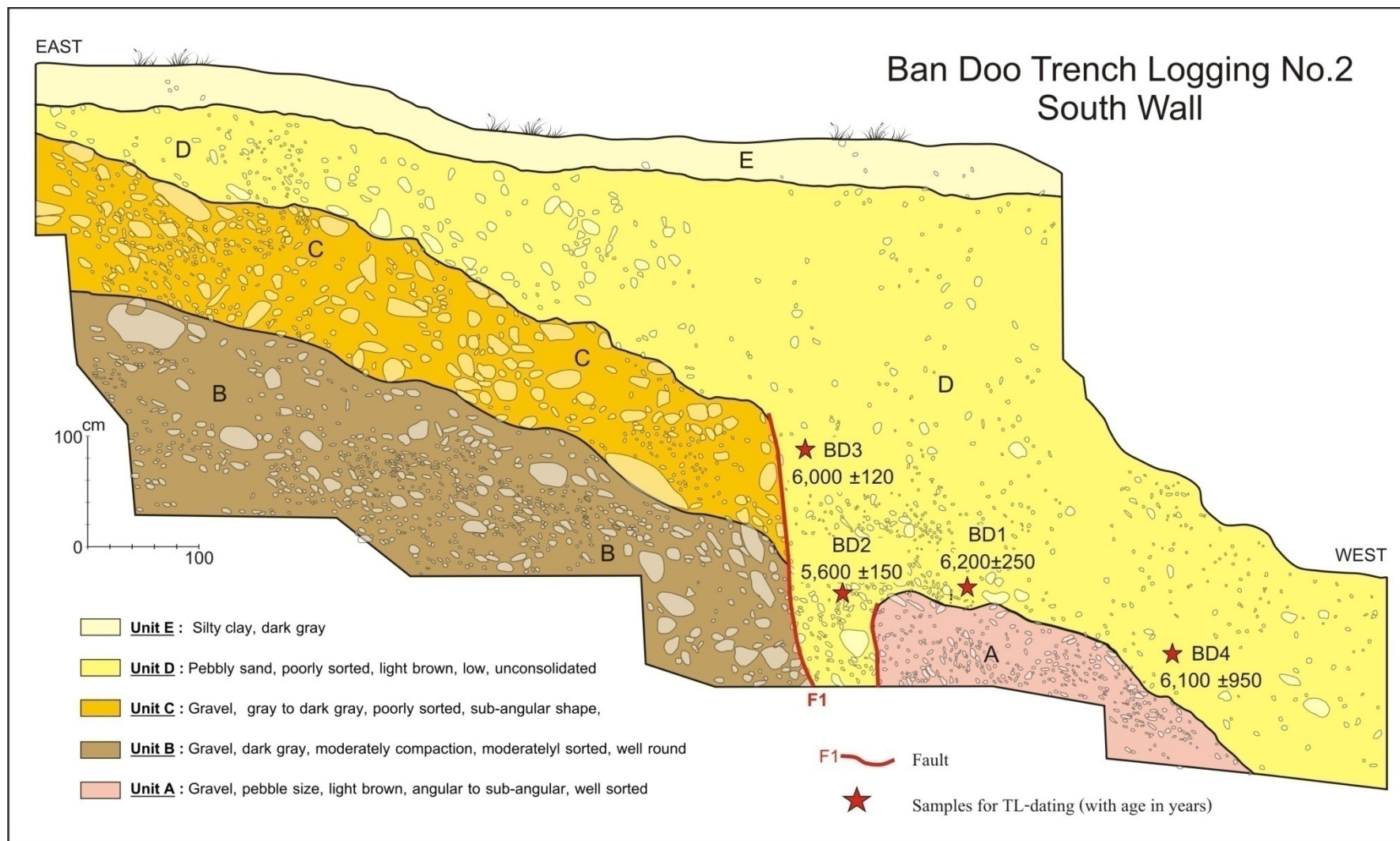


Figure 5.14 Trench-log stratigraphy showing fault orientation, lithostratigraphy and TL ages of sedimentary layer, Ban Doo trench.

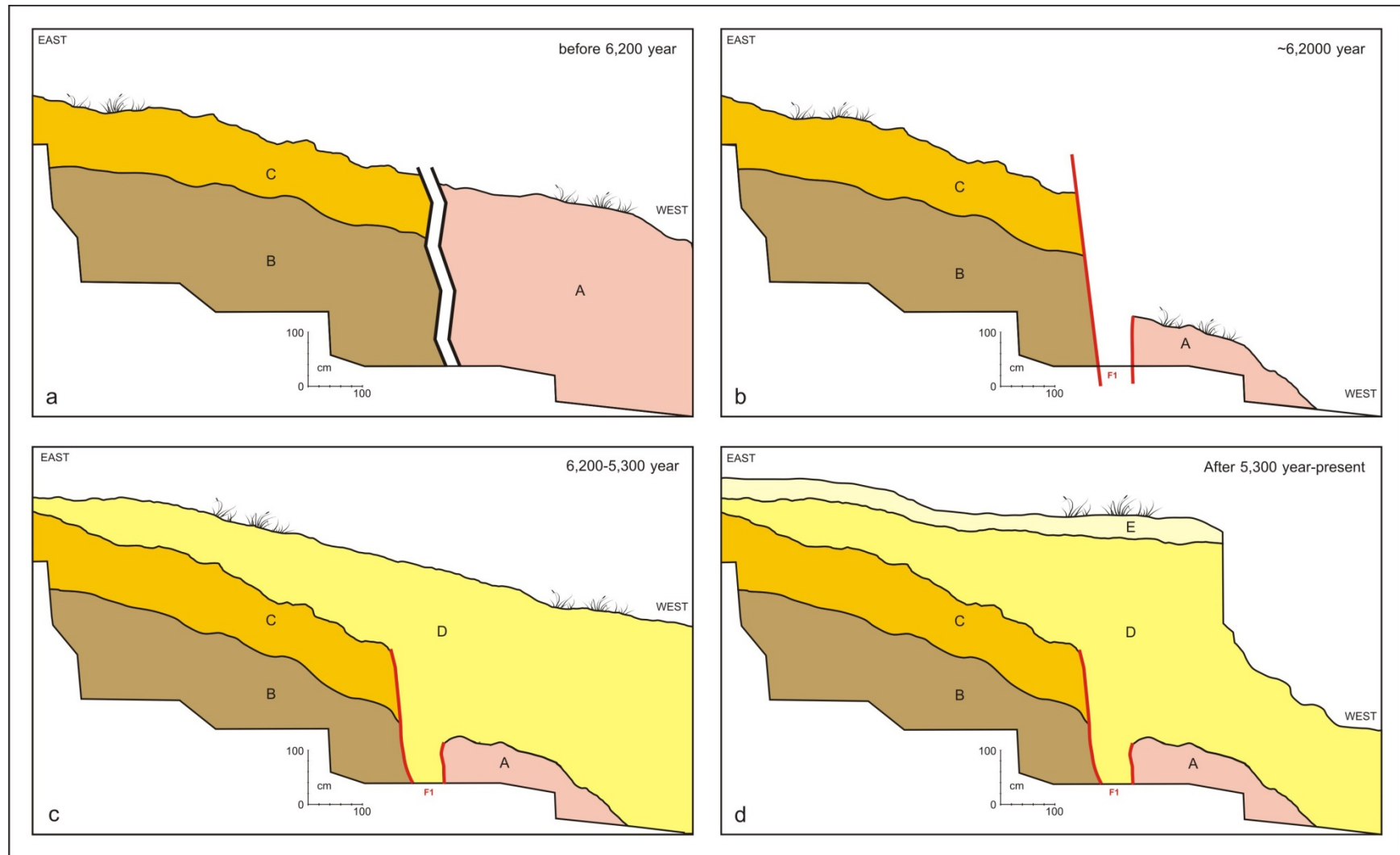


Figure 5.15 Evolution of faulting associated with sediment deposition in Ban Doo trench from 6,200 year to present.

From trench stratigraphical data, sedimentary layers of Ban Wiang Song can be divided into three major units. The oldest is unit A, the deformed sandy clay interbedded fine gravel bed and overlain unconformably by gravel bed of unit B and loosed sediment of Unit C which all of them are covered by unit D, sandy clay.

The deformed sediments from unit A yield TL dates of about 130,000-110,000 years. Unit B, which is the less deformed unit yield the TL dates of about 100,000-72,000 years. The TL date of unit C has a long range from 57,000 to 110,000 years but in a reverse order. As described in Chapter 4, Ban Wiang Song trench is regarded as a historical site named “Ban Pha Wae”, therefore sediments of unit C are moat-filled sediment by human activity. From stratigraphical and age dating data, unit C was probable dug from unit B and filled up the moat suddenly, so these sediments have no time for bleaching TL signal. This is a reason TL dating results from unit C have similar age to the other units. The overall lithostratigraphy with TL-dated sediment samples are shown in Figure 5.16

5.3.3.2 Evolution of sedimentation and faulting

As mentioned above and described in the last chapter, the sedimentary layers at Ban Doo trench is not cut by fault but the deformation of unit A probably occurred by fault movement nearby (see Figure 4.35) at about 130,000 to 100,000 years ago. The evolutionary model for sediment deposition and faulting events is herein proposed and illustrated in Figure 5.17. Starting with deposition of sedimentary layers of the Unit A (more than one beds) before 110,000 years ago (Figure 5.17a). Then the unit A was compressively deformed between 110,000-100,000 years ago (Figure 5.17b). After that deposition of sedimentary layers of Unit B took place between 100,000 and 70,000 years ago onto the underlying Unit A (see Figure 5.17c). Subsequently after 70,000 years man-made moat was created and become part of “the Ban Pa Haew” ancient community.

Table 5.2 displays age and events of the paleoearthquakes with in the Nan-Pua study area. It is quite likely that there are at least 3 faulting events occurring in the study area. The oldest paleoearthquake event may have happened sometime after 70,000 years. The second event may have taken place at about 6,000 years where as the youngest event may have occurred at Ca. 3,000 years. However, as stated in the earlier chapter, the Prathat Din Wai, a historical earthquake was record to have

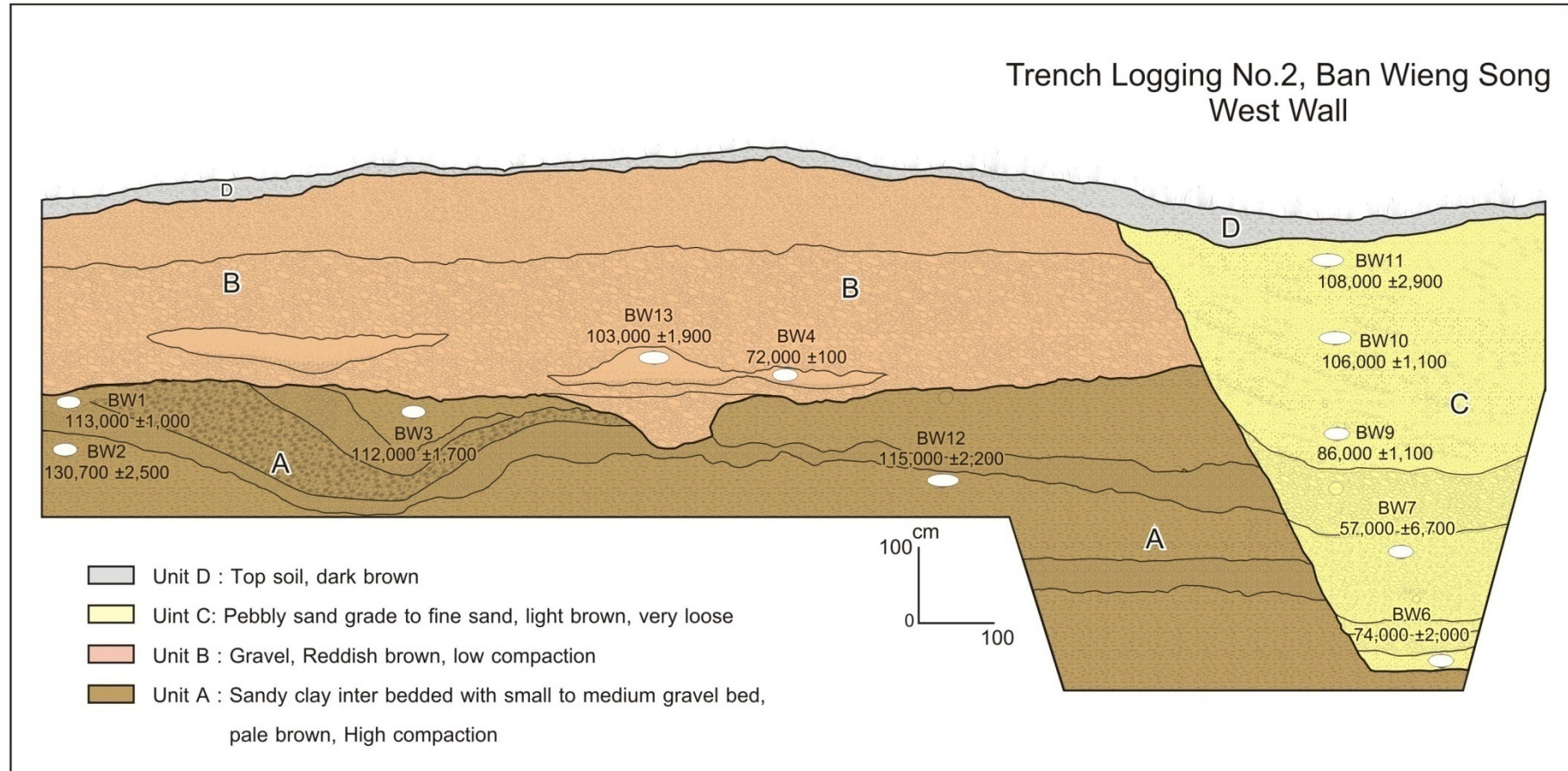


Figure 5.16 Trench-log stratigraphy showing fault orientation and TL ages of sedimentary layer, Ban Doo trench.

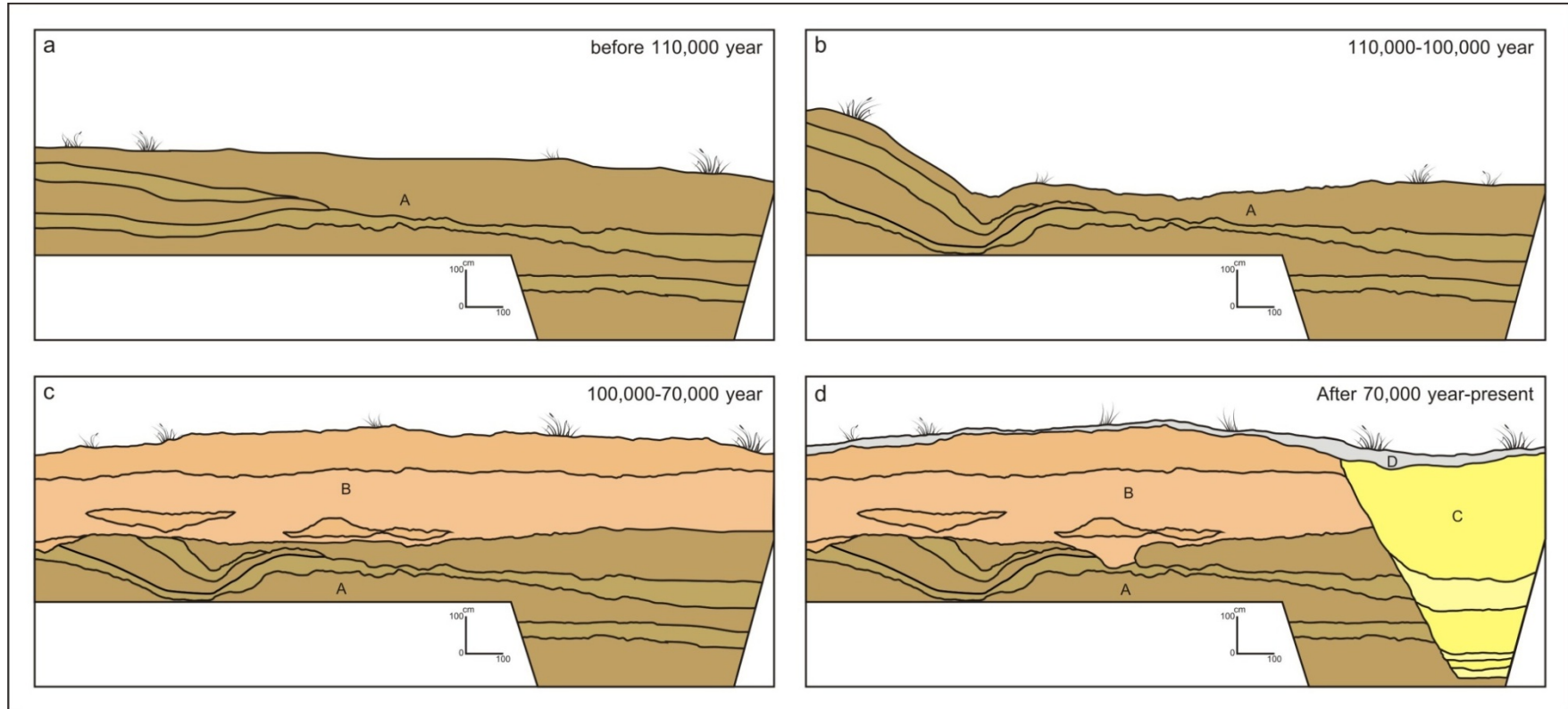


Figure 5.17 Evolution of faulting associated with sediment deposition in Ban Wiang Song trench from 110,000 year to present.

occurred as about the 180 year. Apart from the latest earthquake event, there are 3 earlier events happened in the Pua-Nan area. These earthquake faulting may correspond to some extent with the morphotectonic features what suggest 4 times of large fault movements.

Table 5.2 Estimated timing of paleoearthquakes in the Pua-Nan area before present.

Trench no.	Age and amount of fault displacement	Earthquake event (year)			
		1 st	2 nd	3 rd	4 th
Trench 1	3,000-2,000 year			~ 2,000	
Trench 2	5,300-6,200 year		5,000		
Trench 3	70,000 year	> 70,000			
Prathat Din Wai	180 year				180

CHAPTER VI

DISCUSSION

In this chapter, a focus is made on the discussion related to the results from current paleoseismic investigations along with the existing previous works. The discussion comprises 1) the characteristic of Pua Fault Zone, 2) their paleoearthquake magnitudes, and slip rates, and 3) neotectonic evolution.

6.1 Characteristic of the Pua Fault Zone

This is no doubt that the major basins in the study area, including Nan, Santisuk, and Pua Basins, are mainly controlled by series of faults that are situated in (or bounded by) the basins. These basins were formed as the north-south trending garben-type or half-garben-type basins by the successively vertical and horizontal movements along the faults. The onset of basin developments has been attributed to the Indian-Asian continental collision since 45 million years (Middle Eocene) ago (see Charusiri et al., 1997 and Polachan et al., 1991). Besides, the occurrence of the stratigraphic fault line leads Siribhakdi (1986) to believe that the movement along the fault is still active at present.

Fenton et al. (1997) first used the tectonic geomorphology in the Nan-Pua Basin to indicate active faults. They recognized three major fault segments including Thung Chang, Santisuk and Pua Faults. However no age dating data has been reported for the fault movement.

In this study, not only the detailed morphotectonic evidence was reported for active fault investigation, but also evidence deduced from TL dating data is provided. Our study shows that the 111 km-long active fault in the Nan-Pua Basin is longer than that (68 km-long) reported earlier by Fenton et al. (1997). Moreover, as shown in Figure 6.1, there are 14 fault segments observed in the current study. All of the segments are confirmed by several places of morphotectonic evidence. Moreover, our TL-dating data also show that the Ban Doo and Thung Ao segments were once active at 5,000 and 2,000 Ma, respectively. The TL dating results point to the conclusion that those two fault segments are undoubtedly active, following the nomenclatures of active faults by Hinthong (1995) and Charusiri et al. (2003).

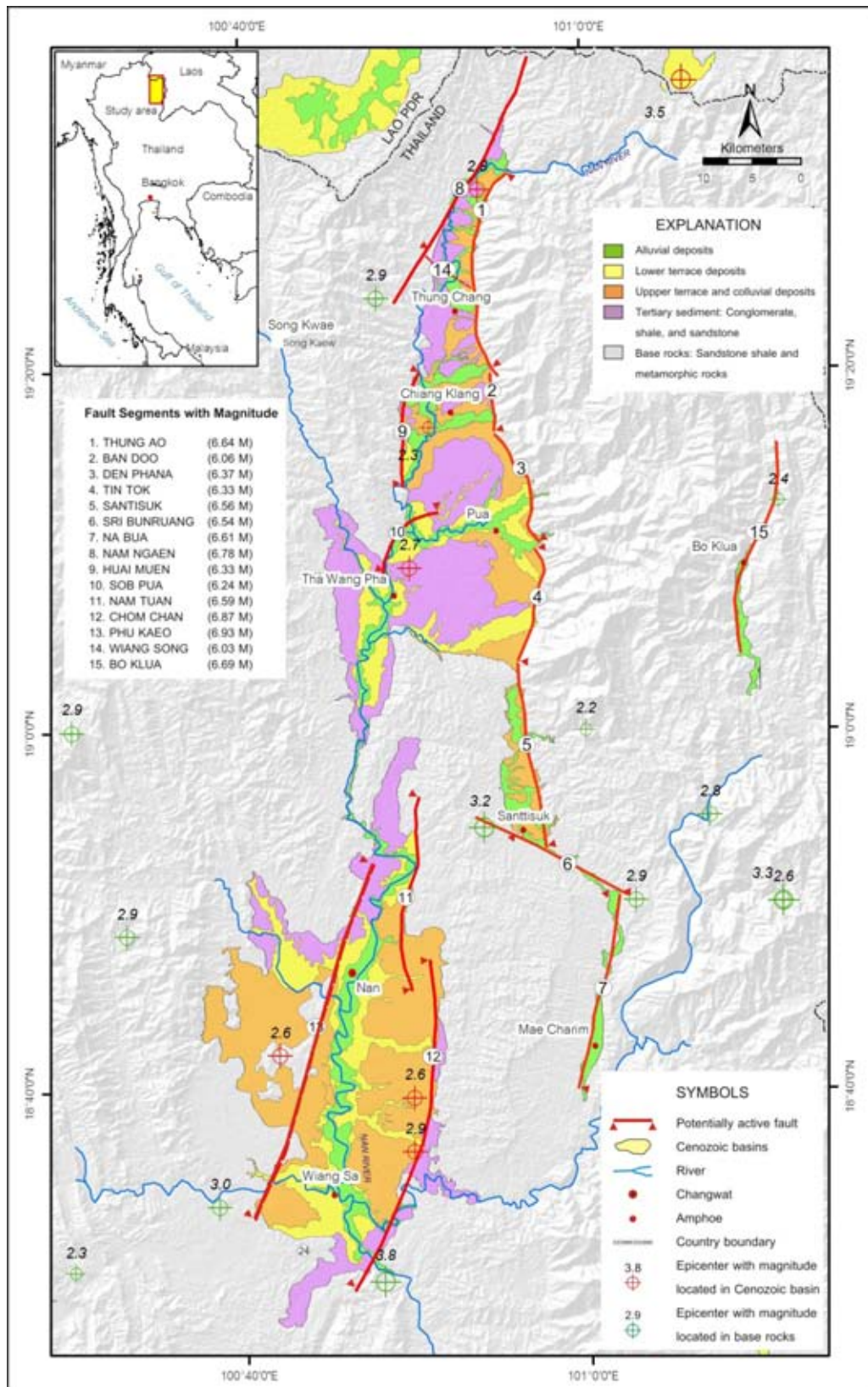


Figure 6.1 Map of Nan and adjacent areas showing epicentral distribution from 1983 to 2008 (Data from Nutalaya et al., 1985; Thai Meteorological Department, 2004; and http://neic.usgs.gov/neis/epic/epic_global.html, 2008). Note that many epicenters are located in the basins, a few in the hard-rock terrain.

Fenton et al. (2003) concluded in their paleoseismic investigations in northern and western Thailand that several epicenters in those two regions do not follow all the active faults and may indicate basin tectonics similar to that of the Basin and Range in southwestern USA. They also considered that seismic sources may have been occurred along the faults as reported earlier by Smith and Arabasz (1991). However, as shown in Figure 6.1, the epicentral distribution from Thailand Meteorological Department (2008) show that almost 70% of the epicenters are located in the basins and the rest are located in hard-rock region. If the locations of epicenters are correct, then many of them can indicate dipping planes of the faults. For example, the Nam Ngaen, Huai Muen, and Sob Pua fault segments are inferred to be the west-dipping plane. It is also considered that if the earthquakes are shallow and occurred at the similar depth, then the Nam Ngaen fault segment become steeper than the other two segments. It is confirmed by epicentral locations that some fault segments showed more lateral movements. Good examples are the Sri Bunruang segment and the Bo Klua segment, the later located to the east, outside of the study area. (see Figures 6.1 and 6.2).

6.2 Paleomagnitude and Slip rate

Well and Coppersmith (1994) reported the relationship between surface rupture length (SRL) along the active faults and the paleoearthquake magnitudes. They also found that the vertical slips are related to the earthquake magnitude. The SRL can be used to calculate the maximum credible earthquake (MCA). These relationships lead them to propose the empirical equations (6.1, 6.1, and 6.3) as shown below.

$$M = 5.08 + 1.16 \log (\text{SRL}) \dots\dots\dots (6.1)^*$$

$$M = 5.16 + 1.12 \log (\text{SRL}) \dots\dots\dots (6.2)**$$

$$M = 6.61 + 0.71 \log (\text{MD}) \dots\dots\dots (6.3)***$$

Whereas: M, moment magnitude; SRL, surface rupture length; MD, maximum displacement;
 *Equation for all fault type; **Equation for strike-slip fault; and ***Equation for normal fault.

Based on the equation (6.1) and as shown as a graph in Figure 6.3, it is likely to estimate the paleoearthquake magnitude of the individual faults as shown below. In this study, since there are 3 basins, so the magnitudes are evaluated for

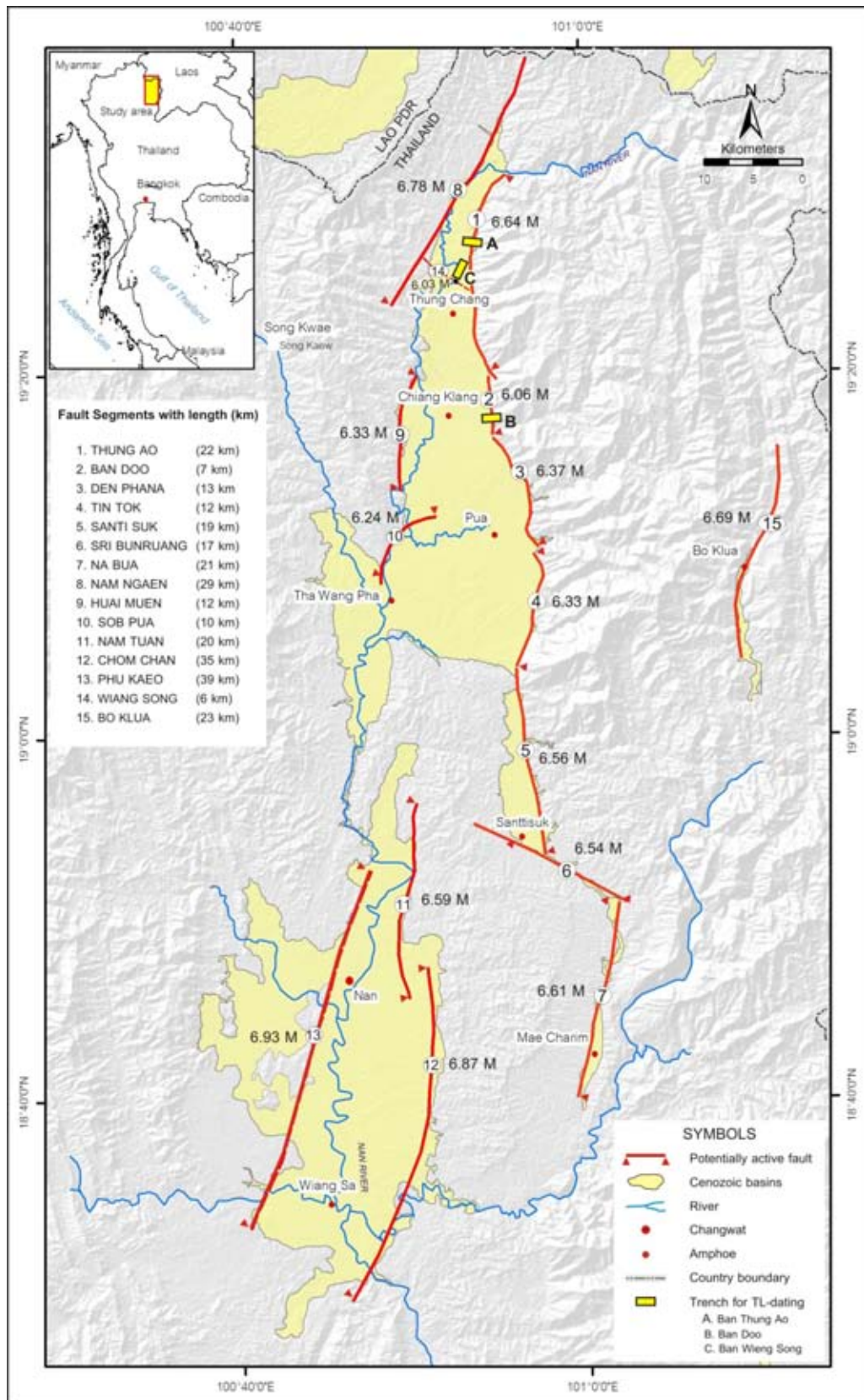


Figure 6.2 Map showing active fault segments, their length and estimated maximum credible earthquakes or paloemagnitudes of the Pua Fault Zone.

individual basins. Tectonically, the Pua Basin has 8 major basin-bounded faults. The longest surface rupture length (SRL) of fault for the Pua basin is that of Nam Ngaen fault segment which is about 29 km long. So the SRL of Nam Ngaen segment gives the paleomagnitude equivalent to 6.78 M. Thung Ao fault segment is about 22 km long and its SRL of Thung Ao segment gives the paleomagnitude equivalent to 6.64 M. Based on the vertical movement which is measured from distance between the location of TL-sample of about 4,000 and 4,200 years (Figure 6.4) as assumed the sediment of 2 locations deposited in the same layer during 4,000 year ago. So, vertical movement of Thung Ao segment is about 1.2 m with using equation (6.3). This segment gives the paleomagnitude equivalent to 6.67 M. Ban Doo fault segment which is about 7 km long, the SRL of Nam Ngaen segment gives the paleomagnitude equivalent to 6.06 M. Based on the vertical movement of 1.75 m (Figure 6.5) using equation (6.3), Ban Doo segment gives the paleomagnitude equivalent to 6.79 M. Den Phana fault segment is about 13 km long which the SRL of Den Phana segment yields the paleomagnitude equivalent to 6.37 M. Tin Tok segment has the SRL of about 12 km long and can give rise to the paleomagnitude equivalent to 6.33 M. Huai Muen fault segment which is about 12 km long. So the SRL of Huai Muen segment gives the paleomagnitude equivalent to 6.33 M. Sob Pua fault segment is about 10 km long which SRL of Sob Pua segment gives the paleomagnitude equivalent to 6.24 M. The shortest is the Wiang Song fault segment which is about 6 km long and its SRL of Wiang Song segment yield the paleomagnitude equivalent to 5.98 M.

Further to the south, the Santisuk Basin consists of 3 major basin-bounded faults; Santisuk, Sri Bunruang and Na Bua segments. The Santisuk segment is about 19 km long and its SRL value yield the paleomagnitude earthquake of about 5.56 M. The NW-tending Sri Bunruang segment has the SRL of about 19 km and this can give rise to the paleomagnitude of about 6.54 M, whereas the NE-trending Nabua segment, which is about 21 km long and orients in the opposite direction, yield the paleomagnitude of about 6.61 M.

The southernmost basin is the Nan Basin which comprises 3 major fault segments- Nam Tuan, Chom Chan, and Pha Kaeo. Among these, the longest SRL is that of the Pha Kaeo which is about 39 km long and can give rise to the paleoearthquake

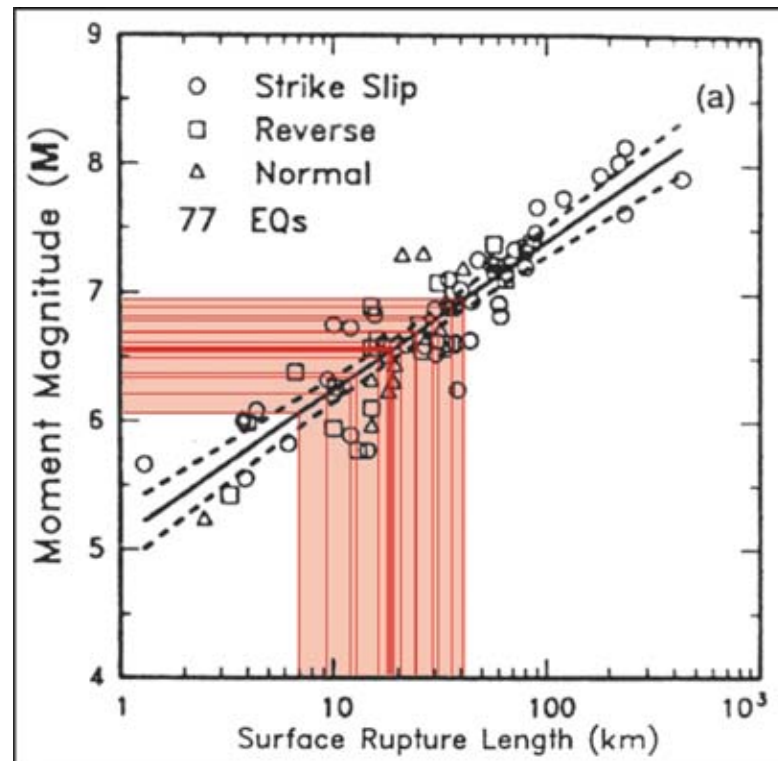


Figure 6.3 Graph showing relationship between surface rupture length and moment magnitude of the data from Pua Fault in comparison with those of the world data of Wells and Coppersmith (1994).

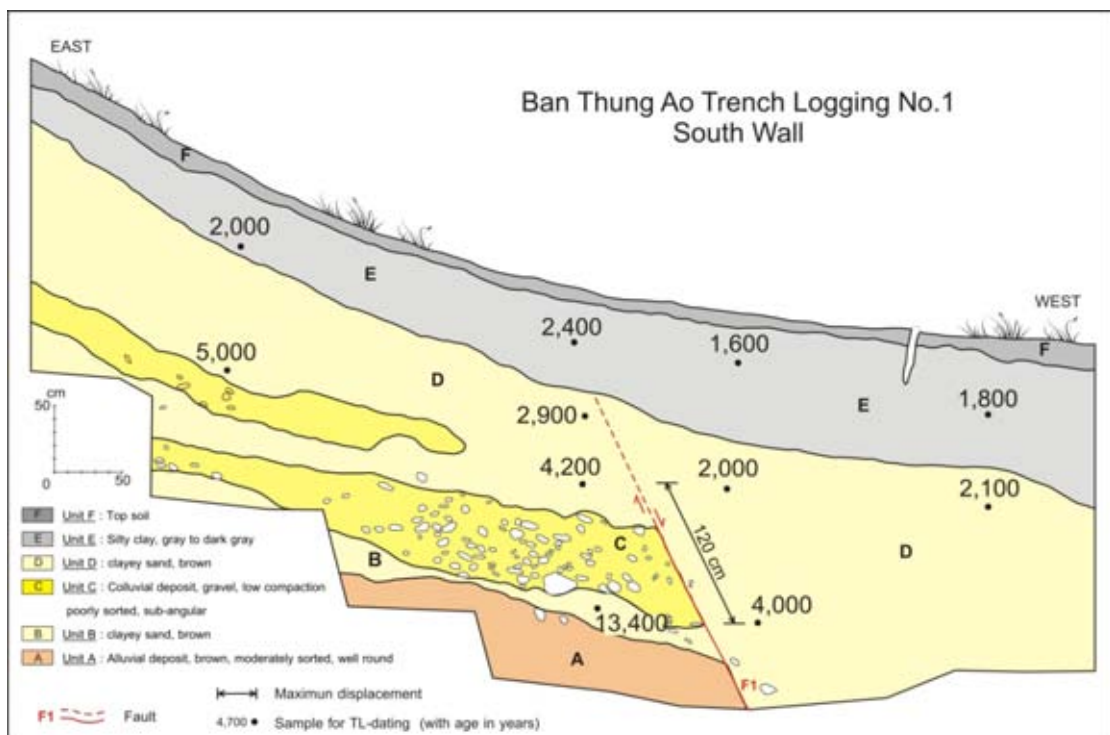


Figure 6.4 Trench log section at the south wall of Ban Thung Ao trench, Nan showing principal stratigraphy and TL ages of each sediment layer.

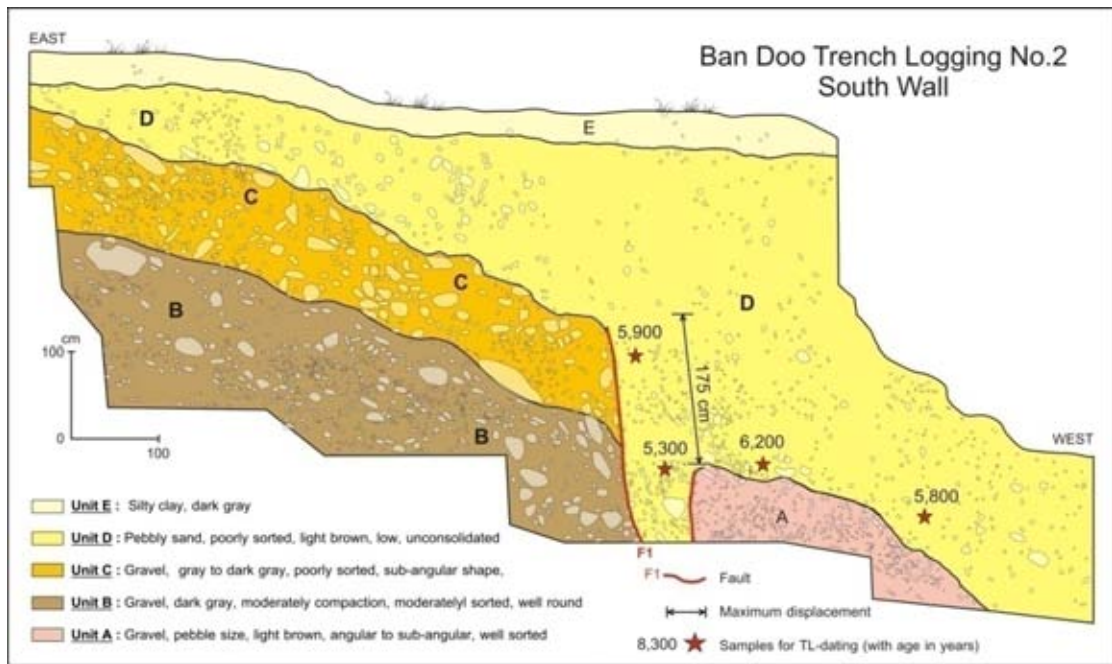


Figure 6.5 Trench log section at the south wall of Ban Doo trench showing principal stratigraphy and TL ages of each sediment layer.

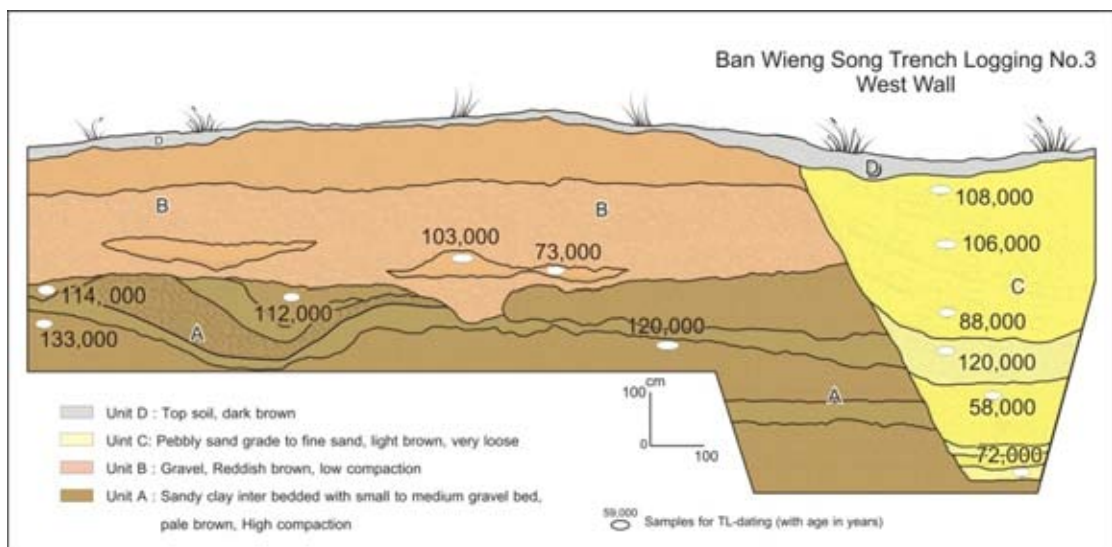


Figure 6.6 Trench log section at the south wall of Ban Doo trench showing principal stratigraphy and TL ages of each sediment layer.

event equivalent to 6.93 M. The Chom Chan segment, which has the SRL of about 35 km, yields the paleomagnitude earthquake of 6.87 M. The shortest is the Nam Tuan segment which is about 20 km long and the SRL value gives the magnitude of about 6.59 M.

There exists the other fault, about 23 km to the east, i.e., the Bo Kua segment. The SRL is about 23 km and render the magnitude of about 6.69 M.

If the Sribunruang segment (17 km-long), Wiang Song (6 km-long) and Bu Klua segment (23 km-long) indicate most lateral movement, then based on the equation 6.2, the better estimated paleomagnitude would be about 6.54 M, 6.03 M and 6.69 M.

Fenton et al. (2003) tried to estimate the slip rate of the Pua Fault to be at ca. 0.6 mm/yr. They applied the Holocene sedimentary layer which was offset at about 6 meters for estimation of slip rate. They also assumed that the age of the Holocene bed would be 10,000 years without any constrain on age dating date.

However, in the current research, we can estimate the slip rate more correctly based on the TL dating data. As shown in Figure 6.4, the Thung Ao fault segment cut the Unit D, two age dates in this unit show the similar date (about 4,000 year) suggesting that these two sample points may be in same level (ca. 1.2 m). After faulting, then the slip rate is estimated by the ratio 1,200 mm/4,000 yr, to be 0.30 mm/yr. The other age date of active fault movement is confirmed by displacement observed in the Ban Doo trench (Figure 6.5). Here at the Ban Doo segment, the sediment Unit D was dated at 6,200 years old. The unit was displaced to about 1.75 m, giving the slip rate of about ca. 0.28 mm/yr. Therefore, it is likely that the Pua Fault, particularly the Ban Doo segment can yield the slip rate within the range of ca. 0.28-0.30 mm/yr.

In order to constrain the recurrence interval, the latest movement for each fault is required which is doubtful at present. As it has been discovered seismically in this thesis that the latest paleoearthquake historically is that of the Prathat Din Wai which occurred at about 180 years ago and is probably equivalent to IV of the modified Mercalli intensity scale. However, geologically the latest movement along the fault (i.e., Ban Doo segment) took place at about 2,000 years. So it is therefore likely that the returns period for the active faults in the Nan-Pua Basin is preliminarily assumed to be around 1,500 to 2,000 years.

6.3 Neotectonic Evolution

As explained in the earlier section (6.1) and the contemporaneous stress regime shown by fault-plane mechanism (Bott et al., 1997 and Fenton et al., 1997), it is therefore likely that the maximum stress has its axis in the north-south direction and may have triggered the development of pull-apart basins in northern and central Thailand in response to the extension in the east-west direction. We considered that the onset of the Nan-Pua basin may have formed in Middle to Late Tertiary time (Figure 6.7). We strongly believe that the strike-slip tectonics in Neogene plays an essential role in the generation of the neotectonic and active faults. Therefore the model for the basin development associated with faulting in the Nan-Pua basin is herein proposed. This model mainly follows that of Sylvester (1988) which mentioned that spatial arrangement (in plan view) of identified structures (folds and faults) is governed by the strike-slip movement.

It is believed that the major fault which has controlled the Nan-Pua Basin and the development of basin-bounding faults is the northeast-southwest-trending Nan-Uttaradit Fault (see Figure 6.8) which also acted as the geosuture as shown in Figure 6.7 (Charusiri et al., 2002). The east-west compressive movements along the major fault (perhaps in Mesozoic) are basically right lateral, similar to that reported by Khaowiset et al. (2007) in the easternmost part of Thailand near Thai-Kampuchea border. However, after the development of the escape tectonics due to Indian-Asian collision at about 45 Ma ago, opposite movement happened, which also changed the compression movement to the north-south direction. The northern part of the fault which was earlier formed as the north-south-trending fractures (reverse fault ?) may become the horsetail splay normal fault system. Perhaps the onset of the (north-south-trending) pull-apart basins (Pua, Nan, and Santisuk basins) may have formed at this stage. Southwestwards, the fault may have become the releasing bend and formed half-graben depression and eventually the Na Noi Basin was created. Further to the south, movement along the faults may have caused the restraining bend whereby thrusting of ophiolite rocks may have been developed along the Nan-Uttaradit geosuture. Mean while, extrusion of Cenozoic basalts may have triggered along the southern part of the strike-slip fault system.

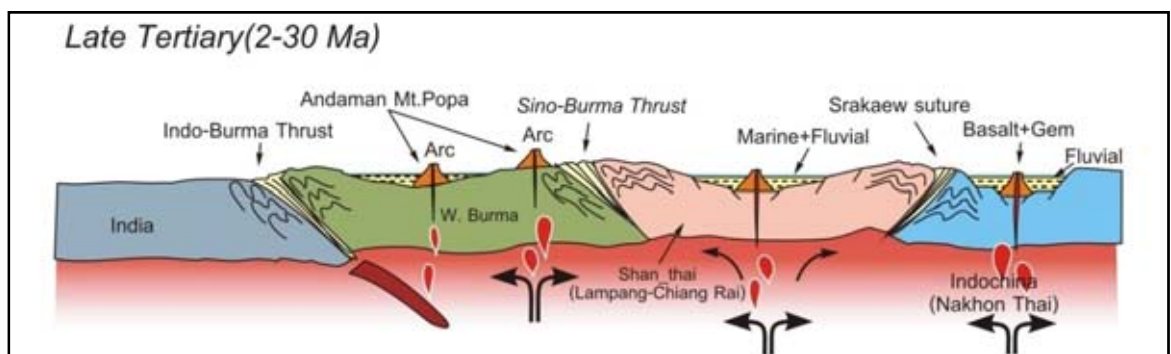
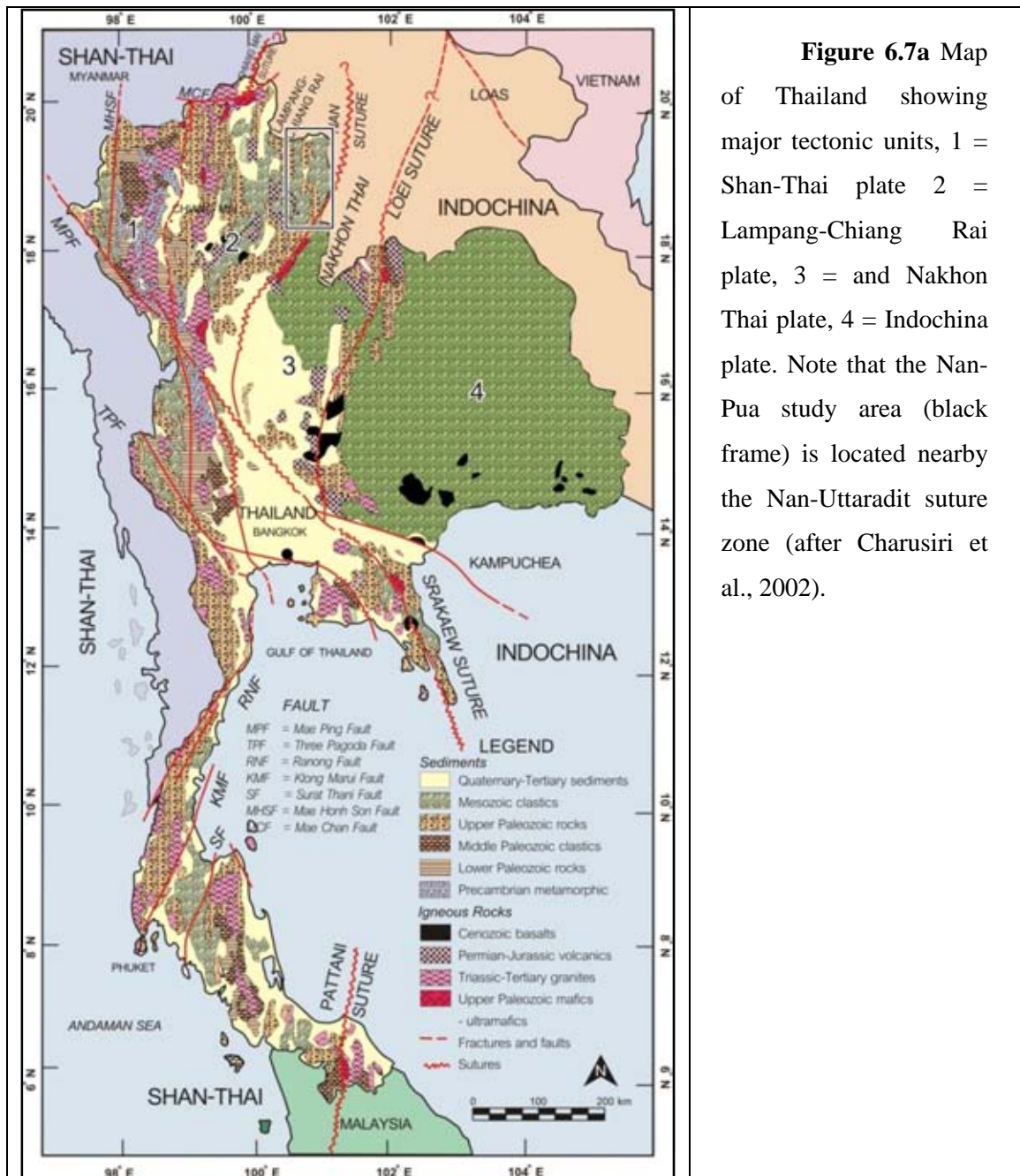


Figure 6.7b Plate tectonic model in Late Tertiary showing the major plate interaction, major structures, and Cenozoic tectonism (modified after Charusiri et al., 2002)

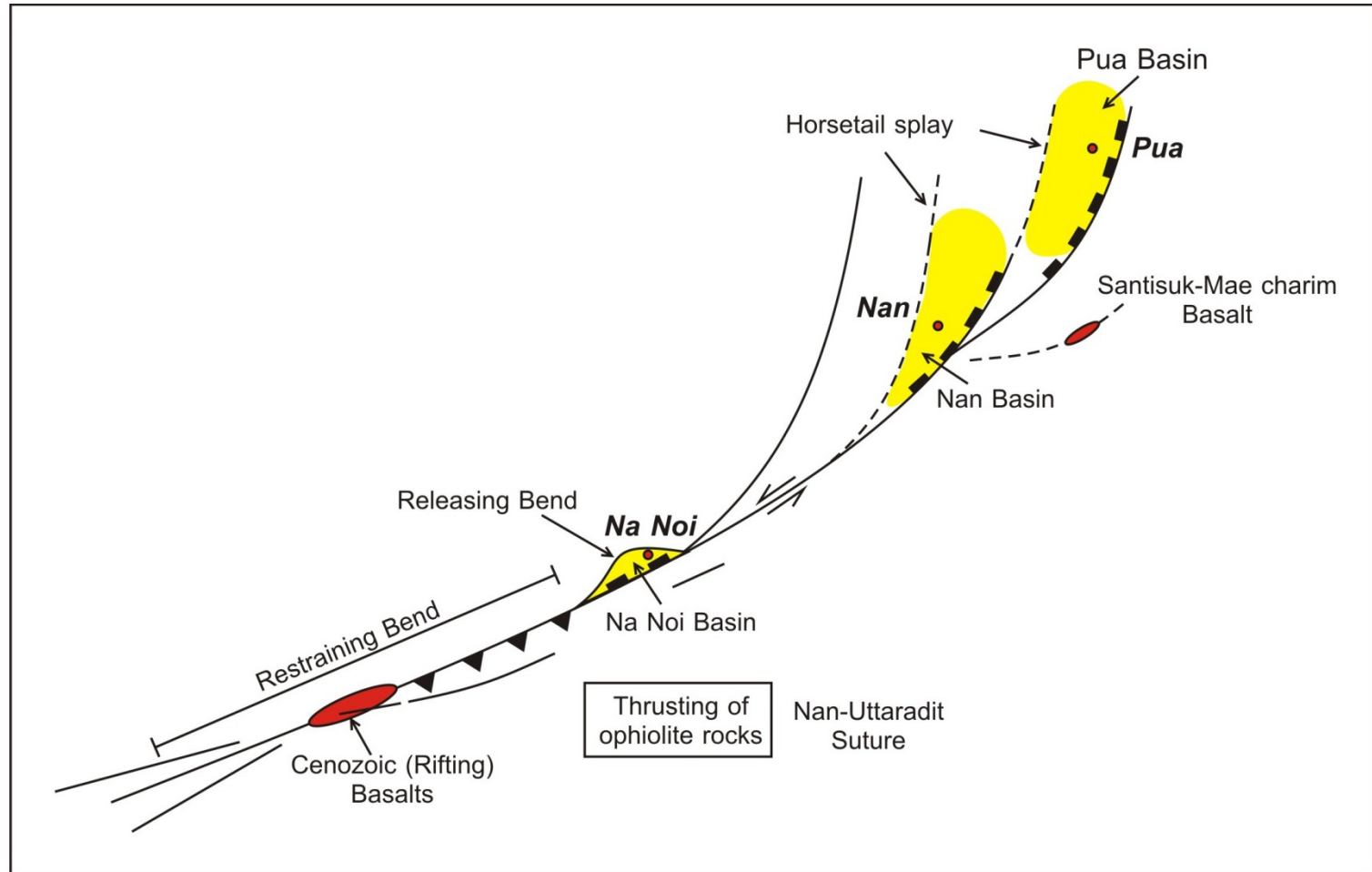


Figure 6.8a A model for the development of the Nan-Pua basins and associated structures by strike-slip tectonics (modified after Christie-Blick and Biddle, 1985 and Sylvester, 1988).

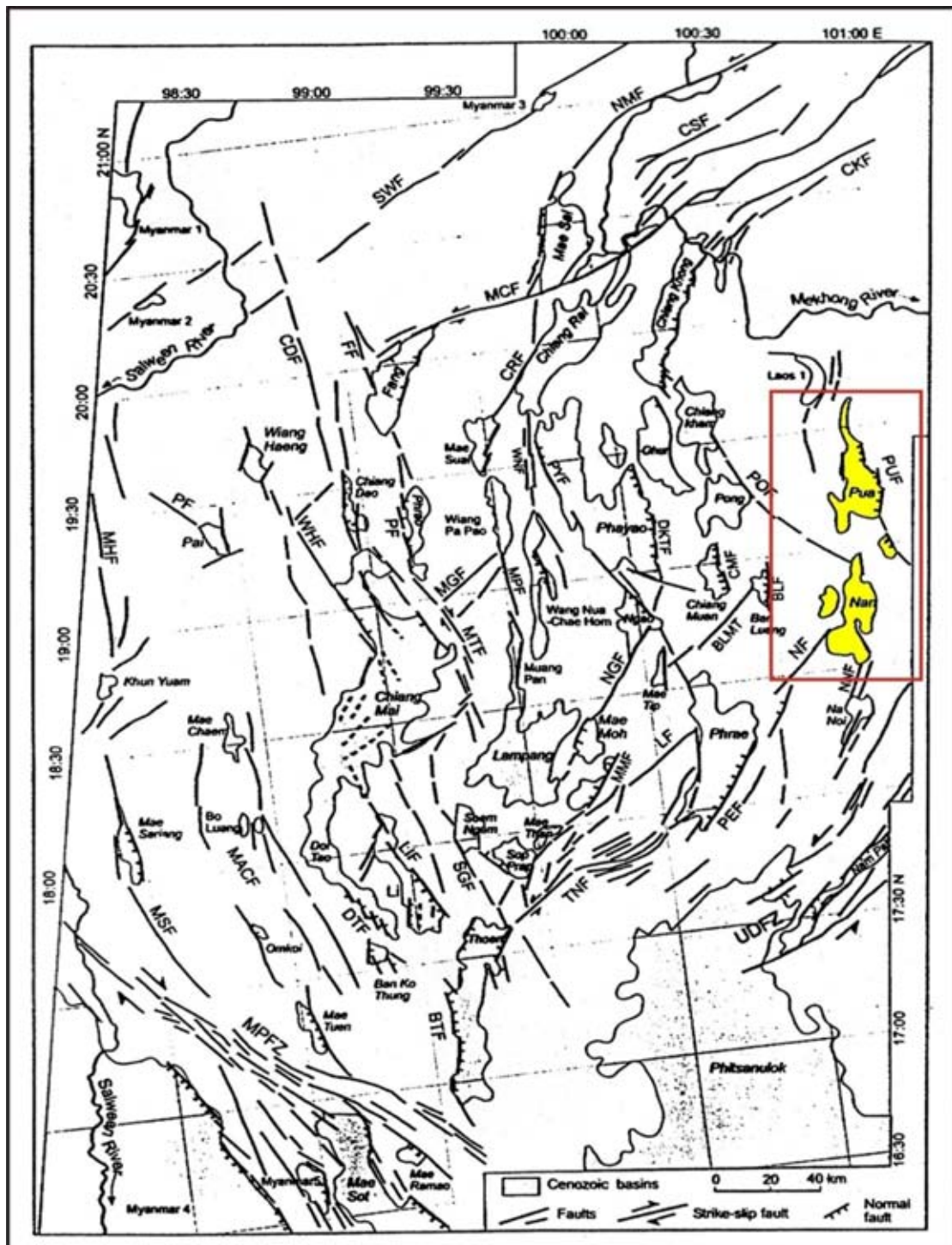


Figure 6.8b Present-day structure relationship between strike-slip faults, and the Cenozoic basins. SWF: Salween fault, NMF: Nam Ma Fault, MCF: Mae Chan fault, CKF: Chiang Khong fault, WHF: Wiang Haeng fault, PYF: Phayao fault, NGF: Ngao fault, LIF Li fault, MMF: Mae Moh fault, TNF: Thoen fault, UDFZ: Uttaradit fault zone, MPFZ: Mae Ping fault zone (after Uttamo et al., 2003).

This perhaps caused the formation of a series of triangular facets as clearly observed at the Den Phana segment. It is inferred herein that the development of vertical movement may become larger than that of the horizontal movement, this perhaps gave rise to the development of wine-glass valley, sag pond, linear ridge and the occurrence of poorly-sorted colluvial deposits (Figure 6.9). Subsequently the enlargement of the Nan-Pua Basin may be more developed. This may have caused the onset of the alluvial fans and terraces at Ban Wiang Song (Figure 6.6), due to both vertical and horizontal movements. By very late Tertiary (or possibly Pleio-Pleistocene time) the left-lateral slip movement may have been prominent for the northeast trending faults. This sometimes caused the s-shape basin (Figure 6.9) where the lateral movement becomes larger than the vertical drop. The occurrence of the early Pleistocene rifting basalts in the south of the Sirikit reservoir provides the good evidence for the extension tectonic associated with the uplifting phenomenon along the Nan suture. By the end of Pleistocene to Holocene, there exists the occurrence of the coarse-grained, poorly-sorted sediments of the Units A and C from the Ban Doo and Ban Thung Ao, respectively. After that the vertical component of the fault movement in several parts of the Nan-Pua Basin became invariably less than those of the horizontal component. Several morphotectonic evidence, such as offset streams and linear valleys, become obvious for the presence of active fault. In the last stage until present, either base level become higher as the uplift stage become minor, there exists the development of the alluvial plain of silty to clayey materials. However the present-day tectonics is still going on. This perhaps gives rise to the activeness of the fault (Figure 6.10).

6.4 Preliminary Seismic Hazard Evaluation

As shown in earlier section (see also Figure 6.1), our result on paleoseismic investigation indicates large paleoearthquakes (> 6.5 M) existing for every fault segment. It is notably important that epicenters have been detected in some active faults, such as Thung Ao, Sob Pua and Chom Chan fault segments. This means that these fault segments have already released appropriate amount of energy for producing earthquakes. Therefore it probably takes some times for these faults to storage energy for the next earthquakes. However, there are some other faults which have not experienced any large movements, such as Ban Doo, Den Phana, Tin Tok,

Santisuk and Nam Tuan segments (Figure 6.11). This is essential for deterministic analysis of the seismic hazard assessment. Therefore we tentatively consider that these afore- mentioned faults may act as the seismic gap within the Nan-Pua basin where the energy becomes progressively accumulated and perhaps produced the major earthquake in the near future, like what the people in Nan have experienced such kind of the shaking phenomenon at Prathat Din Wai about 180 years ago.

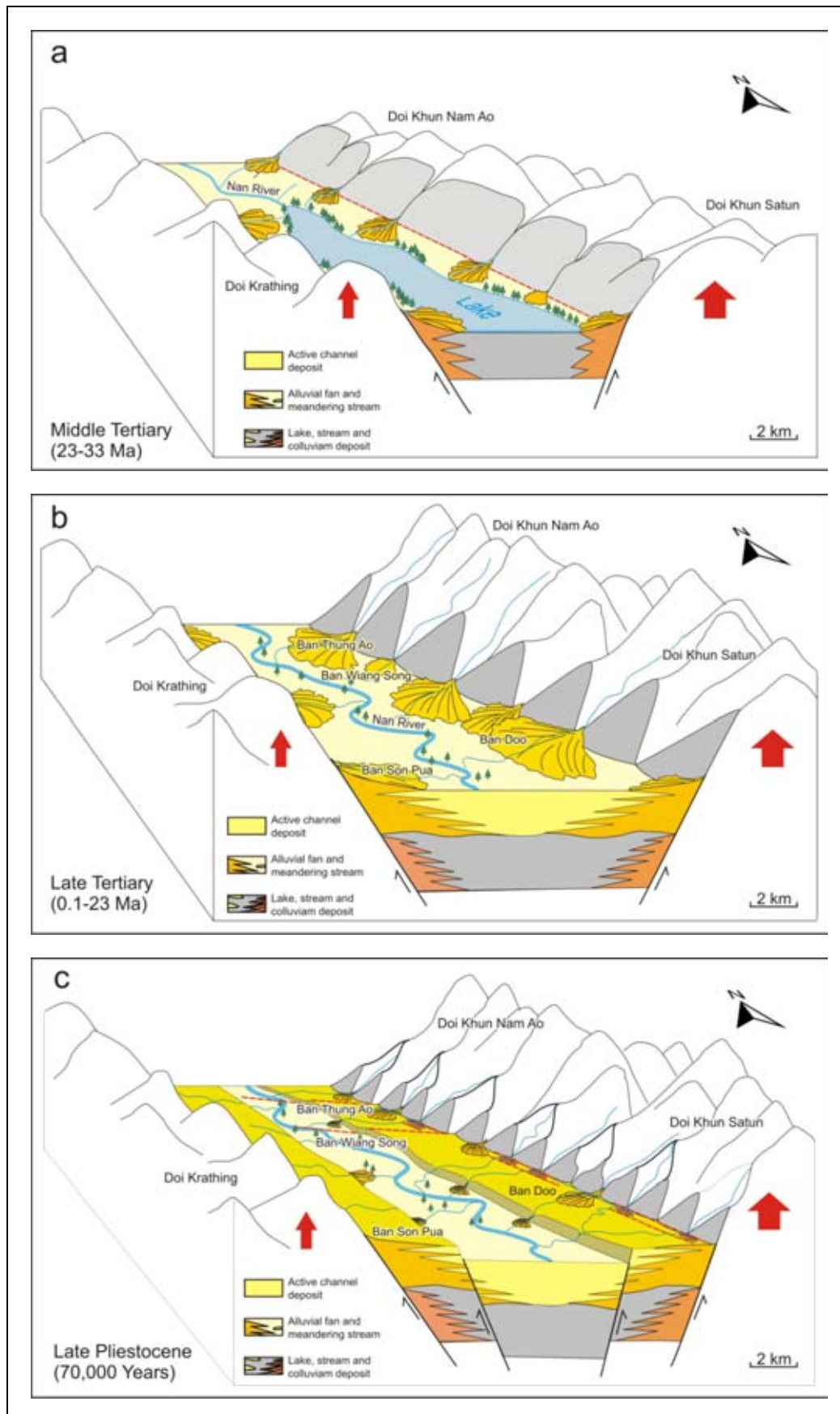


Figure 6.9a Schematic diagram showing evolution of Nan-Pua basin during the Cenozoic time. Note that the red arrows represent the rate of uplift.

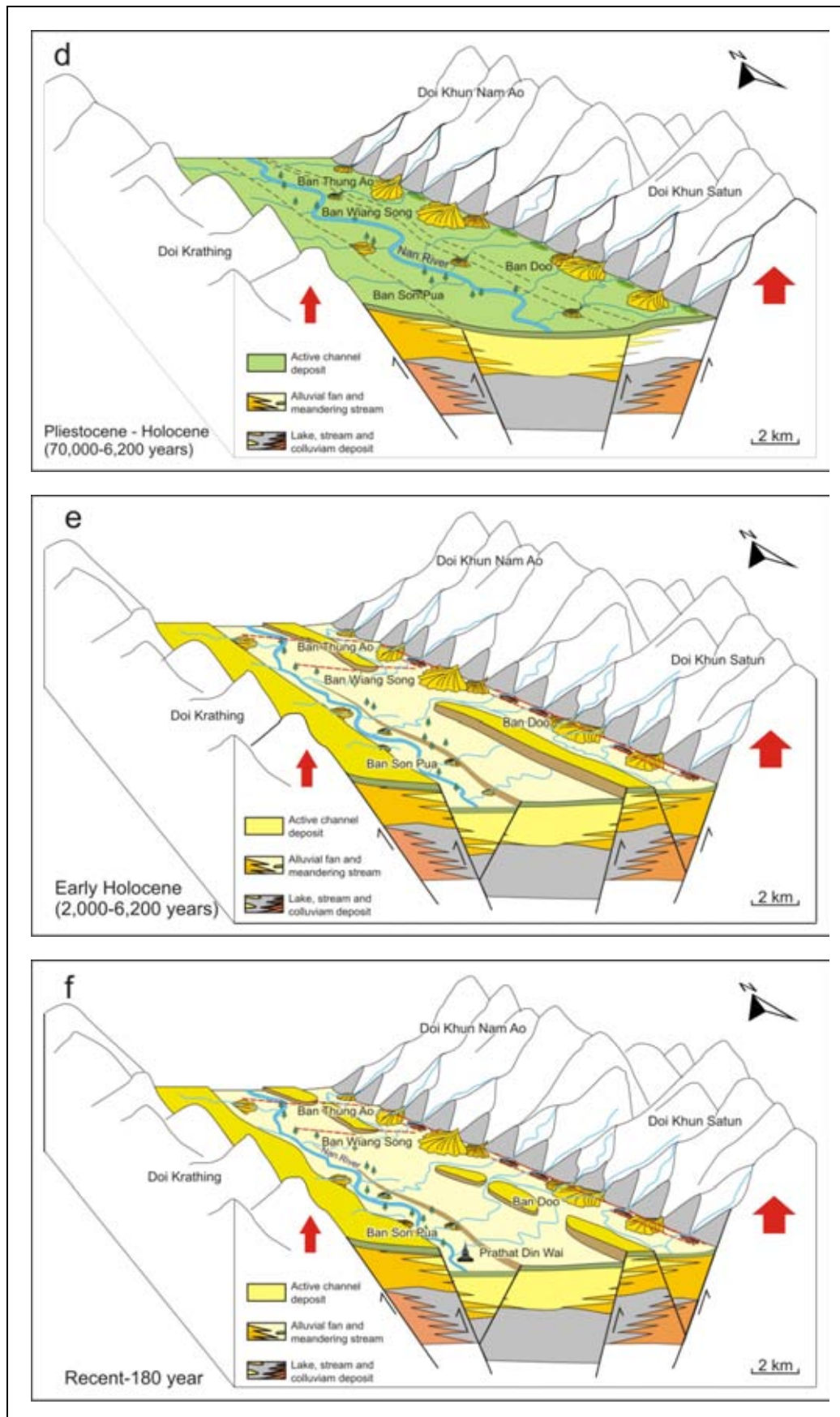


Figure 6.9b Schematic diagram showing evolution of Nan-Pua basin during the Cenozoic time. Note that the red arrows represent the rate of uplift.

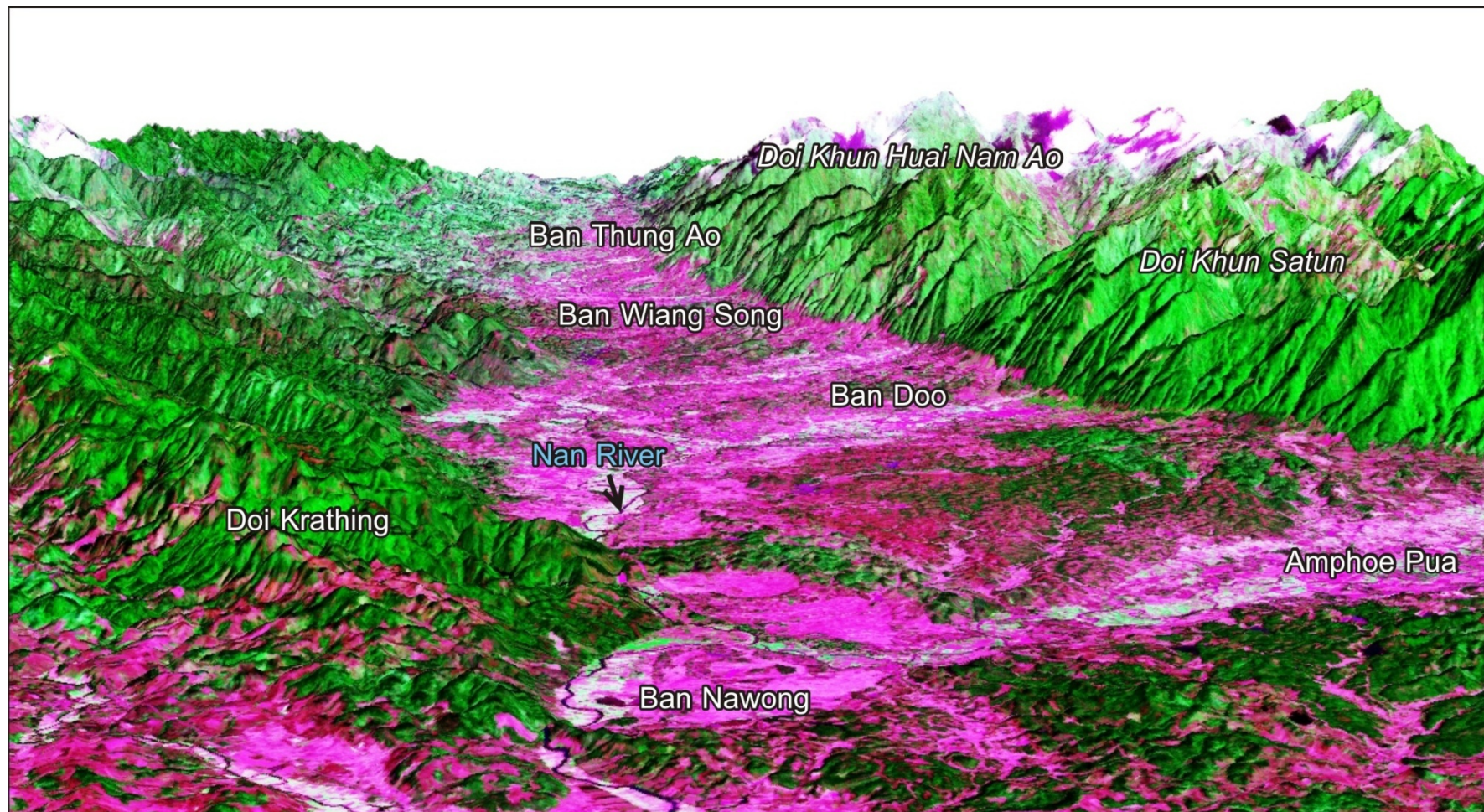


Figure 6.10 The 3D model of ASTER image showing sharp morphotectonic of Pua basin, particularly on the eastern flank of the basin which indicated an active tectonic of this area.

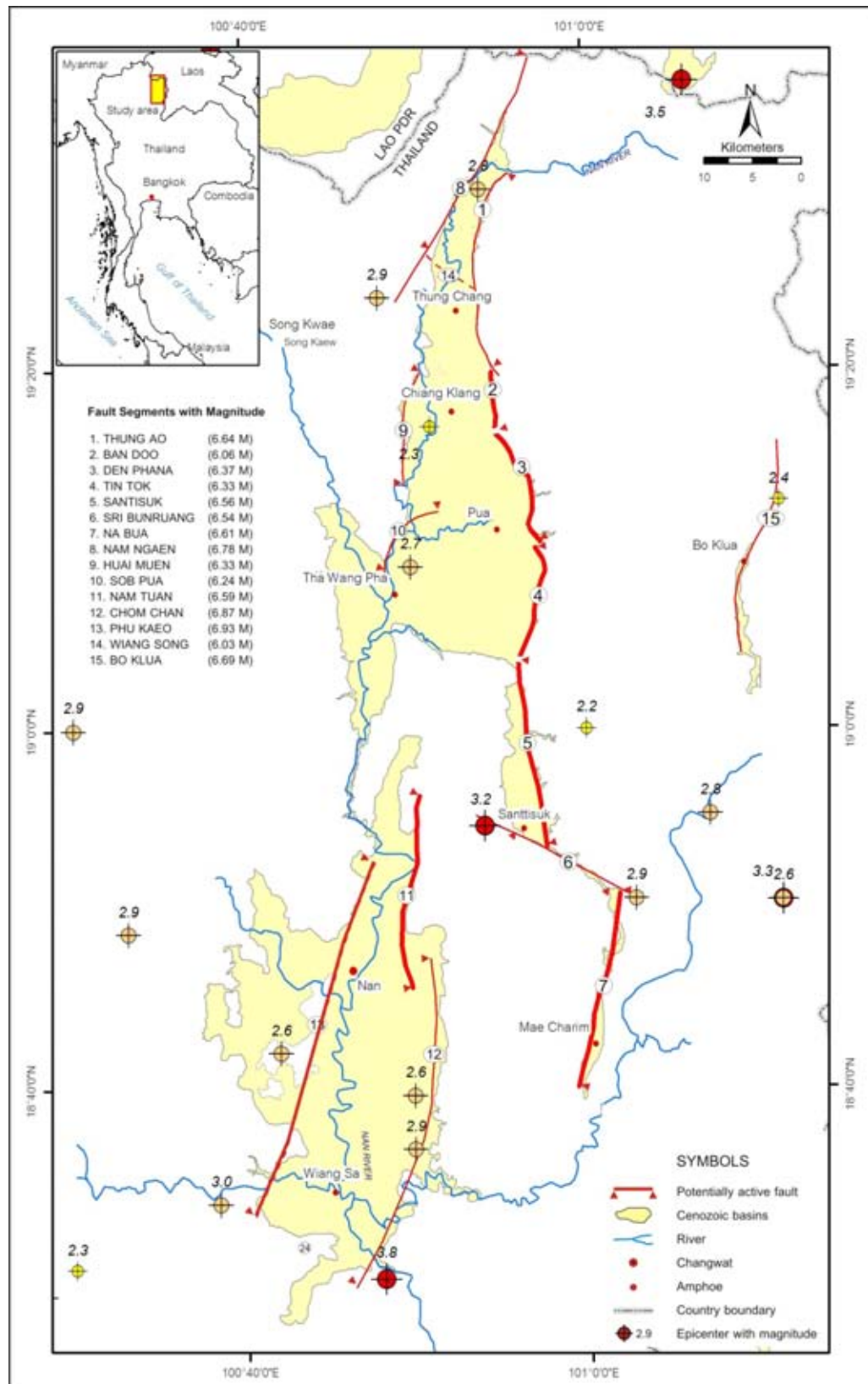


Figure 6.11 Simplify map of Pua Fault zone showing faults are never generated earthquake (thick red lines). Note that the epicentral distribution from 1983 to 2008 (Data from Nutalaya et al., 1985; Thai Meteorological Department, 2002; and http://neic.usgs.gov/neis/epic/epic_global.html, 2008).

CHAPTER VII

CONCLUSIONS

Based on the results of remote-sensing interpretation (Landsat 7 TM, SRTM, ASTER, IKONOS, and aerial photograph) integrated with ground-truth investigation, detailed topographic survey as well as those of TL-dating of fault-related sediments, and neotectonics of the Pau Fault Zone in Changwat Nan, northern Thailand, the conclusions can be drawn as the followings;

1) Pau Fault Zone is the north to north-northwest striking which the longest fault line is Pua Fault, 111 km-long. Fault zone is extending from northern most of Pua basin near Thai-Lao border to southern of Nan basin

2) Most fault traces of the Pau Fault Zone are oriented in north-northwest direction. The fault zone can be divided, based on discontinuity criteria, from north to south in to fourteen fault segments, viz, Thung Ao (22 km), Ban Doo (9), Den Phana (13 km), Tin Tok (12 km), Santisuk (19 km), Sri Bunruang (17 km), Na Bua (21 km), Nam Ngaen (29 km), Huai Muen (12 km), Sob Pua (10 km), Nam Tuan (20 km), Chom Chan (35 km), Phu Kaeo (39 km), and Wiang Song (6 km).

3) Significant and well-defined types of morphotectonic evidences are triangular facets, scarplet, wine-glass canyons, offset streams, shutter ridges, and linear valleys. They are well recognized along the Pua FaultZone, particularly where bed rock connects with the Cenozoic basins boundary.

4) Estimation from the surface rupture length of about 22 km, the Thung Ao segment indicates that an earthquake may have occurred in this area with the maximum magnitude of 6.64 M. If calculate moment magnitude using vertical displacement (1.2 m) would be about 6.67 M. The fault show the Normal-oblique sense of movement at present with the slip rate of this fault segment is about 0.3 mm/yr

5) The Ban Doo segment can be estimated from the surface rupture length of about 7 km. An earthquake may have occurred in Ban Doo area with the maximum magnitude of 6.3 M. If calculate moment magnitude using vertical displacement (1.75 m) would be about 6.79 M. The fault show the Normal-oblique

sense of movement at present with the slip rate of this fault segment is about 0.28 mm/yr

6) Ban Wiang Song area is part of Wiang Song segment. Estimation from the surface rupture length of about 6 km, the Wiang Song segment indicates that an earthquake may have occurred in this area with the maximum magnitude of 6.03 M.

7) Four major earthquakes with the paleoearthquake of about 6-7 M and they occurred of about more than 70,000, 5,000, 2,000 and 180 years ago which the recurrence interval is rounded 1,500 to 2,000 years.

8) Based on classification of active fault as proposed by Charusiri et al., (2001). The Pua fault zone are classified as active following the definition. Additional data of historical and instrumentally earthquake records in Nan and adjacent area also indicated that this area is tectonically active.

REFERENCES

- Academic Center of Khun Ngang School Group. 2003. History of Prathat Din Wai, Wat Sala, Tambol Chedichai, Amphoe Pua, Changwat Nan. Report Submitted to Wat Sala, Tambol Chedichai, Amphoe Pua, Changwat Nan: 12pp (in Thai).
- Aitken, A. J. 1985. Thermoluminescence Dating. New York: Academic Press: 351pp.
- Aki, K. 1984. Asperities of Barrier on an Earthquake Fault and Strong Motion Prediction. Jour. Geophys. Res., 98: 5681-5698.
- Albee, A. L. and Smith, J. L. 1966. Earthquake Characteristics and Fault Activity in Southern California. Engineering Geology in Southern California. Association of Engineering Geologists. Glendale, California. Los Angeles Section Special Publication: 9-34.
- Alderson, A. Holmes, N.A. and Murphy, C. 1994. A summary of the biostratigraphy and biofacies for the Tertiary sequence, Gulf of Thailand, in Proceedings of the International Symposium on Stratigraphic Correlation of Southeast Asia, International Geological Correlation Project 306: 292-295
- Allen, C. R. 1986. Seismological and Paleoseismological Techniques of Research in Active Tectonics. In: Wallace, R. E. ed. In: Active Tectonics: Studies in Geophysics. Natl. Acad. Press. Washington, DC: 148-154.
- Allen, C. R. Armand, F. Richter, C. F. and Nordquist, J. M. 1965. Relationship between Seismicity and Geologic Structure in the Southern California Region. Bulletin of the Seismological Society of America; 55, 4: 753-797.
- Allen, C. R. Gillespie, A. R. Huan, H. Sieh, K. E. Buchanan, Z. and Chengnan, Z. 1984. Red River and associated faults, Yunnan Province, China: Quaternary geology, slip rates, and seismic hazard, Geol. Soc. Am. Bull., 95: 686-700.
- Barr, S. M. and Macdonal, A. S., 1979, Paleomagnetism age and geochemistry of the Denchai basalts, Northern Thailand, Earth Planet Science Letters, 46: 113-124.
- Bell, W. T. 1979. Thermoluminescence dating. Radiation dose-rate data. Archaeometry, 21: 243-245.
- Biddle, K. T. and Christie-Blick, N. 1985. Glossary-Strike-Slip Deformation, Basin Formation, and Sedimentation. In: Biddle, K. T., and Christie-Blick, N. eds. Strike-Slip Deformation, Basin Formation and Sedimentation. Spec. Pub. Soc. Econ. Paleont. Miner. Tulsa, 37: 375-385.
- Bott, J. Wong, I. Prachuab, S. Wechbunthung, B. Hinthong, C. and S. Sarapirome. 1997. Contemporary seismicity in Northern Thailand and its tectonic implications, in

Proceedings of the International Conference on Stratigraphy and Tectonic Evolution of Southeast Asia and the South Pacific, Bangkok, Thailand: 453-464.

- Bunopas, S., 1981, Paleogeographic history of Western Thailand and adjacent parts of Southeast Asia - A plate tectonics interpretation, Ph.D. thesis, Victoria University of Wellington, New Zealand., 810 p.; reprinted 1982 as Geological Survey Paper no.5, Geological Survey Division, Department of Mineral Resources, Thailand.
- Capetta, H., Buffetaut, E. and Suteethorn, V., 1990, A new hypodont shark from the Lower Cretaceous of Thailand, Neues Jahrbuch for Geologie und Paleontologie, Monatshefte, 11: 659-666.
- Carver, G. A. and McCalpin, J. P. 1996. Paleoseismology of Compression Tectonic Environment. In: McCalpin, J. P. ed. Paleoseismology, New York: Academic Press: 183-270.
- Chaodumrong, P. 1992, Stratigraphy, Sedimentology and Tectonic Setting of the Lampang Group, Central North Thailand, unpublished Ph.D. thesis, University of Tasmania: 230 p.
- Charusiri, P. Daorerk, V. and Supajanya, T. 1996. Applications of Remote-Sensing Techniques to Geological Structures Related to Earthquakes and Earthquake-Prone Areas in Thailand and Neighbouring Areas. A Preliminary Study. Journal of Scientific Research. Chulalongkorn University, 21, 1: 14-38.
- Charusiri, P. Daorerk, V. Kosuwan, K. Choowong, M. 2004. Active Fault and Determination of Seismic Parameters Hutgyi Hydropower Project. Department of Geology, Faculty of Science, Chulalongkorn University submitted to Electricity Generating Authority of Thailand: 93pp.
- Charusiri, P. Kosuwan, S. Fenton, C. H. Tahashima, T. Won-in, K. and Udchachon, M. 2001. Thailand Active Fault Zones and Earthquake Analysis: A Preliminary Synthesis. Jour. Asia Earth Sci. (submitted for publication).
- Charusiri, P. Takashima, I. Kosuwan, S. Won-in, Saithong, P. Saensrichan, W Khaowiset, K. Pailoplee, S. and Meetuwong, R. 2006. The Study of Mae Yom Active Fault, Keang Sua Ten, Amphoe Song, Changwat Phare. Department of Geology, Faculty of Science, Chulalongkorn University submitted to Department of Royal Irrigation. Ministry of Natural Resources and Environment. Bangkok: 174pp.
- Charusiri, P., Kosuwan, K., Daorerk, V., Vajbunthoeng, B., and Khutaranon, S. 2000. Final Report on Earthquake in Thailand and Southeast Asia. Final Report Submitted to The Thailand Research Fund (TRF.): 171pp (in Thai).

- Charusiri, P., Kosuwan, S., Imsamut, S. 1997. Tectonic Evolution of Thailand: From Bunopas (1981)'s to a new scenario. The International Conference on Stratigraphy and Tectonic Evolution of Southeast Asia and the South Pacific, Bangkok, Department of Mineral Resources, August 19-24: 436-452.
- Christie-Blick, N. and Biddle, K. T. 1985. Deformation and Basin Deformation along Strike-Slip Fault. In: Biddle, K. T., and Christie-Blick, N. eds. Strike-Slip Deformation, Basin Formation, and Sedimentation, Society of Economic Paleontologists and Mineralogists, Spec. Pub. 37: 1-34.
- Cluff, L. S. and Bolt, B. A. 1969. Risk from Earthquake in the Modern Urban Environment with Special Emphasis on the San Francisco Bay Area, Urban Environmental Geology in the San Francisco Bay Region. In Association Engineering Geologist Sacramento, California: San Francisco Section Special Public: 25-64.
- Daly, M. C. Cooper, M. A. Wilson, I. Smith, D. G. and Hooper, B. G. D. 1991. Cenozoic Plate Tectonics and Basin Evolution in Indonesia. Marine and Petroleum Geology. 8: 2-21.
- Daly, M. C. Cooper, M. A. Wilson, I. Smith, D. G. and Hooper, B. G. D. 1991. Cenozoic Plate Tectonics and Basin Evolution in Indonesia. Marine and Petroleum Geology. 8: 2-21.
- Department of Highways. Highway Map of Thailand. Information Technology Division. Available from <http://map-project.doh.go.th/ZoomRaster.asp?Region=3&Zoom=1> (2007, January 10).
- Department of Mineral Resources. 1999. Geologic Map of Thailand 1: 1,000,000. Department of Mineral Resources. Bangkok (with English explanation).
- Dewey, J. F. Cande, S. and Pitman, W. 1989. Tectonic Evolution of the India/Eurasia Collision Zone. Eclogae Geologica Helvetica, 82: 717-734.
- Fenton, C. H. Charusiri, P. and Wood, S. H. 2003. Recent Paleoseismic Investigations in Northern and Western Thailand, Annals of Geophysics: 957-981.
- Fenton, C. H. Charusiri, P. Hinthong, C. Lumjuan, A. and Mangkonkarn, B. 1997. Late Quaternary faulting in northern Thailand. In: Proceedings of the International Conference on Stratigraphy and Tectonic Evolution of Southeast Asia and the South Pacific, Bangkok, Department of Mineral Resources, August: 436-452.
- Gutenberg, B. and Richter, C. F., 1954, Seismic of the Earth and Associated Phenimena. Priceton University Press, New Jersey.

- Hall, R. 1996. Reconstructing Cenozoic SE Asia. In: Hall, R. and Blundell, D. eds., Tectonic Evolution of Southeast Asia. Geological Society of London Special Publication 106: 153-184.
- Hamblin, W.K. 1976. Patterns of displacement along the Wasatch Fault, *Geology*, 4: 619-622.
- Hinthong, C. 1991. Role of tectonic setting in earthquake event in Thailand. In ASEAM-EC Workshop on Geology and Geophysics. Jakarta, Indonesia: 1-37.
- Hinthong, C. 1995. The Study of Active Faults in Thailand. In: Proceedings of the Technical Conference on the Progression and Vision of Mineral Resources Development, Department of Mineral Resources, Bangkok: 129-140.
- Hinthong, C. 1997. The Study of Active Faults in Thailand. Report of EANHMP. An Approach to Natural Hazards in the Eastern Asia: 17-22.
- Hobbs, W. H. 1972. Earth Features and Their Meaning. New York: Macmillan: 506pp.
- Hoke, L. and Campbell, H. J. 1995. Active mantle melting beneath Thailand?. in Proceedings of the International Conference on Geology, Geotechnology, and Mineral Resources of Indochina, Department of Geotechnology, Khon Kaen University, Khon Kaen: 13-22.
- Hongjatsee, U. 1999. Major fault and seismic hazard in northern, Thailand. Master's Thesis. Department of Geology, Faculty of Science, Chiang Mai University: 128pp.
- Huchon, P. LePichon, X. and Rangin, C. 1994. Indochina Peninsula and the collision of India and Eurasia. *Geology*, 22: 27-30.
- International Atomic Energy Agency. 1988. Code on the Safety of Nuclear Power Plants: Siting, Code 50-C-S. IAEA. Vienna.
- International Atomic Energy Agency. 1992. Code on the Safety of Nuclear Research Reactors: Design, Safety Series 35-S1. IAEA. Vienna.
- Keller, E. A. and Pinter, N. 1996. Active tectonics: Earthquake, uplift, and landscape, New Jersey: Prentice-Hall, 338pp.
- Khaowiset, K., Charusiri, C., Chutakositkanon, V. and Takashima, I. 2007. Batdabong Fold Complex in Khlong Had area, Sa Kaeo, Eastern Thailand: Evidence from Remote Sensing and Structural Analyses. Journal of Remote Sensing and GIS Association of Thailand. 8. 1: 14-30.
- Knuepfer, P. L. K. 1989. Implications of the Characteristics of End-Points of Historical Surface Fault Ruptures for the Nature of Fault Segmentation. In: Schwartz, D. P. and Sibson, R. H. eds., Fault Segmentation and Controls of Rupture Initiation and Termination, U.S. Geological Surv. Open File Rep.89-315: 193-228.

- Kosuwan, S. Saithong, P. Lumjuan. A. Takashima, I. and Charusiri, P. 1999. Preliminary Results of Studies on the Mae Ai Segment of the Mae Chan Fault Zone, Chiang Mai Northern Thailand. The CCOP Meeting on Exodynamic Geohazards in East and Southeast Asia. July 14-16, Pattaya, CCOP: 1-8.
- Lacassin, R. Maluski. P. Leloup, P. H. Tapponnier, P. Hinthong, C. Siribhakdi, K. Chuavithit, S. and Charoenpravat, S. 1997. Tertiary Diachronic Extrusion and Deformation of western Indochina: Structural and $^{40}\text{Ar}/^{39}\text{Ar}$ evidence from NW Thailand. Journal of Geophysical Research, 102: 10013-10037.
- Lee, T. Y. and Lawver, L. A. 1995. Cenozoic plate reconstructions of Southeast Asia. Tectonophysics, 251: 85–138.
- Lorenzetti, E.A. Brennan, P.A. and Hook, S.C. 1994. Structural styles in rift basins: interpretation methodology and examples from Southeast Asia, Bull. Am. Assoc. Pet. Geol., 78, 1,152.
- MaCalpin, J. P. 1996. Paleoseismology, California. Academic press, 588pp.
- Macdonald, A.S., Barr, S.M. Dunning, G.R. and Yaowanoyothin, W. 1993. The Doi Inthanon metamorphic core complex in NW Thailand: age and tectonic significance, J. Southeast Asian Earth Sci., 8 (1-4), 117-125.
- Matthews, S. J. Fraser, A. J. Lowe, S. Todd, S. P. and Peel, F. J. 1997. Structure, Stratigraphy and Petroleum Geology of the SE Nam Con Son Basin, Offshore Vietnam. In: Fraser, A. Matthews, S. Murphy, R. eds., Petroleum Geology of Southeast Asia. Geol. Soc. London, Spec. Publ., 126: 89–106.
- Mccabe, R. Celaya, M. Cole, J. Han, H.C. OHNSTAD, T. PAIJITPRAPAPON, V. and Thitipawarn, V. 1988. Extension tectonics: the Neogene opening of the north-south trending basins of Central Thailand, J. Geophys. Res., 93, 11,899-11,910.
- Mccabe, R. Harder, S. Cole, J.T. and Lumadyo, E. 1993. The use of paleomagnetic studies in understanding the complex Tertiary tectonic history of east and southeast Asia, J. Southeast Asian Earth Sci., 8 (1-4), 257-268.
- Meesook, A., 2000, Cretaceous environments of Northeastern Thailand, in H. Okada and N.J. Mateer, eds. Cretaceous environment of Asia, Elsevier Science B.V.: 207-223
- Molnar, P. and Deng, Q. 1984. Faulting Associated with Large Earthquake and the Average Rate of Deformation in Central and Eastern Asia. Journal of Geophysical Research, 89: 6203-6227.
- Molnar, P. and Tapponnier, P. 1975. Cenozoic tectonics of Asia: effects of a continental collision. Science, 280: 419–426.

- Ni, J. and York, J. E. 1978. Late Cenozoic Tectonics of the Tibetan Plateau. J. Geophys. Res., 83: 5377-5384.
- Nutalaya, P. Sodsri, S. and Arnold, E. P. 1985. Series on Seismology-Volume II-Thailand. In: Arnold, E. P ed., Southeast Asia Association of Seismology and Earthquake Engineering: 402pp.
- O' Leary, D. W. and Simson, S. L. 1977. Remote Sensing Application to Tectonism and Seismicity in the Northern Part of the Mississippi Embayment. Geophysics, 42, 3: 542-548.
- O' Leary, D. W. Fridman, J. D. and Pohn, H. A. 1976. Lineament, Linear, Lination: Some Proposed New Standards for Old Terms. Bull. Geol.soc.Am, 87: 1463-1469.
- O'LEARY, J. and HILL, G. S. (1989): Tertiary basin development in the Southern Central Plains, Thailand, in Proceedings of the International Symposium on Intermontaine Basins: Geology and Resources, Chiang Mai University, Chiang Mai, Thailand: 254-264.
- Packham, G. 1996. Cenozoic SE Asia: reconstructing its aggregation and reorganization. In: Hall R., and Blundell, D. J. eds., Tectonic Evolution of Southeast Asia. Geol. Soc. London Spec. Publ, 106:123-152.
- Park, R. G. and Jaroszewski, W. 1994. Craton Tectonics, Stress and Seismicity. In: Hancock, P. L. ed., Continental Deformation. Oxford: Pergomon Press, 200-222.
- Peltzer, G. and Tapponnier, P. 1988. Formation and evolution of strike-slip faults, rifts, and basins during the India-Asia collision: an experimental approach, J. Geophys. Res., 93, 15,085-15,117.
- Phillip, H. Pogozhin, E. Cisternas, A. Bousquet, J. C. Borison, B. and Karakhanian, A. 1992. The Armenian Earthquake of 1988 December7; Faulting and Folding, Neotectonics and Paleoseismicity. Geophys. Jour. Int, 110: 141-158.
- Polachan, S. 1988. The Geological Evolution of the Mergui Basin, SE Andaman Sea, Thailand. PhD thesis. Royal Holloway and Bedford New College, Univesity of London: 218pp.
- Polachan, S. and Satayarak, N. 1989. Strike-Slip Tectonics and the Development of Tertiary Basins in Thailand. In: Proceedings of the International Symposium on Intermountain Basin, Geology and Resources, 30 Jan-2 Feb 1989, Chiang Mai, Thailand: 243-253.
- Polachan, S. Pradidtan, S. Tongtaow, C. Janmaha, S. Intrawijitr, K. and Sangsuwan, C. 1991. Development of Cenozoic basins in Thailand, Mar. Pet. Geol., 8: 84-97.

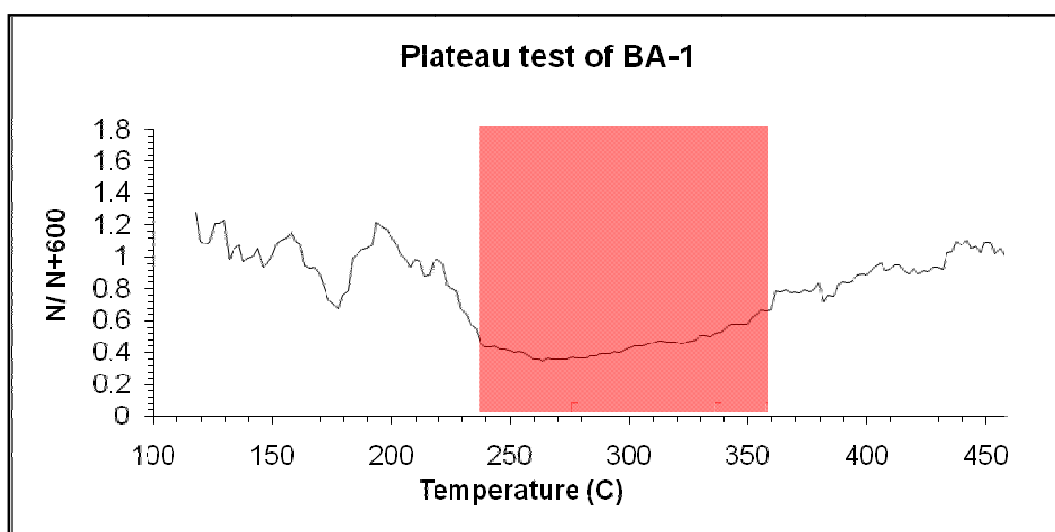
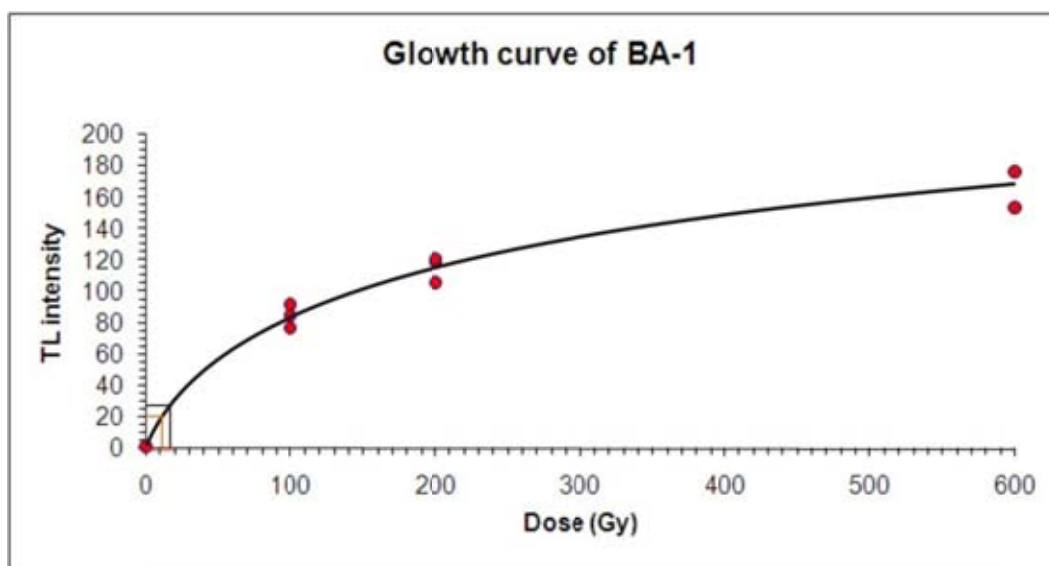
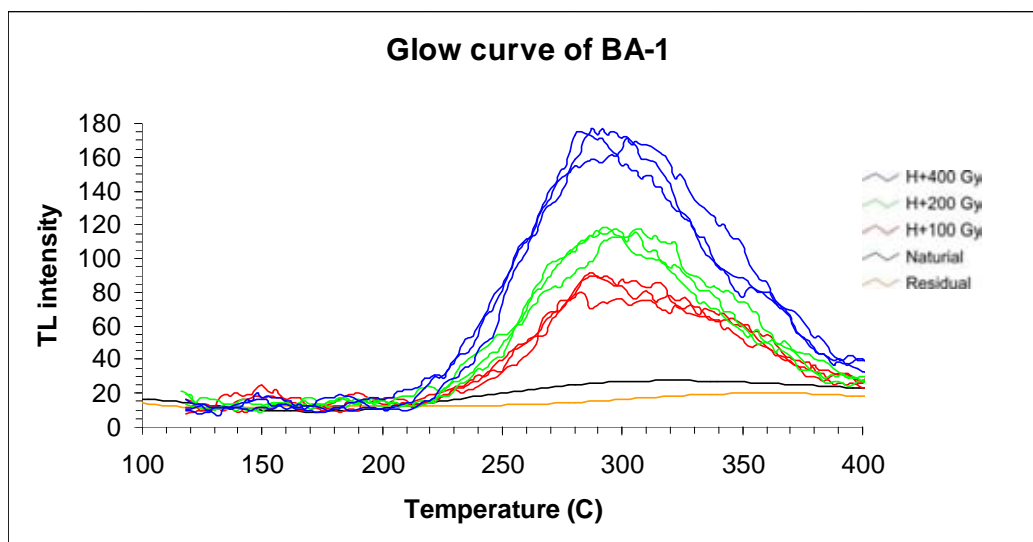
- Rangin, C. Jolivet, L. and Pubellier, M. 1990. A Simple Model for the Tectonic Evolution of Southeast Asia and Indonesia Region for the past 43 m.y. Bulletin de la Société géologique de France, 8 VI: 889-905.
- Remus, D. Webster, M. and Keawkan, K. 1993. Rift architecture and sedimentology of the Phetchabun intermontaine basin, Central Thailand, J. Southeast Asian Earth Sci., 8 (1-4): 421-432.
- Rhodes, B. P. Perez, R. Lamjuan, A. and Kosuwan, S. 2002. Kinematics of the Mae Kuang Fault, Northern Thailand Basin and Range Province. The Symposium on Geology of Thailand. August 2002, Bangkok Thailand: 298-308.
- Ricter, B. Fuller, M. Schmidtke, E. Myint, U.T. Ngwe, U.T. Win, U.M. and Bunopas, S. 1993. Paleomagnetic results from Thailand and Myanmar: implications for the interpretation of tectonic rotations in Southeast Asia, J. Southeast Asian Earth Sci., 8 (1-4): 247-255.
- Saithong, P. 2006. Characteristics of the Moei-Mae Ping Fault Zone, Changwat Tak, Northwestern, Thailand. Master's Thesis. Department of Geology, Faculty of Science, Chulalongkorn University: 218pp.
- Sattayarak, N., Polachan, S. and Charusirisawad, R., 1991, Cretaceous rock salt in the northeastern part of Thailand, the Seventh Regional Conference on Geology, Mineral and Energy Resources of Southeast Asia (GEOSEA VII), Bangkok, November 5-8, Geological Society of Thailand, Abstract Volume: 36pp.
- Schwartz, D. P. 1998. Geological Characterization of Seismic Sources: Moving into the 1990's. In J.L. von Thun (ed.), Earthquake Engineering & Soil Dynamics II Proceedings; 2, Recent Advances in Group Motion Evaluation. Spec. Publ. Am. Soc. Civil Engineers Geotech. 20: 1-42.
- Segall, D. and Pollard, D. D. 1980. Mechanics of Discontinuous Faults. J. Geophys. Res., 85: 4337-4350.
- Siribhakdi, K. 1986. Seismicity of Thailand and Periphery. Geological Survey Division, Department of Mineral Resources Bangkok. In: Panitan Lukleunaprasit et al. eds., Proceedings of the 1 st Workshop on Earthquake Engineering and Hazard Mitigation. Bangkok, November 1986, Chulalongkorn University: 151-158.
- Slemmons, D. B. 1982. Determination of Design Earthquake Magnitudes for Microzonation. 3rd International Earthquake Microzonation Conference Proceedings: 119-130.
- Smith, R.B. and Aabas, W.J. 1991. Seismicity of the Intermountain Seismic Belt, in Neotectonics of North America, Geological Society of America Decade Map, vol. 1: 185-228.

- Srisuwan, P. 2002. Structural and Sedimentological Evolution of the Phrae Basin, Northern, Thailand. PhD. thesis. Department of Geology, Royal Holloway, University of London: 502pp.
- Strandberg, C. H. 1967. Aerial Discovery Manual. New York: John Wiley & Son.
- Sylvester, A. G. 1988. Strike-Slip Faults. Geol. Soc. Am. Bull., 100: 1666-1703.
- Takashima, I. and Honda, S. 1989. Comparison between K-Ar and TL Dating Results of Pyroclastic Flow Deposits in the Aizutajima Area, Northeast Japan. Journal of Geological Society, 95: 807-816.
- Takashima, I. and Watanabe, K. 1994. Thermoluminescence Age Determination of Lava Flows/Domes and Collapsed Materials at Unzen Volcano, SW Japan. Bulletin of the Volcanological Society of Japan, 39: 1-12.
- Tanaka, K. Hataya, R. Spooner, N. A. Questiaux, D. G. Saito, Y. and Hashimoto, T. 1997. Dating of Marine Terrace Sediments by ESR, TL and OSL Methods and their Applicabilities. Quaternary Science Reviews, 16: 257-264.
- Tapponnier, P. Peltzer, G. and Armijo, R. 1986. On the Mechanics of Collision between India and Asia. In: Coward, M. P., and Ries, A. C. eds., Collision Tectonics. Journal of the Geological Society of London. Special Publication, 19: 115-157.
- Tapponnier, P. Peltzer, G. Armijo, R. Le Dain, A. and Coorbald, P. 1982. Propagating Extrusion Tectonics in Asia: New insights from simple experiments with plasticine. Geology, 10: 611-616.
- Thailand Meteorological Department. 2008. Earthquake Information Catalogue. Report of Thailand Meteorological Department. Bangkok (digital files and unpublished).
- Tulyatid, J. 1999. The Ancient Tethys in Thailand as Indicated by Nationwide Airborne Geophysical Data. In: Proceedings of the International Symposium on Shallow Tethys. February 1-5, 1999. Chiang Mai, Thailand: 335-351.
- U.S. Nuclear Regulatory Commission. 1982. Appendix A: Seismic and geologic siting criteria for nuclear power plants. Code of Fed. Regul. 10. Chap. 1, Part 100. 1 September, 1982: 549-559.
- Udachachon, M. Charusiri, P. Daorerk, V. Won-in, K. and Takashima, I. 2005. Paleoseismic Studies along the Southeastern portion of the Phrae Basin, Northern Thailand. In: Proceedings of the International Conference on Geology, Geotechnology and Mineral Resources of Indochina. November 28-30, 2005. Khon Kaen, Thailand: 511-516.

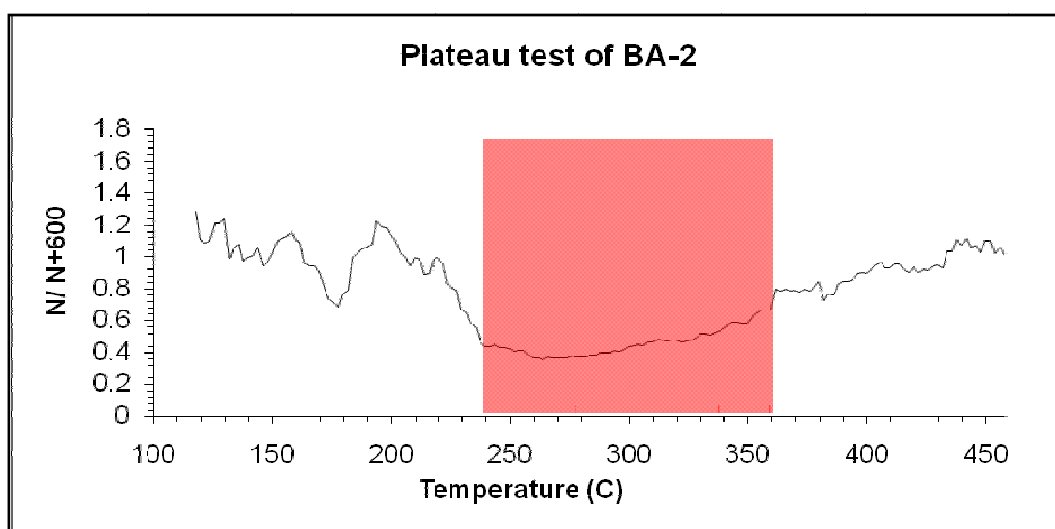
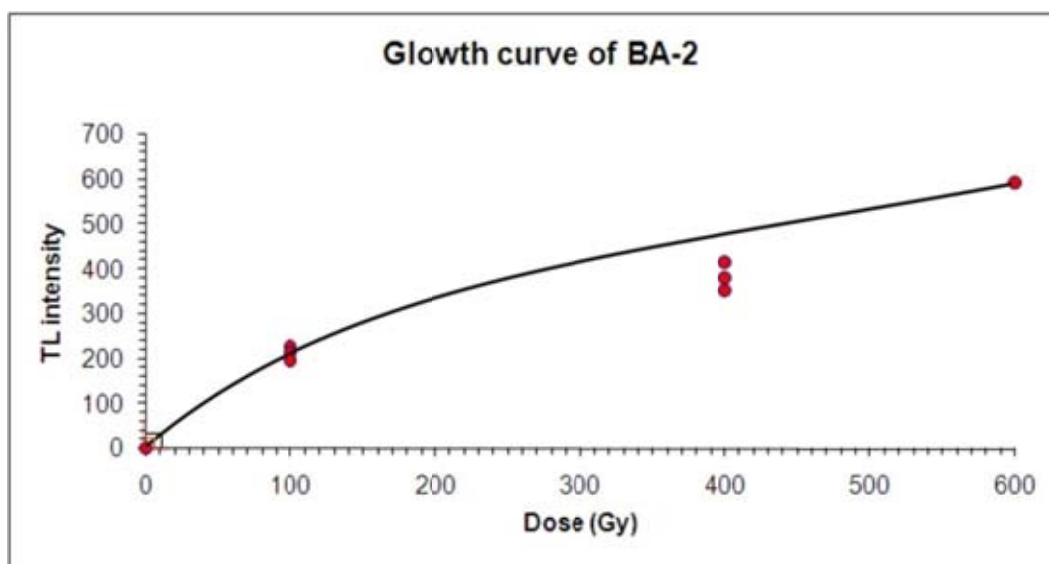
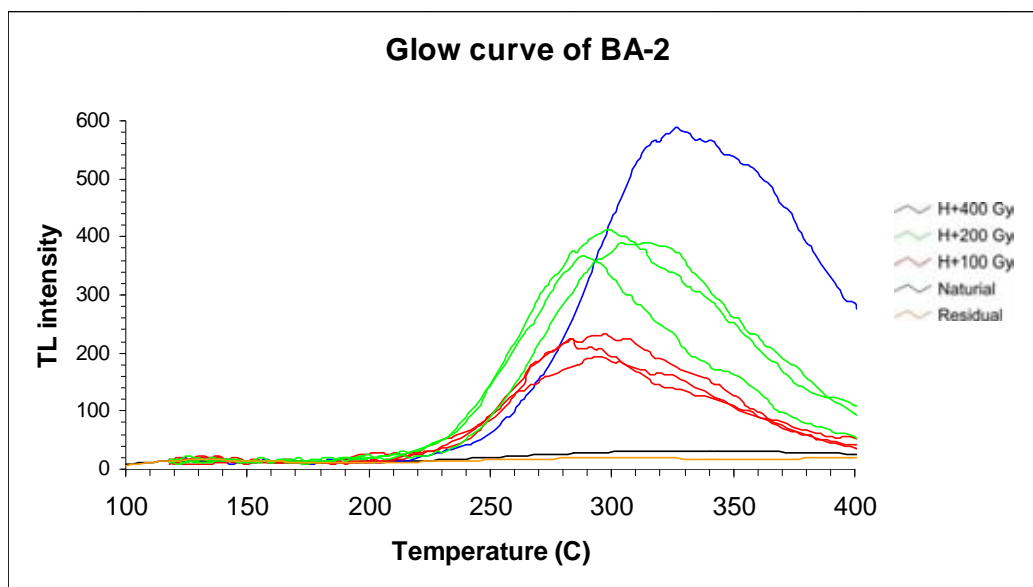
- Wallace, R. E. 1980. Active fault, Paleoseismology, and Earthquake Hazards. Proceedings of the Seventh World Conference on Earthquake Engineering. Istanbul, Turkey, 1: 115-122.
- Ward, D.E. and Bunnag, D., 1964, Stratigraphy of the Mesozoic Khorat Group in Northeast Thailand. Department of Mineral Resources, Bangkok, Report of Investigation, 6, 95 p.
- Weldon, R. J. McCalpin, J. P. and Rockwell, T. K. 1996. Paleoseismology of Strike-Slip Tectonic Environments. In: McCalpin, J. P. ed. Paleoseismology, New York: Acad. Press, 271-329.
- Wells, D. L. and Coppersmith, K. J. 1994. New Empirical Relationships among Magnitude, Rupture Width, Rupture Area, and Surface Displacement. In: Bulletin of the Seismological Society of America, 84: 974-1002.
- Western States Seismic Policy Council. 1997. Active Fault Definition for the Basin and Range Province. WSSPC Policy Recommendation 97-1 White Paper. May 22, 1997., San Francisco, CA: 3pp.
- Wheeler, R. L. 1989. Persistent Segment Boundaries on Basin-Range Normal Faults. In: Stewart D. P. and Sibson, R. H. eds., Fault Segmentation and Controls of Rupture Initiation and Termination. U.S. Geol. Surv., Open File Rep. 89-135: 432-444.
- Willis, B. 1923. A Fault Map of California. Bulletin of the Seismological Society of America, 13: 1-12.
- Wintle, A. G. and Huntley, D. J. 1980. Thermoluminescence Dating of Ocean Sediments. Canadian. Journal of Earth Sciences, 17: 348-360.
- Won-in, K. 1999. Neotectonic evidences along the Three Pagoda Fault Zone, Changwat Kanchanaburi. Master's Thesis. Department of Geology, Faculty of Science, Chulalongkorn University, 188pp.
- Won-in, K. 2003. Quaternary Geology of the Phrae Basin, Northern Thailand and Application of Thermoluminescence Technique for Quaternary Chronology. PhD. Thesis. Graduate School of Mining and Engineering, Akita University: 200pp.
- Wood, H. O. 1915. California Earthquake, A Synthetic Study of Recorded Shocks. Bulletin of the Seismological Society of America, 6: 54-196.
- Woodward Clyde Federal Services. 1996. Seismic hazards evaluation, Environmental Impact Assessment: Geological Aspect, Kaeng Sua Ten Dam Project Changwat Phrae. unpublished report prepared by GMT Corporation and other for the Department of Mineral Resources.

APPENDICES

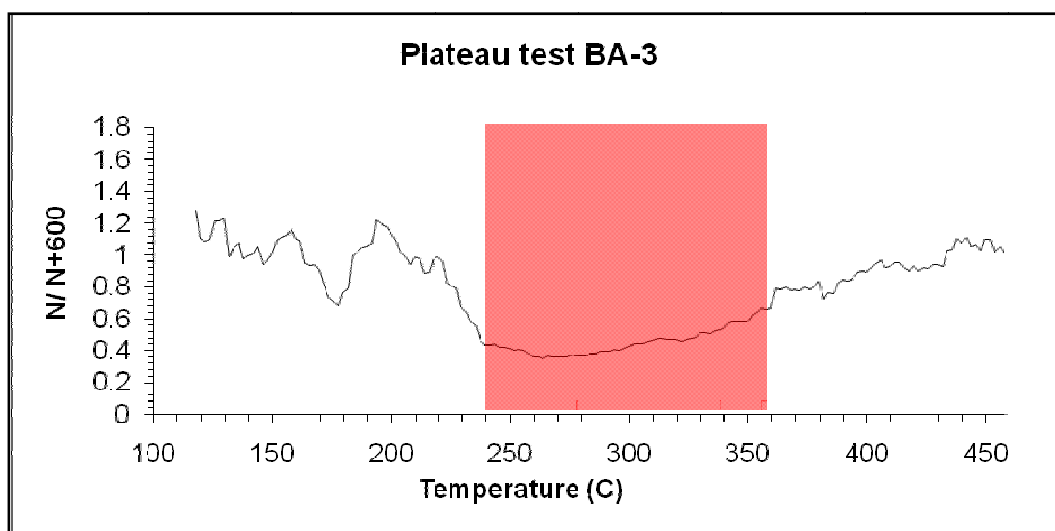
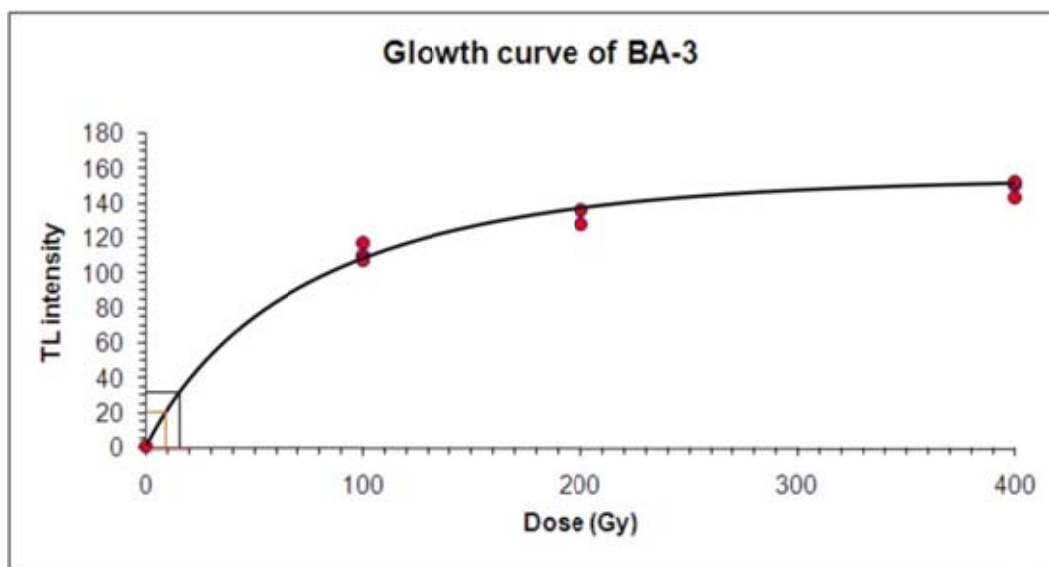
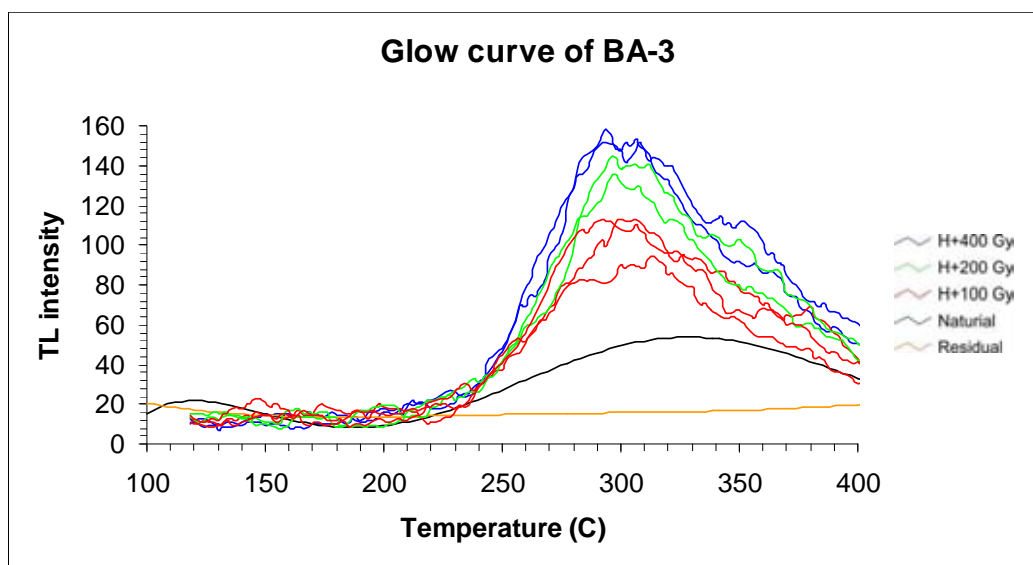
Sample No. BA - 1



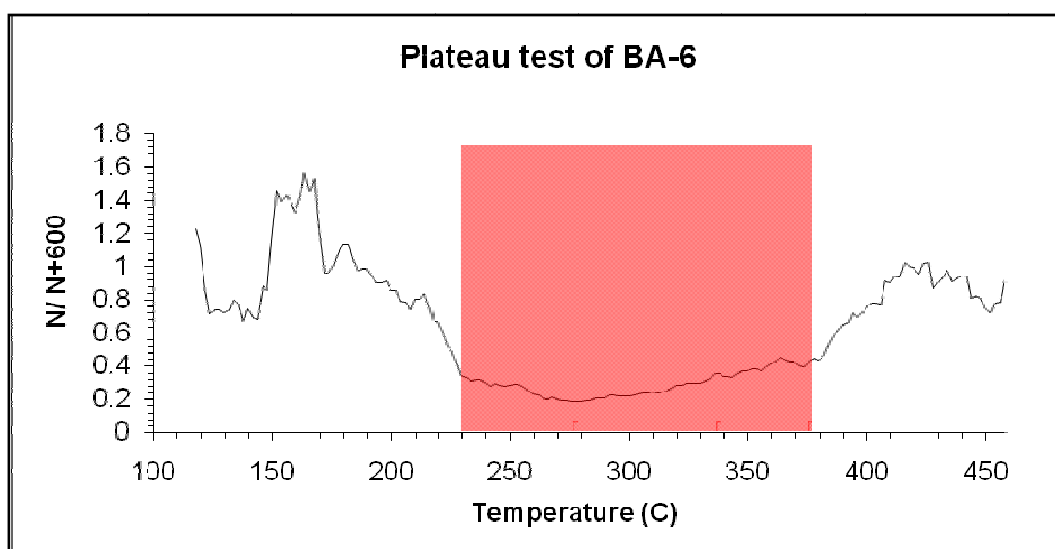
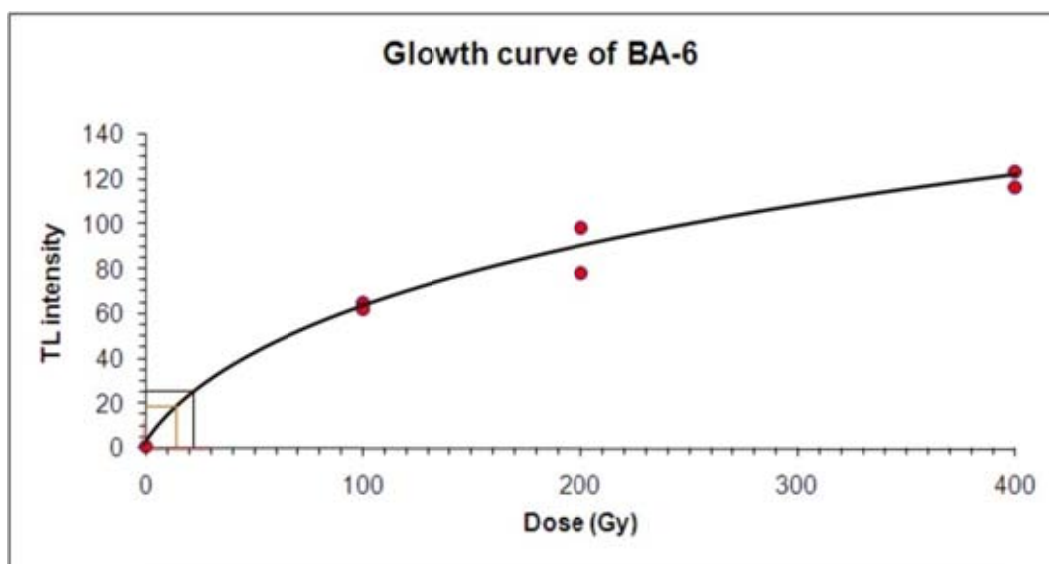
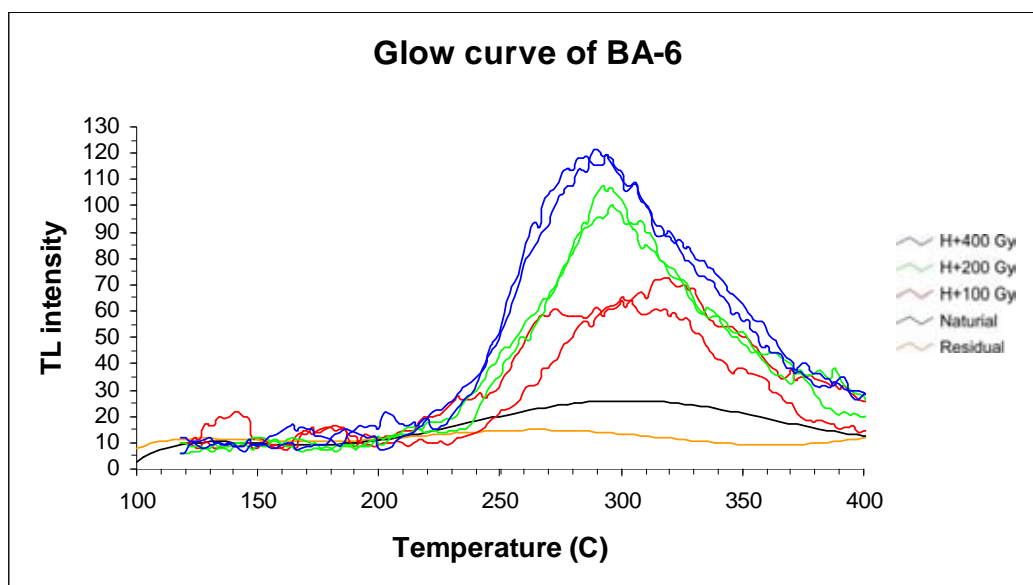
Sample No. BA – 2



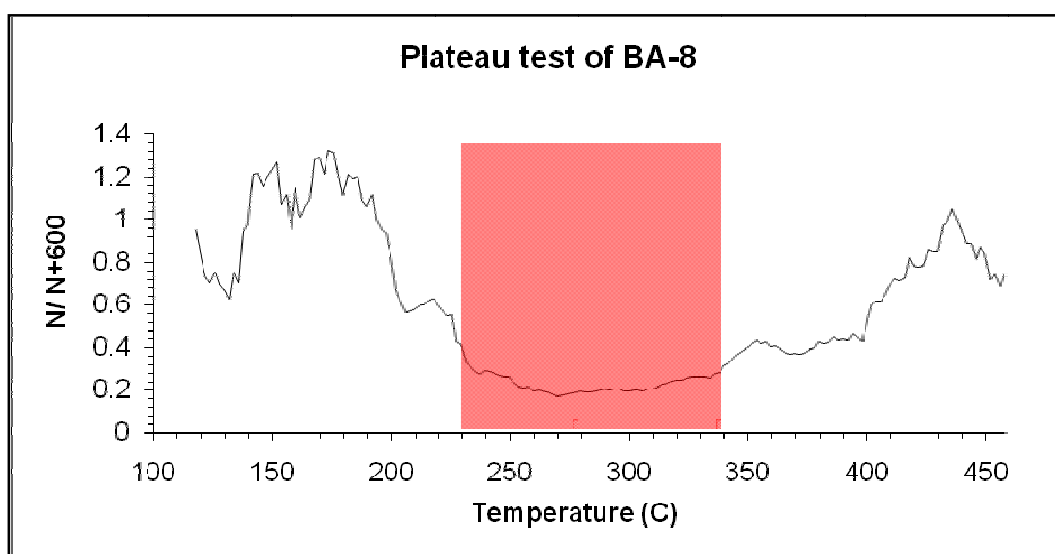
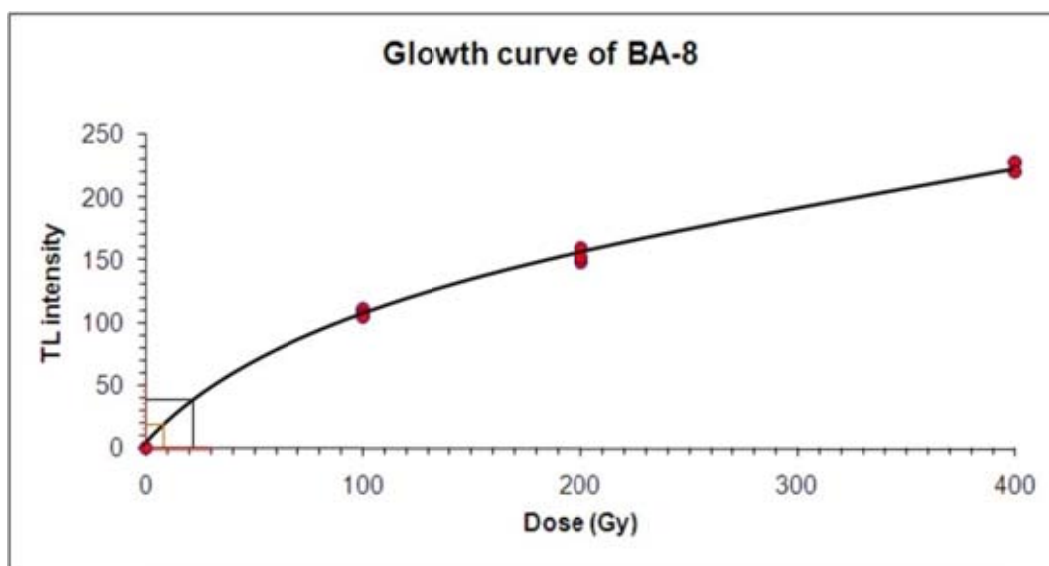
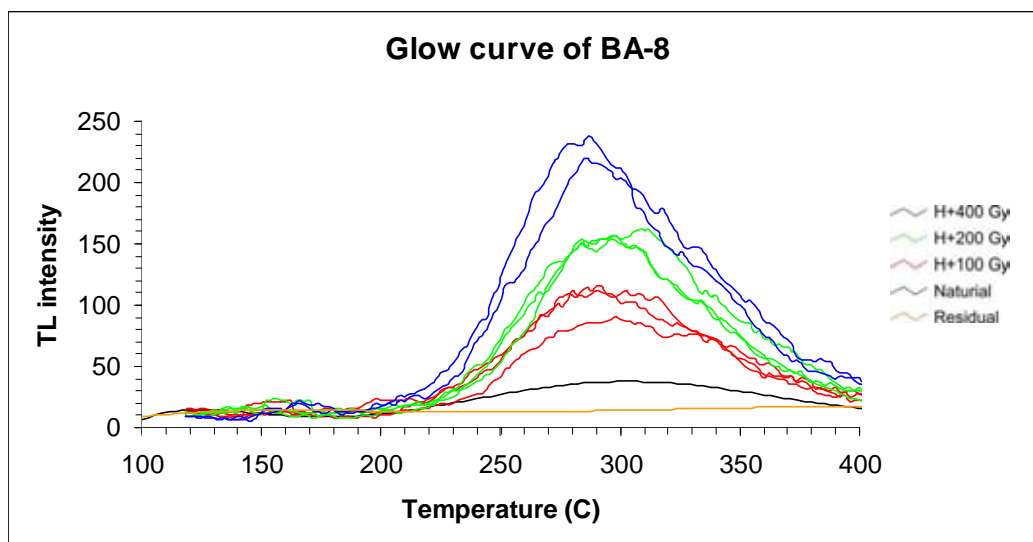
Sample No. BA - 3



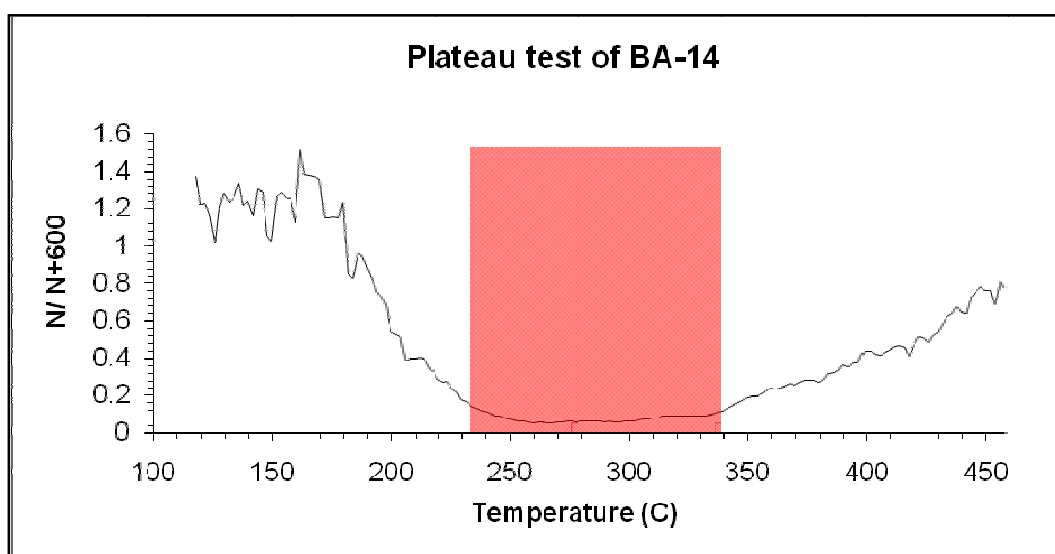
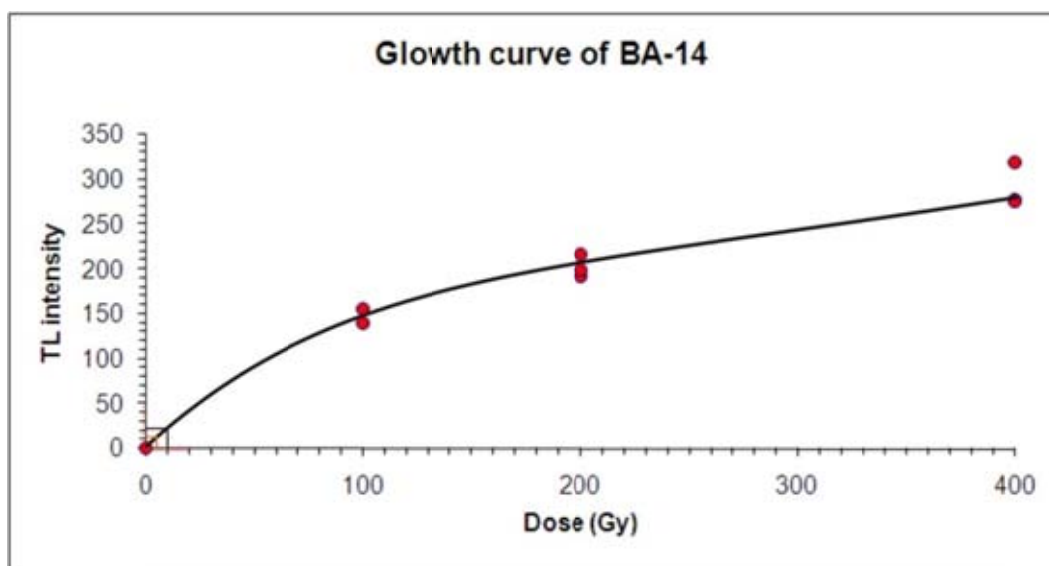
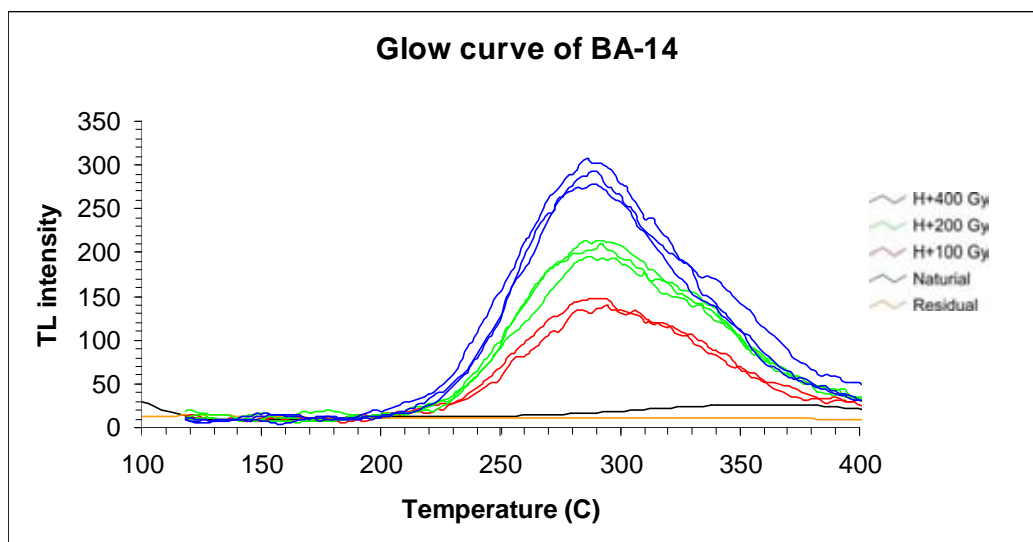
Sample No. BA – 6



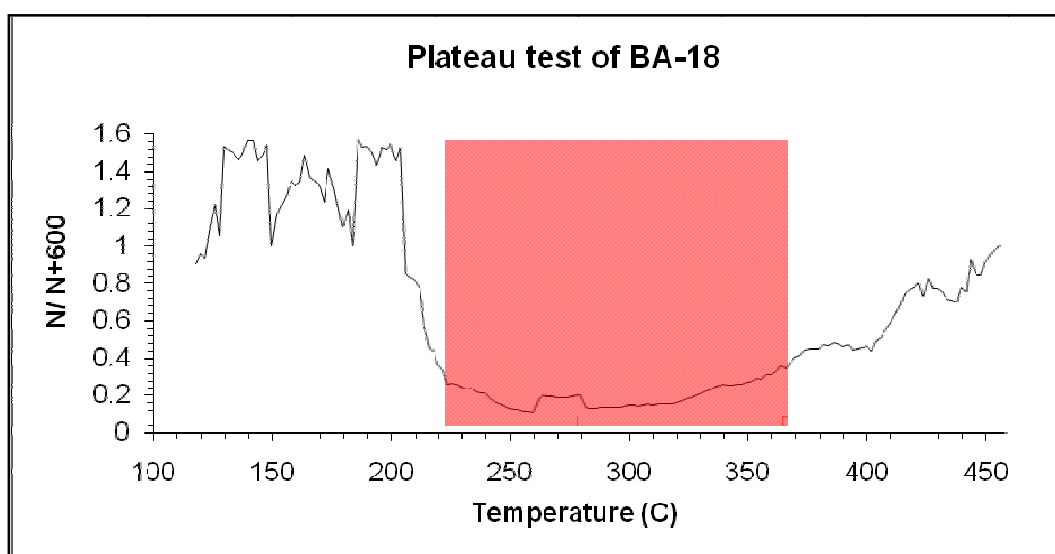
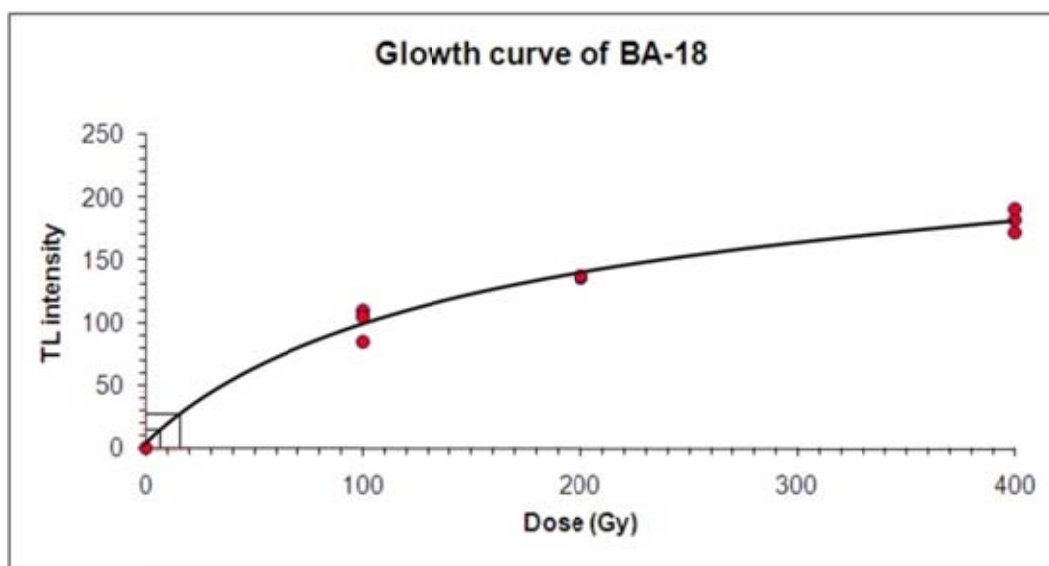
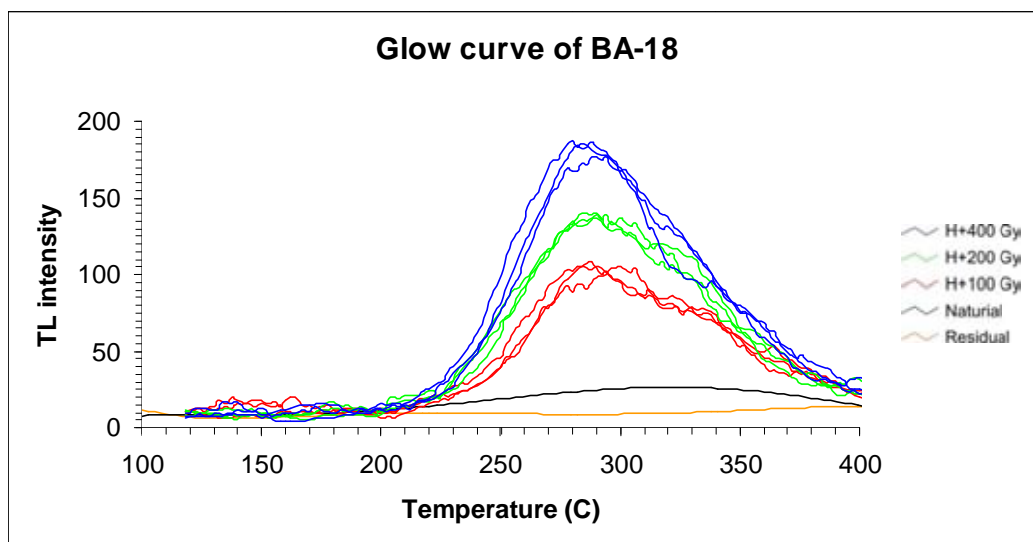
Sample No. BA – 8



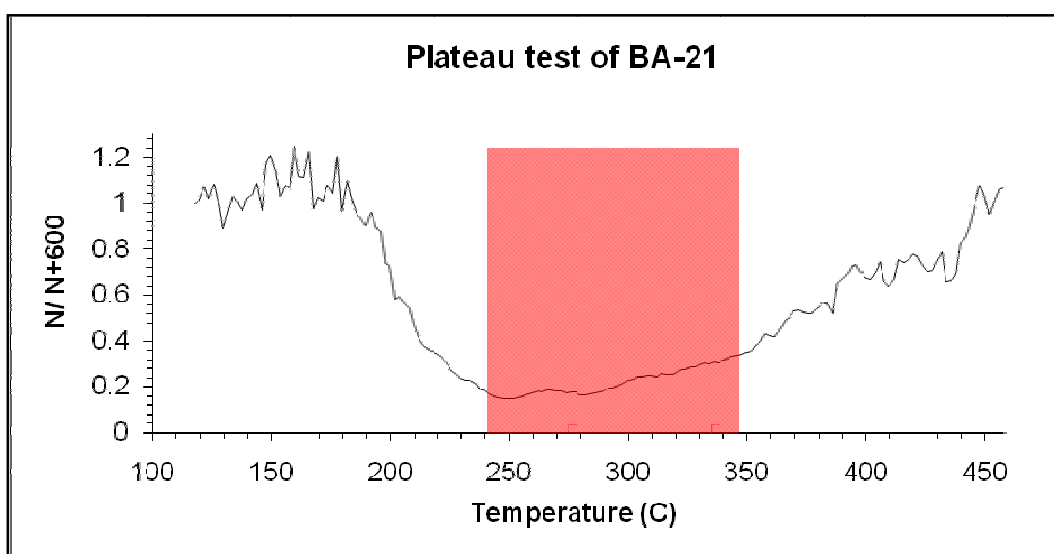
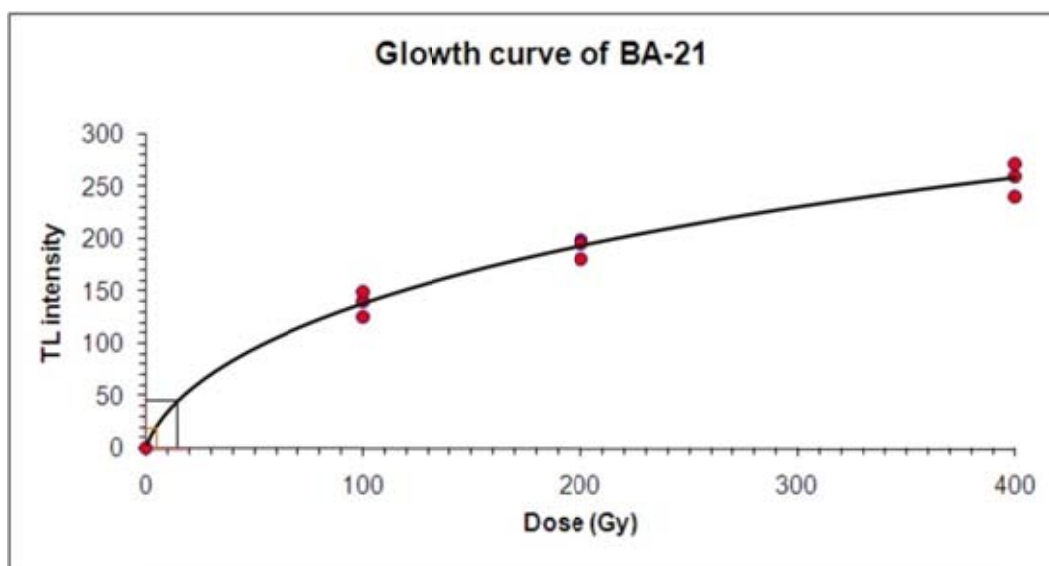
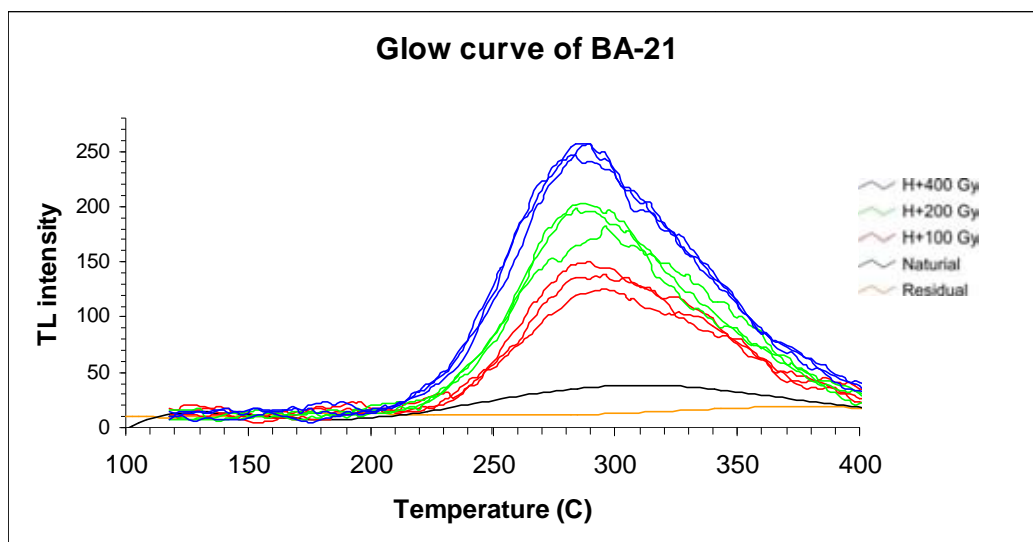
Sample No. BA-14



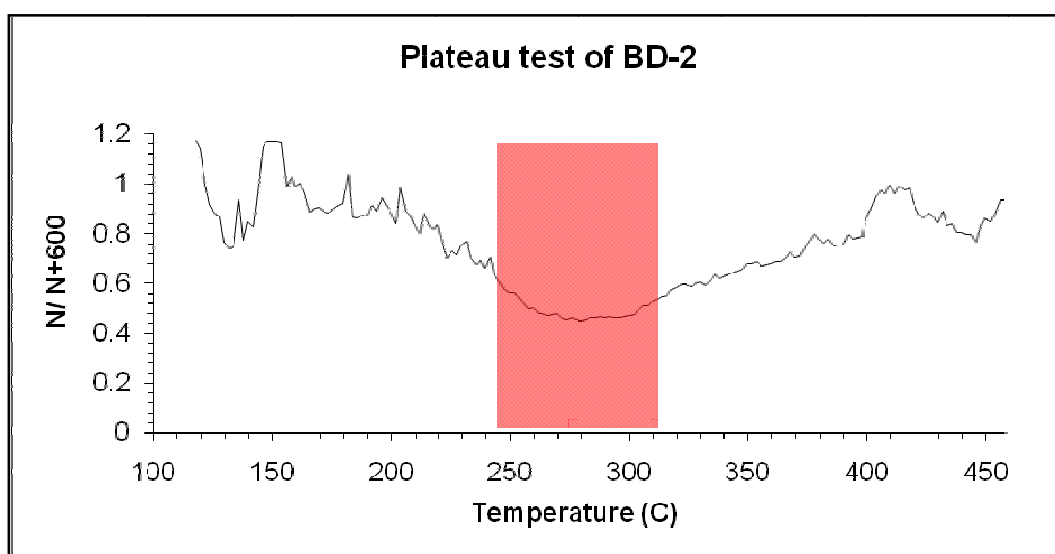
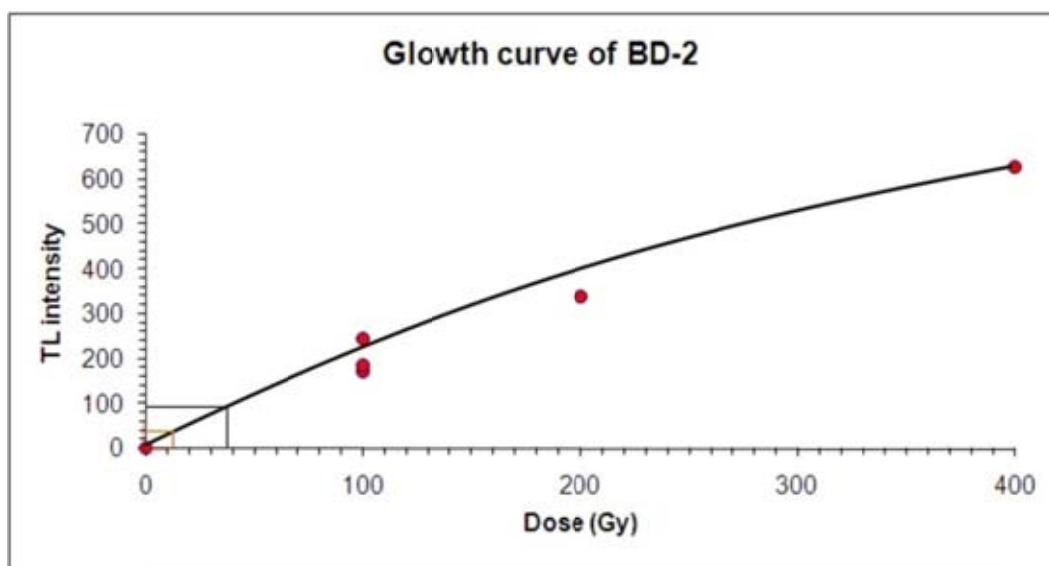
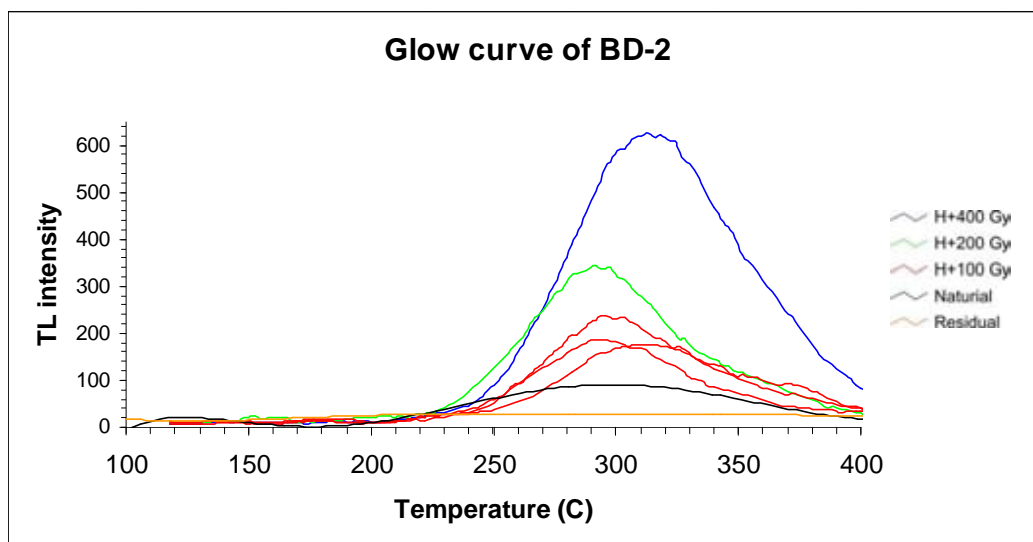
Sample No. BA-18



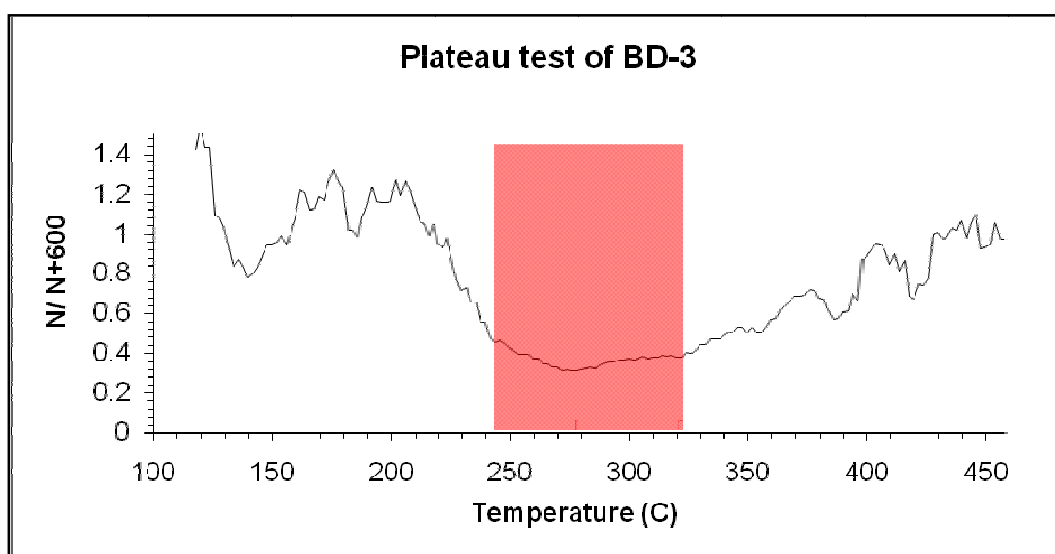
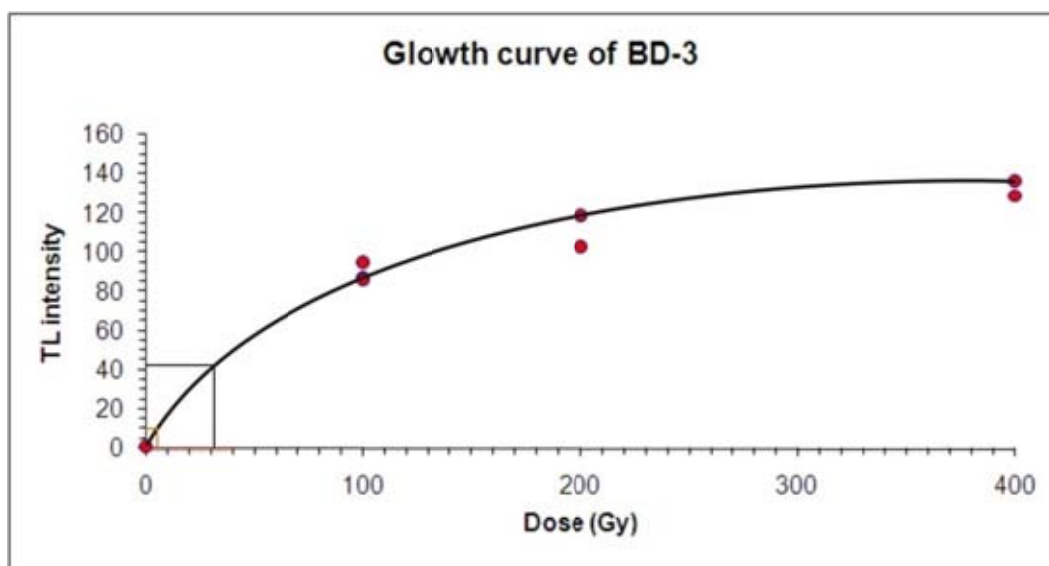
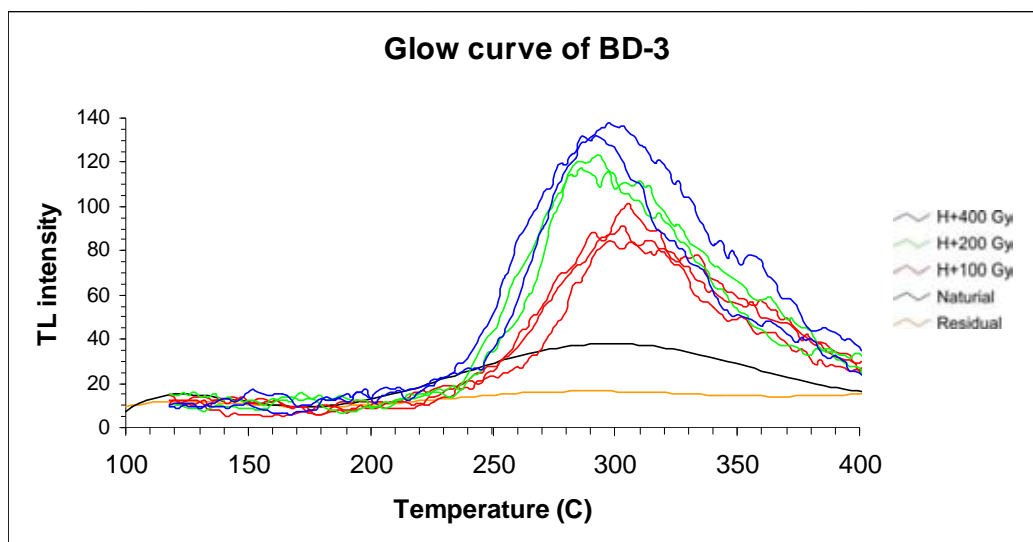
Sample No. BA-21



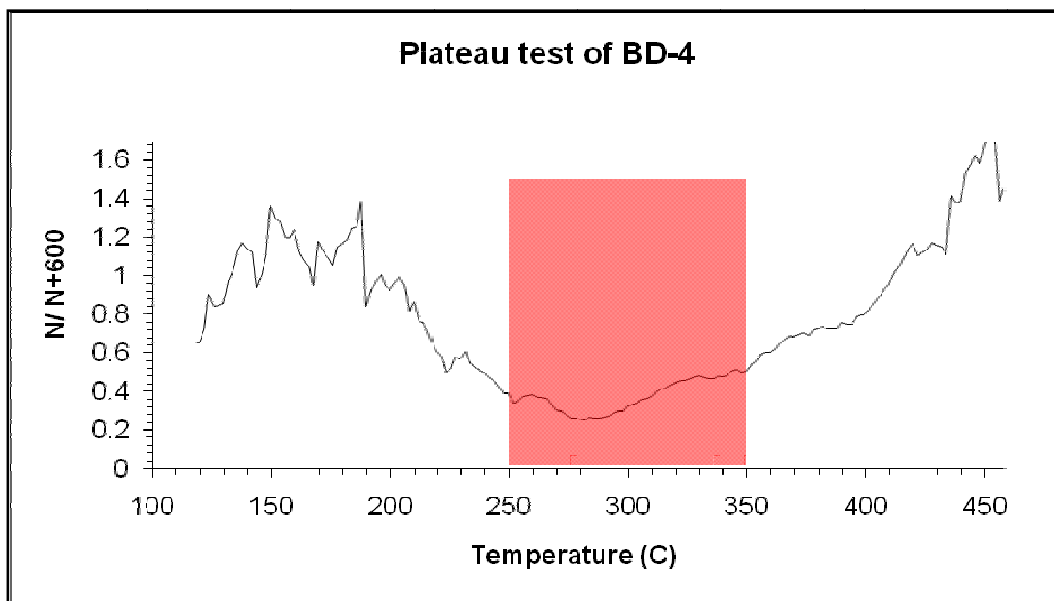
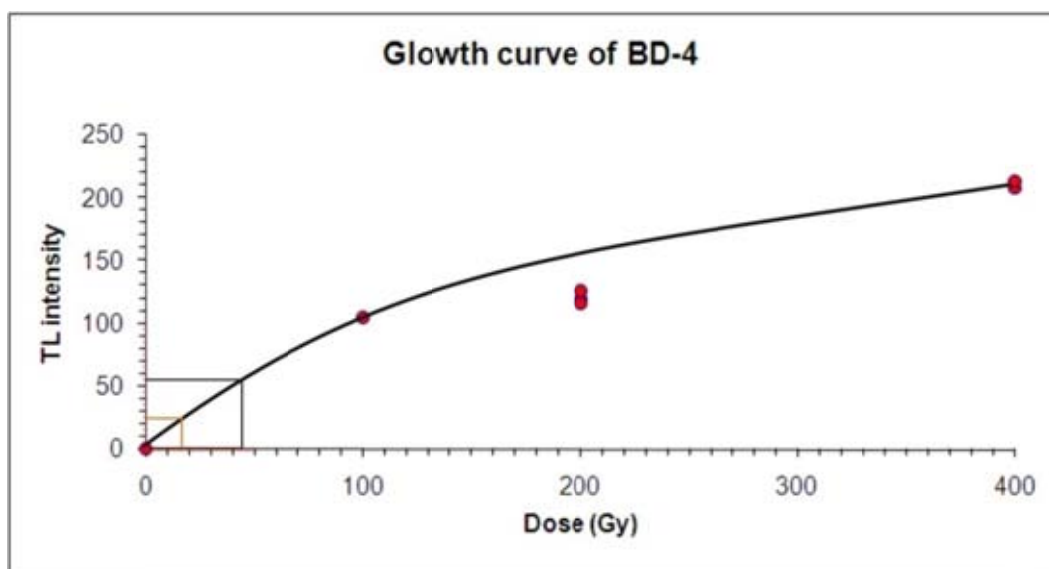
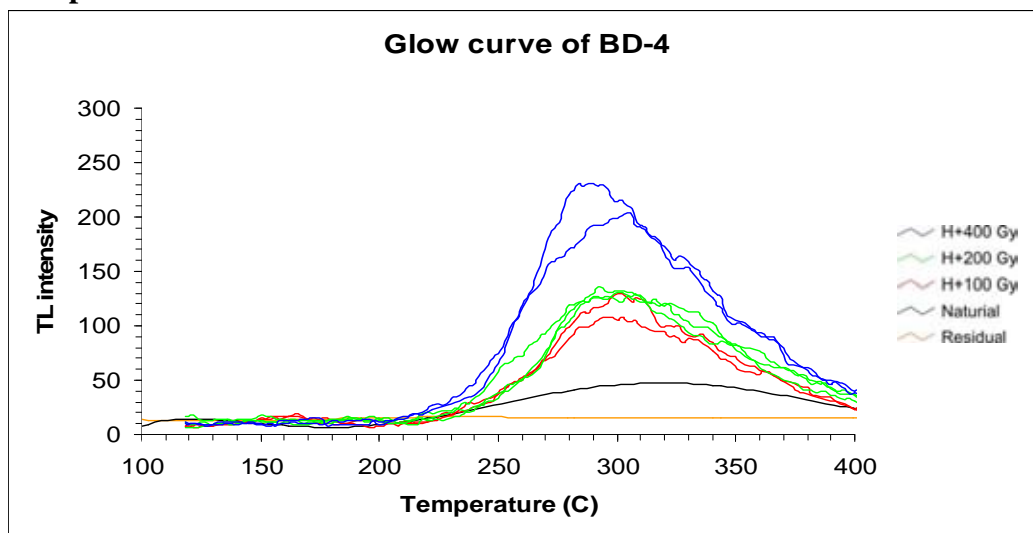
Sample No. BD – 2



Sample No. BD – 3



Sample No. BD - 4



BIOGRAPHY

Mr. Kitti Khaowiset was born on August 23, 1976 in Suphanburi, central Thailand. He graduated at high school level from Kannasootsuksalai School, Suphanburi, in 1995. In 1999, he received a B.Sc. degree in Geology from the Department of Geology, Faculty of Science, Chulalongkorn University, Thailand. After his graduation, he started his work in 1999 as a government official at the Geological Information Section, Geological Survey Division, Department of Mineral Resources (DMR). In 2002, he has moved to work in the different section, the Geological Section 4, Bureau of Geological Survey, Department of Mineral Resources (DMR), and have been employed until present time. In 2004 he enrolled as a graduate student for the M.Sc. program of Geology programme at Graduate School, Chulalongkorn University, Bangkok, Thailand. He published a geoscientific paper on “Batdabong Fold Complex in Khlong Had area, Sa Kaeo, Eastern Thailand: Evidence from Remote Sensing and Structural Analyses” which appeared in Journal of Remote Sensing and GIS Association of Thailand in 2006.